PRECURSOR TRNA PROCESSING BY PROTEIN ONLY RNASE PS AND ITS CONNECTION TO MITOCHONDRIAL DISEASES

by

Agnes Karasik

Dissertation submitted to the Faculty of the
Molecular and Cellular Biology Graduate Program
Uniformed Services University of the Health Sciences
In partial fulfillment of the requirements for the degree of
Doctor of Philosophy 2018

[Dissertation approval form inserted here]

UNIFORMED SERVICES UNIVERSITY, SCHOOL OF MEDICINE GRADUATE PROGRAMS
Graduate Education Office (A 1045), 4301 Jones Bridge Road, Bethesda, MD 20814

APPROVAL OF THE DOCTORAL DISSERTATION IN THE MOLECULAR & CELL BIOLOGY GRADUATE PROGRAM

Title of Dissertation: "Precursor tRNA processing by Protein Only RNase Ps and its connection to mitochondrial diseases"

Name of Candidate: Agnes Karasik
Doctor of Philosophy
March 14, 2018

DISSERTATION AND ABSTRACT APPROVED:

DATE:

[redacted]
March 23, 2018
Tharun Sundaresan, PhD
DEPARTMENT OF BIOCHEMISTRY
Committee Chairperson

[redacted]
3/14/18
Markos Koutmos, PhD
DEPARTMENT OF BIOCHEMISTRY
Dissertation Advisor

[redacted]
3/14/18
Frank Shewmaker, PhD
DEPARTMENT OF PHARMACOLOGY
Committee Member

[redacted]
3/14/18
Sc, MS, PhD
DEPARTMENT OF IMMUNOLOGY
Committee Member

[redacted]
3/14/2018
Adrian Ferre-D'Amare, PhD
NATIONAL INSTITUTES OF HEALTH, NHLBI
Committee Member

ACKNOWLEDGMENTS

First of all, I would like to thank to my advisor, Dr. Markos Koutmos for guiding me throughout my graduate years. I feel that his mentorship was a giant step in my life that not only enhanced my scientific views and skills but also helped me to become a better person. He always encouraged and supported me in achieving my goals. Thank you for believing in me!

I am also very grateful to my co-mentor, Dr. Carol Fierke for insightful comments and discussions about my work. I have learnt a lot from you!

I would like to also acknowledge my co-workers whom I worked with on different projects during my PhD; Dr. Aranganathan Shanmuganathan, Dr. Mike Howard, Dr. Bradley Klemm and Dr. Nancy Wu. During the summers I also had the opportunity to supervise talented high school students; Nathaniel Jackson and Sonia He. It was fun to work with you!

Special thanks to Dr. Kristin Koutmou, who taught me many techniques to kick-start my projects, read my manuscripts and was always available to answer my questions.

I am grateful to all at USUHS who followed and supported my graduate career; especially to Dr. Saibal Dey and Dr. Mary Lou Cutler. I am thankful for my thesis committee members who always had great questions and advise on my research; Dr. Tharun Sundaresan, Dr. Joseph Mattapallil, Dr. Frank Shewmaker and Dr. Adrian Ferre-D'Amare. My research was generously supported by American Heart Association pre-doctoral fellowship and USU student (TO) grant.

This thesis could not be written without the help of my family in the U.S. and overseas. I really appreciate the help of my grandma, Erzsebet, and my in-laws, Natalie and Isak who were with me in the most difficult times.

Last but not least, I would like to say a special thanks to Dr. Max Karasik, who besides being a great husband also acted as my “unofficial advisor”. He always encouraged me to think critically and deal with my scientific problems. Without you I would not be the same person! You and our sons born during my graduate years, Marton and Aron, brought a lot of joy and fun to my life. Thank you!

DEDICATION

I dedicate my dissertation to all women who could not pursue their dream of becoming a scientist due to discrimination or commitment to family.

COPYRIGHT STATEMENT

The author hereby certifies that the use of any copyrighted material in the dissertation manuscript entitled: “Precursor tRNA processing by Protein Only RNase Ps and its connection to mitochondrial diseases” is appropriately acknowledged and, beyond brief excerpts, is with the permission of the copyright owner.

[Signature] 

Agnes Karasik

March 26th, 2018

DISCLAIMER

The views presented here are those of the author and are not to be construed as official or reflecting the views of the Uniformed Services University of the Health Sciences, the Department of Defense or the U.S. Government.

ABSTRACT

Precursor tRNA processing by Protein Only RNase Ps and its connection to mitochondrial diseases

Agnes Karasik, PhD, 2018

Thesis directed by: Dr. Markos Koutmos, associate professor, Department of Biochemistry and Molecular Biology

A plethora of human diseases are linked to mutations in human mitochondrial transfer RNAs (tRNA). In most cases, it is unknown how these mutations contribute to disease. tRNAs are matured by several enzymes acting in a sequential manner. Mutations in tRNAs could impair interactions with these enzymes causing precursor RNA accumulation leading to mitochondrial dysfunction.

RNase P is one of the first tRNA maturation enzymes catalyzing the removal of the 5' extraneous end of precursor tRNAs. Protein Only RNase Ps (PRORPs) are found in eukaryotes and divided into two major classes. In most unicellular eukaryotes and plants, PRORPs are stand-alone enzymes that localize in the nucleus and organelles, while metazoan PRORPs, also known as MRPP3s (Mitochondrial RNase P Protein), are found only in mitochondria and form the mitochondrial RNase P complex with accessory partners MRPP1 and 2. mtRNase P is proposed to play a central role in human health and disease. Despite the importance of PRORPs, knowledge of their structure and function

and their relations to human diseases is still very limited. Hence, I have investigated the following overall questions: (1) How do PRORPs recognize and cleave their substrates? (2) Are PRORPs structurally conserved? (3) Is there any link between PRORPs and mitochondrial diseases?

In order to answer these questions I studied a stand-alone PRORP (PRORP2 from *A.thaliana*) and human MRPP3 using X-ray crystallography and biochemical assays. I found that the biochemical and structural properties of PRORP2 are highly conserved with minor differences compared to other *A.thaliana* paralogs. Furthermore, my work resulted in a detailed model of PRORP-substrate interactions. Later, I demonstrated that single unit and multi-subunit PRORPs employ different substrate recognition mechanisms. In addition, I observed that there is a complex interplay between components of mtRNase P that can drive substrate recognition. Further confirming the important role of mtRNase P in human mitochondria, I also found that pathogenic mutations in pre-tRNAs significantly affected functions of mtRNase P *in vitro*.

Taken together, my work offers insights into the functions of different PRORPs and provides a framework for further characterization of their working mechanism and connections to human health and disease.

TABLE OF CONTENTS

LIST OF TABLES xii

LIST OF FIGURES xiv

CHAPTER 1: Introduction 1

1.1 Maturation and classification of mitochondrial pre-tRNAs 1
1.1.1 Maturation of precursor transfer RNAs 1
1.1.2 Pre-tRNA maturation in the mitochondria 2
1.1.3 Classification and structure of human mitochondrial tRNAs 3
1.2 A Diverse group of RNase Ps catalyze the 5'end cleavage of precursor tRNAs 5
1.2.1 Ribozyme RNase Ps 5
1.2.2 Protein Only RNase Ps 6
1.2.3 *Arabidopsis thaliana* single unit PRORPs 8
1.3 Structure and function of PRORPs 9
1.3.1 PRORPs process the 5' end of pre-tRNAs 9
1.3.1 Crystal Structures of PRORPs 11
1.3.2 Catalytic mechanism of PRORPs 15
1.3.4 Metal dependence of PRORPs 17
1.3.5 Substrate specificity of PRORPs 18
1.3.6 Substrate recognition by PRORPs 20
1.4 Role of mitochondrial PRORP in human health and disease 23
1.5 Significance 24
1.5.1 Single unit PRORPs 24
1.5.2 Multi-subunit PRORPs 26
References 27

CHAPTER 2: Structure, substrate specificity and binding of *A.thaliana* PRORPs 32

Paper1: Nuclear Protein-only ribonuclease P 2 Structure and Biochemical Characterization Provide Insight Into the Conserved Properties of tRNA 5'-end Processing Enzymes 32
Abstract 33
Introduction 34
Results 36
PRORP2 uses Mg^{2+} as a catalytic co-factor 36
PRORP2 preferentially binds pre-tRNA substrates with short 5' leader and 3' trailer sequences 37
PRORP2 inefficiently cleaves mitochondrial encoded nad6 t-element 39
PRORP1 and PRORP2 share overall structural characteristics 40
PRORP2 is a dimer in crystallo and monomeric in solution 41
PPR domains of PRORP1 and PRORP2 exhibit structural differences 43
Central domain of PRORP2 harbors a conserved structural zinc binding site 45

Active sites in the metallonuclease domains of A. thaliana PRORPs are conserved 45
Discussion 47
Materials and methods 51
Supplemental Material 67
Supplemental methods 74
References 75
Crystal structure of inhibitor bound Protein Only RNase P 1 79
Introduction 79
Materials and Methods 80
Results 81
Juglone covalently binds surface cysteines in PRORP1 81
Discussion 83
References 90

CHAPTER 3: Precursor tRNA binding, processing and methylation by human mtRNase P and its connection to diseases 92

Manuscript 1: Interplay between substrate recognition, 5'end processing and methylation activity of human mitochondrial RNase P 92
Abstract 93
Introduction 93
Materials and Methods 96
Results 101
mtRNase P binds mitochondrial precursor-tRNAs non-uniformly 101
mtRNase P exhibits 5' end processing of tightly bound (mt)pre-tRNAs 103
MRPP3 can enhance the methylation activity of the MRPP1/2 sub-complex.... 104
SAM is required for mtRNase P to efficiently bind and process some human mitochondrial pre-tRNAs 105
Discussion 107
Tables 113
Figures 114
Supplemental Material 120
References 122
Manuscript 2: Disease associated mutations in precursor tRNAs affect binding, m1R9 methylation and 5' end precursor tRNA processing by mtRNase P in human mitochondria 126
Abstract 128
Introduction 128
Materials and Methods 131
Results 134
Disease-related mutations in human mitochondrial pre-tRNAs affect substrate binding of mtRNase P 134
Mitochondrial pre-tRNA mutations decrease 5' end cleavage activity of mtRNase P 136
Disease-linked pre-tRNA$^{Leu(UUR)}$ mutations severely affect m1G9 methylation activity in the mitochondria. 136

Mutations in mitochondrial pre-tRNAs can alter their folding and structure. 138
Discussion 140
Figures 146
Supplemental material 150
References 152

CHAPTER 4: CONCLUSIONS 156

4.1 Single Unit PRORPs 156
4.1.1 *A.thaliana* PRORPs are structurally and functionally conserved 156
4.1.2 PRORPs employ a different substrate recognition and cleavage mechanism than ribozyme RNase P 157
4.1.3 The PRORP inhibitor juglone covalently modifies surface cysteine residues 158
4.1.4 Limitations of study: co-crystallization of PRORP and pre-tRNA 159
4.1.5 Future directions 160
4.2 Multi-Subunit PRORPs 161
4.2.1 Proper substrate recognition is the determinant of mtRNase P 5' pre-tRNA processing activity 161
4.2.2 Interplay between the pre-tRNA processing and methylation functions of mtRNase P 162
4.2.3 Single unit and multi-subunit PRORPs employ different substrate recognition mechanism 162
4.2.4 Physiological mutations in human mitochondrial pre-tRNAs have negative effects on mtRNase P functions 163
4.2.5 Loss of mtRNase complex leads to accumulation of mitochondrial RNA precursors in *D.melanogaster* 163
4.2.5 Limitations of study – pre-tRNA$^{Ser(UCN)}$ is not an efficient substrate for mtRNase P 164
4.2.6 Future directions 165
References 166

APPENDIX 168

Paper 2: Differential substrate recognition by isozymes of plant protein-only Ribonuclease P 168
Abstract 170
Introduction 171
Results 174
PRORP1 substrate recognition has little dependence on leader and trailer length 174
PRORP reactivity with model substrates reveals the importance of the D-arm in recognition 176
Arabidopsis PRORP isozymes display differential catalytic efficiencies with four pre-tRNAs 177
PRORPs bind individual pre-tRNAs similarly 178
Product release is not rate-limiting for MTO catalysis by PRORP 178
PRORPs have varying cleavage fidelities 179

3’ discriminator base can contribute to PRORP cleavage fidelity..... 180
Discussion..... 181
Material and Methods..... 185
Tables..... 191
Figures..... 193
References..... 206
Paper 3: Molecular recognition of pre-tRNA by *Arabidopsis* protein-only Ribonuclease P..... 209
Abstract..... 211
Introduction..... 212
Results..... 215
AtPRORP-substrate recognition mode..... 215
AtPRORP1 does not have specific anion binding sites that compete with substrate binding..... 218
AtPRORP1 makes fewer contacts to substrate leader than the bacterial ribozyme..... 219
The PRORP PPR domain recognizes tRNAs using non-canonical positions..... 220
The AtPRORP2 PPR domain recognizes tRNAs using a similar binding surface..... 223
PRORP PPR domain appears not to recognize tRNAs with base-specificity..... 225
Na^+ screening inhibits AtPRORP1 single-turnover activity..... 226
Discussion..... 227
Materials and methods..... 236
Figures..... 244
Supplemental Methods..... 251
Supplemental Figures..... 257
References..... 262
Paper 4: Loss of the mitochondrial protein-only Ribonuclease P complex causes aberrant tRNA processing and lethality in Drosophila..... 267

LIST OF TABLES

Chapter 1. - Introduction
Table 1. Comparison of the *in vitro* multiple turnover enzymatic activity of PRORP1 and ribozyme RNase P from *B.subtilis*. Table has been modified from [17]. 11
Table 1. Dissociation (K_D) and single-turnover rate constants (k_{obs}) for PRORP2 with (nu)pre-tRNA^{Gly} substrates containing varying 5' leader and 3' trailer lengths..... 58
Table 2. Crystallographic data. Data processing and refinement statistics. 59
Table 3. Single turnover rate constants for PRORP2 cleaving (nu)pre-tRNA$^{Gly\ 8:1}$. 60
Supplemental table 1. Intramotif angles of PRORP1 and PRORP2 calculated by PROMOTIF. 67
Supplemental table 2. Binding of (nu) pre-tRNA$^{Gly\ 8:1}$ to PRORP2 active site mutants. 68
Supplemental table 3. k_{obs} values and standard errors (SE) derived from individual single turnover experiments for PRORP2..... 69
Table 1. X-Ray Crystallography Data Collection and Refinement Statistics..... 89
Table 1. Human mtRNase P binds and processes a subset of mitochondrial pre-tRNA substrates efficiently. 113
Table 2. 5' end cleavage of mitochondrial pre-tRNAs by the mtRNase P complex..... 113
Supplemental Table 1. *A.thaliana* PRORP1 and PRORP2 do not bind and process most human mitochondrial pre-tRNAs efficiently. 120
Supplemental Table 2. Summary of binding and single turnover cleavage experiments for wild type and methylation site mutant tRNA$^{Val7:0}$. 120
Supplemental Table 3. Binding and 5' end cleavage of human pre-tRNAs by mtRNase P in the presence of excess SAM. 120
Supplement Table 1. Disease-linked tRNA mutations affect binding and cleavage rates of mtRNase P. 150
Supplement Table 2. Melting temperature values for first transitions for wild type pre-tRNAs and pre-tRNA$^{Ile\ 7:0}$ mutants. 150
Table 1. Dissociation constant (K_D) and STO observed rate constant (k_{obs}) for PRORP1 with *B. subtilis* pre-tRNA containing varying leader lengths 191
Table 2. Kinetic parameters for pre-tRNA cleavage catalyzed by *A. thaliana* PRORP1, 2 and 3..... 191
Table 3. Dissociation constants (K_D in nM) for PRORP1, 2, and 3 binding to pre-tRNAs[a] 192
Table S1. STO miscleavage kinetics catalyzed by PRORP1, 2, and 3[a] 200
Table S2. Single-turnover observed rate constants (k_{obs}) for cleavage of model substrates 200
Table 1. Na^+-dependence of binding affinity. 242
Table 2. Na^+-dependence of *At*PRORP1 variants affinity for *B. subtilis* pre-tRNA^{Asp}. 243
Table S1. Effects of anion identity on affinity for pre-tRNA^{Asp}. 254
Table S2. Effects of mutation to *At*PRORP2 PPRs on affinity for pre-tRNA. 255
Table S3. Effects of *B. subtilis* pre-tRNA^{Asp} mutants on affinity for *At*PRORP1. 256
Table S4. Effects of mutations on *At*PRORP1 affinity for pre-tRNA. 256

LIST OF FIGURES

Chapter 1-Introduction
Figure 1. Schematic representation of tRNA maturation. 2
Figure 2. RNA processing in the mitochondria. 3
Figure 3. Predicted secondary structures of different types (type 0-II) of human mitochondrial tRNAs. 5
Figure 4. Structure of *B. subtilis* ribozyme RNase P with in complex with pre-tRNA (PDB ID: 3Q1Q)[20]. 6
Figure 5. Structure and composition of PRORPs. 8
Figure 6. Crystal structure of (A) PRORP1 (PDB ID:4G24 [33]) and (B) human mitochondrial MRPP3 (PDB ID: 4XGL [34, 35]). 14
Scheme 1. Minimal kinetic mechanism of (A) ribozyme RNase P and (B) PRORPs. 16
Figure 7. Two metal ion mechanism of (A) *B.subtilis* ribozyme RNase P (B) and PRORP1 [20]. Figure is adopted from [44]. 17
Scheme 1. Minimal kinetic mechanism for PRORP2. 57
Figure 1. Metal dependence of PRORP2. 61
Figure 2. PRORP2 discriminates betweeen binding, but not cleaving, substrates with varied 5' leader and 3' trailer lengths. 62
Figure 3. PRORP2 cleaves mitochondrial pre-nad6 t-element. 63
Figure 4. Comparison of PRORP1 and PRORP2 crystal structures. 64
Figure 5. PRORP2 is a monomer in solution. 65
Figure 6. Comparison of the PPR, central and metallonuclease domains of PRORP1 and PRORP2. 66
Supplemental figure 1. Representative gels showing cleavage activity of PRORP2 in the presence of A. Mg^{2+}, B. Ca^{2+}, C. Mn^{2+} and D. Zn^{2+}. 70
Supplemental Figure 2. Comparison of cleavage activity of PRORP2 and truncated 21-515 PRORP2 with (nu)$tRNA^{Gly}$ 8:1 using standard reaction conditions. 71
Supplemental Figure 3. Clustal W 2.1 analysis of PRORP1 and PRORP2. 72
Supplemental Figure 4. Differences in disordered loops in the A. PPR and B. metallonuclease domains. 73
Figure 1. Chemical composition of juglone. 86
Figure 2. Crystal structure of PRORP1 in complex with juglone after overnight incubation. 87
Figure 3. 88
Figure 1. Proposed secondary structures of different types of human mitochondrial pre-tRNAs used in this study. 114
Figure 2. Presence of MRPP1/2 is required for efficient recognition of mitochondrial pre-tRNAs. 115
Figure 3. Some human mitochondrial pre-tRNAs are efficiently cleaved by the mtRNase P complex *in vitro*. 116
Figure 4. MRPP1/2 methylates human mitochondrial pre-tRNAs. 117
Figure 5. Presence of SAM enhances recognition and 5' end processing of some mitochondrial pre-tRNAs by mtRNase P. 119
Supplemental Figure 1. 121

Figure 1. Locations of the investigated mitochondrial tRNA mutations in the predicted secondary structure of **A.** pre-tRNA^{Ile}, **B.** pre-tRNA$^{Leu(UUR)}$ and **C.** pre-tRNA^{Met}. 146
Figure 2. Disease-related tRNA mutations affect binding and 5' end pre-tRNA processing by the mtRNase P. 147
Figure 3. Disease-linked mutations in human mitochondrial pre-tRNA$^{Leu(UUR)}$ decrease methylation efficiency of the human mtRNase P complex. 148
Figure 4. Disease-associated tRNA mutations alter the structure of pre-tRNAs. 149
Supplemental Figure 1. Human mtRNase Ps do not process some pre-tRNAs at physiological temperatures. 151
Figure 1. A. *A. thaliana* encodes three PRORP enzymes, PRORP1, 2 and 3 193
Figure 2. Binding affinity and STO activity of PRORP1 for varying leader lengths of *B. subtilis* pre-tRNA. 194
Figure 3. A. Predicted secondary structures of *A. thaliana* pre-tRNA substrates used in this study. 195
Figure 4. Multiple-turnover cleavage of pre-tRNA catalyzed by PRORPs. 196
Figure 5. 197
Figure 6. PAGE analysis of reaction products from RNase P-catalyzed STO cleavage of pre-tRNA 198
Figure 7. Miscleavage of pre-tRNA catalyzed by PRORP is alleviated by removal of the discriminator base. 199
Figure S1. Competition binding assays using unlabeled pre-tRNAs. 201
Figure S2. STO cleavage kinetics of Phe-nuc pre-tRNA catalyzed by PRORP. 203
Figure S3. STO cleavage kinetics of phe-nuc pre-tRNA catalyzed by PRORP analyzed by reverse transcription. 204
Figure S4. Miscleavage of pre-tRNA Cys-mito catalyzed by PRORP3 is reduced by removal of the discriminator base. 205
Figure 1. Structure of *Arabidopsis thaliana* PRORP1 (PDB 4g24), generated in PyMOL [57]. 244
Figure 2. Substrates used for functional assays. 245
Figure 3: Cation (M^{n+}) dependence of dissociation constants for *At*PRORP1 binding to *B. subtilis* fluorescein-labeled pre-tRNA^{Asp} 246
Figure 4. Sodium dependence of *At*PRORP1 affinity for substrates with varied leader lengths. 247
Figure 5: Residues selected for mutation in the PPRs of *At*PRORPs, generated in PyMOL [57]. 248
Figure 6. Na^+-dependence of *At*PRORP1 cleavage activity. 249
Figure 7: Model of the PRORP-substrate complex. 250
Figure S1. Alignment of PRORP PPR domains (Clustal Omega) [63, 64]. 257
Figure S2. Stability of Y140A and R184A *At*PRORP1 or Y74S *At*PRORP2. 259
Figure S3. Defects in R212A *At*PRORP1 catalysis and substrate binding with *B. subtilis* pre-tRNA^{Asp}. 261

CHAPTER 1: Introduction

1.1 MATURATION AND CLASSIFICATION OF MITOCHONDRIAL PRE-TRNAS

1.1.1 Maturation of precursor transfer RNAs

Transfer RNAs (tRNAs) are essential elements of the protein translation machinery and therefore for cellular function. tRNAs are transcribed from the genome as precursors (pre-tRNAs) that have to go through many processing and maturation steps by the sequential action of tRNA processing and editing enzymes [1]. In many organisms, the first step of pre-tRNA maturation is the removal of the extraneous 5'end catalyzed by Ribonuclease Ps (RNase Ps). This is followed by the cleavage of the 3' overhanging end by RNase Z (ELAC2 in humans) or exonucleases (e.g Rex1p) [2]. Then, a CCA adding enzyme acts on the processed 3' end of the tRNA (Figure 1) [3, 4]. Additionally, most of the tRNAs acquire distinct posttranscriptional base modifications through the action of tRNA modifying enzymes. Up to date more than 90 different tRNA modifications have been observed in the tRNA body [5]. This includes hypermodifications, such as 7-deaza-guanosine and wybutozine, where the actions of several tRNA modification enzymes are required for the formation of the modified base [5]. In contrast, some modifications, including methylation, are catalyzed by a single enzyme most of the times. These modifications can facilitate proper folding, anticodon recognition and function of the tRNAs [5]. After processing and modification, the mature tRNA is loaded with amino acids by aminotransferases at the 3' end where the CCA bases serve as a recognition site. In addition, most nuclear pre-tRNAs include introns that are spliced out during tRNA maturation.

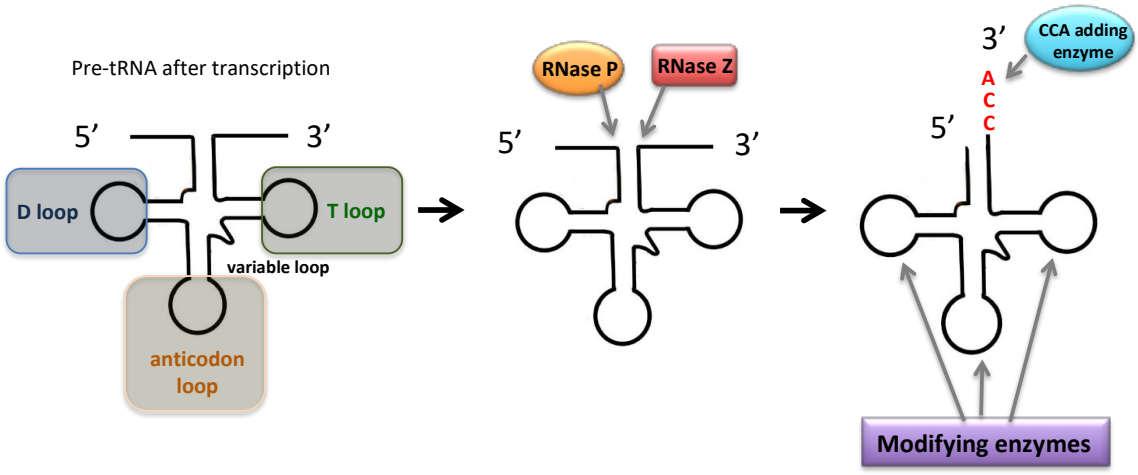


Figure 1. Schematic representation of tRNA maturation.
After transcription, RNase P and RNase Z cleave the 5' and 3' end of the tRNAs. The tRNA body can acquire different base modifications by editing enzymes. Mature tRNAs harbor CCA termini at the 3' end.

1.1.2 Pre-tRNA maturation in the mitochondria

Although maturation of mitochondrial tRNAs is very similar to that of nuclear ones, there are few characteristic differences. Pre-tRNAs in mitochondria do not include introns and are transcribed as a part of longer polycistronic units engaged with mitochondrial mRNAs and rRNAs [6]. According to the punctuation model [7], tRNAs are interspersed between 2 rRNAs and 13 mRNAs as precursor RNAs in mammals (Figure 2A). When tRNAs are processed, the product of the 5' or 3' end cleavage of tRNAs can also result in mature rRNAs and mRNAs [6, 7] (Figure 2B). This model highlights the importance of 5' and 3' processing in mitochondria, since impaired tRNA processing could not only affect levels of mature tRNAs, but also influence levels of matured mRNAs and rRNAs. Perturbation of mature RNA levels can lead to dysfunction of the mitochondria, reduced ATP levels and therefore development of diseases.

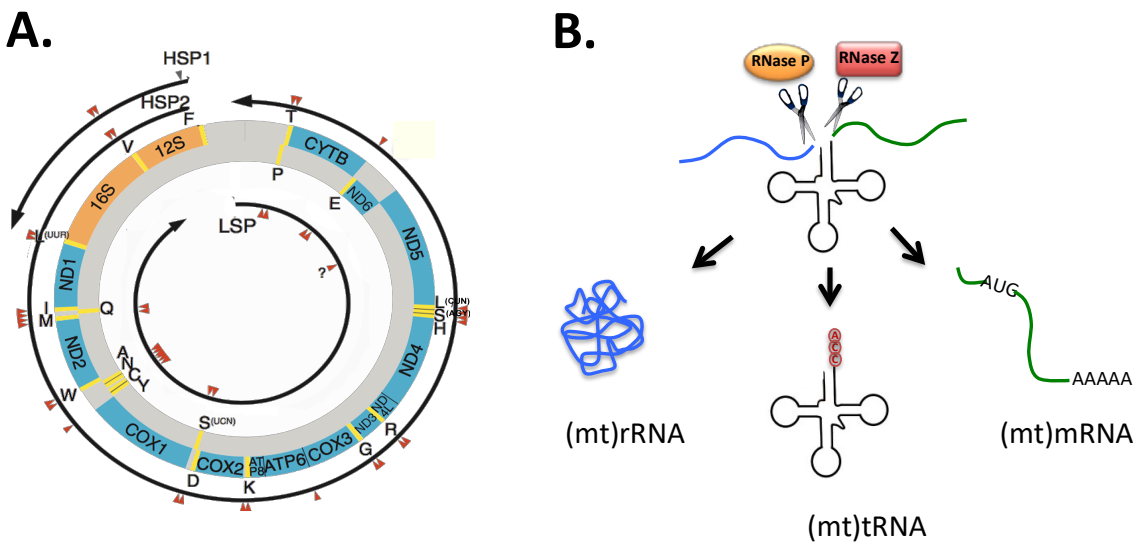


Figure 2. RNA processing in the mitochondria.
A. RNA transcripts are transcribed from the circular mitochondrial genome as polycistronic units. In human mitochondria there are three polycistronic units transcribed (indicated by black arrows); two from the heavy chain (HSP1 and 2) and one from the light chain (LSP). Red arrows indicate mitochondrial processing sites. tRNA genes (yellow) are interspersed between mRNA (blue) and rRNA (orange) genes. Figure is adopted from [8]. **B.** 3' and 5' end tRNA processing in the human mitochondria can produce 3' or 5' end mature rRNA and mRNA transcripts.

1.1.3 Classification and structure of human mitochondrial tRNAs

The human mitochondrial genome encodes for all 22 tRNAs involved in mitochondrial protein translation. The secondary structure of mitochondrial tRNAs ((mt)tRNAs) provides the basis for their categorization (Type 0-III), which often differs from that of nuclear ones [9, 10]. Type I and III are only represented by one mitochondrial tRNA, respectively, and both significantly deviate from nuclear tRNAs in their secondary structure. $tRNA^{Ser(UCN)}$ (Type I) has a longer anticodon stem and shorter D-, variable loops and connector than the canonical tRNAs (Figure 3). The type III tRNA, $tRNA^{Ser(AGY)}$, lacks the entire D-loop and D-stem (Figure 3). Most human

mitochondrial tRNAs belong to Type 0 or II and their secondary structures are predicted to be more closely aligned to nuclear ones with slight variations on the size of the D- and T-loops. Supporting the distinctness of mitochondrial tRNA and pre-tRNA structures, it has been shown that human *in vitro* transcribed mitochondrial (mt)tRNA^{Asp} can adopt several conformations besides the expected cloverleaf secondary structure [5, 11]. In addition, (mt)tRNA^{Lys} only adopts its predicted secondary structure when the base in the 9th position is methylated (m1A9 methylation). This methylation disrupts base pairing responsible for the alternative conformation and allows for proper folding into the classical L-shaped 3D-structure [12]. Nuclear tRNAs adopt a conserved L-shaped tertiary structure when they are properly folded [13]. However, the tertiary structures of human mitochondrial tRNAs are mostly based on predictions [14].

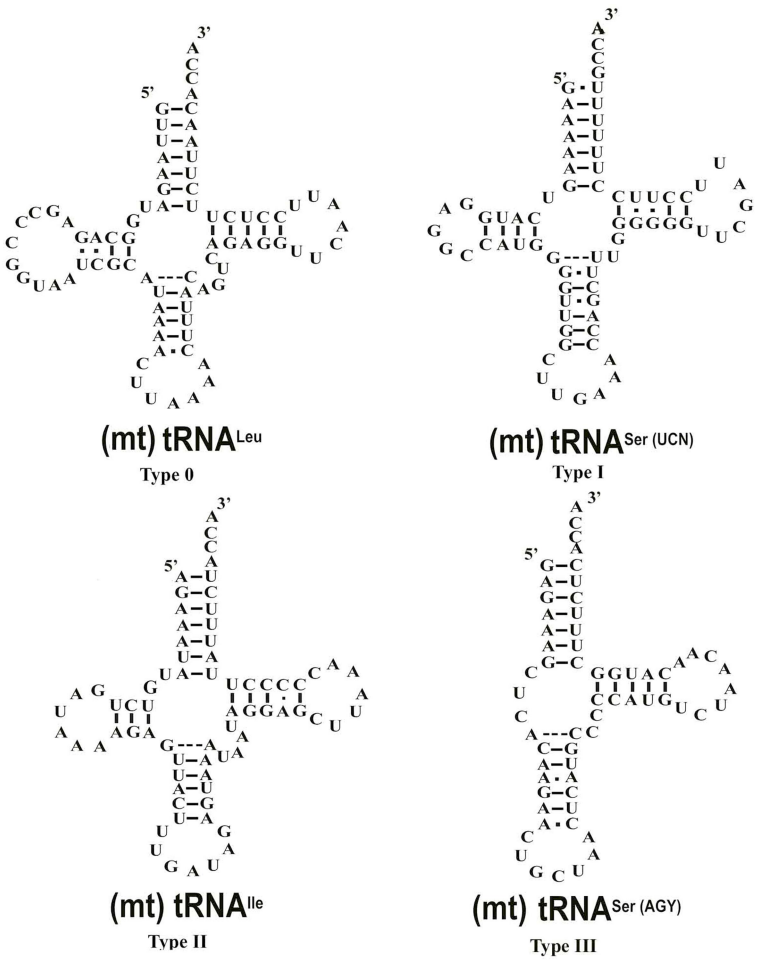


Figure 3. Predicted secondary structures of different types (type 0-II) of human mitochondrial tRNAs.
Other Type 0 pre-tRNAs: Asn, Gln, Leu (CUN)
Other Type II pre-tRNAs: Ala, Arg, Asp, Cys, Glu, Gly, His, Lys, Met, Phe, Pro, Thr, Trp, Tyr, Val

1.2 A DIVERSE GROUP OF RNASE PS CATALYZE THE 5'END CLEAVAGE OF PRECURSOR TRNAS

1.2.1 Ribozyme RNase Ps

RNase P - that cleaves the 5' tRNA end of immature tRNAs - is an essential enzyme found in most organisms. Notably, it was also the first ribozyme discovered in

the 1970's [15]. In general, RNase P consists of one RNA and one to ten protein components, depending on the organism. The RNA moiety serves as a catalyst, while proteins facilitate substrate binding and catalysis (Figure 4) [15-17]. In bacteria, the RNase P complex contains only one protein required for *in vivo* function, however *in vitro*, the RNA component of bacterial RNase P itself is capable of processing pre-tRNAs at high ion concentrations [18]. In contrast to bacteria, archaea and eukaryotes have five to ten protein components in their ribozyme RNase P, where the function of the RNA catalyst is increasingly dependent on their presence [19].

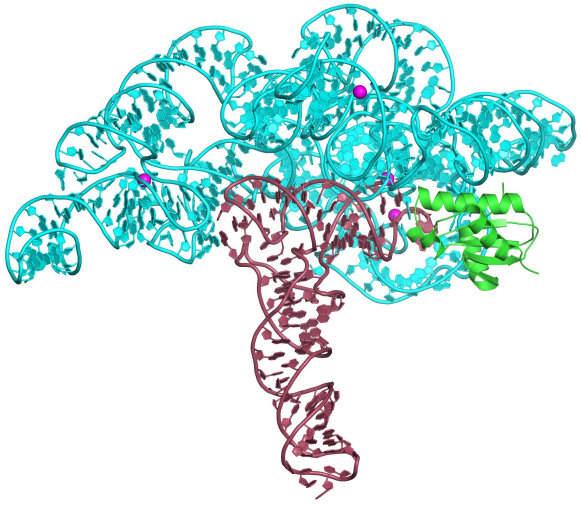


Figure 4. Structure of *B. subtilis* ribozyme RNase P with in complex with pre-tRNA (PDB ID: 3Q1Q)[20].
Cyan: RNA moiety of ribozyme RNase P, Green: protein component of ribozyme RNase P, Raspberry: Modified pre-tRNA^{Phe} from *Thermatoga maritima*.

1.2.2 Protein Only RNase Ps

A novel group of 5' end tRNA processing enzymes called Protein Only RNase Ps (PRORPs) was discovered a decade ago [21-23]. While canonical RNase Ps are present in every kingdom of life, protein only RNase Ps were only found in Eukaryotes (Figure

5). Although these enzymes are catalyzing the same reaction and are functionally similar [22-25], they are not homologs of any components of the ribozyme RNase P. PRORPs can be distinguished based on their ability to interact with other proteins and their localization. In some land plants, exemplified by *Arabidopsis thaliana* [23, 26], and other unicellular Eukaryotic organisms, like *Trypanosoma bruceii* [22], PRORP enzymes carry out the 5' end cleavage of tRNAs in both the nucleus and the organelles without any known interaction partners. Depending on the organism, one to three PRORP paralogs are present and these are frequently localized into different cell compartments [22, 26-29]. It is noteworthy that in archaea and bacteria, 5' tRNA enzymes containing a similar catalytic domain to PRORPs were also recently identified (HARPs, Homologs of Aquifex RNase P). These enzymes were shown to be the smallest RNase P with independent 5' end pre-tRNA processing endonuclease activity [30]. In contrast, metazoans - including humans - typically contain a complex-forming PRORP in their mitochondria, and a ribozyme-based RNase P in their nucleus [23]. In humans, PRORP (here referred as MRPP3, Mitochondrial RNase P Protein 3) is only active in the presence of auxiliary proteins, MRPP1 and MRPP2 (Mitochondrial RNase P Protein 1 and 2) forming the mitochondrial RNase P complex (mtRNase P). Although human PRORP has very low activity by itself and miscleaves some of the human tRNAs (collaborators unpublished data), *in vitro* and *in vivo* formation of the complex is necessary for proper 5' end cleavage and mitochondrial function, respectively [21, 31]. The sub-complex consisting of MRPP1 and MRPP2 has tRNA methyltransferase activity, and this function is not directly linked to the 5' tRNA processing activity of the mtRNase P [32]. MRPP1 is required for methylation of the 9^{th} position of most mitochondrial tRNAs. MRPP2 is a

dehydrogenase, however it likely functions as a scaffold protein for the formation of the MRPP 1 and 2 sub-complex [32]. The stoichiometry and the mechanism of how these proteins work together still remains a question.

While ribozyme RNase P has been studied extensively in the last decades, knowledge on PRORPs - their structural and biochemical properties - has been limited due to their novelty.

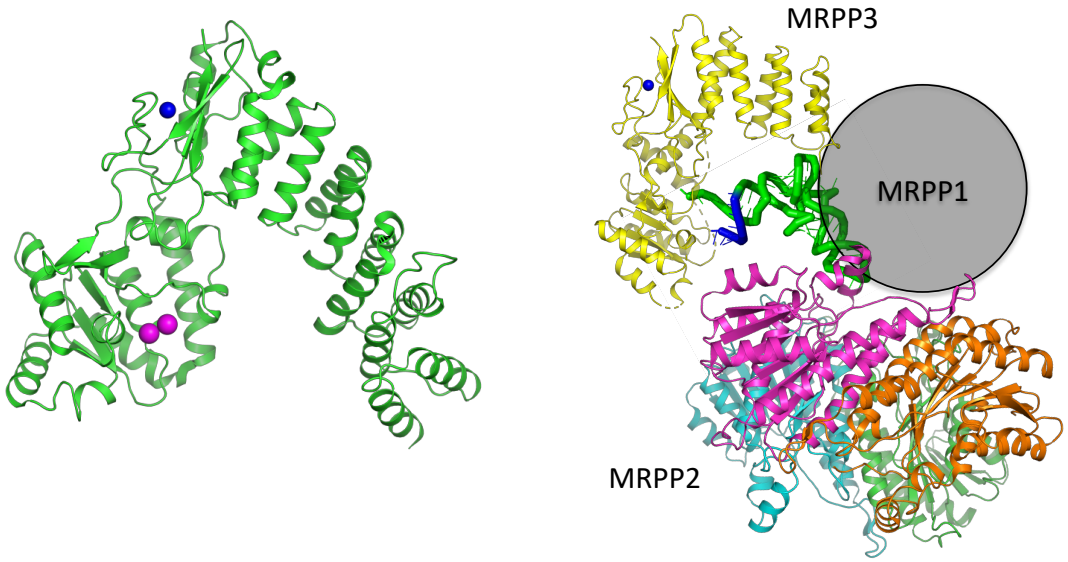


Figure 5. Structure and composition of PRORPs.
Left: Structure of a single subunit PRORP from *A.thaliana* (PDB ID: 4G24)[33]. Right: Components of complex-forming PRORPs. MRPP3 (yellow, PDB ID: 4XGL[34, 35]) is proposed to form a transient complex with MRPP1 (grey circle) and the homotetramer MRPP2 (PDB ID: 1U7T) [36] when the pre-tRNA substrate is present (green, modified from PDB ID: 1EHZ [37]).

1.2.3 *Arabidopsis thaliana* single unit PRORPs

As in most land plants [28, 38], in *Arabidopsis thaliana (A.thaliana)*, three single-protein PRORPs have been identified [23, 26] but not ribozyme RNase P. The three paralog PRORPs localize to different compartments in the cell; PRORP1 is localized in mitochondria, while PRORP2 and PRORP3 are found in the nucleus [23]. All *A.thaliana* PRORPs are essential, however PRORP2 and PRORP3 have redundant functions [26]. Knock down of any PRORPs by *in vivo* virus induced gene (VIGS) silencing in *A.thaliana* leads to the accumulation of tRNA precursors, supporting their 5' end tRNA cleavage function. Silencing of nuclear PRORPs affects only nuclear transcripts but not organellar ones, while down-regulating PRORP1 decreases the level of mitochondrial and chloroplast RNA transcripts but not nuclear ones. This highlights the connection between function and localization of different *A.thaliana* PRORPs [26]. Notably, silencing of organellar PRORP1 resulted in defects in photosynthesis but not in mitochondrial function [39]. These enzymes are likely to fulfill the same or greatly overlapping functions to the prototypical ribozyme RNase Ps since *A.thaliana* PRORPs are able to functionally replace the ribozyme RNase P in *E.coli* and therefore maintain its viability [23, 26].

1.3 STRUCTURE AND FUNCTION OF PRORPS

1.3.1 PRORPs process the 5' end of pre-tRNAs

A.thaliana PRORPs provide excellent models to study the kinetics of pre-tRNA cleavage by PRORPs mainly due to their easy expression, handling and robustness in *in vitro* assays. Accordingly, initial kinetic studies have been focusing on *A.thaliana*

PRORPs, especially on PRORP1. All recombinantly expressed and purified *A.thaliana* PRORPs are capable of cleaving the 5' end of pre-tRNAs *in vitro* [23, 26, 40]. Since the discovery of PRORP enzymes it has been of interest to study and compare the endonuclease mechanism of PRORPs with ribozyme RNase Ps. Early studies on the kinetics of PRORPs have shown that multiple turnover kinetic parameters of PRORP1 and 3 were comparable to that of eukaryotic ribozyme RNase P [17, 26], however both PRORPs were significantly slower than the bacterial ribozyme RNase P (Table 1). Additionally, single turnover reaction rates were also found to be at least 10 fold slower for *A.thaliana* PRORPs (observed kinetic constant is between 1-8 min^{-1} depending on reaction conditions) compared to the bacterial ribozyme RNase P [17, 33, 40]. However, these studies on PRORP kinetics were rudimentary (e.g non-native bacterial substrates were used) and focused primarily on the comparison of ribozyme RNase Ps and PRORPs with a lesser emphasis on differences between the different PRORP paralogs.

Since reconstitution of the three-component metazoan PRORPs is challenging, there are no major kinetics studies on this enzyme complex. Thus far, reported observed single turnover rate constants (k_{obs}) for mtRNase P with human mitochondrial $tRNA^{Leu(UUR)}$ and $tRNA^{Ile}$ substrates have been found to be ~1 min^{-1} and ~4.5 min^{-1}, respectively [41, 42]. This measured activity is comparable with that of single subunit PRORPs.

	k_{cat} (sec^{-1})	K_M (nM)	k_{cat}/K_M ($M^{-1}sec^{-1}$)
B.subtilis ribozyme RNase P	~ 1	230	4 X 10^6
A.thaliana PRORP1	~ 0.1	850	1 X 10^5

Table 1. Comparison of the *in vitro* multiple turnover enzymatic activity of PRORP1 and ribozyme RNase P from *B.subtilis*. Table has been modified from [17].

1.3.1 Crystal Structures of PRORPs

The crystal structure of *A.thaliana* PRORP1 was the first PRORP structure solved [33] (Figure 6A), followed by crystal structures of severely truncated human MRPP3s [34, 35] (Figure 6B). PRORP1 has three distinct domains forming an overall V-shaped molecule. While human MRPP3's overall domain structure is similar to that of PRORP1, the distinct domains adopt a more relaxed conformation resulting in a L-shaped molecule [34, 35].

The N-terminal, PentatricoPeptide Repeat domain (PPR domain) consists of five PPR motifs (each formed by two antiparallel helixes interconnected by a disordered loop) and is part of the putative binding site of the pre-tRNA. This is evidenced by N-terminal truncations that not only severely reduce tRNA binding but also impair the nuclease ability of PRORP1 [33, 43]. Similarly, N-terminally truncated human MRPP3 lacks cleavage activity when reconstituted with MRPP1 and 2 [38].

The C-terminal metallonuclease domain (Ned4-Bp1, YacP Nuclease domain; NYN-domain) houses the active site of PRORPs. In the active site of PRORP1 conserved aspartate residues have been identified (D399, D474, D475 and D493) as the key players of the cleavage reaction (Figure 6C). Substitutions of these aspartates to alanines resulted in catalytically inactive PRORP1 validating their importance in 5' tRNA processing [33]. H498 and H438 in PRORP1, which are located near the catalytic site, were thought to play a role in the catalysis, but it was later found that substitution of these residues does

not fully abolish catalytic activity and does not significantly alter single turnover pH dependence [44] suggesting that they are not involved in catalysis directly.

All RNase Ps are metallonucleases that require the presence of metal ions for function. Therefore, in order to identify the catalytical metal(s) in PRORP structure, PRORP1 crystals were soaked in different metal ions. One Ca^{2+} or Sr^{2+} has been found at the catalytic center when PRORP1 crystals were soaked into 50 mM $CaCl_2$ or $SrCl_2$, respectively. However, soaking into $MnSO_4$ yielded two metal ions present at the active site. Based on PRORP1 crystal structure, it has been proposed that at least two metal ions are required for 5' end pre-tRNA cleavage [33]. This was later confirmed by investigating the metal dependence of k_{cat}/K_M where derived hill coefficients were in good agreement with a two metal ion mechanism [44].

In human MRPP3, three of the four PRORP1 active site aspartate residues are present (D409, D478 and D479) and mutations of these also significantly decrease the activity of mtRNase P complex [34] suggesting a similar catalytic mechanism for single and complex-forming PRORPs. However, instead of the fourth catalytic aspartate an arginine residue is found in MRPP3 (R498) that blocks the metal binding site by interacting with D478 (Figure 6D and E). Therefore, it has been proposed that activation of MRPP3 requires conformational changes at the catalytic core [34, 35]. However, replacing the active site by swapping the full metallonuclease domain of MRPP3 with that of PRORP1 resulted in limited 5' end tRNA processing activity [34, 35]. This indicates that other rearrangements might be needed for correct MRPP3 function.

The third, central PRORP domain holds the PPR and the metallonuclease domains together in such a position where the two functionally relevant domains are facing towards each other. The central domain contains a structurally important zinc-binding site, where conserved cysteine and histidine residues (C347, C344, C565 and H548 in PRORP1) interact with the Zn^{2+} ion (Figure 6F). A long and disordered loop (lariat loop) is located between the metallonuclease and the PPR domain. This lariat loop is stabilized by H-bonds and salt bridges and in the case of MRPP3, it is in close proximity to the active site [34]. In contrast, PRORP1's lariat loop is shorter and does not interact with the metallonuclease domain but forms inter loop H-bonds. However, the function of this region has not been evaluated yet in PRORPs.

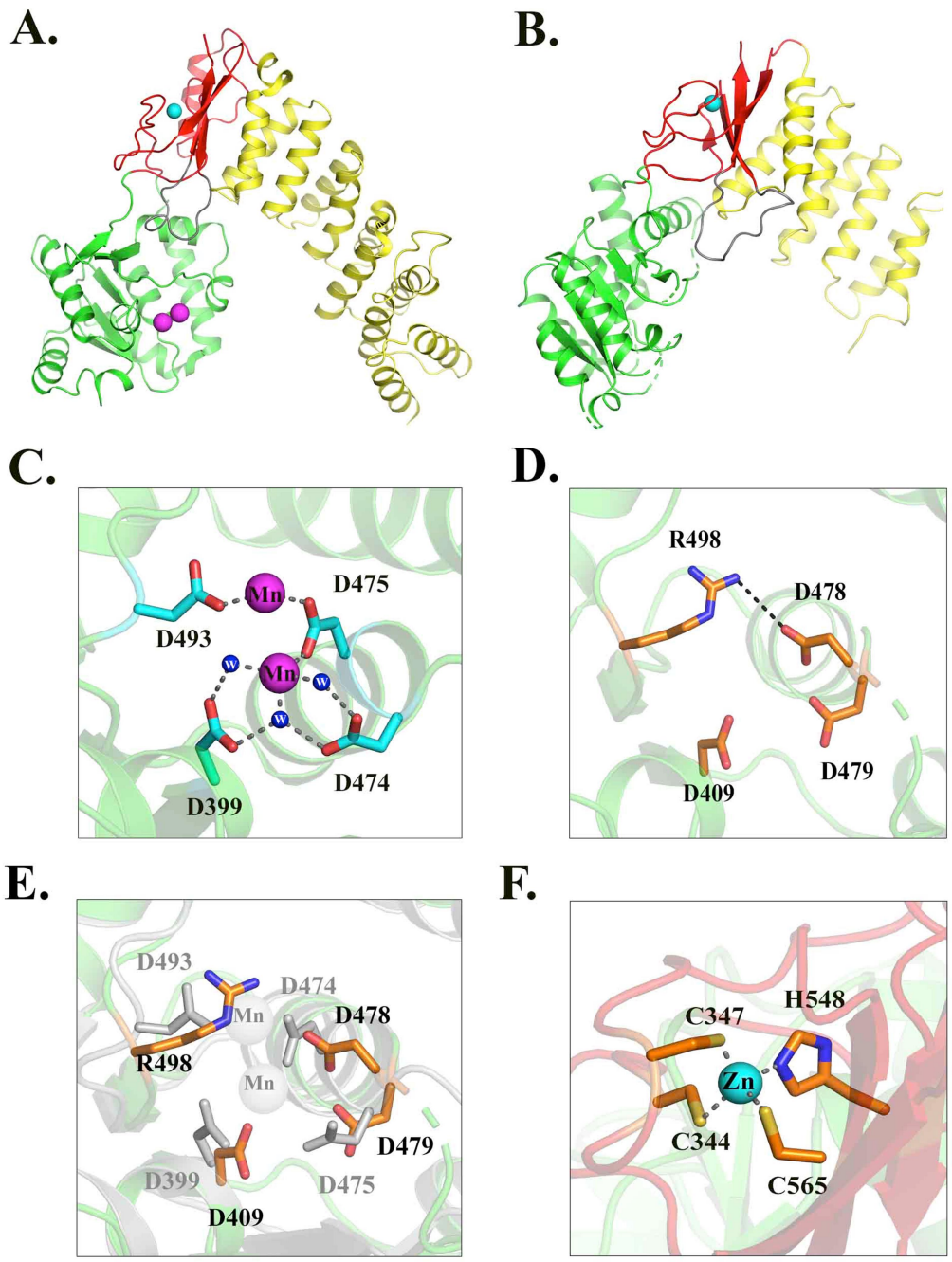


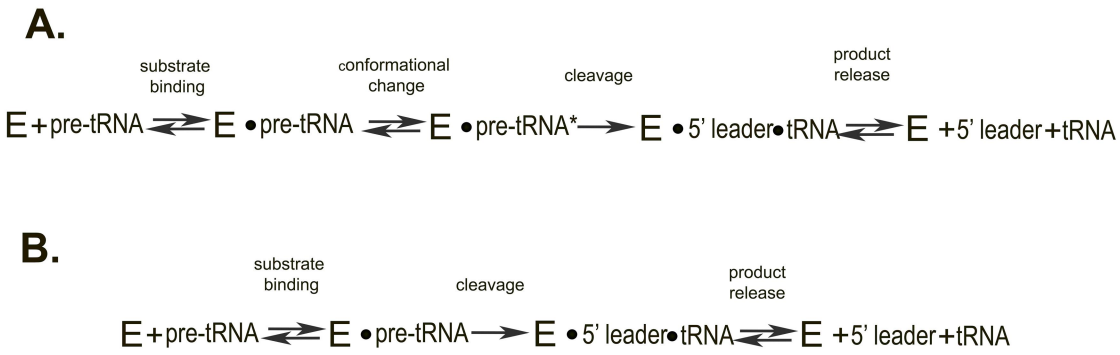
Figure 6. Crystal structure of (A) PRORP1 (PDB ID:4G24 [33]) and (B) human mitochondrial MRPP3 (PDB ID: 4XGL [34, 35]).
Green: metallonuclease domain, Red: central domain, Yellow: PPR domain, Magenta: manganese ions, Cyan: Zinc ion. C. Catalytically active aspartate residues coordinate pre-tRNA cleavage at the active site of PRORP1. D. R498 locks the active site by blocking metal binding in MRPP3 structure. E. Superposition of PRORP1's (grey) and MRPP3's (colored) catalytic core. F. Zinc binding site of the central domain of PRORP1.

1.3.2 Catalytic mechanism of PRORPs

The crystal structures and biochemical characterization of PRORPs provided early insights into the differences in the catalytic mechanism of the distinct group of RNase Ps. This contributed to the initial understanding of how an RNA and a protein can catalyze the exact same reaction.

The most kinetically studied RNase P is the ribozyme from *B.subtilis*. For this enzyme a four step minimal kinetic model has been proposed (Scheme 1A) [45]. Ribozyme RNase P first rapidly associates with the substrate to form the enzyme-substrate complex. Then a conformational step occurs prior to the cleavage step. After the cleavage of the pre-tRNA, the 5' cleaved fragment and the 5' mature tRNA products are released. The latter step of product release is the rate-limiting step in the kinetic cycle [46]. In contrast, the working model for PRORPs corresponds to a three step minimal kinetic mechanism, where the "conformational change" step found in the ribozyme mechanism is not present [33]. However, it is still not clear whether a conformational change is also required for PRORPs. By comparing single turnover and multiple turnover rate constants for PRORP1 and a model *B.subtilis* substrate, it has been shown that product release is not the rate-limiting step for this enzyme in contrast to the bacterial

ribozyme RNase P [44].



Scheme 1. Minimal kinetic mechanism of (A) ribozyme RNase P and (B) PRORPs.

One of the major questions that the discovery of PRORPs raised relates to the details of the similarities and differences between ribozyme and protein only RNase P's mechanism of action. Similarly to ribozyme RNase P, PRORP1 has at least two catalytically important metal ions in the active site [20, 33]. However, the mechanism is suggested to be distinct for PRORP1 compared to the bacterial RNase P due to the different chemical composition of the active site. In the proposed mechanism for the ribozyme RNase P, the first metal ion (M1) positions the substrate and deprotonates the nucleophile, a water molecule, while the second metal ion (M2) mediates a proton transfer to the 3' scissile oxygen during product release (Figure 7A). In contrast to the ribozyme RNase P, in PRORP1, the conserved D399 is proposed to mediate the deprotonation of the nucleophile [33], while protonation of the leaving group occurs by a metal bound water nucleophile similarly to the ribozyme RNase P [44] (Figure 7B). In agreement with this model, a single ionization event was observed for pH dependence of PRORP1's single turnover activity (pK_a ~8.7) that could account for ionization of the metal bound water [44]. Furthermore, another difference is that the pro-Rp oxygen is

coordinated by the metal ions in ribozyme RNase P, whereas in the proposed PRORP1 mechanism, the pro-Sp oxygen interacts with the metal ions during the pre-tRNA cleavage reaction. This is supported by the observation that Rp-phosphorothioate modification at the canonical cleavage site of a model precursor tRNA did not affect the activity of PRORPs significantly but had an impact on *E.coli* ribozyme RNase P activity [40, 47]. In addition, it has also indicated that the 2'OH of the nucleotide upstream of the cleavage site (N_{-1}) coordinates the metal ion required for PRORP1 catalysis similarly to the ribozyme RNase P [48, 49].

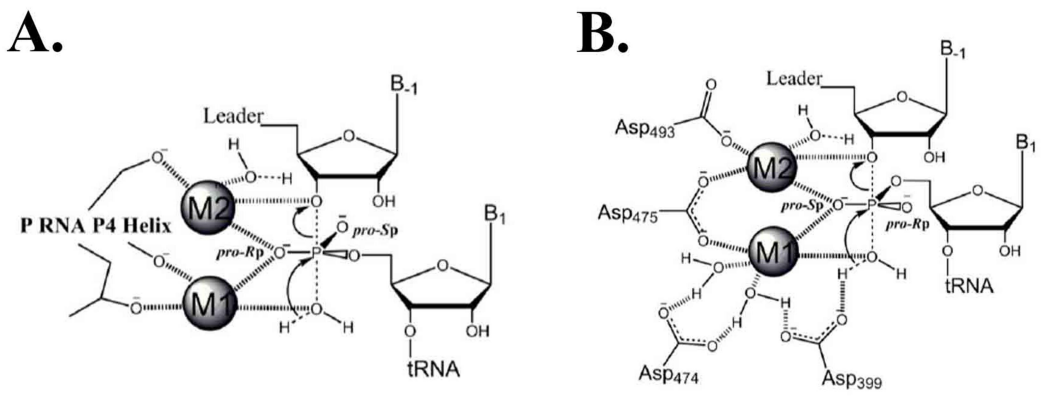


Figure 7. Two metal ion mechanism of (A) *B.subtilis* ribozyme RNase P (B) and PRORP1 [20]. Figure is adopted from [44].

1.3.4 Metal dependence of PRORPs

The most likely physiological metal ion important for MRPP3 catalytic activity is Mg^{2+}, similarly to the RNase P ribozyme [33, 50]. PRORP1 had the highest activity in $MgCl_2$, but it was also active in the presence of Mn^{2+}, Co^{2+} and Ni^{2+} [40]. On the other hand, in the presence of Ca^{2+}, Cd^{2+} and Zn^{2+} PRORP1 did not exhibit processing

activity suggesting that these ions are dispensable for cleavage activity [40]. Like other metallonucleases, PRORP1 in the presence of Ca^{2+} does not cleave but binds its substrate allowing determination of dissociation constants in binding assays [33].

1.3.5 Substrate specificity of PRORPs

Although bacterial ribozyme RNase P is primarily known to process pre-tRNAs it can also cleave a wide variety of other substrates, including 4.5S RNA (part of a signal recognition particle targeting ribosomes to the plasma membrane), tmRNA (transfer messenger RNA), snoRNAs, viral pseudoknots and mRNAs [51-54]. Since *A.thaliana* PRORPs are capable of replacing the bacterial ribozyme in *E.coli* the two groups of RNase P must have largely overlapping substrate profiles [24]. In agreement with this, several studies have shown that recombinant PRORPs are able to bind and cleave pre-tRNAs derived from both *A.thaliana* and bacteria [23, 26, 33, 40]. Similarly to the ribozyme RNase P, PRORPs were also shown to mediate cleavage of snoRNAs and mRNAs *in vivo* in *A.thaliana* [26, 39]. However, ribozyme RNase P deficient but PRORP containing *E.coli* accumulates 4.5S RNA, indicating that this RNA is not a target of PRORPs. The inability of all *A.thaliana* PRORPs to cleave 4.5S RNA was further confirmed by *in vitro* cleavage assays [24].

The *A.thaliana* chloroplast genome encodes for tRNA like structures, termed t-elements that are often present at the 5' end of mRNAs [55]. It has been shown that at least a couple of such tRNA like structures (nad6 and orf138 t-element) are processed by PRORP1 based on *in vivo* and *in vitro* biochemical assays [23, 26] supporting the notion that PRORPs are capable of processing a wide variety of substrates.

In most bacteria, in contrast to eukaryotes, pre-tRNA^{His} and pre-tRNA^{Sec} are cleaved at a non-canonical cleavage site (N_{-1}:N_{73} site) by ribozyme RNase P due to additional base pairing that leads to formation of an 8 base pair long acceptor stem [56, 57]. *In vivo* and *in vitro* experiments showed that PRORP2 and 3 mostly cleave at the non-canonical site of these bacterial pre-tRNAs similarly to bacterial RNase P [24]. In contrast, PRORP1 cleaved most of these substrates at the canonical sites suggesting different a mechanism in cleavage site selection as compared to *A.thaliana* PRORP1 and 2 or the ribozyme RNase P [24].

In addition to tRNAs with non-canonical cleavage sites, cleavage of model hairpin substrates by PRORPs has also been evaluated. These studies found that unlike ribozyme RNase P, PRORPs process these hairpin substrates significantly slower than pre-tRNAs [58, 59].

Since the exact sequence of 5' and 3' end tRNA processing is not fully understood in many organisms, it is unknown if PRORPs process pre-tRNAs with or without a mature 3' end. Bacterial ribozyme RNase P favors substrates with mature 3'end with an added CCA sequence that promotes substrate recognition by the RNA catalyst [20]. However, the effects of the 3' CCA presence have been controversial for PRORPs. Gobert et al have found that addition to the 3' CCA to pre-tRNA^{Cys} from plant mitochondria prevented 5' end cleavage [60], while in other studies no significant effect was found when a model hairpin and bacterial pre-tRNA^{Gly} substrate were used [58, 59].

Taken together, ribozyme and protein only RNase Ps both have similar and wide range of substrate recognition. However, how paralog PRORPs from the same organism differ in substrate specificity is still largely unknown.

1.3.6 Substrate recognition by PRORPs

Despite the available crystal structures of PRORPs, the molecular details of how pre-tRNAs are recognized is still unknown. Besides PRORPs, PPR motif containing proteins are rich in plants (>400 PPR proteins in *A.thaliana*) and there are also eight PPR proteins found in human mitochondria [61-63]. In spite of the abundance of PPR proteins, there are only a few studies investigating the mode of substrate recognition by PPRs, and there is only a single crystal structure where a single stranded (ss) RNA was co-crystallized with a PPR-containing protein (PPR10 from maize) [59, 64].

A.thaliana PRORPs contain five PPR motifs in their substrate binding domains (PPR domain) [33]. Canonical PPR motifs are 35 amino acid long sequences that form two antiparallel α-helixes joined by a short coil and are associated with single stranded RNA binding [63, 65]. However, it is hard to predict how the pre-tRNA and the PPR motifs interact due to the highly degenerate nature of PPR motif amino acid sequences even among PRORPs [66-68]. Despite this unpredictability, several studies attempted to uncover the mode of substrate recognition by PRORPs.

In the first such study, Gobert et al. highlighted the importance of the D-and T-loops (forming the "elbow" region in the 3D structure of tRNAs) in PRORP1's substrate recognition [60]. In *A.thaliana* mitochondrial $tRNA^{Cys}$ residues G18, G19, C56 and G57 are found to play a potential role in interactions with PRORP1 based on tRNA mutational

analysis and footprinting studies [60]. Later, residues in PRORP1's and PRORP3's PPR domain that potentially played a role in substrate recognition were also evaluated [43, 58]. Mutation of the 6th residue in PRORP1's 2nd, 3rd and 4th PPR motif (N136, T180 and G215 respectively) resulted in reduction of the cleavage activity indicating the potential role of these residues in substrate recognition. This together with additional tRNA mutational analysis (mutagenesis of A58 and A59 in the pre-tRNA) yielded the first detailed model of PRORP-tRNA interaction ("Imai-model") [43]. However, this model and analysis has limitations. First, the "Imai-model" only shows interactions with the T-loop but fails to evaluate D-loop interactions between the tRNA and PRORP. Furthermore, the model is based on a crystal structure of pseudouridine synthase (a protein with no sequence homology to PRORPs) crystallized together with its tRNA substrate where the T-loop is turned inside out. However, there is no evidence for such rearrangements in pre-tRNA upon their binding to PRORPs. Contrary to these data, equivalent mutations in the tRNA substrate and in PRORP3 did not abolish PRORP3 catalytic activity. Nonetheless, certain combinations of pre-tRNA and single PPR domain mutations or double mutations in the PPR domain resulted in decreased PRORP3 activity confirming the importance of the 3rd PPR domain and the pre-tRNA T-loop for substrate recognition [58]. Mutagenesis studies in the PPR domain of PRORP2 also pointed out the involvement of the 2nd and 3rd PPR motif [69], and in combination with single anomalous X-ray scattering (SAXS) studies allowed Pinker et al. to propose a new PRORP-tRNA model ("Pinker-model") [70] (this work was published around the same time as my work relating to PRORP2 that is presented in Chapter 2; Paper 3). An

alternative, third PRORP1 substrate recognition model ("Chen-model") has been also proposed based on chemical modification of lysines conjoined with multiple reaction monitoring mass-spectrometry and a mutagenesis study of selected lysine residues at the tip of the metallonuclease and PPR domains [71]. This model differs from the above-mentioned models; it proposes that PRORP interacts with the pre-tRNA through lysine residues at the tip of the metallonuclease and PPR domain. However, this model also has significant limitations; (i) it assumes that most protein-RNA interactions are mediated through lysine residues and (ii) it doesn't take it into account that PRORP1 can adopt a different conformation to accommodate substrate binding through flexible hinges near the metallonuclease domain and the PPR domain.

Additionally, how the 5' end (leader) and 3'end (trailer) of the pre-tRNA substrate may potentially interact with PRORPs hasn't been thoroughly addressed. The RNase P ribozyme makes direct contacts with the 3' mature CCA end (discussed in section 1.3.5) and at least the first 4 bases in the 5' overhanging end of the pre-tRNA substrate [20, 72]. In contrast, variation of the length of the 3' end of the pre-tRNA did not affect activity of PRORP3 indicating no contact between the trailer sequence and the enzyme. Moreover, PRORP3 was able to process substrates with up to 2 nucleotide long 5' ends, suggesting that it only makes contact at most with the first couple of bases in the 5' leader pre-tRNA sequences [58].

1.4 ROLE OF MITOCHONDRIAL PRORP IN HUMAN HEALTH AND DISEASE

One out of every 4,000 children in the US is born with a mitochondrial disease, however the pathogenesis of most mitochondrial diseases is still not clearly understood. Moreover, there are no cures for mitochondrial diseases, and the available treatments are limited. The majority of mitochondrial disease-causing mutations are in (mt)tRNAs. A link between mitochondrial diseases and impaired tRNA maturation in the mitochondria is beginning to emerge [73, 74]. Because (mt)DNA is transcribed as a polycistron with tRNAs punctuating rRNA and coding regions [7], improper tRNA processing may influence maturation of other essential mRNAs and rRNAs [75, 76]. When tRNA maturation is disturbed, the amount of mature RNAs available for normal function is likely to be decreased, which can lead to mitochondrial dysfunction. Since mitochondria are the major source of energy of the cell, decrease in their function may contribute to the development of diseases.

Human mtRNase P is proposed to be the first processing enzyme acting on RNA transcripts in human mitochondria [31]. Highlighting its importance, this enzyme complex has been implicated in several mitochondrial diseases, such us maternally inherited essential hypertension [73], mitochondrial myopathy [77, 78], MELAS [79] and HSD10- disease [80, 81]. As an example, maternally inherited essential hypertension is linked to a 4263A>G mutation in mitochondrial $tRNA^{Ile}$ [73]. This mutation both reduces the efficiency of the human mitochondrial 5' tRNA processing enzyme MRPP3 *in vitro* and decreases mature mitochondrial $tRNA^{Ile}$ levels *in vivo*, suggesting that the perturbed processing of $tRNA^{Ile}$ is likely an underlying cause of this disease.

Recently, the essential function of MRPP3 was also pointed out; MRPP3 knockout mice were arrested in development in a very early stage [82]. In addition, it was shown that MRPP3 is also essential later in life, since conditional knockout of MRPP3 in the heart leads to rapid development of cardiomyopathy due to accumulation of mitochondrial RNAs in mice [82]. It is also likely that MRPP3 affects other functions in the mitochondria. In support of this a missense mutation in MRPP3 was identified as an important factor that causes differences in mitochondrial tRNA methylation pattern amongst individuals [83]. Furthermore, it is also demonstrated that MRPP3 plays an important role in the unfolded protein response in *C.elegans* [84].

1.5 SIGNIFICANCE

Although PRORPs were discovered nearly a decade ago, many questions remain to be answered on their working mechanism, structure and *in vivo* function. Investigation of PRORPs is of particular interest since comparison of those to the ribozyme RNase P can give us an insight into how different enzymes of distinct composition can catalyze the same reaction. Human mitochondrial MRPP3 is also implicated as a key player in human health and disease. Investigation of this enzyme can potentially provide us further understanding of the development of diseases and mitochondrial function.

1.5.1 Single unit PRORPs

Since single unit PRORPs catalyze the 5’ end pre-tRNA cleavage without any known interaction partners, they provide an excellent model to study PRORP function

and structure. Additionally, land plants, such as *A.thaliana* contain three paralog PRORP enzymes that offer the opportunity to compare different PRORPs from the same organism. Investigation of similar enzymes can lead to more detailed understanding of enzyme function. Most studies so far were focused on *A.thaliana* PRORP1. Unlike PRORP1, little is known about *A.thaliana* nuclear PRORPs, in particular PRORP2. Therefore, in the first half of my dissertation research I was focusing on the mechanism, structure and function of PRORP2.

In the beginning of my thesis research, there was only one PRORP structure available (PRORP1) and only very limited biochemical analysis indicating a general hiatus in understanding the structure and function of PRORPs. In detail, the following questions were unanswered: (i) what is the physiological metal for PRORP2 (ii) if there are any differences in PRORP2's structure compared to that of PRORP1 (iii) how PRORP2 interacts with the 5' leader and 3' trailer of pre-tRNAs (iv) if there are any differences in substrate specificity between *A.thaliana* PRORP paralogs and (v) what is the difference between the kinetic mechanism of PRORPs and RNase Ps?

Furthermore, despite the availability of a PRORP1 crystal structure, it is not obvious how PRORPs interact with their pre-tRNA substrate. PPR proteins, including PRORPs, are abundant in plants in mammalian mitochondria [63]. Since little is known about how PPR motifs are making contacts with their RNA substrate, understanding PRORP substrate binding could contribute to elucidation of the general RNA binding mechanism of these motifs.

Additionally, there are no known inhibitors of PRORPs. Specific inhibitors can be helpful in further studying the *in vitro* function and *in vivo* role of enzymes. Therefore, it

is important to find potential inhibitors and then evaluate the mode of inhibition in functional and structural studies.

1.5.2 Multi-subunit PRORPs

After investigating single unit PRORPs, the next logical step is to apply the acquired knowledge to study metazoan mitochondrial MRPP3 (complex forming PRORP homologues) that form the mtRNase P complex. It is still largely unknown how metazoan mtRNaseP interacts, methylates and processes mitochondrial pre-tRNAs. Moreover, the interplay between the different components and functions of mtRNase P has not been explored and is poorly understood.

Characterization of human mitochondrial MRPP3 is also an important step for understanding the link between tRNA processing and mitochondrial diseases. It has been shown that abnormal 5'-end tRNA processing of mutant precursor tRNAs can influence mitochondrial function [73]. This begs the question whether more mitochondrial diseases arise from improper 5' tRNA processing by human PRORP. Therefore, there is a need to further establish the connections between mitochondrial tRNA 5'-end processing and mitochondrial diseases. Since it is challenging to investigate the effects of tRNA mutations in the mitochondria *in vivo* (limited to mutant cell lines derived from patients) the first step could be to evaluate the effects of tRNAs carrying pathogenic mutations by *in vitro* methods.

REFERENCES

1. Phizicky, E.M. and A.K. Hopper, *tRNA biology charges to the front.* Genes Dev, 2010. **24**(17): p. 1832-60.
2. Maraia, R.J. and T.N. Lamichhane, *3′ processing of eukaryotic precursor tRNAs.* Wiley Interdiscip Rev RNA, 2011. **2**(3): p. 362-75.
3. Betat, H., C. Rammelt, and M. Morl, *tRNA nucleotidyltransferases: ancient catalysts with an unusual mechanism of polymerization.* Cell Mol Life Sci, 2010. **67**(9): p. 1447-63.
4. Xiong, Y. and T.A. Steitz, *A story with a good ending: tRNA 3'-end maturation by CCA-adding enzymes.* Curr Opin Struct Biol, 2006. **16**(1): p. 12-7.
5. Lorenz, C., C.E. Lunse, and M. Morl, *tRNA Modifications: Impact on Structure and Thermal Adaptation.* Biomolecules, 2017. **7**(2).
6. Stewart, J.B. and A.T. Beckenbach, *Characterization of mature mitochondrial transcripts in Drosophila, and the implications for the tRNA punctuation model in arthropods.* Gene, 2009. **445**(1-2): p. 49-57.
7. Ojala, D., J. Montoya, and G. Attardi, *tRNA punctuation model of RNA processing in human mitochondria.* Nature, 1981. **290**(5806): p. 470-4.
8. Chujo, T., et al., *LRPPRC/SLIRP suppresses PNPase-mediated mRNA decay and promotes polyadenylation in human mitochondria.* Nucleic Acids Res, 2012. **40**(16): p. 8033-47.
9. Helm, M., et al., *Search for characteristic structural features of mammalian mitochondrial tRNAs.* Rna, 2000. **6**(10): p. 1356-79.
10. Suzuki, T., A. Nagao, and T. Suzuki, *Human mitochondrial tRNAs: biogenesis, function, structural aspects, and diseases.* Annu Rev Genet, 2011. **45**: p. 299-329.
11. Messmer, M., et al., *Tertiary network in mammalian mitochondrial tRNAAsp revealed by solution probing and phylogeny.* Nucleic Acids Res, 2009. **37**(20): p. 6881-95.
12. Helm, M., et al., *The presence of modified nucleotides is required for cloverleaf folding of a human mitochondrial tRNA.* Nucleic Acids Res, 1998. **26**(7): p. 1636-43.
13. Shi, H. and P.B. Moore, *The crystal structure of yeast phenylalanine tRNA at 1.93 A resolution: a classic structure revisited.* Rna, 2000. **6**(8): p. 1091-105.
14. Mustoe, A.M., et al., *Noncanonical secondary structure stabilizes mitochondrial tRNA(Ser(UCN)) by reducing the entropic cost of tertiary folding.* J Am Chem Soc, 2015. **137**(10): p. 3592-9.
15. Altman, S., *Ribonuclease P.* Philos Trans R Soc Lond B Biol Sci, 2011. **366**(1580): p. 2936-41.
16. Kazantsev, A.V. and N.R. Pace, *Bacterial RNase P: a new view of an ancient enzyme.* Nat Rev Microbiol, 2006. **4**(10): p. 729-40.
17. Howard, M.J., et al., *RNase P enzymes: divergent scaffolds for a conserved biological reaction.* RNA Biol, 2013. **10**(6): p. 909-14.
18. Guerrier-Takada, C., et al., *The RNA moiety of ribonuclease P is the catalytic subunit of the enzyme.* Cell, 1983. **35**(3 Pt 2): p. 849-57.

19. Kikovska, E., S.G. Svard, and L.A. Kirsebom, *Eukaryotic RNase P RNA mediates cleavage in the absence of protein.* Proc Natl Acad Sci U S A, 2007. **104**(7): p. 2062-7.
20. Reiter, N.J., et al., *Structure of a bacterial ribonuclease P holoenzyme in complex with tRNA.* Nature, 2010. **468**(7325): p. 784-9.
21. Holzmann, J., et al., *RNase P without RNA: identification and functional reconstitution of the human mitochondrial tRNA processing enzyme.* Cell, 2008. **135**(3): p. 462-74.
22. Taschner, A., et al., *Nuclear RNase P of Trypanosoma brucei: a single protein in place of the multicomponent RNA-protein complex.* Cell Rep, 2012. **2**(1): p. 19-25.
23. Gobert, A., et al., *A single Arabidopsis organellar protein has RNase P activity.* Nat Struct Mol Biol, 2010. **17**(6): p. 740-4.
24. Gossringer, M., et al., *Protein-only RNase P function in Escherichia coli: viability, processing defects and differences between PRORP isoenzymes.* Nucleic Acids Res, 2017. **45**(12): p. 7441-7454.
25. Weber, C., et al., *Playing RNase P evolution: swapping the RNA catalyst for a protein reveals functional uniformity of highly divergent enzyme forms.* PLoS Genet, 2014. **10**(8): p. e1004506.
26. Gutmann, B., A. Gobert, and P. Giege, *PRORP proteins support RNase P activity in both organelles and the nucleus in Arabidopsis.* Genes Dev, 2012. **26**(10): p. 1022-7.
27. Bonnard, G., et al., *Transfer RNA maturation in Chlamydomonas mitochondria, chloroplast and the nucleus by a single RNase P protein.* Plant J, 2016. **87**(3): p. 270-80.
28. Sugita, C., et al., *Molecular Characterization of Three PRORP Proteins in the Moss Physcomitrella patens: Nuclear PRORP Protein Is Not Essential for Moss Viability.* PLoS One, 2014. **9**(10): p. e108962.
29. Rossmanith, W., *Of P and Z: mitochondrial tRNA processing enzymes.* Biochim Biophys Acta, 2012. **1819**(9-10): p. 1017-26.
30. Nickel, A.I., et al., *Minimal and RNA-free RNase P in Aquifex aeolicus.* Proc Natl Acad Sci U S A, 2017. **114**(42): p. 11121-11126.
31. Sanchez, M.I., et al., *RNA processing in human mitochondria.* Cell Cycle, 2011. **10**(17): p. 2904-16.
32. Vilardo, E., et al., *A subcomplex of human mitochondrial RNase P is a bifunctional methyltransferase--extensive moonlighting in mitochondrial tRNA biogenesis.* Nucleic Acids Res, 2012. **40**(22): p. 11583-93.
33. Howard, M.J., et al., *Mitochondrial ribonuclease P structure provides insight into the evolution of catalytic strategies for precursor-tRNA 5′ processing.* Proc Natl Acad Sci U S A, 2012. **109**(40): p. 16149-54.
34. Reinhard, L., S. Sridhara, and B.M. Hallberg, *Structure of the nuclease subunit of human mitochondrial RNase P.* Nucleic Acids Res, 2015. **43**(11): p. 5664-72.
35. Li, F., et al., *Auto-inhibitory Mechanism of the Human Mitochondrial RNase P Protein Complex.* Sci Rep, 2015. **5**: p. 9878.

36. Kissinger, C.R., et al., *Crystal structure of human ABAD/HSD10 with a bound inhibitor: implications for design of Alzheimer's disease therapeutics.* J Mol Biol, 2004. **342**(3): p. 943-52.
37. Shi, H. and P.B. Moore, *The crystal structure of yeast phenylalanine tRNA at 1.93 A resolution: a classic structure revisited.* Rna, 2000. **6**(8): p. 1091-105.
38. Lechner, M., et al., *Distribution of Ribonucleoprotein and Protein-Only RNase P in Eukarya.* Mol Biol Evol, 2015. **32**(12): p. 3186-93.
39. Zhou, W., et al., *Multiple RNA processing defects and impaired chloroplast function in plants deficient in the organellar protein-only RNase P enzyme.* PLoS One, 2015. **10**(3): p. e0120533.
40. Pavlova, L.V., et al., *tRNA processing by protein-only versus RNA-based RNase P: kinetic analysis reveals mechanistic differences.* Chembiochem, 2012. **13**(15): p. 2270-6.
41. Falk, M.J., et al., *A novel HSD17B10 mutation impairing the activities of the mitochondrial RNase P complex causes X-linked intractable epilepsy and neurodevelopmental regression.* RNA Biol, 2016. **13**(5): p. 477-85.
42. Vilardo, E. and W. Rossmanith, *Molecular insights into HSD10 disease: impact of SDR5C1 mutations on the human mitochondrial RNase P complex.* Nucleic Acids Res, 2015. **43**(13): p. 6649.
43. Imai, T., et al., *Pentatricopeptide repeat motifs in the processing enzyme PRORP1 in Arabidopsis thaliana play a crucial role in recognition of nucleotide bases at TpsiC loop in precursor tRNAs.* Biochem Biophys Res Commun, 2014. **450**(4): p. 1541-6.
44. Howard, M.J., B.P. Klemm, and C.A. Fierke, *Mechanistic Studies Reveal Similar Catalytic Strategies for Phosphodiester Bond Hydrolysis by Protein-only and RNA-dependent Ribonuclease P.* J Biol Chem, 2015.
45. Hsieh, J. and C.A. Fierke, *Conformational change in the Bacillus subtilis RNase P holoenzyme--pre-tRNA complex enhances substrate affinity and limits cleavage rate.* RNA, 2009. **15**(8): p. 1565-77.
46. Beebe, J.A. and C.A. Fierke, *A kinetic mechanism for cleavage of precursor tRNA(Asp) catalyzed by the RNA component of Bacillus subtilis ribonuclease P.* Biochemistry, 1994. **33**(34): p. 10294-304.
47. Howard, M.J., et al., *Differential substrate recognition by isozymes of plant protein-only Ribonuclease P.* Rna, 2016. **22**(5): p. 782-92.
48. Walczyk, D., et al., *Analysis of the Cleavage Mechanism by Protein-Only RNase P Using Precursor tRNA Substrates with Modifications at the Cleavage Site.* J Mol Biol, 2016. **428**(24 Pt B): p. 4917-4928.
49. Zahler, N.H., et al., *The pre-tRNA nucleotide base and 2'-hydroxyl at N(-1) contribute to fidelity in tRNA processing by RNase P.* J Mol Biol, 2005. **345**(5): p. 969-85.
50. Beebe, J.A., J.C. Kurz, and C.A. Fierke, *Magnesium ions are required by Bacillus subtilis ribonuclease P RNA for both binding and cleaving precursor tRNAAsp.* Biochemistry, 1996. **35**(32): p. 10493-505.
51. Coughlin, D.J., et al., *Genome-wide search for yeast RNase P substrates reveals role in maturation of intron-encoded box C/D small nucleolar RNAs.* Proc Natl Acad Sci U S A, 2008. **105**(34): p. 12218-23.

52. Mans, R.M., et al., *Interaction of RNase P from Escherichia coli with pseudoknotted structures in viral RNAs.* Nucleic Acids Res, 1990. **18**(12): p. 3479-87.
53. Alifano, P., et al., *Ribonuclease E provides substrates for ribonuclease P-dependent processing of a polycistronic mRNA.* Genes Dev, 1994. **8**(24): p. 3021-31.
54. Komine, Y., et al., *A tRNA-like structure is present in 10Sa RNA, a small stable RNA from Escherichia coli.* Proc Natl Acad Sci U S A, 1994. **91**(20): p. 9223-7.
55. Forner, J., et al., *Mapping of mitochondrial mRNA termini in Arabidopsis thaliana: t-elements contribute to 5' and 3' end formation.* Nucleic Acids Res, 2007. **35**(11): p. 3676-92.
56. Burkard, U. and D. Soll, *The unusually long amino acid acceptor stem of Escherichia coli selenocysteine tRNA results from abnormal cleavage by RNase P.* Nucleic Acids Res, 1988. **16**(24): p. 11617-24.
57. Brannvall, M., B.M. Fredrik Pettersson, and L.A. Kirsebom, *The residue immediately upstream of the RNase P cleavage site is a positive determinant.* Biochimie, 2002. **84**(8): p. 693-703.
58. Brillante, N., et al., *Substrate recognition and cleavage-site selection by a single-subunit protein-only RNase P.* Nucleic Acids Res, 2016. **44**(5): p. 2323-36.
59. Mao, G., et al., *Cleavage of Model Substrates by Arabidopsis thaliana PRORP1 Reveals New Insights into Its Substrate Requirements.* PLoS One, 2016. **11**(8): p. e0160246.
60. Gobert, A., et al., *Structural insights into protein-only RNase P complexed with tRNA.* Nat Commun, 2013. **4**: p. 1353.
61. Barkan, A. and I. Small, *Pentatricopeptide repeat proteins in plants.* Annu Rev Plant Biol, 2014. **65**: p. 415-42.
62. Pinker, F., et al., *PPR proteins shed a new light on RNase P biology.* RNA Biology, 2013. **10**(9): p. 1274-1285.
63. Rackham, O. and A. Filipovska, *The role of mammalian PPR domain proteins in the regulation of mitochondrial gene expression.* Biochim Biophys Acta, 2012. **1819**(9-10): p. 1008-16.
64. Yin, P., et al., *Structural basis for the modular recognition of single-stranded RNA by PPR proteins.* Nature, 2013. **504**(7478): p. 168-71.
65. Saha, D., A.M. Prasad, and R. Srinivasan, *Pentatricopeptide repeat proteins and their emerging roles in plants.* Plant Physiol Biochem, 2007. **45**(8): p. 521-34.
66. Kobayashi, K., et al., *Identification and characterization of the RNA binding surface of the pentatricopeptide repeat protein.* Nucleic Acids Res, 2012. **40**(6): p. 2712-23.
67. Barkan, A., et al., *A combinatorial amino acid code for RNA recognition by pentatricopeptide repeat proteins.* PLoS Genet, 2012. **8**(8): p. e1002910.
68. Small, I.D. and N. Peeters, *The PPR motif - a TPR-related motif prevalent in plant organellar proteins.* Trends Biochem Sci, 2000. **25**(2): p. 46-7.
69. Pinker, F., et al., *Biophysical analysis of Arabidopsis protein-only RNase P alone and in complex with tRNA provides a refined model of tRNA binding.* J Biol Chem, 2017.

70. Pinker, F., et al., *Biophysical analysis of Arabidopsis protein-only RNase P alone and in complex with tRNA provides a refined model of tRNA binding.* J Biol Chem, 2017. **292**(34): p. 13904-13913.
71. Chen, T.H., et al., *Use of chemical modification and mass spectrometry to identify substrate-contacting sites in proteinaceous RNase P, a tRNA processing enzyme.* Nucleic Acids Res, 2016. **44**(11): p. 5344-55.
72. Koutmou, K.S., et al., *Protein-precursor tRNA contact leads to sequence-specific recognition of 5' leaders by bacterial ribonuclease P.* J Mol Biol, 2010. **396**(1): p. 195-208.
73. Wang, S., et al., *Maternally inherited essential hypertension is associated with the novel 4263A>G mutation in the mitochondrial tRNAIle gene in a large Han Chinese family.* Circ Res, 2011. **108**(7): p. 862-70.
74. Chatfield, K.C., et al., *Mitochondrial energy failure in HSD10 disease is due to defective mtDNA transcript processing.* Mitochondrion, 2015.
75. Wittenhagen, L.M. and S.O. Kelley, *Impact of disease-related mitochondrial mutations on tRNA structure and function.* Trends Biochem Sci, 2003. **28**(11): p. 605-11.
76. Levinger, L., M. Morl, and C. Florentz, *Mitochondrial tRNA 3' end metabolism and human disease.* Nucleic Acids Res, 2004. **32**(18): p. 5430-41.
77. Bindoff, L.A., et al., *Abnormal RNA processing associated with a novel tRNA mutation in mitochondrial DNA. A potential disease mechanism.* J Biol Chem, 1993. **268**(26): p. 19559-64.
78. Rossmanith, W. and R.M. Karwan, *Impairment of tRNA processing by point mutations in mitochondrial tRNA(Leu)(UUR) associated with mitochondrial diseases.* FEBS Lett, 1998. **433**(3): p. 269-74.
79. Li, R. and M.X. Guan, *Human mitochondrial leucyl-tRNA synthetase corrects mitochondrial dysfunctions due to the tRNALeu(UUR) A3243G mutation, associated with mitochondrial encephalomyopathy, lactic acidosis, and stroke-like symptoms and diabetes.* Mol Cell Biol, 2010. **30**(9): p. 2147-54.
80. Deutschmann, A.J., et al., *Mutation or knock-down of 17beta-hydroxysteroid dehydrogenase type 10 cause loss of MRPP1 and impaired processing of mitochondrial heavy strand transcripts.* Hum Mol Genet, 2014.
81. Chatfield, K.C., et al., *Mitochondrial energy failure in HSD10 disease is due to defective mtDNA transcript processing.* Mitochondrion, 2015.
82. Rackham, O., et al., *Hierarchical RNA Processing Is Required for Mitochondrial Ribosome Assembly.* Cell Rep, 2016. **16**(7): p. 1874-90.
83. Hodgkinson, A., et al., *High-resolution genomic analysis of human mitochondrial RNA sequence variation.* Science, 2014. **344**(6182): p. 413-5.
84. Munch, C. and J.W. Harper, *Mitochondrial unfolded protein response controls matrix pre-RNA processing and translation.* Nature, 2016. **534**(7609): p. 710-3.

CHAPTER 2: Structure, substrate specificity and binding of *A.thaliana* PRORPs

PAPER1: NUCLEAR PROTEIN-ONLY RIBONUCLEASE P 2 STRUCTURE AND BIOCHEMICAL CHARACTERIZATION PROVIDE INSIGHT INTO THE CONSERVED PROPERTIES OF TRNA 5'-END PROCESSING ENZYMES

Agnes Karasik[1], Aranganathan Shanmuganathan[1], Michael J. Howard[2], Carol A. Fierke[2,3], Markos Koutmos[1,*]

[1]4301 Jones Bridge Road, Department of Biochemistry, Uniformed Services University of the Health Sciences, Bethesda, MD, 28104, USA;

[2]Department of Biological Chemistry, University of Michigan, Ann Arbor, MI, 48109, USA

[3]Department of Chemistry, University of Michigan, Ann Arbor, MI, 48109, USA

* To whom correspondence should be addressed. Tel: [+1 301 295 9419]; Fax: [+1 301 295 3512]; Email: [markos.koutmos@usuhs.edu].

Keywords: pre-tRNA, RNase P, RNA processing, metal dependence, t-element

Author contributions: A.K. cloned PRORP2 gene, designed and executed all kinetic and mutagenesis experiments and analyzed structure of PRORP2. A.S. optimized expression, crystallized PRORP2 and performed AUC experiments. M.H. performed experiments on PRORP1. M.K. solved the crystal structure. A.K., C.A.F. and M.K. wrote and edited the manuscript. A.K. generated all figures and contributed data to Figure 1, Figure 2, Figure 3, Figure 4, Figure 5 and Table 1 and 3.

Abstract

Protein-only RNase Ps (PRORPs) are a recently discovered class of RNA processing enzymes that catalyze maturation of the 5' end of precursor tRNAs (pre-tRNAs) in Eukaryotes. PRORPs are found in the nucleus and/or organelles of most eukaryotic organisms. *Arabidopsis thaliana* is a representative organism that contains PRORP enzymes (PRORP1, PRORP2, PRORP3) in both its nucleus and organelles; PRORP2 and 3 localize to the nucleus, PRORP1 to the chloroplast and the mitochondria. Apart from their identification, almost nothing is known about the structure and function of PRORPs that act in the nucleus. Here we use a combination of biochemical assays and X-ray crystallography to characterize *A. thaliana* PRORP2. We solved the crystal structure of PRORP2 (3.2 Å) revealing an overall V-shaped protein and conserved metallonuclease active site structure. Our biochemical studies indicate that PRORP2 requires Mg^{2+} for catalysis and catalyzes the maturation of nuclear encoded substrates up to 10-fold faster than mitochondrial encoded precursor nad6 t-element under single turnover conditions. We also demonstrate that PRORP2 preferentially binds pre-tRNAs containing short 5' leaders and 3' trailers; however, leader and trailer length do not significantly alter the observed rate constants of PRORP2 in single turnover cleavage assays. Our data provide a biochemical and structural framework to begin understanding how nuclear localized PRORPs recognize and cleave their substrates.

Introduction

RNase P catalyzes the removal of 5' leader sequences from precursor tRNAs (pre-tRNAs) and is found in all three kingdoms of life. The canonical form of RNase P is a ribozyme associated with one to ten proteins depending on the organism [1, 2]. However, a second form of the enzyme, called protein only RNase P (PRORP), comprised solely of protein and lacking an RNA component has been discovered in Eukaryotes [3-5]. It is noteworthy that none of the known protein components of the "ribozyme-based" RNase P have any homology to PRORPs[6]. Beyond the bioinformatic identification of PRORPs in a wide variety of organisms [3, 7, 8] little is known about how they recognize substrates. PRORPs can act either as single protein enzymes or as the catalytic subunit of multi-protein RNase Ps. Metazoans typically possess both RNA and protein based RNase Ps; retaining the traditional RNase P ribozyme in their nuclei, and using a PRORP transiently associated with MRPP1 and 2 (Mitochondrial RNase P Protein 1 and 2) in their mitochondria [4]. In contrast, land plants, exemplified by *A. thaliana* [3, 9], and other unicellular Eukaryotic organisms, such as *Trypanosoma bruceii* [5], appear to lack any RNA-based RNase P and instead utilize single protein versions of PRORP to catalyze the 5' end cleavage of pre-tRNAs in both their nucleus and organelles. The single protein enzymes are related to the catalytic PRORP subunit of the multi-protein RNase Ps found in metazoan mitochondria and provide the simplest system for understanding how this new class of RNA processing enzymes function.

A. thaliana contains three differentially localized PRORPs (PRORP1, PRORP2, PRORP3) that share a high level of protein sequence identity (48-80%). PRORP1 is found in the mitochondria and the chloroplast, and PRORP2 and PRORP3 are present in the nucleus [9]. Thus far, PRORP1 is the best-characterized PRORP from any organism and the only PRORP for which there is a crystal structure where all of its domains are intact [8, 10, 11]. A recent study evaluating the *in vitro* pH profile and metal dependence of PRORP1 cleavage

activity proposed that, like the "ribozyme-based" RNase P, PRORP1 uses a metal-bound water nucleophile to cleave pre-tRNA substrates [12]. The precise molecular recognition strategies used by PRORPs remain largely unknown. The crystal structure of PRORP1 revealed three distinct domains forming an overall V-shaped molecule (pentatricopeptide repeat (PPR) domain, central domain and metallonuclease domain) [8]. The PPR domain, consisting of five PPR motifs, is one of the putative binding sites for pre-tRNA. Canonical PPR motifs are ~35 amino acid long sequences that form two antiparallel α-helices joined by a short loop known to be involved in RNA binding [13]. Truncation of the four PRORP1 N-terminal PPR motifs reduces the ability of the enzyme to bind and cleave pre-tRNAs [8]. The Nedd4-BP1, YacP nuclease (NYN) domain (metallonuclease domain) houses the active site that catalyzes 5' pre-tRNA cleavage. The functional importance of this domain has been validated in mutagenesis studies where mutations of conserved aspartates to alanines resulted in catalytically inactive PRORP1 [8, 14]. The central domain holds the PPR and the metallonuclease domain together in such a way that the two functionally relevant domains face towards each other. The central domain also harbors a structurally important zinc-binding site. Several studies have shown that recombinant PRORP1 is able to bind and cleave pre-tRNAs derived from *A. thaliana* and *E. coli* [3, 8, 9, 15]. Meanwhile, little is known about the nuclear localized PRORPs found in *A. thaliana* or other organisms. Recently, it was shown that *A. thaliana* PRORP2 and PRORP3 can catalyze the maturation of the 5' ends of two nuclear pre-tRNA substrates *in vivo*, confirming their predicted roles as RNase Ps in the nucleus [9]. However, there are no structural and limited mechanistic data available for nuclear localized PRORPs.

While the investigations of PRORP1 provide an important first step towards understanding how PRORPs work [8, 12, 15, 16] the study of a single enzyme cannot reveal how PRORPs generally function; comparison of the structure and function of multiple

proteins is necessary to understand any given class of enzymes. Here, we present the first x-ray structure and biochemical characterization of a nuclear localized PRORP, *A. thaliana* PRORP2. Our crystal structure of PRORP2 (3.2 Å) provides the only structural information available on any nuclear localized PRORP and reveals an overall structure that, while similar to the mitochondria and chloroplast localized PRORP1, exhibits a more open conformation. Thermodynamic binding studies provide insight into the differences between proteinaceous and ribozyme RNase Ps in recognition of the 5' and 3' end of pre-tRNAs. Furthermore, our work demonstrates that PRORP2 exhibits a modest preference against catalyzing maturation of the mitochondrial encoded nad6 t-element, suggesting that there are subtle but important distinctions in how differentially localized PRORPs recognize and process a sub-set of substrates. The data presented here provide a basis for understanding how nuclear localized PRORPs function, and allow us to begin understanding how PRORPs act as a new class of RNA processing proteins to bind and cleave their substrates.

Results

PRORP2 uses Mg^{2+} as a catalytic co-factor

Given that the only mechanistic information available on PRORPs comes from studies of PRORP1 [12, 15] little is known about how the nuclear localized PRORPs recognize and mature their substrates. Here, we begin by assessing how PRORP2 catalyzes pre-tRNA cleavage using single turnover kinetic assays. In these assays, we measure the rate constants (k_{obs}) for single turnover reactions with limiting substrate (nuclear pre-$tRNA^{Gly}$, < 100 nM) and saturating enzyme concentrations (5 μM) (Figure 1A, 1B). These conditions were selected because the k_{obs} values are independent of PRORP2 concentration (Figure 1B).

The k_{obs} values report on steps in the mechanism that occur after substrate binding and before, and including, pre-tRNA cleavage (Scheme 1).

Since all PRORPs contain a conserved metallonuclease domain we first asked if PRORP2, like PRORP1, uses a divalent metal ion as its catalytic co-factor. We measured the single-turnover rate constants for PRORP2 cleaving a nuclear pre-tRNA^{Gly} with an 8 nucleotide long 5' leader and a 1 nucleotide long 3' trailer ((nu)pre-tRNA$^{Gly\ 8:1}$) (Figure 1A) in the presence of four distinct divalent metal ions commonly found in metallonuclease active sites (Mg^{2+}, Mn^{2+}, Ca^{2+}, Zn^{2+})[8, 17-19]. PRORP2 is active in the presence of Mg^{2+} and Mn^{2+} but not Ca^{2+} or Zn^{2+} (Figure 1C, 1D, Supplemental Figure 1) similar to PRORP1 [8]. Given that PRORP2 cleaves substrates with comparable single turnover rate constants in the presence of Mg^{2+} and Mn^{2+} ($k_{obs,\ Mg2+}$= 1.4 ± 0.1 min^{-1}, $k_{obs,\ Mn2+}$= 0.8 ± 0.1 min^{-1}, Figure 1D) and Mg^{2+} is at least 5-fold more abundant in the cell [20] our data suggest that Mg^{2+} is the likely catalytic metal ion *in vivo*.

PRORP2 preferentially binds pre-tRNA substrates with short 5' leader and 3' trailer sequences

The traditional ribozyme form of RNase P has a strong preference for binding and cleaving pre-tRNAs with particular 5' leader and 3' trailer lengths [21, 22]. However, it is unknown if the length of the 5' leader and 3' trailer are also important determinants of PRORPs binding pre-tRNAs. To investigate this question we measured the dissociation constants (K_D) for PRORP2 binding 5' fluorescently labeled nuclear pre-tRNA^{Gly} substrates with varying 5' leader and 3' trailer lengths ((nu)pre-tRNA$^{Gly\ 23:1}$, (nu)pre-tRNA$^{Gly\ 13:1}$, (nu)pre-tRNA$^{Gly\ 8:1}$, (nu)pre-tRNA$^{Gly\ 23:10}$, (nu)pre-tRNA$^{Gly\ 23:5}$, (nu)pre-tRNA$^{Gly\ 23:1}$)

(Table 1). K_D values were determined using a previously described fluorescence polarization assay developed for PRORP1 in which the concentration of 5' "fluorescein-labeled" substrates is held constant (20 nM) and the enzyme is titrated (0-1000 nM) [8]. Since PRORP2 is incapable of cleaving pre-tRNA in the presence of Ca^{2+} (Figure 1C, 1D) and previous studies demonstrated that PRORP1 binds pre-tRNAs in the presence of Ca^{2+} [8], our K_D values were measured in the presence of Ca^{2+} instead of Mg^{2+}.

We found that PRORP2 preferentially binds substrates with short 3' trailers. The affinity of PRORP2 for a (nu)pre-tRNA^{Gly} substrate containing a 23 nucleotide long 5' leader is enhanced by 7-fold when the 3' trailer length is shortened from 10 to 1 nucleotide (Figure 2A, Table 1). Additionally, PRORP2 prefers to bind substrates with shorter (< 23 nucleotide) 5' leaders. When the 5' leader length of (nu)pre-tRNA^{Gly} substrate with a 1 nucleotide 3' trailer is reduced from 23 to 8 nucleotides, the K_D decreases by 5-fold (Figure 2A, Table 1). Thus, PRORP2 has higher affinity for substrates with short 3' trailer and 5' leader.

We also measured the k_{obs} values in single turnover assays for nuclear pre-tRNA^{Gly} substrates with varied 5' leader and 3' trailer lengths ((nu)pre-tRNA$^{Gly\ 23:1}$, (nu)pre-tRNA$^{Gly\ 13:1}$, (nu)pre-tRNA$^{Gly\ 8:1}$, (nu)pre-tRNA$^{Gly\ 23:10}$, (nu)pre-tRNA$^{Gly\ 23:5}$, (nu)pre-tRNA$^{Gly\ 23:1}$). The k_{obs} values are comparable for all five of these substrates (k_{obs} = 0.7-1 min $^{-1}$) (Figure 2B, Table 1) suggesting that the leader and trailer lengths do not affect stabilization of the transition state. Additionally, we measured the k_{obs} values for PRORP1 cleaving the (nu)pre-tRNA$^{Gly\ 23:1}$ and (nu)pre-tRNA$^{Gly\ 8:1}$ substrates (k_{obs} = 1.2 ± 0.06

min^{-1} and 1.2 ± 0.1 min^{-1}, respectively); PRORP1 and PRORP2 cleave both substrates with comparable rate constants.

PRORP2 inefficiently cleaves mitochondrial encoded nad6 t-element

Next, we assessed if PRORP2 can recognize and cleave substrates encoded in the mitochondria using single turnover kinetic assays. For this purpose, we measured the k_{obs} values for PRORP1 and PRORP2 cleaving the mitochondria specific nad6 t-element possessing a 14 nucleotide long 5' leader and 6 nucleotide long 3' trailer sequence ((mt) pre-nad6 t-element$^{14:6}$, Figure 3A); PRORP1 was previously shown to efficiently cleave this substrate [3]. T-elements are encoded near, and in the same transcriptional orientation as, the 5' or 3' ends of many mRNAs and rRNAs in the mitochondrial DNA of plants [23]. These elements assume tRNA-like secondary structures and have been proposed to act as signals for endonucleic cleavage catalyzed by PRORPs [3]. The (mt) pre-nad6 t-element$^{14:6}$ is proposed to fold into a structure much like a tRNA, however it differs significantly from a canonical pre-tRNA substrate because it lacks an anti-codon stem loop (Figure 3A). PRORP1 cleaves the (mt) pre-nad6 t-element$^{14:6}$ with rate constants similar to other substrates (k_{obs}= 1.5 ± 0.2 min^{-1}) [8, 12] in contrast to PRORP2, which exhibited a ~10-fold slower single-turnover rate constant (k_{obs}= 0.13 ± 0.02 min^{-1}, Figure 3B). Furthermore, PRORP2 binds the precursor nad6 t-element significantly less tightly (K_D= 615 ± 100) than the nuclear encoded precursor tRNA^{Gly} substrates. This suggests that differentially localized *A. thaliana* PRORPs exhibit some specificity for binding and cleaving a subset of non-canonical substrates.

PRORP1 and PRORP2 share overall structural characteristics

The existence of three different PRORPs in *A. thaliana* that localize to distinct cellular compartments provides a unique opportunity to investigate general PRORP characteristics by comparing their structural differences and similarities. We solved a 3.2 Å crystal structure of full-length nuclear PRORP2 (Figure 4A, PDB ID 5DIZ) by molecular replacement based on our previously determined 1.98 Å structure of the mitochondrial and chloroplast Δ76 PRORP1 [8] (Figure 4B, PDB ID 4G23, Table 2). In PRORP1, where the N-terminal region is longer than that of PRORP2 (Supplemental Figure 3) due to the presence of an organellar localization sequence, electron density is visible from the 95th residue. This density corresponds to the beginning of the first helix of the PPR domain. Similarly, in PRORP2 electron density is seen from the 28th residue in the beginning of the PPR domain. Since we could map neither the first 28 residues of PRORP2 nor the residues between the localization signal and the 94th residue in PRORP1, we predict that these regions may be structurally disordered. It was previously suggested that this region might be functionally important based on reduced activity of truncated versions of PRORP1 [14]. To test if this region is indeed important for the catalytic activity of PRORP2, we measured the single-turnover rate constants for PRORP2 containing truncations at the N- tand C-termini (residues 21-515). This mutant PRORP2 correlates well with Δ76 PRORP1 in sequence length since it starts at approximately the same residue and lacks the C-terminal extension of PRORP2 (Supplemental Figure 2.). We find that truncated 21-515 PRORP2 cleaves the (nu)pre-tRNA$^{Gly\ 8:1}$ substrate (data not shown) with a single-turnover rate constant similar to that of wild type full-length PRORP2. This suggests that the truncated residues (including the N-terminal disordered region and the PRORP2 specific extension) are not important for the substrate binding and/or cleavage *in vitro* (Scheme 1).

PRORP2 shares the overall V-shaped structure of PRORP1 but has an "open" conformation relative to PRORP1 (Figure 4C). Analysis of PRORP1 and PRORP2 structures by the DynDom protein motion server [24, 25] predicts that both proteins form three rigid bodies: the metallonuclease domain, the first five PPR α-helices, and the central domain with the C-terminal portion of the PPR domain. When the central domains of PRORP1 and PRORP2 are superimposed, the first 5 N-terminal helices are rotated by 34.8˚ and the metallonuclease domain is rotated by 44.5˚ in PRORP2 relative to PRORP1. Potential flexible hinges are present between the metallonuclease and central domain (PRORP2 residues 291-293 and 480-481, and PRORP1 residues 354-56 and 534-35) and in the intra-motif loop of the third PPR motif in the PPR domain (PRORP2 residues 122-123, and PRORP1 residues 189-190) (Figure 4C).

Since macromolecules can undergo many different conformational changes we performed normal mode analysis for PRORP1 and PRORP2 to predict the most probable large-scale functional motions using the ElNemo [26] and iMods [27] normal mode analysis servers. Normal mode analysis further indicates the presence of flexible regions in the PPR domain and between the metallonuclease and central domain. We propose that these potential flexible hinges could facilitate the motion of the metallonuclease domain and the PPR domain towards each other, potentially playing a role in accommodating substrates.

PRORP2 is a dimer in crystallo and monomeric in solution

PPR motif containing proteins can exist as homodimers, exemplified by HCF152 [28] and PPR10 [29, 30], or monomers, such as PPR4 and PPR5 [29-32]. In our crystal structure PRORP2 appears as a homodimer. This is in contrast to PRORP1, which is a monomer in both the crystal and solution. This disparity raises the question whether PRORP2 forms a dimer in the crystal as a consequence of its packing or if its dimerization is physiologically

relevant. The PRORP2 homodimer in the crystal has an unusual inter-domain interaction in which the first PPR motif is inserted into the nuclease active site (Figure 4A). We performed interdomain surface analysis to provide insight into the physiological relevance of this interaction using the PISA webserver [33]. The dimerization interface surface for PRORP2 was 790 $Å^2$ however the Complex Formation Significance Score (CFSS) of zero indicated that PRORP2 dimerization is unlikely *in vivo*.

Nonetheless, we tested if residues involved in dimerization in the crystal structure are important for catalysis. Our structure of PRORP2 suggests that dimerization may be mediated via an interaction between the K42 residue in the first PPR domain of one PRORP2 monomer and the metallonuclease domain active site residues D422 and D421 in an adjacent PRORP2 monomer (Figure 5A). We speculated that if dimerization is important for PRORP2 function then disruption of this putative interaction might alter the activity of PRORP2. However, the K42A mutation does not change the cleavage rate constant of PRORP2 for (nu)pre-tRNA$^{Gly}_{8:1}$ ($k_{obs,wild\text{-}type} = 0.8 \pm 0.1$ min^{-1} and $k_{obs,K42A} = 0.8 \pm 0.03$ min^{-1}) (Figure 5B). Lastly, we directly tested the dimerization state of PRORP2 in solution using Analytical Ultracentrifugation (AUC) with 1 and 10 mg/mL PRORP2. Even at high concentrations of PRORP2 only a single peak representing the monomeric form of PRORP2 is observed at 3.6S (Figure 5C). Analysis of this peak suggests the presence of a 58 kDa protein in solution, which correlates well with the 60 kDa molecular weight of the PRORP2. Our results indicate that PRORP2 is monomeric in solution and that the observed dimerization of PRORP2 in the asymmetric unit is due to crystal packing without *in vivo* relevance.

PPR domains of PRORP1 and PRORP2 exhibit structural differences

PPR motifs are found in all plants and are comprised of ~35 amino acid long sequences forming a helix-turn-helix arrangement (α-hairpin). These motifs can vary in length and their sequences are highly degenerate. The PPR domain of PRORP2 consists of five and a half PPR motifs corresponding to eleven consecutive α-helices similar to PRORP1. Based on the available structures of PPR motif containing proteins [8, 29, 30, 34-36] sequential PPR motifs packing in a parallel fashion results in a spiral of anti-parallel α-helices that form a right-handed superhelical structure. The two helices in a PPR motif are referred to as helix A and helix B, with all odd-numbered helices A in a superhelical PPR arrangement forming an inner concave surface while all even-numbered helices B are facing outwards and form the convex surface. The PPR domains of PRORP1 and PRORP2 share high amino acid identity (~45 %, Supplemental Figure 3) and structural homology. As expected with paralogous proteins [37] most of the differences between PRORP1 and PRORP2 are localized in the loop regions connecting the well-conserved structural elements. Example differences include the observation that the intra-domain loop of the second PPR motif in *A. thaliana* PRORPs is eight amino acids longer than in a canonical PPR repeat (Supplemental Figure 4A), and the presence of a two amino acid insertion in the third motif of the PRORP2 intradomain loop that is missing in PRORP1.

Superimposition of each individual equivalent PPR motif from PRORP1 and PRORP2 shows little variation in their structures (RMSD values = 0.58-0.68 Å) and in the absolute values of the angles between the two antiparallel α-helices (intra-PPR motif A-B angles) as calculated by PROMOTIF [38] (Supplemental Table 1). However, superimposition of the PPR domains of PRORP1 and PRORP2 in their entirety (and not just as individual motifs) no longer demonstrates a high degree of overlap between the structures (RMSD =

2.94 Å). While there is little variation in the angles between sequential PPR motifs (inter-PPR motif angles A-A'), closer examination reveals that the inter-PPR motif angle between helices 5 and 6 in PRORP1 is 153.1˚, in contrast to the corresponding angle in PRORP2 of -166.5˚. Furthermore, PRORP2 has a greater degree of curvature compared to PRORP1 (Figure 6A, Supplemental Table 1) when only the 5th helix of PRORP1 and PRORP2 PPR domains are aligned. The global rearrangement observed in the PPR domains of the two PRORPs is not due to differences between the intra-PPR and inter-PPR motif angles since these are equally and globally distributed among all PPR motifs, but rather results from differences between the orientation of helices 5 and 6 in the third PPR motif. This difference in orientation between helices 5 and 6 in the two proteins is shown in Figure 5A, which displays how PRORP2 helices 4 and 6 on the convex surface have moved away from each other by more than 2 Å compared to the equivalent helices in PRORP1. We speculate that this rearrangement between helices 5 and 6 may be indicative of a flexible connecting loop.

We performed normal mode analysis of PRORP1 and PRORP2 independently using the iMod and DynDom servers [24, 25, 27]. Our analyses indicate that the PPR domain displays a potential mechanical hinge between the two helices 5 and 6 of the PPR3 motif in both PRORPs (PRORP2 residues 122-123, and PRORP1 residues 190-191). This would permit motion between two rigid domains (where the first domain is defined by the 5 first helices and second domain is comprised of the subsequent 6 helices) and is consistent with our observed structural differences between helices 5 and 6. We hypothesized that such a motion might be relevant to catalysis and tested the potential contribution of the first three PPR motifs to PRORP function by measuring the catalytic activity of an N-terminal truncated version of PRORP2 (Δ141) lacking the first three PPR motifs. This mutant cleaves (nu)pre-tRNA$^{Gly\ 8:1}$ with a single turnover rate constant (k_{obs} < 0.001 min $^{-1}$) that is over 100-fold slower than wild-type PRORP2 (Table 3) under conditions where wild-type PRORP2 is

saturating. To test if Δ141 PRORP2 cleaves slowly under these conditions due, at least in part, to an inability to bind substrate tightly we measured the K_D of this mutant for (nu)pre-tRNA$^{Gly\ 8:1}$. We find that the affinity of the mutant for (nu)pre-tRNA$^{Gly\ 8:1}$ is over 58-fold weaker (K_D > 1 μM) than the wild-type enzyme. Our data indicate that the first three PPR motifs of PRORP2 contribute significantly to substrate binding.

Central domain of PRORP2 harbors a conserved structural zinc binding site

The central domain of PRORP2 is sandwiched between the PPR and metallonuclease domain and harbors a zinc-binding motif that is a conserved in all of the PRORPs. The Zn^{2+} binding motif observed in our PRORP2 structure is comprised of four conserved residues (C281, C284, H494 and C511) that coordinate a Zn^{2+} ion. As in PRORP1, Zn^{2+} binding appears to be important for structure as the metal is distal from the enzyme active site and the Zn^{2+} does not directly participate in substrate cleavage. The central domain interacts with the PPR domain through a four-stranded antiparallel β-sheet and is anchored to the metallonuclease domain through two long loops similar to that of PRORP1 (Figure 6B). Overall, the structure of the central domain is highly similar between PRORP1 and PRORP2 (RMSD = 0.644 Å).

Active sites in the metallonuclease domains of A. thaliana PRORPs are conserved

The metallonuclease domains of PRORP1 and PRORP2 are nearly structurally identical (overall RMSD= 0.956 Å, Figure 4C and 6C) based on their superposition. The few differences between PRORP1 and PRORP2 metallonuclease domains occur primarily in loop

regions (e.g. the connecting loop between α-helices (PRORP2 residues 349-358, PRORP1 residues 403-411)) that possess different conformations (Supplemental Figure 4B)). In the structure of PRORP1, two Mn^{2+} ions were observed in the active site[8] when Mn^{2+} ions were soaked into PRORP1 crystals. In the absence of any added heavy metals, the electron density of water and Mg^{2+} ions cannot be unambiguously discerned. This is especially true for our PRORP2 crystal structure, where due to the limited resolution and the absence of any added heavy metals, we were unable map Mg^{2+} ions in the active site. The core of PRORP1 and PRORP2 active sites share very high amino acid identity (~80 %) and structure (RMSD < 0.8 Å). The conserved aspartate residues of the active site (D343, D421, D422, D440 in PRORP2 and D399, D474, D475, D493 in PRORP1) overlap when superimposed (Figure 5C). The histidine residue in the active site (H445 in PRORP2, H498 in PRORP1) is found in a different position in the structures of PRORP2 and PRORP1 (Figure 6C) suggesting flexibility in this region. This residue was initially proposed to protonate the leaving product [8] but was later shown not to participate in acid-base chemistry [12].

To verify that the putative active site residues are essential for PRORP2 catalysis, we created a series of mutants where the active site aspartate and histidine residues are substituted with alanine (D343A, D421A, D422A, D440A, H445A). We find that all of the aspartate to alanine mutants are unable to cleave (nu)pre-$tRNA^{Gly\ 8:1}$ in our single turnover assays (Table 3), and some of these mutants have significantly weaker substrate affinity than the wild type enzyme (Supplemental Table 2) [6]. The H445A PRORP2 mutant reduced the k_{obs} value measured in cleavage assays by approximately 50-fold relative to the wild type protein. Since we expect that mutation of active site residues that directly participate in the pre-tRNA cleavage reaction to lower activity by more than 50-fold, we tested if H455 plays a role in pre-tRNA binding and recognition by measuring the K_D of the PRORP2 H455A

mutant for (nu)pre-tRNA$^{Gly\ 8:1}$. We find that this mutant does not alter substrate binding relative to the wild-type enzyme (Supplemental Table 2). Given that H455A binds substrates well and, in contrast to the aspartate active site mutants, does not render the enzyme entirely inactive, we suggest that H455 might play an indirect role in catalysis such as orienting the substrate for cleavage following binding.

Discussion

While protein only RNase Ps are found in many eukaryotic organisms (including humans) how this new class of RNA processing enzymes generally functions remains poorly understood. In some Eukaryotes, such as land plants, PRORPs have entirely taken over the role of "ribozyme-based" RNase Ps [4-6, 9]. Despite their essential nature [9] to date only a single PRORP, the *A. thaliana* PRORP1 localized to mitochondria and chloroplast, has been characterized biochemically and structurally [4, 6, 8, 12, 15]. To broadly understand how PRORPs function, our work here is the first structure and function study of a nuclear localized PRORP, *A. thaliana* PRORP2.

Our 3.2 Å crystal structure of *A. thaliana* PRORP2 demonstrates that the overall structure of single enzyme PRORPs, including the active site and structural zinc site, are conserved. We were unable to visualize the active site metal(s) previously seen in the PRORP1 structure [8] in our PRORP2 crystal structure. However, our biochemical data indicate that PRORP2, like PRORP1, uses a catalytic Mg^{2+} cofactor (Figure 1C, 1D). Interestingly, we discovered that PRORP2 exhibits a more open conformation than PRORP1; this difference cannot be explained simply by crystal contacts and suggests that despite a high degree of sequence identity (~48%) there can be significant variation even between PRORP paralogues from a single organism. The structural differences that we observe are localized to the PPR domain and the region connecting the central and metallonuclease domains. Within

the PPR domain we found that the different rotation angles of the A-B helices of the third PPR motif in PRORP1 and PRORP2 account for much of the difference in protein conformations. Additionally, normal mode analysis of PRORP1 and PRORP2 revealed the presence of putative mechanical hinges in the intra-motif loop of the third PPR and between the metallonuclease domain and central domain in both PRORPs. These crystal structures combined with the normal mode analysis are the first evidence of potential flexibility within the PPR motifs. Kinetic assays with truncated PRORP2 indicate that the first three PPR helices, forming the first rigid group in the PRORP2 PPR domain, are relevant to PRORP2 function since truncation leads to reduced activity. The N-terminal helices may be important for both providing residues that mediate protein-nucleic acid interactions and helping to accommodate conformational changes within the PPR domain necessary for substrate binding. Our structural analysis suggests that the relative motion of the two observed rigid group of helices within the PPR domain could permit two different superhelical arrangements of the PPR domain. These arrangements potentially represent different PPR domain conformations during the PRORP catalytic cycle and reveal how the PPR domain might adopt different conformations in response to RNA binding.

We find that PRORP2 has high affinity for pre-tRNA (K_D values in low nanomolar range) consistent with dissociation constants reported for PRORP1 [8, 12] and other PPR proteins (eg. PPR 10) [29]. Furthermore, the single turnover rate constants that we measure for PRORP2 cleaving (nu)pre-tRNA^{Gly} substrates are comparable with previously published rate constants for PRORP1 catalyzing cleavage of (mt)pre-tRNAs under the same conditions[8, 12]. However these activities are at least 10-fold lower than that of bacterial and yeast RNA based RNase P [6].

"Ribozyme-based" RNase P typically recognizes pre-tRNA substrates using a variety of sequence and secondary structural characteristics (e.g. D and T-stem loops, 5' leader

length) based on *in vitro* kinetic experiments and the co-crystal structure of RNase P with $tRNA^{Phe}$ [21, 39-48]. Activity assays and footprinting experiments indicate that PRORP1 recognizes individual residues in the pre-tRNA D- and T-loops [49] but it is unknown if, like RNA-based RNase P, the pre-tRNA 5' leader and immature 3' trailer length are also determinants of PRORP substrate recognition. Our binding studies (Figure 2A, Table 1) indicate that PRORP2 preferentially associates with pre-tRNA substrates containing short 3' trailers and 5' leaders. This is in contrast to the bacterial RNA-based form of the enzyme, which does not discriminate between binding pre-tRNAs with leaders longer than 5 nucleotides [21, 22, 39]. PRORP2 demonstrates a preference towards binding pre-tRNAs with short 3' trailers, making it unlikely that 3' trailers of pre-tRNAs are important in substrate recognition. The preference for pre-tRNAs with short 3' trailers differs from the eukaryotic nuclear RNA-based RNase P found in yeast [39], indicating that there are potential differences between how eukaryotic RNA based RNase-P and PRORPs recognize their substrates. It is possible that PRORP2 prefers to bind pre-tRNAs with short 5' leader and 3' trailer sequences because extended single stranded RNA regions have the potential to base pair and/or form secondary structures, thereby altering the substrate structure. While pre-tRNA 5' end processing by RNase P is conserved, tRNA 3' end maturation is not; depending on the organism 3' maturation is catalyzed by different endo- (e.g. RNase Z, RNase PH) and exonucleases (e.g Rex1.), and even sometimes requires multiple enzymes [7]. Furthermore, the order of 3' and 5' pre-tRNA maturation is not conserved [7]. While in human human mitochondria 5' end processing is proposed to be the first step [50], given the substrate preferences that we observe we speculate that nuclear pre-tRNAs in *A. thaliana* may be first processed by 3' end tRNA processing enzymes before 5' end maturation by PRORP2 *in vivo*.

Whether or not differentially localized PRORPs in a single organism display specificity for substrates localized to their compartments is mostly unknown[51]. Answering this question is of interest because it might help us to rationalize why some organisms evolved multiple PRORP paralogs. We first approached this by measuring the single-turnover rate constants for PRORP2 cleaving a mitochondria specific t-element and nuclear encoded pre-tRNAs. Our *in vitro* studies demonstrate that PRORP1 single turnover activity for the mitochondrial t-element is 10-fold higher than that of PRORP2, suggesting that some differences in cleavage specificity amongst PRORPs exist. Moreover, despite the similarity of PPR domains in PRORP proteins, there are not only sequence differences but also structural dissimilarities within PRORP PPR domains. These observed subtle variances in the PPRs may account for differences in substrate recognition strategies between PRORPs of different organellar localization. This observation can help to explain why PRORPs with different sequences and slight structural variations may be required within a single organism.

It has been proposed that PPR domains interact with RNAs via both the RNA sugar-phosphate backbone and/or base specific contacts [14, 29, 49]. These types of contacts are more likely to be made between the PRORP PPR domains and pre-tRNA D- and T-arms, and the leader sequences [49] than with pre-tRNA aniticodon loops. This is reinforced by the observation that PRORPs process precursor forms of t-elements that completely lack the anticodon loop (Figure 3A). Bioinformatic analyses of PPR proteins suggest that amino acids that potentially interact with the RNA substrates are typically found in the first, third, sixth, tenth and thirteenth position of a given PPR motif (when the first residue of a PPR motif is defined as the first amino acid of the first α-helix of a PPR motif) [29, 52, 53]. The crystal structure of maize PPR10 PPR protein with its cognate RNA substrate provided hints as to the potential importance of amino acids in the third and the sixth position of PPR motifs in substrate binding. Mutagenesis studies have shown that amino acids in the 6^{th} position of the

second and third PPR motif of PRORP1 might play a role in recognition of the tRNA substrate [14]. We mapped the positions of all the residues thus far identified as potentially important for *A. thaliana* PRORPs binding pre-tRNAs onto the PRORP1 and PRORP2 crystal structures. The positions of these residues on the two structures are similar, consistent with our findings suggesting that the enzymes typically have similar reactivity toward pre-tRNAs. We expect that this will not be the case for non-canonical substrates, such as the mitochondrial t-elements. Further studies, including foot-printing, crosslinking, and crystal structures of PRORPs bound to their substrates will be necessary to tease out the precise contributions of individual PRORP structures to substrate recognition.

The work presented here provides the first biochemical and structural insight into a nuclear localized PRORP. This work demonstrates that there are subtle, but potentially important, differences between the structures of PRORPs and identifies a number of structural features likely important for substrate recognition. Furthermore, we reveal that differentially localized PRORPs exhibit some preference for cleaving a subset of localized non-canonical substrates, partially explaining the need for multiple PRORP paralogs in a single organism. In summary, our findings further our knowledge of a new class of RNA processing enzymes by providing mechanistic insight into how they recognize and cleave their substrates, and uncovering a number of conserved and non-conserved features of their structure and function.

Materials and methods

Protein expression. Δ75 PRORP1 was prepared according to previously published protocols [8, 12]. Full length PRORP2 was cloned into pMCSG7 vector (add plasmid name?). Mutants were generated by Quickchange mutagenesis. Expression of full-length wild type PRORP2 was induced upon addition of 200 μM IPTG to BL21(DE3) pMCSG7 *E.* coli at 18 ˚C.

Bacterial cells were collected by centrifugation (10.000 x g, 15 minutes), resuspended in lysis buffer (20 mM MOPS pH 7.8, 1 M NaCl, 1 mM TCEP, 0.2 % Tween, 0.1 mg/ml lysozyme and 0.1 mg/ml phenylmethylsulfonyl fluoride), and incubated for 1 hour at 4 ˚C. The cells were subsequently subjected to sonication, and the resulting suspension was centrifuged at 34.000 x g at 4˚C for 1 hour. The supernatant was loaded onto a HisTrap (GE Healthcare) nickel column and protein was eluted with 500 mM imidazole. The purified His_6-PRORP were dialyzed into 20 mM MOPS pH 7.8, 150 mM NaCl, 1 mM TCEP and 5 % glycerol overnight at 4 ˚C and incubated with TEV protease (1:20 protein:TEV protease molar ratio) to remove the His tag. His_6-TEV protease was removed by running the sample through the HisTrap nickel column. For *in vitro* assays PRORP2 was dialyzed into 20 mM MOPS pH 7.8, 1 mM TCEP, 150 mM NaCl and 2 mM EDTA overnight at 4 ˚C to remove any possible metal contamination. Then, buffer was exchanged for 20 mM MOPS pH 7.8, 1 mM TCEP, 150 mM NaCl using a desalting column (BioRad). For crystallization purposes, PRORP2 was further fractionated using a size exclusion column before setting up crystallization trays.

Transcription and 5' labeling of precursor tRNAs. Pre-tRNA sequences were commercially synthesized and cloned into pCR vector (Zero Blunt Topo PCR cloning kit, Invitrogen) and templates were amplified by PCR for *in vitro* transcription. The Nad6 t-element sequence was cloned into a pUC18 vector; the final vector contains a T7 promoter and a Bstn1 restriction site at the 5' and 3' of the template, respectively. Bstn1 was used for linearizing the template for run-off transcription reactions. Reactions were carried out in 50 mM Tris-HCl pH 8.0, 4 mM (for pre-tRNA) or 25 mM (pre- nad6 t-element) $MgCl_2$, 1 mM spermidine, 5 mM DTT, 4 mM ATP, 4 mM CTP, 4 mM UTP, 1 mM GTP, 4 mM guanosine-5'-O-monophosphorothioate (GMPS), 350 µg/ml purified T7 RNA polymerase, 12.5 µM purified DNA template containing T7 promoter and 4 U/µl SUPERaseIn. After stopping the

transcription by addition of 50 mM EDTA and 500 mM NaCl, the pre-tRNA was washed with degassed TE pH 7.2 three times using an Amicon spin column (10 kDa MWCO). The washed pre-tRNA (~200 µl) was incubated with 20 µl 45 mM fluorescein overnight at 37 ˚C to label the 5'end. The reaction was stopped by addition of equal volume of 2X loading dye (0.05 % Bromo-Phenol-Blue, 0.05 % Xylene Cyanol dye, 50 % m/v urea, 0.1 M EDTA) and run on a 12% urea-polyacrylamide gel. The pre-tRNA was eluted into crush-soak buffer (TE, 0.1 % SDS and 0.5 M NaCl) overnight at 4˚C. The next day the mixture was filtered, concentrated and washed with degassed TE using an Amicon spin column (10 kDa MWCO). The pre-tRNA was ethanol precipitated and the resulting pellet was re-suspended in RNase free H_2O. The concentrations of total and labeled pre-tRNA were measured from absorbance using a Nanodrop spectrophotometer.

Crystallization of PRORP2. Protein samples were concentrated to 8 mg ml^{-1} in 50 mM MOPS buffer at pH 7.8, 100 mM NaCl, 1 mM TCEP. The PRORP2 crystals were grown under oil (mixture containing 1:2 paraffin to silicone oil) in microbatch trays at 4 ºC by mixing 0.3 µl of protein solution with 0.6 µl of reservoir solution, which contained 19.9 % (w/v) PEG3000, and 0.21 M sodium citrate. Crystals were cryoprotected for a few minutes before being flash frozen in liquid N_2, by transfer to a solution of 20 % glycerol, 20% PEG3000 (w/v), and 0.2 M sodium citrate, in 20 mM MOPS pH 7.8. Crystals of PRORP2 were of space group *P*1 (a= 70.0 Å, b= 77.0 Å, c= 80.1 Å, α= 72.6°, β= 64.1°, γ= 77.8°) with 2 monomers in the asymmetric unit (Matthews' coefficient, V_M = 3.1 $Å^3$/Da for 2 PRORP2 monomers, 60.6% solvent content).

Data collection, structure determination and refinement. Diffraction data were collected at GM/CA-CAT 23-IDB (Advanced Photon Source, Argonne National Laboratory) on a Mar

300 detector and processed with HKL2000 [54] to 3.2 Å resolution. Initial phases were obtained by the molecular replacement (MR) method with Phaser [55] using the three domains of PRORP1 (PDB accession number 4G26) separately as search models. Specifically a molecular replacement strategy was employed to search firstly for two excised PRORP1 metallonuclease domains, followed by two PPR and then finally by two central domains. It has to be noted that all loops and areas with high B-factors were omitted from the search models. Phaser successfully obtained a solution with all 6 individual domains The PRORP2 structure was refined originally with PHENIX [56] including rigid body refinement of the individual domains followed by simulated annealing in torsional and Cartesian space, coordination minimization, and restrained individual B-factor adjustment with maximum-likelihood targets. Refmac5 [57] in the CCP4i suite [58] was subsequently employed for restrained refinement of using isotropic individual B-factors with maximum-likelihood targets using a simple model for bulk solvent scaling, followed by model building and modification with Coot [59]. Several iterative rounds of refinement followed by model building/modifications were performed. In the early rounds of refinement, restraints and ideal targets for tetrahedral geometry at zinc were added. Crystallographic information as well as refinement statistics are provided in the Table 3. The geometric quality of the model and its agreement with the structure factors were assessed with MolProbity For PRORP2, MolProbity [60] reported a clash and a molprobity score of 1.62 (100^{th} percentile) and1.48 (100^{th} percentile) respectively, while 92.52 % of the residues were in the favored Ramachandran plot regions with 0.96% residues in outlier regions. Figures showing crystal structures were generated with PyMOL [61].

Analytical Ultracentrifugation. All the AUC sedimentation velocity experiments were carried out in 20 mM MOPS (pH 7.8), 100 mM NaCl, and 1 mM TCEP buffer using a

Beckman ProteomeLab XL-1 instrument with An-50 Ti rotor at 2000xg and 20 ˚C using 1 and 10 mg/mL of protein concentrations. The values for buffer density, viscosity and protein partial specific volume were calculated using Sednterp [62]. During the runs, changes in the concentration gradient were monitored by absorbance at 280 nm. The data were analyzed by the SEDFIT using the continuous $C(s)$ distribution model.

Single turnover assays. All single turnover reactions were conducted in buffer containing 30 mM MOPS pH 7.8, 150 mM NaCl, 1 mM $MgCl_2$ (or $CaCl_2$, $MnCl_2$, $ZnCl_2$ for data displayed in Figure 1C,D), 1 mM DTT at 25 ˚C. To initiate the reaction 20-100 nM fluorescently labeled substrate was added to 5 μM of recombinant purified PRORP2. Reactions were incubated for up to 60 minutes at 25 ˚C, time points were obtained by stopping the reactions with 0.05 % Bromo-Phenol-Blue, 0.05 % Xylene Cyanol dye, 50 % m/v urea, 0.1 M EDTA. Samples were visualized on a polyacrylamide-urea gel (8-20%) by direct scanning on a Storm 860 imager. Densitometry was performed with ImageQuant and data from at least three independent experiments were analyzed using Kaleidagraph 4.1.3. Eq 1. was fit to the data, as described in Howard et al, 2012 [8] to calculate the observed rate constant (k_{obs}) and the standard error .

Eq 1. $$\text{Fraction cleaved} = 1 - e^{-kt}$$

Fluorescent polarization binding assay. The binding assays were performed in 30 mM MOPS pH 7.8, 150 mM NaCl, 6 mM $CaCl_2$, 1 mM DTT at 25 ˚C. For all assays, 20 nM of 5' fluorescein labeled pre-$tRNA^{Gly}$ was incubated with increasing concentrations (0-1000 nM) of PRORP2 for 5 minutes before changes in anisotropy was measured. Data were corrected with the anisotropy measured in the absence of the protein. The quadratic form of a binding

isotherm (Eq. 2) [22] was fit to the fluorescence polarization data from at least three independent experiments using Kaleidagraph 4.1.3 software to calculate the dissociation constant (K_D) and the standard error.

Eq 2. $\Delta FP = \Delta FP_0 + (\Delta FP_{max} - \Delta FP_0) \times \frac{[(-K_D+[E]+[S]_T)-\sqrt{(K_D+[E]+[S]_T)2-4\,[E][S]_T}}{2[S]_T}$

ΔFP= Observed enhancement in fluorescent anisotropy

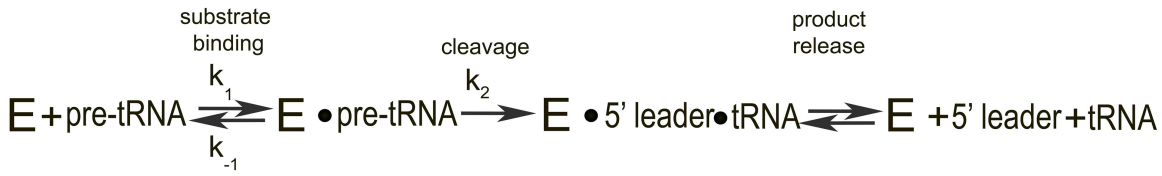
ΔFP_0= Fluorescent anisotropy in the absence of enzyme

ΔFP_{max}= Fluorescent anisotropy at enzyme saturation

ACCESSION NUMBERS: Coordinates and structure factors have been deposited in the Protein Data Bank with accession number 5DIZ.

Acknowledgements

We would like to thank the National Institute of General Medical Sciences and National Cancer Institute Collaborative Access Team (GM/CA CAT) at the Advanced Light Source for beam time. We also thank Dr. Kristin S. Koutmou for her advice in setting up kinetic experiments and reading this manuscript. This work was supported by the National Institutes of Health [R01 GM055387 to C.A.F]; in part by the Molecular Biophysics Training Grant [T32 GM8270-25 to M.J.H.] and by Uniformed Services University of the Health Sciences start-up funds (R071KB to M.K.).



Scheme 1. Minimal kinetic mechanism for PRORP2.
PRORP2 (E) binds pre-tRNA to form an enzyme-substrate complex. The substrate is then cleaved (k_2), resulting in an enzyme-tRNA-5' leader complex. The products of the reaction (tRNA and 5' leader) are subsequently released.

Nuclear Substrate	5’ leader sequence	3’ trailer sequence	K_D (nM)	k_{obs} (min^{-1})
pre-tRNA$^{Gly\ 23:10}$	GGGUAUUUGCUCGAUAUGCAAAA	UUUAUAUUUU	118 ± 26	0.7 ±0.1
pre-tRNA$^{Gly\ 23:5}$	GGGUAUUUGCUCGAUAUGCAAAA	UUUAU	52 ± 12	1.0 ±0.1
pre-tRNA$^{Gly\ 23:1}$	GGGUAUUUGCUCGAUAUGCAAAA	U	17 ± 5	0.7 ±0.1
pre-tRNA$^{Gly\ 13:1}$	GGGAUAUGCAAAA	U	6 ± 1	0.7 ±0.1
pre-tRNA$^{Gly\ 8:1}$	GGGCAAAA	U	3 ± 1	1.1 ±0.1

Table 1. Dissociation (K_D) and single-turnover rate constants (k_{obs}) for PRORP2 with (nu)pre-tRNA^{Gly} substrates containing varying 5’ leader and 3’ trailer lengths. The data were measured in buffers containing 30 mM MOPS pH 7.8, 150 mM NaCl, 1 mM DTT and 1 mM $MgCl_2$ (k_{obs}) or $CaCl_2$ (K_D). The standard error values displayed were obtained from at least three independent experiments.

Table 2. Crystallographic data. Data processing and refinement statistics.

Protein	**PRORP2**
Data Collection	
Space Group	*P*1
Cell Dimensions	
a, b, c (Å)	70.0, 77.0, 80.1
α, β, γ (°)	72.7, 64.1, 77,8
Wavelength (Å)	1.033
Resolution (Å)	50-3.20 (3.31-3.20)
R_{sym} (%)	5.9 (65.4)
I/σI	8.7 (1.4)
Completeness (%)	99.1 (98.6)
Redundancy	2.2 (2.2)
Refinement	
Resolution (Å)	45.6-3.2
No. reflections	23,241
R_{work} / R_{free}	0.228 / 0.272
No. atoms	
Protein	7493
Water	5
Zn	2
B-factors	
Protein	123.5
Water	66.8
Zn	127.8
R.m.s Deviations	
Bond lengths (Å)	0.007
Bond angles (°)	0.970
Ramachandran plot (%)	
Favored/allowed/outliers	93.70/5.66/0.64
MolProbity Score	1.23 (100^{th} percentile)
Protein Data Bank code	**5DIZ**

PRORP2	k_{obs} (min^{-1})
Wild type	1.1 ± 0.1
D393A	< 0.001
D421A	< 0.001
D422A	< 0.001
D440A	< 0.001
H445A	0.02 ± 0.004
Δ141	< 0.001

Table 3. Single turnover rate constants for PRORP2 cleaving (nu)pre-$tRNA^{Gly\ 8:1}$. The reactions were perfomed at 25°C in the presence of 30 mM MOPS pH 7.8, 150 mM NaCl, 1 mM DTT and 1 mM $MgCl_2$ with 50 nM 5' "fluorescein-labeled" (nu)pre-$tRNA^{Gly\ 8:1}$ and 5 μM PRORP2. The k_{obs} values and standard errors reflect at least three independent experiments.

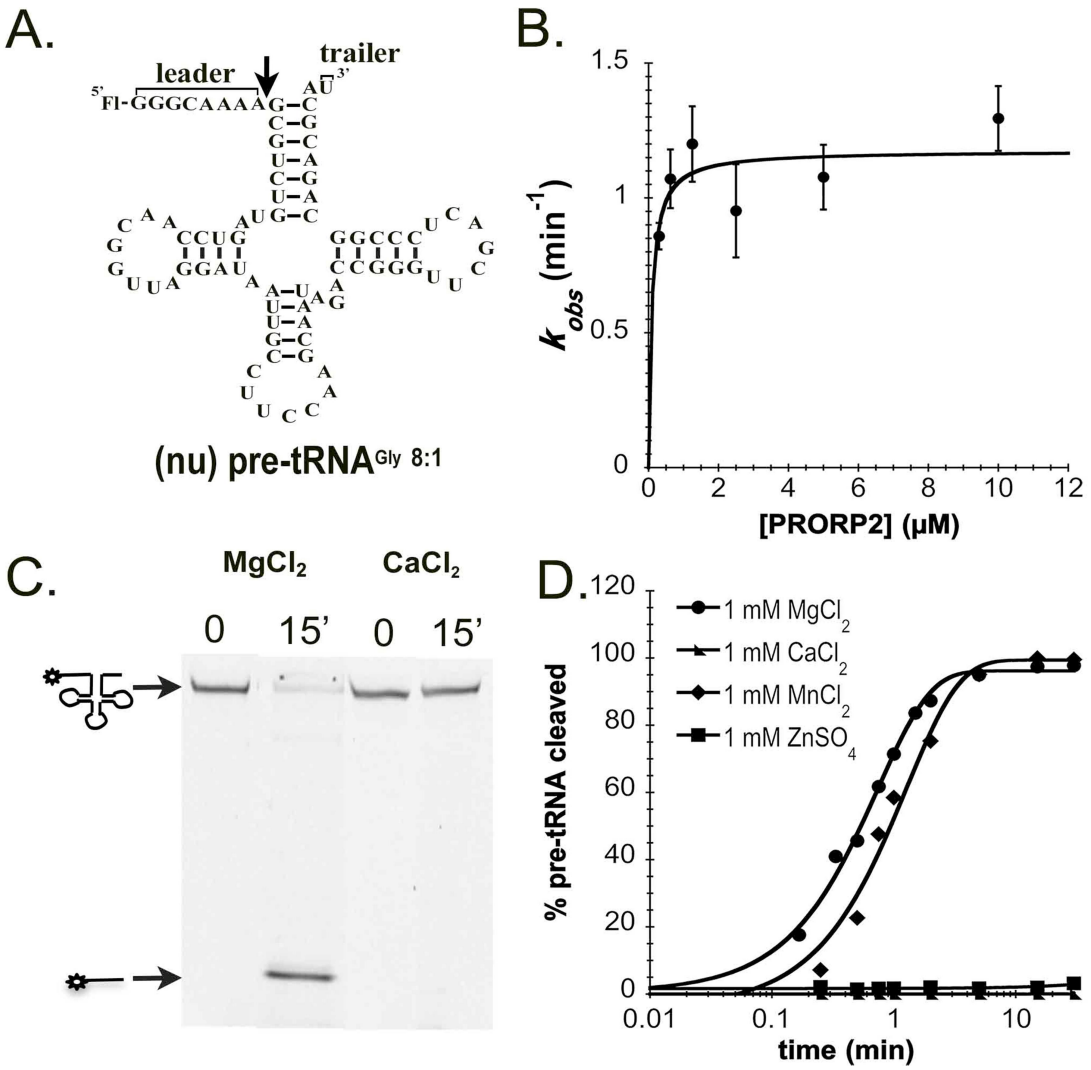


Figure 1. Metal dependence of PRORP2.

A. Proposed secondary structure of nuclear pre-tRNA$^{Gly\ 8:1}$ used in our *in vitro* assays. Pre-tRNAs are 5' fluorescently labeled by fluorescein (Fl). The 5' leader and 3' trailer are noted, and the black arrow indicates the cleavage site. B. The dependence of the single turnover cleavage rate constant (k_{obs}) on the PRORP2 concentration for (nu)pre-tRNA$^{Gly\ 8:1}$. C. Representative denaturing PAGE gel displaying the cleavage activity of PRORP2 for (nu)pre-tRNA$^{Gly\ 8:1}$ after a 15 min incubation with buffer containing 1 mM $MgCl_2$ or $CaCl_2$. Cleavage is observed in the presence of $MgCl_2$ but not $CaCl_2$ under standard reaction conditions. D. Representative timecourses for the cleavage of a 5' "fluorescein-labeled" (nu)pre-tRNA$^{Gly\ 8:1}$ substrate catalyzed by PRORP2 under standard single turnover conditions in the presence of $MgCl_2$ (circle), $MnCl_2$ (diamond), $ZnCl_2$ (square) and $CaCl_2$ (triangle).

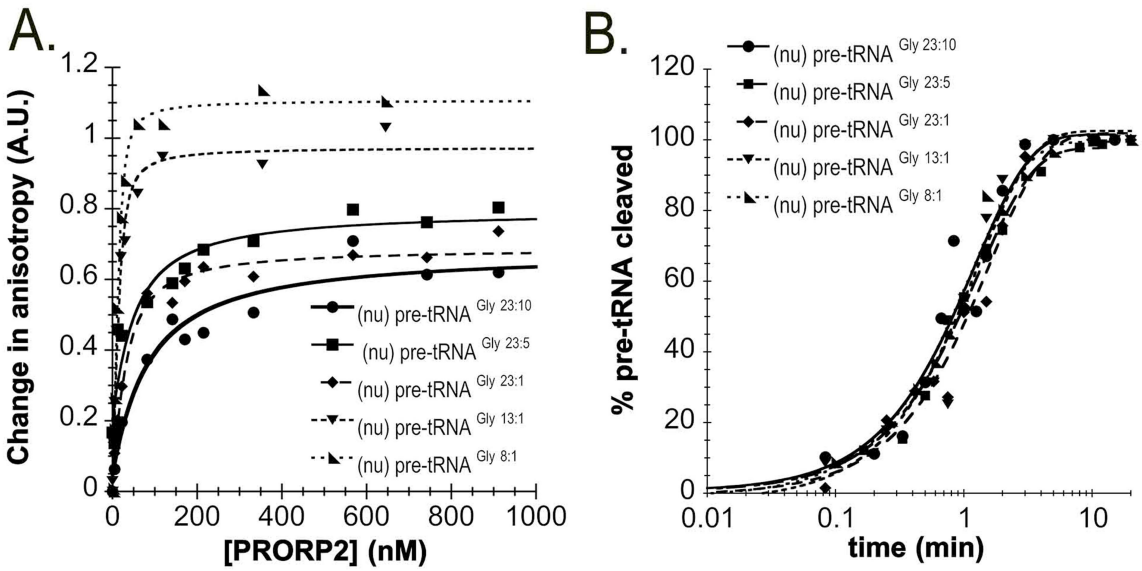


Figure 2. PRORP2 discriminates betweeen binding, but not cleaving, substrates with varied 5' leader and 3' trailer lengths.
A. Representative plots of fluorescent polarization assays performed at 25 ^{o}C in 30 mM MOPS pH 7.8, 150 mM NaCl, 1mM DTT and 6 mM $CaCl_2$ with varied PRORP2 (0-1000 nM) and 20 nM 5' fluorescently labeled: (nu)pre-tRNA$^{Gly\ 23:10}$ (closed circle), (nu)pre-tRNA$^{Gly\ 23:5}$ (closed square), (nu)pre-tRNA$^{Gly\ 23:1}$ (diamond), (nu)pre-tRNA$^{Gly\ 13:1}$ (closed upside down triangle), and (nu)pre-tRNA$^{Gly\ 8:1}$ (right triangle). B. Representative single turnover assays using standard assay conditions with 5 μM PRORP2 and 50 nM nuclear fluorescently labeled (nu)pre-tRNA$^{Gly\ 23:10}$ (closed circle), (nu)pre-tRNA$^{Gly\ 23:5}$ (closed square), (nu)pre-tRNA$^{Gly\ 23:1}$ (diamond), (nu)pre-tRNA$^{Gly\ 13:1}$ (closed upside down triangle), and (nu)pre-tRNA$^{Gly\ 8:1}$ (right triangle).

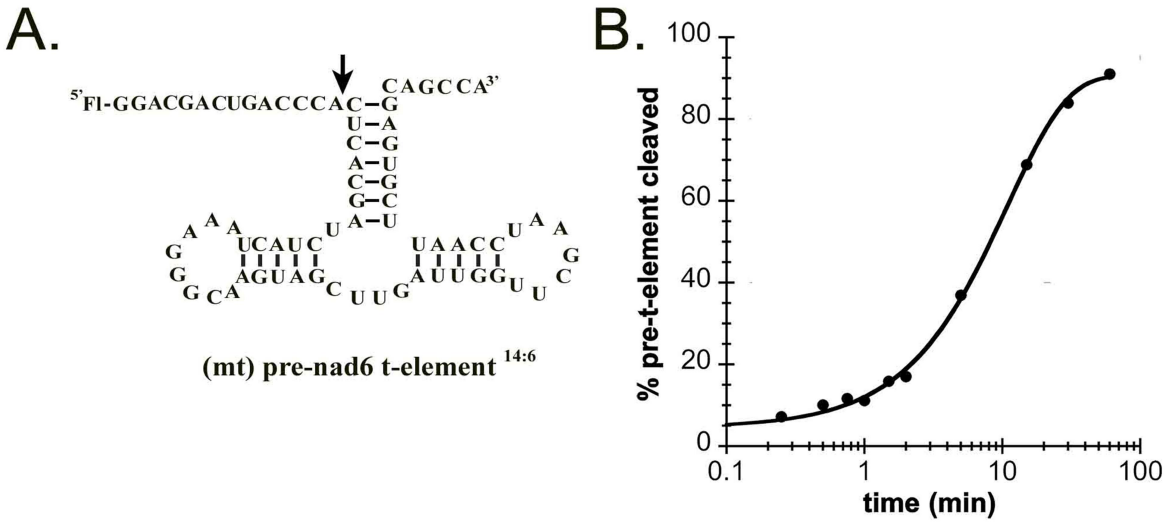


Figure 3. PRORP2 cleaves mitochondrial pre-nad6 t-element.

A. Proposed secondary structure of the (mt)pre-nad6 t-element$^{14:6}$ used in our *in vitro* assays. B. Percentage of the (mt)pre-nad6 t-element$^{14:6}$ cleaved as a function of time under single turnover conditions (50 nM 5' fluorescein end labeled (mt)pre-nad6 t-element$^{14:6}$, 5 µM PRORP2, 25^{o}C, 30 mM MOPS pH 7.8, 150 mM NaCl, 1 mM DTT and 1 mM $MgCl_2$).

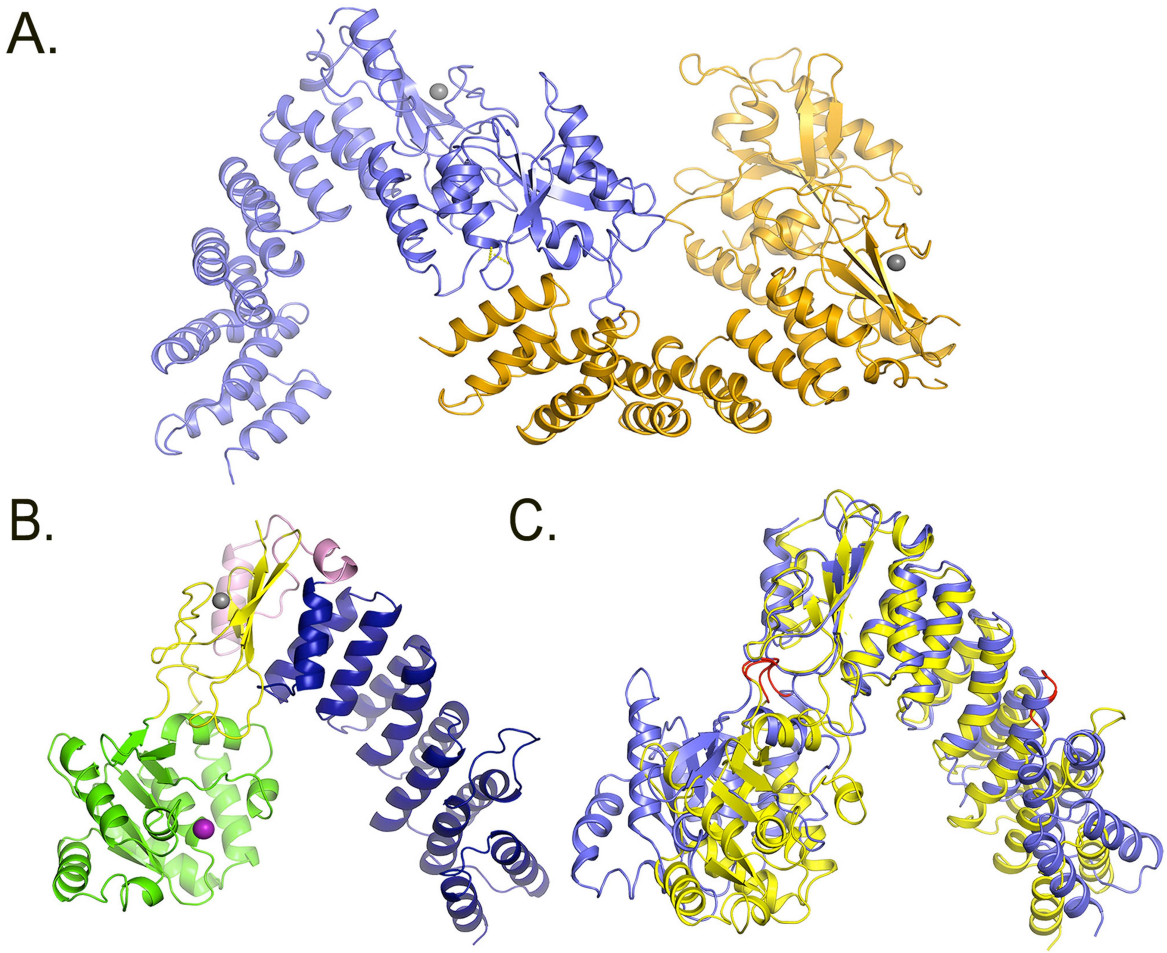


Figure 4. Comparison of PRORP1 and PRORP2 crystal structures.
A. Crystal structure of the two monomers of PRORP2 in the asymmetric unit. B. Crystal structure of PRORP1. blue: PPR domain, yellow: central domain, Pink: *A. thaliana* specific insertion, green: metallonuclease domain, Grey: zink ion, Purple: modeled magnesium ion. C. PRORP1 and PRORP2 superimposition based on the central domains. The structure of PRORP2 (blue) is in an "open" conformation, while PRORP1 (yellow) is in a "closed" conformation. The predicted PRORP2 mechanical hinges are shown in red in the metallonuclease domain and the 3rd PPR motif.

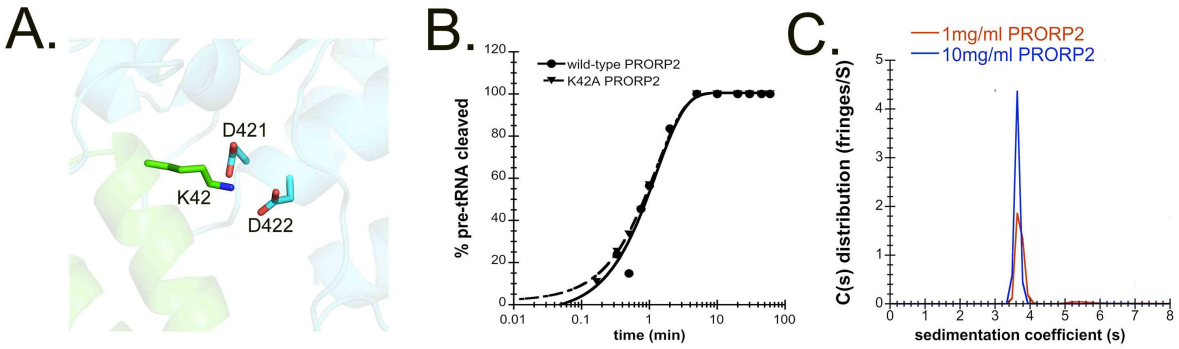


Figure 5. PRORP2 is a monomer in solution.

A. Residue K42 in the PPR domain and active site residues of two adjacent *in crystallo* PRORPs (residues D421 and D422). B. Representative plot of 5 µM K42A PRORP2 cleaving 50 nM (nu)tRNAGly $^{8:1}$ in single turnover cleavage assays under standard reaction conditions. C. Analytical Ultracentrifugation experiment with 1 and 10 mg/ml PRORP2.

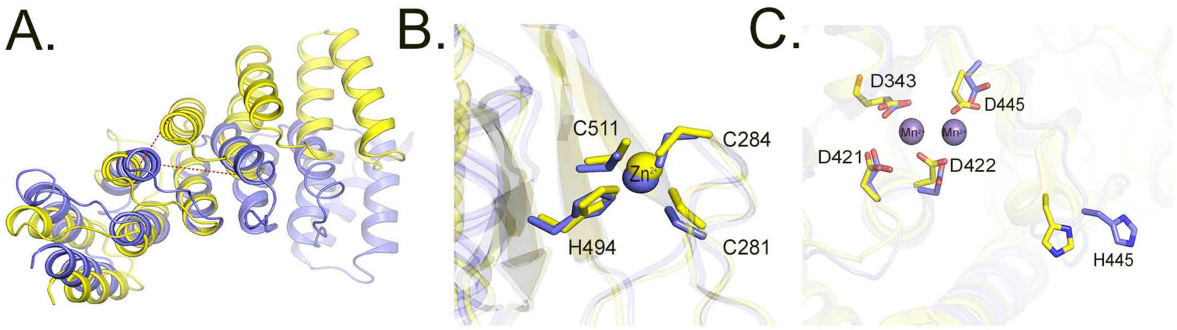


Figure 6. Comparison of the PPR, central and metallonuclease domains of PRORP1 and PRORP2.
A. Superimposition of the 5th PPR motif of PRORP1 and PRORP2. Dotted red lines indicate differences in distance between the same residues in the 4th and 6th PPR helices in PRORP1 and PRORP2. B. Superimposition of the central domains of PRORP1 and PRORP2. Residues numbering correspond to the conserved amino acids in PRORP2. C. Superimposition of the active sites of PRORP1 (yellow) and PRORP2 (blue). Residue numbers correspond to conserved amino acids in PRORP2. Positions of Mn^{2+} ions are depicted based on the structure of PRORP1.

Supplemental Material

helices	PRORP1	PRORP2	Δ˚
A1-B1	-171.1 ˚	-161.4˚	9.7˚
A2-B2	-157.1˚	-154.6˚	2.5 ˚
A3-B3	153.1˚	-166.5˚	-321.5˚
A4-B4	-163.9˚	-169.1˚	-5.2˚
A4-B5	-160.2˚	-157.0˚	3.2˚

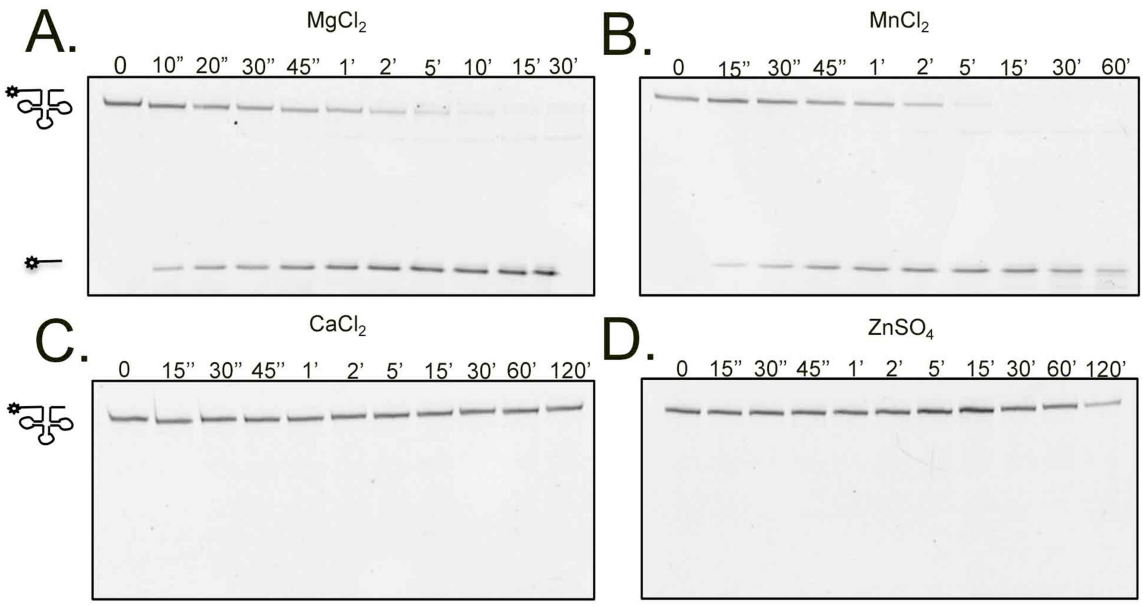
Supplemental table 1. Intramotif angles of PRORP1 and PRORP2 calculated by PROMOTIF.

PRORP2	K_D (nM)
D343A	177 ± 74
D421A	17 ± 5
D422A	757 ± 243
D440A	67 ± 28
H445A	17 ± 4
Δ 141	>1 µM

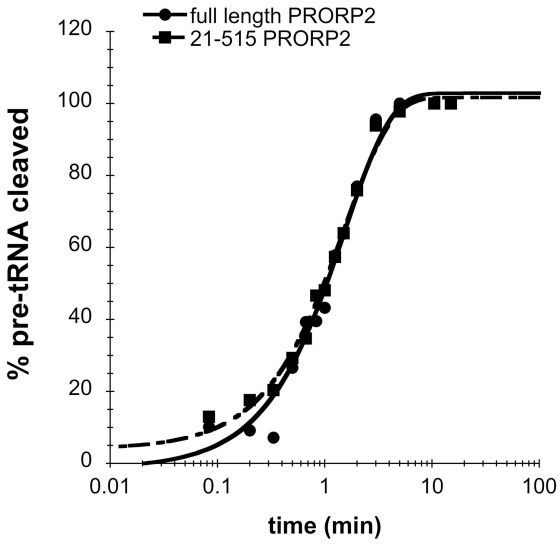
Supplemental table 2. Binding of (nu) pre-tRNA$^{Gly\ 8:1}$ to PRORP2 active site mutants. The data were measured in buffers containing 30 mM MOPS pH 7.8, 150 mM NaCl, 1 mM DTT and 1 mM $CaCl_2$. The standard error values displayed were obtained from at least three independent experiments.

substrate	No. of experiment	k_{obs} (min^{-1})	k_{obs} SE
(nu) pre- $tRNA^{Gly\ 8:1}$ with Mg^{2+}	1	1.05	± 0.12
	2	1.56	± 0.13
	3	0.98	± 0.11
	4	0.87	± 0.07
with Mn^{2+}	5	0.08	± 0.07
(nu) pre-$tRNA^{Gly\ 13:1}$	1	0.99	± 0.23
	2	0.45	± 0.15
	3	0.68	± 0.12
	4	0.64	± 0.07
(nu) pre-$tRNA^{Gly\ 23:1}$	1	1.62	± 0.17
	2	0.83	± 0.08
	3	0.78	± 0.11
(nu) pre-$tRNA^{Gly\ 23:5}$	1	1.39	± 0.09
	2	0.96	± 0.22
	3	0.77	± 0.07
(nu) pre-$tRNA^{Gly\ 23:10}$	1	0.76	± 0.10
	2	0.53	± 0.17
	3	0.82	± 0.13
	4	0.99	± 0.06
pre-nad6 t-element $^{14:3}$	1	0.19	± 0.04
	2	0.09	± 0.05
	3	0.09	±0.01

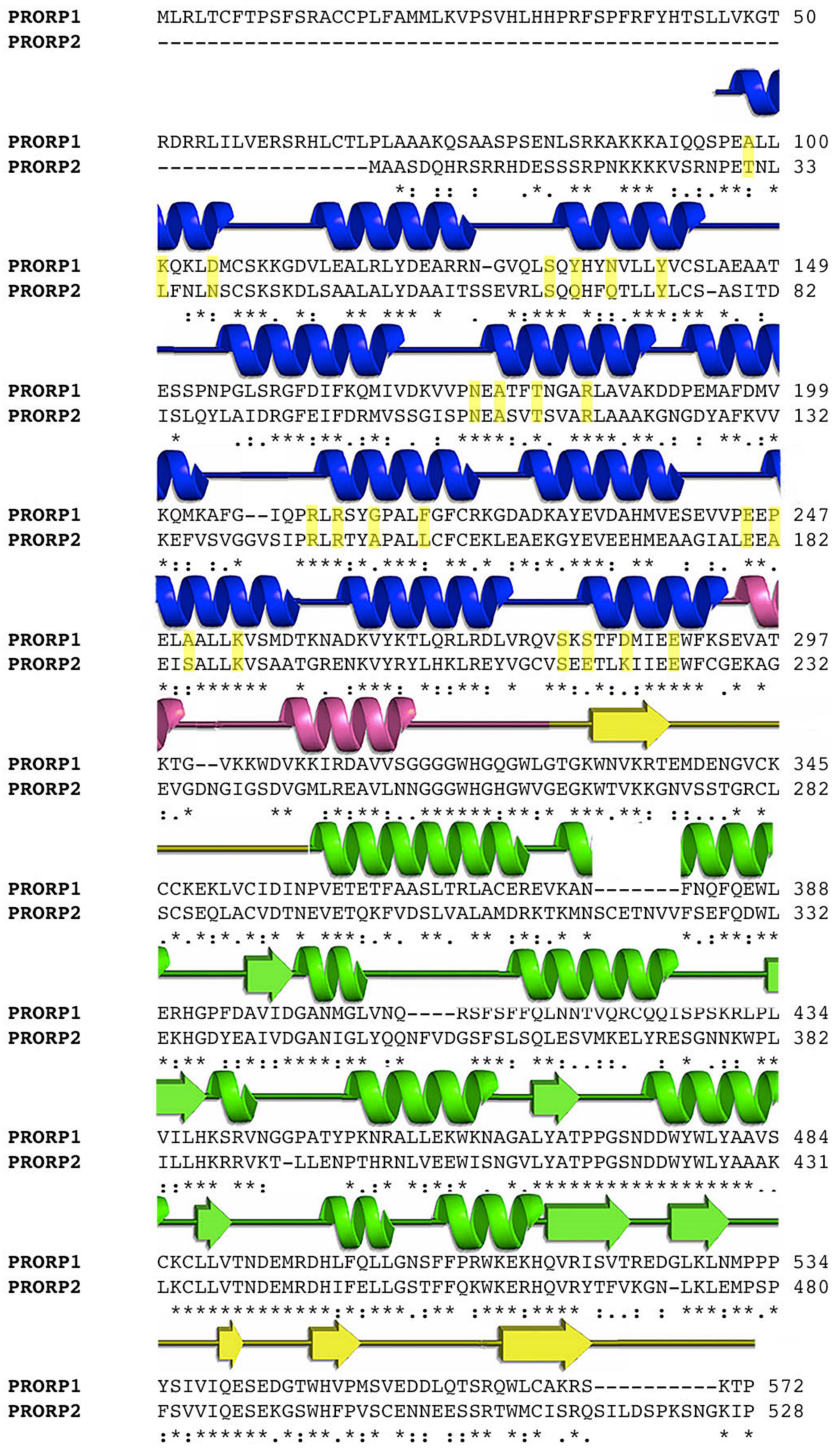
Supplemental table 3. k_{obs} values and standard errors (SE) derived from individual single turnover experiments for PRORP2.



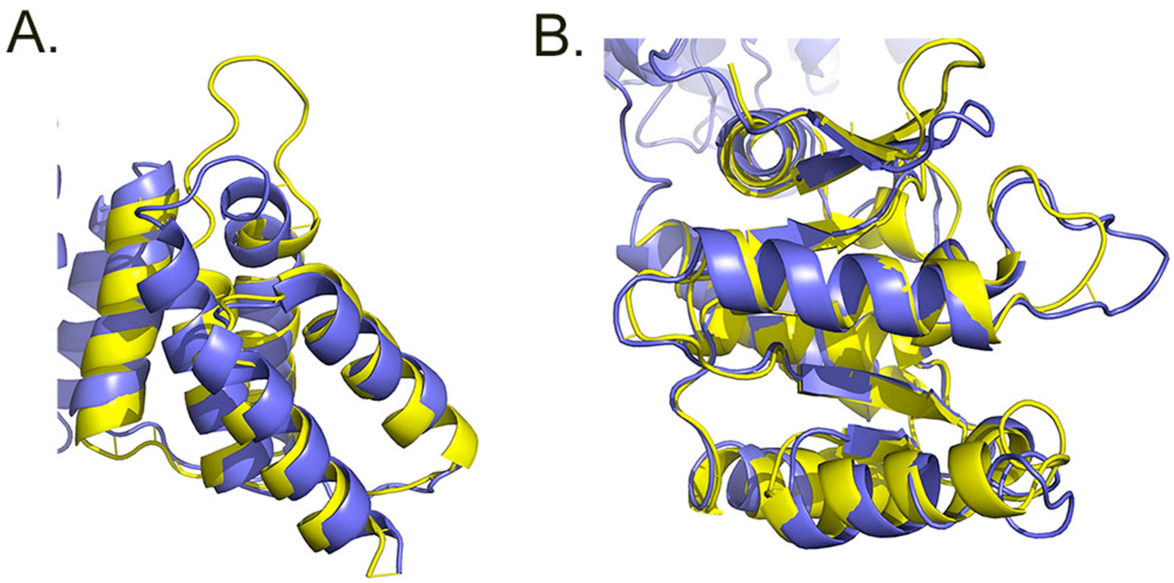
Supplemental figure 1. Representative gels showing cleavage activity of PRORP2 in the presence of A. Mg^{2+}, B. Ca^{2+}, C. Mn^{2+} and D. Zn^{2+}.



Supplemental Figure 2. Comparison of cleavage activity of PRORP2 and truncated 21-515 PRORP2 with (nu)tRNA^{Gly} 8:1 using standard reaction conditions.



Supplemental Figure 3. Clustal W 2.1 analysis of PRORP1 and PRORP2.
blue: PPR domain, yellow: central domain, Pink: *A. thaliana* specific insertion, green: metallonuclease domain, yellow highlights: residues predicted to be potentially involved in tRNA binding.



Supplemental Figure 4. Differences in disordered loops in the A. PPR and B. metallonuclease domains.

Supplemental methods

Pre-tRNA sequences used in this study are:

(nu)pre-tRNA$^{Gly\ 23:10}$:

GGGUAUUUGCTCGAUAUGCAAAAGCGUCUGUAGUCCAACGGUUAGGAUAAUUGCCU

UCCAAGCAAUAGACCCGGGUUCGACUCCCGGCAGACGCAUUUAUAUUUU

(nu)pre-tRNA$^{Gly\ 23:5}$:

GGGUAUUUGCTCGAUAUGCAAAAGCGUCUGUAGUCCAACGGUUAGGAUAAUUGCCU

UCCAAGCAAUAGACCCGGGUUCGACUCCCGGCAGACGCAUUUAU

(nu)pre-tRNA$^{Gly\ 23:1}$:

GGGUAUUUGCTCGAUAUGCAAAAGCGUCUGUAGUCCAACGGUUAGGAUAAUUGCCU

UCCAAGCAAUAGACCCGGGUUCGACUCCCGGCAGACGCAU,

(nu)pre-tRNA$^{Gly\ 13:1}$:

GGGAUAUGCAAAAGCGUCUGUAGUCCAACGGUUAGGAUAAUUGCCUUCCAAGCAAUA

GACCCGGGUUCGACUCCCGGCAGACGCAU

(nu)pre-tRNA$^{Gly\ 8:1}$:

GGGCAAAAGCGUCUGUAGUCCAACGGUUAGGAUAAUUGCCUUCCAAGCAAUAGACCC

GGGUUCGACUCCCGGCAGACGCAU,

(mt) pre-nad-6 t-element$^{14:6}$:
GGACGACUGACCCACUCACGAUCUACUAAAGGGCAAGUAGCUUGAUUGGUUCGAAU
CCAAUUCGUGAGCAGCCA,

REFERENCES

1. Altman, S., *Ribonuclease P.* Philos Trans R Soc Lond B Biol Sci, 2011. **366**(1580): p. 2936-41.
2. McClain, W.H., L.B. Lai, and V. Gopalan, *Trials, travails and triumphs: an account of RNA catalysis in RNase P.* J Mol Biol, 2010. **397**(3): p. 627-46.
3. Gobert, A., et al., *A single Arabidopsis organellar protein has RNase P activity.* Nat Struct Mol Biol, 2010. **17**(6): p. 740-4.
4. Holzmann, J., et al., *RNase P without RNA: identification and functional reconstitution of the human mitochondrial tRNA processing enzyme.* Cell, 2008. **135**(3): p. 462-74.
5. Taschner, A., et al., *Nuclear RNase P of Trypanosoma brucei: a single protein in place of the multicomponent RNA-protein complex.* Cell Rep, 2012. **2**(1): p. 19-25.
6. Howard, M.J., et al., *RNase P enzymes: divergent scaffolds for a conserved biological reaction.* RNA Biol, 2013. **10**(6): p. 909-14.
7. Rossmanith, W., *Of P and Z: mitochondrial tRNA processing enzymes.* Biochim Biophys Acta, 2012. **1819**(9-10): p. 1017-26.
8. Howard, M.J., et al., *Mitochondrial ribonuclease P structure provides insight into the evolution of catalytic strategies for precursor-tRNA 5′ processing.* Proc Natl Acad Sci U S A, 2012. **109**(40): p. 16149-54.
9. Gutmann, B., A. Gobert, and P. Giege, *PRORP proteins support RNase P activity in both organelles and the nucleus in Arabidopsis.* Genes Dev, 2012. **26**(10): p. 1022-7.
10. Li, F., et al., *Auto-inhibitory Mechanism of the Human Mitochondrial RNase P Protein Complex.* Sci Rep, 2015. **5**: p. 9878.
11. Reinhard, L., S. Sridhara, and B.M. Hallberg, *Structure of the nuclease subunit of human mitochondrial RNase P.* Nucleic Acids Res, 2015. **43**(11): p. 5664-72.
12. Howard, M.J., B.P. Klemm, and C.A. Fierke, *Mechanistic Studies Reveal Similar Catalytic Strategies for Phosphodiester Bond Hydrolysis by Protein-only and RNA-dependent Ribonuclease P.* J Biol Chem, 2015.
13. Small, I.D. and N. Peeters, *The PPR motif - a TPR-related motif prevalent in plant organellar proteins.* Trends Biochem Sci, 2000. **25**(2): p. 46-7.
14. Imai, T., et al., *Pentatricopeptide repeat motifs in the processing enzyme PRORP1 in Arabidopsis thaliana play a crucial role in recognition of nucleotide bases at TpsiC loop in precursor tRNAs.* Biochem Biophys Res Commun, 2014. **450**(4): p. 1541-6.
15. Pavlova, L.V., et al., *tRNA processing by protein-only versus RNA-based RNase P: kinetic analysis reveals mechanistic differences.* Chembiochem, 2012. **13**(15): p. 2270-6.
16. Zhou, W., et al., *Multiple RNA processing defects and impaired chloroplast function in plants deficient in the organellar protein-only RNase P enzyme.* PLoS One, 2015. **10**(3): p. e0120533.
17. Nemeth, E., et al., *Preorganization of the catalytic Zn-binding site in the HNH nuclease motif-A solution study.* J Inorg Biochem, 2015.
18. Chinami, M. and M. Shingu, *Hydrogen-1 nuclear magnetic resonance studies of staphylococcal nuclease variant H124L: pH dependence of histidines and tyrosines.* Arch Biochem Biophys, 1989. **270**(1): p. 126-36.
19. Hsiao, Y.Y., et al., *Crystal structure of CRN-4: implications for domain function in apoptotic DNA degradation.* Mol Cell Biol, 2009. **29**(2): p. 448-57.

20. Finney, L.A. and T.V. O'Halloran, *Transition metal speciation in the cell: insights from the chemistry of metal ion receptors.* Science, 2003. **300**(5621): p. 931-6.
21. Crary, S.M., S. Niranjanakumari, and C.A. Fierke, *The protein component of Bacillus subtilis ribonuclease P increases catalytic efficiency by enhancing interactions with the 5′ leader sequence of pre-tRNAAsp.* Biochemistry, 1998. **37**(26): p. 9409-16.
22. Hsieh, J. and C.A. Fierke, *Conformational change in the Bacillus subtilis RNase P holoenzyme--pre-tRNA complex enhances substrate affinity and limits cleavage rate.* RNA, 2009. **15**(8): p. 1565-77.
23. Forner, J., et al., *Mapping of mitochondrial mRNA termini in Arabidopsis thaliana: t-elements contribute to 5′ and 3′ end formation.* Nucleic Acids Res, 2007. **35**(11): p. 3676-92.
24. Hayward, S. and H.J. Berendsen, *Systematic analysis of domain motions in proteins from conformational change: new results on citrate synthase and T4 lysozyme.* Proteins, 1998. **30**(2): p. 144-54.
25. Hayward, S., A. Kitao, and H.J. Berendsen, *Model-free methods of analyzing domain motions in proteins from simulation: a comparison of normal mode analysis and molecular dynamics simulation of lysozyme.* Proteins, 1997. **27**(3): p. 425-37.
26. Suhre, K. and Y.H. Sanejouand, *ElNemo: a normal mode web server for protein movement analysis and the generation of templates for molecular replacement.* Nucleic Acids Res, 2004. **32**(Web Server issue): p. W610-4.
27. Lopez-Blanco, J.R., et al., *iMODS: internal coordinates normal mode analysis server.* Nucleic Acids Res, 2014. **42**(Web Server issue): p. W271-6.
28. Nakamura, T., et al., *RNA-binding properties of HCF152, an Arabidopsis PPR protein involved in the processing of chloroplast RNA.* Eur J Biochem, 2003. **270**(20): p. 4070-81.
29. Yin, P., et al., *Structural basis for the modular recognition of single-stranded RNA by PPR proteins.* Nature, 2013. **504**(7478): p. 168-71.
30. Li, Q., et al., *Examination of the Dimerization States of the Single-stranded RNA-recognition Protein PPR10.* J Biol Chem, 2014.
31. Meierhoff, K., et al., *HCF152, an Arabidopsis RNA binding pentatricopeptide repeat protein involved in the processing of chloroplast psbB-psbT-psbH-petB-petD RNAs.* Plant Cell, 2003. **15**(6): p. 1480-95.
32. Barkan, A. and I. Small, *Pentatricopeptide repeat proteins in plants.* Annu Rev Plant Biol, 2014. **65**: p. 415-42.
33. Krissinel, E. and K. Henrick, *Inference of macromolecular assemblies from crystalline state.* J Mol Biol, 2007. **372**(3): p. 774-97.
34. Ban, T., et al., *Structure of a PLS-class pentatricopeptide repeat protein provides insights into mechanism of RNA recognition.* J Biol Chem, 2013. **288**(44): p. 31540-8.
35. Gully, B.S., et al., *The solution structure of the pentatricopeptide repeat protein PPR10 upon binding atpH RNA.* Nucleic Acids Res, 2015. **43**(3): p. 1918-26.
36. Schwinghammer, K., et al., *Structure of human mitochondrial RNA polymerase elongation complex.* Nat Struct Mol Biol, 2013. **20**(11): p. 1298-303.
37. Joseph, A.P., et al., *Local structural differences in homologous proteins: specificities in different SCOP classes.* PLoS One, 2012. **7**(6): p. e38805.
38. Hutchinson, E.G. and J.M. Thornton, *PROMOTIF--a program to identify and analyze structural motifs in proteins.* Protein Sci, 1996. **5**(2): p. 212-20.
39. Ziehler, W.A., et al., *Effects of 5′ leader and 3′ trailer structures on pre-tRNA processing by nuclear RNase P.* Biochemistry, 2000. **39**(32): p. 9909-16.
40. Loria, A., et al., *Recognition of a pre-tRNA substrate by the Bacillus subtilis RNase P holoenzyme.* Biochemistry, 1998. **37**(44): p. 15466-73.

41. Loria, A. and T. Pan, *Recognition of the T stem-loop of a pre-tRNA substrate by the ribozyme from Bacillus subtilis ribonuclease P.* Biochemistry, 1997. **36**(21): p. 6317-25.
42. Loria, A. and T. Pan, *Recognition of the 5' leader and the acceptor stem of a pre-tRNA substrate by the ribozyme from Bacillus subtilis RNase P.* Biochemistry, 1998. **37**(28): p. 10126-33.
43. Loria, A. and T. Pan, *The cleavage step of ribonuclease P catalysis is determined by ribozyme-substrate interactions both distal and proximal to the cleavage site.* Biochemistry, 1999. **38**(27): p. 8612-20.
44. Koutmou, K.S., J.J. Day-Storms, and C.A. Fierke, *The RNR motif of B. subtilis RNase P protein interacts with both PRNA and pre-tRNA to stabilize an active conformer.* RNA, 2011. **17**(7): p. 1225-35.
45. Zahler, N.H., E.L. Christian, and M.E. Harris, *Recognition of the 5' leader of pre-tRNA substrates by the active site of ribonuclease P.* RNA, 2003. **9**(6): p. 734-45.
46. Christian, E.L., D.S. McPheeters, and M.E. Harris, *Identification of individual nucleotides in the bacterial ribonuclease P ribozyme adjacent to the pre-tRNA cleavage site by short-range photo-cross-linking.* Biochemistry, 1998. **37**(50): p. 17618-28.
47. Brannvall, M., et al., *RNase P RNA structure and cleavage reflect the primary structure of tRNA genes.* J Mol Biol, 1998. **283**(4): p. 771-83.
48. Lustbader, J.W., et al., *ABAD directly links Abeta to mitochondrial toxicity in Alzheimer's disease.* Science, 2004. **304**(5669): p. 448-52.
49. Gobert, A., et al., *Structural insights into protein-only RNase P complexed with tRNA.* Nat Commun, 2013. **4**: p. 1353.
50. Brzezniak, L.K., et al., *Involvement of human ELAC2 gene product in 3' end processing of mitochondrial tRNAs.* RNA Biol, 2011. **8**(4): p. 616-26.
51. Sugita, C., et al., *Molecular Characterization of Three PRORP Proteins in the Moss Physcomitrella patens: Nuclear PRORP Protein Is Not Essential for Moss Viability.* PLoS One, 2014. **9**(10): p. e108962.
52. Kobayashi, K., et al., *Identification and characterization of the RNA binding surface of the pentatricopeptide repeat protein.* Nucleic Acids Res, 2012. **40**(6): p. 2712-23.
53. Barkan, A., et al., *A combinatorial amino acid code for RNA recognition by pentatricopeptide repeat proteins.* PLoS Genet, 2012. **8**(8): p. e1002910.
54. Otwinowski, Z. and W. Minor, *Processing of X-ray diffraction data collected in oscillation mode.* Methods Enzymol, 1997. **276**: p. 307-26.
55. McCoy, A.J., et al., *Phaser crystallographic software.* J Appl Crystallogr, 2007. **40**(Pt 4): p. 658-674.
56. Adams, P.D., et al., *PHENIX: building new software for automated crystallographic structure determination.* Acta Crystallogr D Biol Crystallogr, 2002. **58**(Pt 11): p. 1948-54.
57. Murshudov, G.N., et al., *REFMAC5 for the refinement of macromolecular crystal structures.* Acta Crystallogr D Biol Crystallogr, 2011. **67**(Pt 4): p. 355-67.
58. Potterton, E., et al., *A graphical user interface to the CCP4 program suite.* Acta Crystallogr D Biol Crystallogr, 2003. **59**(Pt 7): p. 1131-7.
59. Emsley, P., et al., *Features and development of Coot.* Acta Crystallogr D Biol Crystallogr, 2010. **66**(Pt 4): p. 486-501.
60. Davis, I.W., et al., *MolProbity: all-atom contacts and structure validation for proteins and nucleic acids.* Nucleic Acids Res, 2007. **35**(Web Server issue): p. W375-83.
61. Schrodinger, *The PyMOL Molecular Graphics System, Version 1.4.* LLC, 2010.

62. Cole, J.L., et al., *Analytical ultracentrifugation: sedimentation velocity and sedimentation equilibrium.* Methods Cell Biol, 2008. **84**: p. 143-79.

CRYSTAL STRUCTURE OF INHIBITOR BOUND PROTEIN ONLY RNASE P 1

Agnes Karasik and Markos Koutmos

Author contributions: A.K. and M.K. designed crystallography experiments and analyzed data. A.K. crystallized PRORP1, performed soaking experiments, collected data and generated all figures.

Introduction

Protein specific inhibitors can be useful tools to understand protein function *in vivo* and *in vitro*. Besides their potential applications as research tools, they can also allow for development of therapeutic treatments. However, there are currently no known inhibitors for PRORP enzymes. Therefore, our collaborators (Dr. Carol Fierke's laboratory) used an adapted fluorescent polarization tRNA cleavage assay to screen a small molecule compound library (containing compounds extracted from microbes and pharmacologically active molecules) to find specific PRORP inhibitors (Nancy Wu et al, unpublished). In these biochemical assays two compounds were identified that are at least 50-fold more potent against *A.thaliana* PRORP1 and human mtRNase P relative to bacterial ribozyme RNase P. One of these compound hits, gambodic acid, a naturally occurring compound in some evergreens, is a rapidly binding uncompetitive inhibitor of PRORPs. The second identified compound, juglone (5-hydroxy-1,4-naphthalenedione) (Figure 1), is a toxic compound most prevalent in the plant family Juglandaceae (e.g. black walnut). In biochemical assays, juglone appears to be a time-dependent PRORP inhibitor. While initial kinetic characterization gave an initial insight into how these inhibitors act on

PRORPs, the molecular details of inhibition are still unknown; the inhibitor binding sites and the exact chemical mode of inhibition needs to be further clarified. In order to answer these questions I solved the crystal structures of juglone-PRORP complexes and identified several cysteine residues that juglone covalently modifies. My data not only convey the potential mechanism of action of this PRORP inhibitor but also provide with the first crystal structures of a protein modified by juglone.

Materials and Methods

Protein preparation. Recombinant *A. thaliana* PRORP1, in where the first 76 residues on the N terminus were truncated, was used in this study. Wild type and mutant PRORP1 were purified from *E. coli* as previously described [1] and the N-terminal His_6-tag was removed during the purification. Before crystallization purified PRORP1 was loaded onto a Sephacryl-200 gel-filtration column (GE Healthcare) that was pre-equilibrated with the dialysis buffer (20 mM MOPS pH=7.8, 150 mM NaCl, 1 mM TCEP). Protein was eluted at 1 mL/min and the A_{280} value was monitored. Peak fractions were analyzed by SDS-PAGE and coomassie blue stain. Protein concentrations were calculated as described in [1].

Crystallization, Data processing and Refinement. Δ76-PRORP1 crystals were grown in 0.1 M sodium citrate pH 5.5 and 18 % (w/v) PEG 3350 at 4 ˚C by the sitting drop method using a 2:1 ratio of protein to reservoir solution [1]. Δ76-PRORP1 crystals were soaked in reservoir solution (14% PEG 3,350, 0.08 M sodium citrate tribasic (pH 5.5)) containing a saturating amount of juglone (>10 μM) and incubated for 45 min, 3h, and overnight in the presence or absence of 50 mM $MnCl_2$ before harvesting. Harvested crystals were cryoprotected by soaking in 14% PEG 3,350,

0.08 M sodium citrate tribasic (pH 5.5), 20% (v/v) glycerol and 10 μM juglone for a few minutes prior to flash cooling in liquid N_2.

Diffraction data were collected on beamline GM/CA-CAT 23 ID-D and 23 ID-B with a Mar 300 CCD and a DECTRIS EIGER X 16M detectors respectively at Advanced Photon Source, Argonne National Laboratory (Argonne, IL). The data were processed with XDS and subsequently Phaser MR, in the CCP4 software package, was used to obtain a solution by molecular replacement [28-30]. Energy-minimized coordinates for juglone-cysteine conjugates were obtained by ProDrg webserver [2]. Refmac5 in the CCP4i suite was subsequently employed for restrained refinement, and model building and modification was performed with Coot [3, 4]. Crystallographic information and refinement statistics are provided in Table 1. The geometric quality of the model and its agreement with the structure factors were assessed with MolProbity [5]. Figures showing crystal structures were generated with PyMOL [6].

Results

Juglone covalently binds surface cysteines in PRORP1

To understand the molecular basis for time-dependent inhibition of PRORP1 by juglone, PRORP1 was crystallized as previously described [7] and subsequently soaked in juglone containing crystallization solutions. Crystallization conditions are essentially different than what was used in the biochemical assays, and therefore time dependence of juglone inhibition of PRORP could differ between the crystallographic experiments and the functional assays. Hence, I first optimized the time course of juglone-PRORP1 soaking experiments. I have co-incubated PRORP1 crystals and juglone for 45 minutes, 3 hours and overnight (~16 hours) before

harvesting and flash-freezing the crystals in liquid nitrogen. Upon soaking the crystals in juglone, that has yellow color in solution, transparent PRORP1 crystals turned dark yellow, indicating the presence of juglone in the crystals. For all different soaking times the resulting PRORP1 juglone soaked crystals diffracted between 1.8-2.2 Å and structures were solved by molecular replacement. In all solved structures, PRORP1 was covalently modified by juglone at C353, which is located in a solvent accessible, flexible region between the metallonuclease and zinc binding central domains making several stacking and polar interactions with surrounding side chains (Figure 2A and B). Observed electron densities for JCC353 (JCC = juglone-cysteine conjugate) indicated full occupancies for this site in all crystal structures (juglone B factors are comparable with B factors of nearby surrounding residues) (Figure 2B). While crystals exposed to juglone for 45 minutes were containing only one identifiable juglone binding site (C353, PDB ID: 6BV5), structures based on crystals soaked for 3 hours (PDB ID: 6BV6) contained two additional sites; JCC373 and JCC346, the electron density however for these sites indicated not fully occupied by JCC sites (Figure 3). JCC373 is found near the active site in the metallonuclease domain making several interactions with nearby amino acid side chains, whereas JCC346 is located next to C345, which coordinates a structural Zinc ion in the central domain. Besides the confirmation of the presence of JCC373 and JCC353, overnight soaking with juglone revealed an additional modification site in the PPR domain, at residue C222 (PDB ID: 6BV9). For modification sites JCC373 and JCC222 only partial juglone electron densities were observed in the overnight structure (Figure 3). Although PRORP1 crystal structures were solved in the presence of juglone and several binding sites were identified, it remained the question whether juglone could also bind to the active site when the catalytic metal

ions are present. Therefore, I have performed juglone-soaking experiments with PRORP1 in the presence of an active site metal, Mn^{2+}, to determine if juglone influences metal binding or if it binds directly to the metal thus directly affecting chemistry. I have found that presence of Mn^{2+} did not affect juglone binding to the previously identified sites and juglone was not present in the active site and therefore did not modify or influence metal or the active site environment (PDB ID: 6BV8).

Discussion

Juglone was found to be a potent inhibitor of PRORPs, acting in low molecular concentrations (IC_{50} = 1 μM, Nancy Wu et al., unpublished). While biochemical assays revealed that juglone is a time-dependent inhibitor of PRORPs, the exact mode of inhibition remained a question. Therefore, I employed X-ray crystallography to uncover the mode of inhibition of PRORP1 by juglone. I found that in several PRORP1-juglone structures juglone forms a covalent bond modifies any of four potential surface exposed cysteine residues in PRORP1.

Juglone, like other quinones, is a potent electrophile that reacts with thiol groups of cysteine residues in proteins [8, 9] similarly to my finding with PRORP1, even though there was no structural data available for this modification till now. A juglone-cysteine conjugate can form through a S-C covalent bond between either of C-2 or C-3 positions in juglone and the thiol group of the cysteine side chain [10]. In the PRORP-juglone crystal structures, based on our electron density conjugation between the C-3 of juglone and the cysteine side chain's thiol group was observed at all modified sites. Based on solution studies with small molecules, where H_2S is added to juglone, the relative susceptibility of C-2 and C-3 in juglone to nucleophilic attack by sulfur dependents on pH. C-2 is more susceptible to nucleophilic attack

than C-3 at pH < pKa through a “Michael addition” mechanism whereas the inverse was observed at pH > pKa proposed to proceed through a “radical” mechanism [10]. The juglone soakings in our experiments are performed under pH 5.5, which is well below the pK_a for a cysteine thiol, therefore C-2 juglone conjugation was to be expected. We however clearly observe only C-3 juglone indicating that in the protein environment the reactivity of cysteine sulfides towards juglone may differ slightly from what has proposed for small sulfur containing molecules. We propose that conjugation on the C-3 juglone position still proceeds through a modified Michael’s addition mechanism, however this still needs to be experimentally verified.

In PRORP1-juglone crystal structures altogether four juglone binding sites were identified that could potentially inhibit protein function. In all PRORP1-juglone crystal structures, C353 is found to form a conjugate with juglone. This residue is located at the flexible hinge between the metallonuclease and central domain. This flexible hinge could play a role in allowing the pre-tRNA substrate to be accommodated in its binding site by allowing PRORP1 to adopt a wider conformation that would fit the substrate (Chapter 2, Paper 1 and Paper 3). It is possible that modification of C353 by juglone influences the flexibility of this region, and therefore inhibits proper substrate binding by PRORP1. Another conjugation site was observed in two PRORP1-juglone structures; C373 is located in the metallonuclease domain near the active site, although it is unlikely that it influences the 5’ end cleavage directly, but may interfere with substrate binding. Two additional modification sites, C222 and C346, situated in the PPR and central domain, respectively, were found in only one crystal structure (overnight and 3 hour juglone soaked crystal structures, respectively). However, juglone-cysteine conjugates at these positions are not predicted to interfere with PRORP1 function based on the

crystal structure. In order to identify the functionally important juglone modification sites further studies are needed, such as mutagenesis of cysteine residues targeted by juglone conjoined by activity assays (ongoing project by our collaborators).

The other potent PRORP inhibitor in our collaborator's screen was gambodic acid (IC_{50} = 100 nM). However, this compound was found to be an uncompetitive inhibitor by biochemical assays that bind the enzyme-substrate complex (Nancy Wu et al, unpublished). Since crystallization of PRORP-pre-tRNA complex is not yet established, it is challenging to determine the inhibition site of gambodic acid and should be subject of further future examination.

Overall, here I present the first crystal structure of an inhibitor bound PRORP which is also a first crystal structure revealing the details of mode of protein inhibition by juglone. Juglone however is known to target and inhibit other proteins in the cell [8, 9] and therefore it is not a specific PRORP inhibitor. In order to find a potent and specific PRORP inhibitor modified juglones should be further tested in *in vitro* assays.

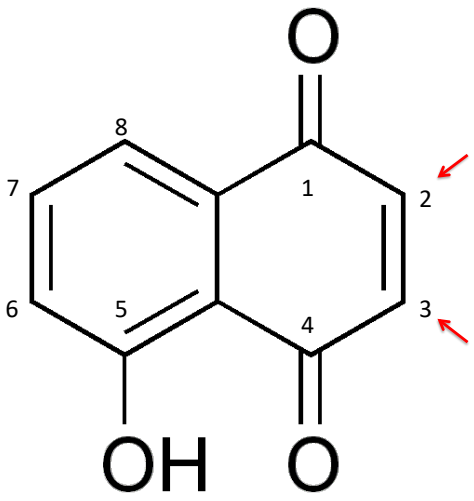


Figure 1. Chemical composition of juglone.
Red arrows indicate potential thiol conjugation sites.

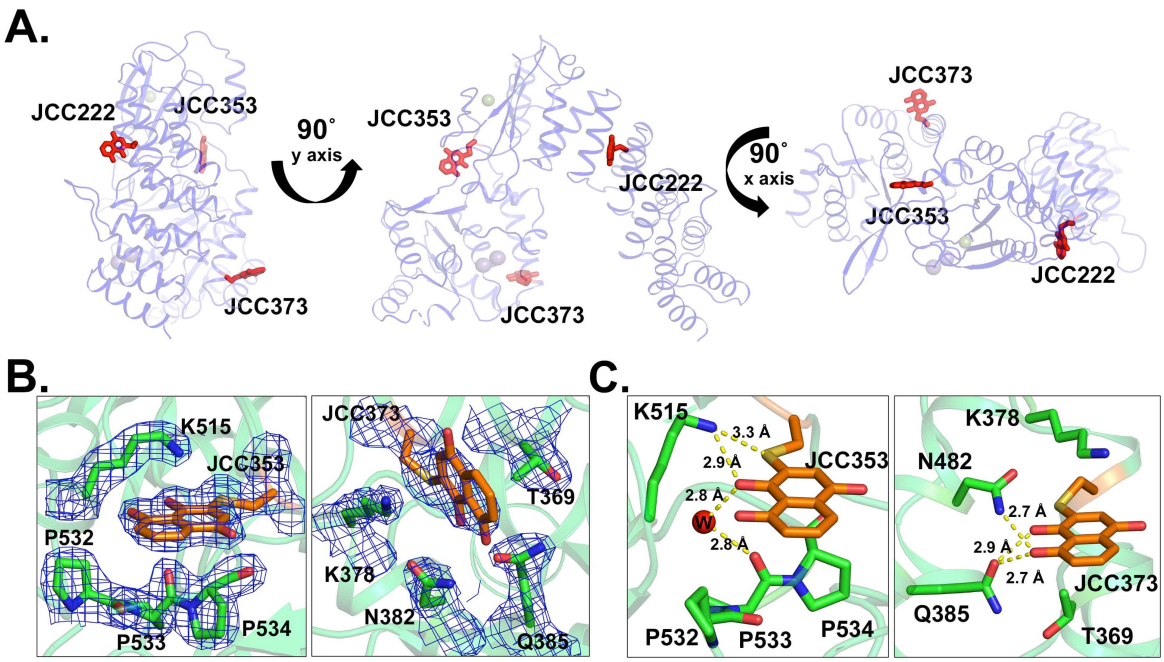


Figure 2. Crystal structure of PRORP1 in complex with juglone after overnight incubation. (**A**) PRORP1 makes a covalent interaction with juglone (red, JCC= juglone cysteine conjugate) through cysteine thiol side chains at C222, C353, and C373. Active site metals were modeled from a previously solved structure of WT PRORP1 with Mn^{2+} ions [1] shown as spheres. Electron densities (**B**) and interactions (**C**) of juglone-cysteine conjugates (JCC 353 and 373) with surrounding residues.

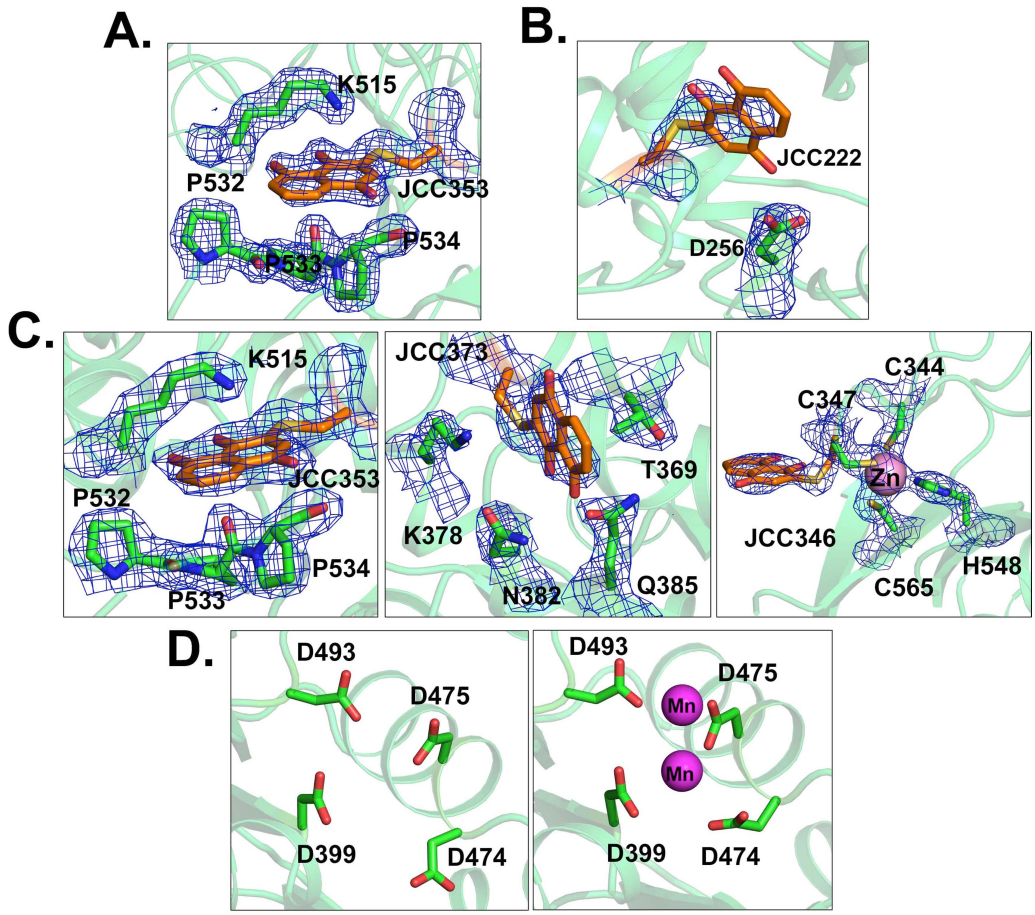


Figure 3.

A. Electron densities of residue JCC 353 and nearby amino acids in PRORP1 crystals soaked in juglone for 45 minutes (PDB ID: 6BV5). B. Electron densities of residue JCC 222 and nearby amino acid in PRORP1 crystals soaked in juglone for overnight (PDB ID: 6BV9). C. Electron densities of residues JCC 353, 373, 346 and nearby amino acids in PRORP1 crystals soaked in juglone for 3 hours (PDB ID: 6BV6). D. Active site residues of PRORP1 in the absence (first panel) and presence (second panel) of active site metal (Mn^{2+}) in 3 hours juglone soaked crystals (PDB IDs: 6BV8).

Table 1. X-Ray Crystallography Data Collection and Refinement Statistics

	PRORP1/Mn + Juglone (45 min soaks)	PRORP1 + Juglone (3 hour soaks)	PRORP1/Mn + Juglone (3 hour soaks)	PRORP1 + Juglone (overnight soak)
Data collection				
Beamline	APS, GMCA 23-IDD	APS, GMCA 23-IDD	APS, GMCA 23-IDD	APS, GMCA 23-IDB
Wavelength (Å)	1.0332	1.0332	1.0332	1.0332
Resolution (Å)	50.0-1.79 (1.83-1.79)	50.0-2.20 (2.26-2.20)	50.0-2.10 (2.16-2.10)	50.0-2.10 (2.16-2.10)
Space group	$P2_12_12_1$	$P2_12_12_1$	$P2_12_12_1$	$P2_12_12_1$
Cell dimensions (Å)	a = 41.6, b = 110.8, c = 140.7	a = 41.7, b = 112.2, c = 139.2	a = 41.7, b = 112.2, c = 139.2	a = 41.8, b = 111.8, c = 139.3
Cell dimensions (°)	α = β = γ = 90	α = β = γ = 90	α = β = γ = 90	α = β = γ = 90
R_{sym} (%)	3.6 (47.8)	4.0 (69.2)	4.8 (63.6)	5.5 (71.7)
<I/σ>	15.9 (1.9)	11.2 (2.1)	13.4 (1.6)	17.5 (2.2)
CC(1/2)	1.0 (0.75)	1.0 (0.74)	1.0 (0.56)	1.0 (0.75)
Multiplicity	3.7 (3.9)	3.4 (3.3)	3.5 (3.4)	6.7 (6.5)
Completeness (%)	99.1 (96.3)	98.1 (95.8)	99.2 (97.9)	100 (99.7)
Refinement				
Resolution range	87.1-1.79	87.3-2.20	87.0-2.10	87.2-2.10
Number of reflections (work/test set)	57980/3033	31891/1637	36554/1900	37078/1982
R_{work}/R_{free} (%)	19.6/22.3	20.6/23.6	20.0/24.7	19.6/24.2
No. of atoms				
Protein	3769*	3755*	3758*	3760*
Water	239	118	173	193
Modified Cysteines	19	57	38	57
Zn/Mn	1/1	1/0	1/2	1/0
B-factors ($Å^2$)				
Protein	48.4	59.0	59.2	62.4
Water	42.0	43.7	51.5	50.7
Modified Cysteines	53.2	77.5	71.0	78.4
Zn/Mn	39.7/32.0	45.8/na	52.8/63.2	51.3/na
Rmsd deviations				
Bond lengths (Å)	0.010	0.010	0.011	0.012
Bond angles (°)	1.28	1.35	1.39	1.45
Ramachandran plot				
E.s.d.s.[$]	0.111	0.228	0.191	0.183
Favored/allowed/outliers	98.3/1.7/0.0	97.8/2.0 /0.2	98.1/1.7/0.2	98.0/2.0/0.0
MolProbity Score	0.64 (100^{th} percentile)	0.93 (100^{th} percentile)	1.00 (100^{th} percentile)	0.97 (100^{th} percentile)
PDB	6BV5	6BV6	6BV8	6BV9

* not counting the modified cysteines

[$] E.s.d.s. = Estimated overall coordinate error

REFERENCES

1. Howard, M.J., et al., *Mitochondrial ribonuclease P structure provides insight into the evolution of catalytic strategies for precursor-tRNA 5′ processing.* PNAS, 2012. **109**(40): p. 16149-16154.
2. Schuttelkopf, A.W. and D.M.F. van Aalten, *PRODRG: a tool for high-throughput crystallography of protein-ligand complexes.* Acta Crystallographica Section D, 2004. **60**(8): p. 1355-1363.
3. Murshudov, G.N., et al., *REFMAC5 for the refinement of macromolecular crystal structures.* Acta Crystallographica Section D, 2011. **67**(4): p. 355-367.
4. Emsley, P., et al., *Features and development of Coot.* Acta Crystallographica Section D, 2010. **66**(4): p. 486-501.
5. Davis, I.W., et al., *MolProbity: all-atom contacts and structure validation for proteins and nucleic acids.* Nucleic Acids Research, 2007. **35**(suppl_2): p. W375-W383.
6. Delano, W.L. *The PyMOL Molecular Graphics System, Version 1.4 (Shrödinger, LLC, Porland, OR)*. 2002; Available from: http://www.pymol.org.
7. Howard, M.J., et al., *Mitochondrial ribonuclease P structure provides insight into the evolution of catalytic strategies for precursor-tRNA 5′ processing.* Proc Natl Acad Sci U S A, 2012. **109**(40): p. 16149-54.
8. Fila, C., C. Metz, and P. van der Sluijs, *Juglone inactivates cysteine-rich proteins required for progression through mitosis.* J Biol Chem, 2008. **283**(31): p. 21714-24.
9. Chao, S.H., A.L. Greenleaf, and D.H. Price, *Juglone, an inhibitor of the peptidyl-prolyl isomerase Pin1, also directly blocks transcription.* Nucleic Acids Res, 2001. **29**(3): p. 767-73.
10. Perlinger, J.A., et al., *Addition of Hydrogen Sulfide to Juglone.* Environmental Science & Technology, 2002. **36**(12): p. 2663-2669.

CHAPTER 3: Precursor tRNA binding, processing and methylation by human mtRNase P and its connection to diseases

MANUSCRIPT 1: INTERPLAY BETWEEN SUBSTRATE RECOGNITION, 5'END PROCESSING AND METHYLATION ACTIVITY OF HUMAN MITOCHONDRIAL RNASE P

Agnes Karasik[1], Carol A. Fierke[2], Markos Koutmos[3*]

[1]Department of Biochemistry and Molecular Biology, Uniformed Services University of the Health Sciences, Bethesda, MD, 20814, USA

[2]Department of Chemistry, Department of Biological Chemistry, University of Michigan, Ann Arbor, MI 48109, USA

[3]Department of Chemistry, Program in Biophysics, University of Michigan, Ann Arbor, MI, 48109, USA

*Corresponding author (mkoutmos@umich.edu, Tel: 734 936-2678)

Author contributions: A.K. designed and executed all experiments, A.K., C.A.F and M.K. wrote and edited the manuscript. A.K. generated data for all figures and tables.

Abstract

Human mitochondrial ribonuclease P (mtRNase P) is an essential three protein complex that catalyzes the 5' end maturation of mitochondrial precursor tRNAs (pre-tRNAs). MRPP3 (Mitochondrial RNase P Protein 3), a protein-only RNase P (PRORP), is the nuclease component of the mtRNase P complex and requires a two-protein S-adenosyl methionine (SAM)-dependent methyltransferase MRPP1/2 sub-complex to function. Dysfunction of mtRNase P is linked to several human mitochondrial diseases. Despite its central role in mitochondrial RNA processing, little is known about how the protein subunits of mtRNase P function synergistically. Here we use purified mtRNase P to demonstrate that mtRNase P recognizes, cleaves, and methylates some, but not all, mitochondrial pre-tRNAs *in vitro*. Additionally, mtRNase P does not process all mitochondrial pre-tRNAs uniformly, suggesting the possibility that some pre-tRNAs require additional factors to be cleaved *in vivo*. Consistent with this, we found that addition of the MRPP1 co-factor SAM enhances the ability of mtRNase P to bind and cleave some of mitochondrial pre-tRNAs. Furthermore, the presence of MRPP3 can enhance the methylation activity of MRPP1/2. Taken together, our data demonstrate that the subunits of mtRNase P work together to efficiently recognize, process and methylate human mitochondrial pre-tRNAs.

Introduction

Ribonuclease P (RNase P) catalyzes one of the first steps in tRNA maturation, the removal of the 5' leader sequences from precursor tRNAs (pre-tRNAs). There are two classes of evolutionarily distinct RNase Ps: RNA-based (ribozyme) and protein-based enzymes. RNase P is essential wherever pre-tRNAs are transcribed and is present in the nucleus, mitochondria and chloroplasts of cells. The protein-only form of RNase P was first identified in human mitochondria and consists of three subunits: Mitochondrial RNase P Protein 1

(MRPP1, TRM10C), Mitochondrial RNase P Protein 2 (MRPP2, 17β-hydroxysteroid dehydrogenase type 1, SDR5C1), and Mitochondrial RNase P Protein 3 (MRPP3, catalytic nuclease subunit) [1-3]. Subsequently, Protein-Only RNase Ps (PRORPs) have been discovered in some land plants, (e.g. *Arabidopsis thaliana* [3, 4]) and other unicellular Eukaryotic organisms (e.g. *Trypanosoma bruceii* [2]). In contrast to human mtRNase P, PRORPs are stand-alone enzymes that do not require accessory protein partners. Most studies of protein-based RNase Ps have focused on PRORPs because these enzymes are homologous to MRPP3 and provide a tractable system for study [3-10]. As a consequence, little is known about how the components of the metazoan mtRNase P complex function.

In mitochondria, RNAs are transcribed in polycistronic units. In each polycistronic unit most protein coding and rRNA transcripts are separated (or 'punctuated') by tRNAs. Therefore 5' end and 3' end tRNA processing are required for the processing of most key mitochondrial RNAs [11]. 5' end cleavage by mtRNase P has been suggested to be the first step in the hierarchical tRNA processing in mitochondria [12, 13]. More than 50% of mitochondrial disease-causing mutations in the mitochondrial genome are found in tRNA genes [14]. Since precursor tRNA processing is likely the first step in the mitochondrial tRNA maturation pathway, disabling this function leads to accumulation of mitochondrial precursor tRNAs along with unprocessed RNA transcripts [15, 16]. This affects downstream processes such as mitochondrial ribosome assembly and translation with detrimental effects on mitochondrial function and viability. It was therefore predicted that mitochondrial 5' end processing plays a role in mitochondrial diseases. Consistent with this, mtRNase P dysfunction is linked to several mitochondrial diseases including maternally inherited essential hypertension [17], mitochondrial myopathy [18, 19], MELAS [20], and HSD10-disease[21-24].

All three subunits of mtRNase P are strictly required *in vivo*; knockout of any component in flies leads to larval lethality [15]. Similarly, knock-out of the MRPP3 gene in mice arrests embryogenesis at a very early stage [16]. Furthermore, mice containing a conditional knock-out of MRPP3 develop cardiomyopathy, show signs of mitochondrial dysfunction, and exhibit severe defects in 5' end RNA processing [16]. MRPP3 has also been shown to further influence tRNA modifications, for example a missense mutation in MRPP3 was identified as an important factor responsible for differences in mitochondrial tRNA methylation patterns amongst individuals [25]. Thus, correct mtRNase P function is likely to be essential for human health.

Little is known about the structure and function of the mtRNase P complex; there are no structures or structural models available, and limited mechanistic and biochemical information, although structures of truncated MRPP3 have been solved [7, 9, 26, 27]. As such, the role of the interaction between MRPP3 and the MRPP1/2 sub-complex in enhancing substrate binding and catalysis is a key question in the function of human mtRNase P [1]. The MRPP1/2 sub-complex has been predicted to methylate the N1 of adenine or guanine residues at the 9^{th} position of 19 mitochondrial tRNAs [28]. Previous reports indicate that this methylation activity is dispensable for the cleavage of pre-tRNAs by human mtRNase P [28]. MRPP1 is the S-adenosyl-methionine (SAM) dependent methyltransferase subunit in the MRPP1/2 sub-complex, and MRPP2 likely acts as a scaffold protein [28].

Here we investigate how MRPP1, MRPP2, and MRPP3 work together to recognize and cleave pre-tRNA substrates. Our work with recombinant mtRNase P reveals that the complex can specifically bind, process and methylate several human mitochondrial pre-tRNAs, which are not recognized and processed by single-subunit plant PRORPs. Additionally, a subset of human mitochondrial pre-tRNA substrates are not processed efficiently by the recombinant mtRNase P complex suggesting that additional components or

modifications may be required to facilitate the cleavage of these substrates. We further demonstrate that the MRPP1 cofactor SAM enhances the ability of the mtRNase P complex to bind and cleave some substrates. Overall, our studies provide the first insight into how the components of mtRNase P synergistically act to bind, process and methylate human mitochondrial pre-tRNAs.

Materials and Methods

***In vitro* transcription and 5' end labeling of pre-tRNAs.** Pre-tRNAs were prepared as previously described [7, 9]. To label the 5' end of tRNA with fluorescein, the ~200 µL *in vitro* transcribed pre-tRNA was incubated overnight with 20 µl 45 mM fluorescein at 37 ˚C and purified on a 12% urea-polyacrylamide gel. After gel purification, pre-tRNAs were ethanol precipitated and the resulting pellet was re-suspended in RNase free H_2O. The concentrations of total and labeled pre-tRNA were measured from absorbance readings at 260 nm using a Nanodrop (Thermo Scientific) spectrophotometer using the following extinction coefficients: 909,100 cm^{-1} mol^{-1} for (mt)pre-$tRNA^{Ile7:0}$, 927,300 cm^{-1} mol^{-1} for (mt)pre-$tRNA^{Leu6:0}$, 848,600 cm^{-1} mol^{-1} for (mt)pre-$tRNA^{Val7:0}$, 838,200 cm^{-1} mol^{-1} for (mt)pre-$tRNA^{Met6:0}$, 848,600 cm^{-1} mol^{-1} for (mt)pre-$tRNA^{Ser(UCN)7:0}$, 737,900 cm^{-1} mol^{-1} for (mt)pre-$tRNA^{Ser(AGY)7:0}$.

Protein expression and purification. His_6-Δ95 MRPP3 was cloned into pMCSG7 vector and transformed into *E. coli* BL21(DE3) cells. Transformed bacteria were grown overnight (5 mL LB media, 100 µg/ml ampicillin, 37 ˚C (220 rpm)), and used to inoculate 500 mL of TB media with 50 µg/ml ampicillin. Cultures were grown at 37^{o}C to an OD ~0.8-1.0, then shifted to 18 ˚C for 1 hour. 200 µM of final concentration of Isopropyl β-D-1 thiogalactopyranoside (IPTG) was added to induce protein expression and the culture was grown overnight (~16

hours) at 18 ˚C, 220 rpm. Bacterial cells were collected by centrifugation (10,000 x g, 15 minutes), re-suspended in lysis buffer (20 mM MOPS pH 7.8, 1 M NaCl, 1 mM TCEP, 0.2 % Tween, 0.1 mg/ml lysozyme and 0.1 mg/ml phenylmethylsulfonyl fluoride).
Cells were lysed by sonication, and the resulting suspension was centrifuged at 34,000 x g at 4˚C for 1 hour. The supernatant was loaded onto a HisTrap (GE Healthcare) nickel column and protein was eluted with 500 mM imidazole, 20 mM MOPS pH 7.8, 100 mM NaCl and 1 mM TCEP. The purified Δ95 MRPP3 was dialyzed against 20 mM MOPS pH 7.8, 150 mM NaCl, 1 mM TCEP and 15 % glycerol overnight at 4 ˚C and incubated with TEV protease (1:20 protein:TEV protease ratio) to remove the His tag. His_6-TEV protease was removed by running the sample through a HisTrap nickel column. Δ95 MRPP3 was then dialyzed against 20 mM MOPS pH 7.8, 1 mM TCEP, 150 mM NaCl and 2 mM EDTA overnight at 4 ˚C to remove any possible metal contamination, followed by buffer exchange with 20 mM MOPS pH 7.8, 1 mM TCEP and 150 mM NaCl using a desalting column (BioRad). Protein concentration was measured using a Nano spectrophotometer (Thermo scientific) with molecular weight and extinction coefficient values of 56.4 kDa and 82500 cm^{-1} mol^{-1}, respectively.

Full length MRPP2 and His_6-Δ40 MRPP1 were cloned into a pCDFDuet-1 (Novagen) vector for co-expression (Liu et al, submitted in conjunction with this manuscript). The MRPP1 N-terminal deletion corresponds to the predicted mitochondrial targeting sequence. Initial steps for protein expression and purification, including nickel column purification, histidine tag and TEV removal are identical to those detailed above for Δ95MRPP3, with the following exceptions: the antibiotic used was streptomycin (50 μg/ml) and 10% glycerol was added to each purification buffer. The resulting Δ40MRPP1/MRPP2 sub-complex was further purified by size exclusion chromatography in 20 mM MOPS pH 7.8, 1 mM TCEP, 100 mM NaCl and 10 % glycerol. Final protein samples were concentrated to 2-4 mg/ml. The

ratio of the MRPP1 and MRPP2 proteins in the sub-complex was determined to be 1:4 based on analytical ultracentrifugation experiments (Liu et al, submitted in conjunction with this manuscript). Therefore, protein concentration was measured based on molecular weight and extinction coefficient values of 149 kDa and 79520 cm^{-1} mol^{-1}. *A. thaliana* PRORP1 and PRORP2 were expressed and purified from *E. coli* as previously described [7, 9].

5' end cleavage single turnover cleavage assays. (mt)pre-tRNA substrates were re-folded prior to each cleavage reaction. First, pre-tRNAs in water were heated at 95 ˚C for 3 minutes. Samples were then cooled down to room temperature (~10-15 minutes). Cleavage reaction buffer (final: 30 mM MOPS pH 7.8, 150 mM NaCl, 1 mM $MgCl_2$, 1 mM DTT) was added and (mt)pre-tRNAs were further incubated for 30 min at room temperature. All single turnover reactions were performed in the cleavage reaction buffer at 28 ˚C. To initiate a reaction, a mixture of 500 nM Δ40 MRPP1/MRPP2 complex and variable concentrations (100 nM - 2 μM) of Δ95 MRPP3 in cleavage reaction buffer were added to 20 nM fluorescently labeled pre-tRNA. Changes in fluorescent polarization were followed at 28 ˚C using a ClarioStar plate reader (BMG LabTech). In these assays we found that the changes in anisotropy observed in the presence of the MRPP1/2 sub-complex and MRPP3 in isolation are small (<1-10%) relative to the significant changes in anisotropy due to cleavage catalyzed by the mtRNase P complex and as such do not impact the rate constants that we measure (Figure 3A). The results of our fluorescence polarization kinetic assays were verified using traditional gel-based cleavage assays. For gel-based assays, various time points were obtained by quenching the reaction with the addition of 0.05 % Bromo-Phenol-Blue, 0.05 % Xylene Cyanol dye, 50 % m/v urea and 0.1 M EDTA. The resulting samples were fractionated on a polyacrylamide-urea gel (12-20%) and visualized by direct scanning on a Storm 860 imager. Densitometry was performed with ImageQuant. Data from at least three independent

experiments were analyzed using Kaleidagraph 4.1.3. Eq 1. was fit to the data to calculate the observed rate constant (k) and the standard error where A is the endpoint, B is the amplitude, and t is the time.

Eq 1. $$\text{Fraction cleaved} = A - B*e^{-kt}$$

Fluorescent polarization binding assays. Binding assays were performed in 30 mM MOPS pH 7.8, 150 mM NaCl, 6 mM $CaCl_2$, 1 mM DTT at 28 ˚C and 20 nM of 5' fluorescein labeled and folded (mt)pre-tRNA. The (mt)pre-tRNA substrates were incubated with increasing concentrations (0-50 μM) of Δ95MRPP3 or MRPP1/2 (0-2 μM) for 5 minutes before changes in anisotropy were measured with ClarioStar plate reader (BMG LabTech). 20 nM fluorescent pre-tRNA (Fl-pre-tRNA) was titrated by adding increasing concentrations (0-50 μM) of Δ95MRPP3 in the presence of 150 nM Δ40 MRPP1/MRPP2. In some experiments, 25 μM SAM was added to Δ40 MRPP1/MRPP2 and Fl-(mt)pre-tRNA and incubated for 5 minutes before the addition of MRPP3. Basal anisotropy values measured in the absence of the protein but presence of the Fl-pre-tRNA were extracted from measured values. The dissociation constant (K_D) for PRORPs and apparent dissociation constant ($K_{D,app}$) for MRPP1/MRPP2 and mtRNase P and the standard errors were calculated by fitting a binding isotherm (Eq. 2) to the fluorescence polarization data from at least three independent experiments using Kaleidagraph 4.1.3 software. In Eq 2, A is the observed anisotropy, A_o is the initial anisotropy, ΔA is the total change in anisotropy, P is the concentration of MRPP3, and $K_{D,app}$ is the dissociation constant.

Eq 2. $$A = A_0 + \frac{\Delta A\,[P]}{[P]+[K_{D,app}]}$$

Primer extension methylation assays. Pre-tRNA was folded as described above before each experiment. Methylation reactions were initiated by mixing the fluorescently labeled

pre-tRNA and Δ40MRPP1/MRPP2 to final concentrations of 800 nM of and 5 μM, respectively, in 30 mM MOPS pH 7.8, 150 mM NaCl, 1 mM $CaCl_2$ and 1 mM DTT at 28 ˚C. To terminate the methylation reaction, 2 μL of enzyme-pre-tRNA reaction mixture was removed, incubated at 95 ˚C for 30 seconds and then placed on ice. Annealing reactions for primer extensions were set up as follows for each quenched time point. A final volume of a 5 μl annealing reaction contained 1 μl of a quenched methylation reaction time point, and 2 μM of fluorescently labeled primers in 50 mM Tris-HCl (pH 8.1), 30 mM NaCl, and 10 mM DTT. Annealing primer sequences were designed against the anticodon loop for (mt)pre-$tRNA^{Ile}$, (mt)pre-$tRNA^{Leu}$, (mt)pre-$tRNA^{Val}$ and (mt)pre-$tRNA^{Met}$ (6-FAM-CTATTATTTACTCTATC; 6-FAM-CCTCTGACTGTAAAG; 6-FAM-CCTAAGTGTAAGTTGGG; and 6-FAM-CGGGGTATGGGCCCG, respectively). Next, annealing reaction mixtures were incubated at 95˚C for 3 minutes followed by cool down to 37˚C for 10-15 minutes. As a control, previously folded pre-tRNA was used that was not incubated with the enzymes. 2 μl of annealed primer/(mt)pre-tRNA mixture was added to a final volume of 5 μl reverse transcriptase reaction mixture containing 0.7 U of AMV-Reverse transcriptase (Promega), 1× AMV-RT reaction buffer (Promega) and 0.5 mM dNTP. The reverse transcription reactions were incubated for 1 hour at 37 ˚C and were subsequently quenched with an equal amount of 0.05 % Bromo-Phenol-Blue, 0.05 % Xylene Cyanol dye, 50 % m/v urea, 0.1 M EDTA and run on 12 % polyacrylamide gel. The gels were scanned in a Storm 860 imager and results were evaluated by densitometry (ImageQuant). As a negative control, we substituted S-adenosyl homocysteine (SAH) for SAM. SAH mimics SAM but lacks the methyl group that is required for the methylation reaction carried out by MRPP1/2. As expected, we did not observe any stops due to methylation in the presence of SAH (Figure 4C-E). Data from at least three independent experiments were analyzed using Kaleidagraph

4.1.3. Eq 1. was fit to the data to calculate the single turnover rate constants ($k_{obs,\ m}$) and the standard error.

Results

mtRNase P binds mitochondrial precursor-tRNAs non-uniformly

Although the human mtRNase P complex was discovered almost a decade ago, it is largely unknown how it recognizes and binds its mitochondrial substrates [1]. The pool of native mtRNase P substrates is diverse; in human mitochondria there are four subtypes of tRNAs (Type 0-III). The (mt)tRNAs belonging to types I, II, and III all differ from the canonical cloverleaf secondary structure of nuclear tRNAs [29, 30]. We selected six mitochondrial pre-tRNA ((mt)pre-tRNAs) substrates to study representatives of all four classes including a substrate ((mt)pre-tRNA$^{Ser(AGY)}$) that human mtRNase P is not proposed to process *in vivo* [31] (Figure 1). We used our knowledge of *A. thaliana* single subunit PRORP enzymes that are homologous to MRPP3 to design the 5' and 3' ends of our (mt)pre-tRNA substrates. PRORPs preferentially bind substrates with short (< 5-8 nucleotide) 5' leaders and do not bind the overhanging 3' end of pre-tRNAs [7]. Thus, the (mt)pre-tRNA substrates studied here possess 6-7 nucleotide long 5' leader sequences and lack mature 3' CCA ends (Figure 1).

To determine how each component of the mtRNase P complex interacts with (mt)pre-tRNAs we measured the binding constant ($K_{D\ or}\ K_{Dapp}$) for the mtRNaseP complex components (MRPP1/2 sub-complex and MRPP3) and six (mt)pre-tRNAs of interest using fluorescent anisotropy. We find that the isolated mtRNase P components generally do not associate tightly with the selected substrates (Table 1, Figure 2A and B). MRPP3 alone binds all of the (mt)pre-tRNAs substrates weakly with K_D values > 4 μM (Table 1 and Figure 2A). The MRPP1/2 sub-complex similarly binds most substrates weakly ($K_{D,app}$ > 2 μM) with the

exception of (mt)pre-tRNA^{Ile} and (mt)pre-tRNASer^{UCN}, which it binds more tightly ($K_{D,app}$ values of 104 ± 24 nM and 730 ± 196 nM, respectively) (Table 1, Figure 2B).

We next sought to establish how the fully-reconstituted mtRNase P complex (MRPP1/2:3) interacts with (mt)pre-tRNA substrates. We measured the apparent dissociation constant ($K_{D,app}$) for the substrates binding to the complex using our fluorescence anisotropy binding assay. For these assays, first we incubated pre-folded (mt)pre-tRNAs with 150 nM MRPP1/2. After MRPP1/2 and pre-tRNA binding reached equilibrium (5 minutes) we added varying concentrations of MRPP3 (0-10 μM, Figure C and D) and measured additional changes in fluorescent anisotropy. In general, we find that the presence of the MRPP1/2 sub-complex enhances (mt)pre-tRNA binding by 3 to 330-fold over binding to MRPP3 alone (Figure 2C and D), as also observed for *B. subtilis* pre-tRNA^{Asp} (Liu et al, submitted in conjunction with this manuscript) . However, these enhancements are not uniform. The substrates fall into two categories: those that bind the complex somewhat tighter than MRPP3 alone (3-5 fold: (mt)pre-tRNA^{Val}, (mt)pre-tRNASer^{UCN}, (mt)pre-tRNA^{AGY}) and those that bind the complex significantly tighter (30-330 fold: (mt)pre-tRNA^{Leu}, (mt)pre-tRNA^{Ile}, (mt)pre-tRNA^{Met}). As anticipated, the substrate that binds the weakest is (mt)pre-tRNASer^{AGY}, which was not expected to be processed by mtRNase P. Notably, the mtRNase P complex exhibits the tightest $K_{D,app}$ (13.5 ± 2.33 nM) for (mt)pre-tRNA^{Ile}. These results indicate that while a subset of human (mt)pre-tRNAs are recognized with high affinity by mtRNase P ($K_{D,app}$ values are in the nanomolar range), there are other (mt)pre-tRNAs that have weaker afffinity ($K_{D,app}$ values in the micromolar range) and may require additional factors or modifications to bind tightly to mtRNase P.

To compare the substrate selectivity of human mtRNase P complex with single component PRORPs we tested the ability of *A. thaliana* PRORP1 and PRORP2 to bind our six human (mt)pre-tRNA substrates using fluorescent anisotropy binding assays. We find that

only (mt)pre-tRNA$^{Ser(UCN)}$ binds to PRORP1 and 2 with a comparable K_D value (60-120 nM) to that of their native *A. thaliana* substrates, all other (mt)pre-tRNAs were bound at least 7-fold less tightly (K_D = 880 nM to > 10 μM) Figure 2E, Supplement Table 1). Thus, the mtRNase P complex uses strategies or interactions for recognizing its substrates that are different from the single-component PRORP1 and 2 enzymes.

mtRNase P exhibits 5' end processing of tightly bound (mt)pre-tRNAs

To further understand mtRNaseP substrate selectivity we measured single turnover cleavage rate constants for the six (mt)pre-tRNAs discussed above (Figure 1). Previously, we used fluorescent polarization-based multiple turnover assays for monitoring pre-tRNA 5' end cleavage by RNA-based and single-component protein only RNase Ps (*A. thaliana* PRORPs)[10, 32]. Here, we adapted this method to monitor the cleavage of 5'-fluorescein labeled (mt)pre-tRNAs by the fully-reconstituted human mtRNase P complex in single turnover cleavage assays. We measured the single turnover rate constants (k_{obs}) and $K_{1/2}^{MRPP3}$ values for mtRNaseP using limiting substrate (20 nM fluorescent pre-tRNA) and range (100 nM- 2 μM) of MRPP3 concentrations at 28 ˚C while MRPP1/2 concentration was maintained constant (Figure 3A and B, Supplement Figure 1B).

All of the (mt)pre-tRNAs that bind with high affinity to the mtRNase P complex ((mt)pre-tRNA^{Leu}, (mt)pre-tRNA^{Ile}, (mt)pre-tRNA^{Met}) have $K_{1/2}^{MRPP3}$ values (ranging from 400 ± 85 nM to 1000 ± 300 nM) greater than the measured binding affinities ($K_{D,app}$ values in $CaCl_2$), suggesting that under STO conditions $K_{1/2}^{MRPP3}$ does not reflect a thermodynamic binding equilibrium. The k_{obs} values for these substrates are between 0.007-0.014 sec^{-1} (Figure 3C, Table 2) and correlate well with rate constants previously measured for single-subunit PRORPs cleaving their native substrates [7, 10, 33]. In contrast, (mt)pre-tRNAs that have low affinities for mtRNase P ((mt)pre-tRNA^{Val}, (mt)pre-tRNASer^{UCN}, (mt)pre-

tRNA^{AGY})) exhibit ~ 10-fold lower single turnover activity (k_{obs} ~0.0008 sec^{-1}) (Figure 3C and Table 2); the cleavage of these substrates was so slow that we were unable to accurately measure $K_{1/2}^{MRPP3}$ values. Our findings suggest that recognition of unmodified human mitochondrial pre-tRNAs is likely to be an important determinant for efficient 5' end cleavage of pre-tRNA catalyzed by mtRNase P.

As mentioned earlier, we find that most human mitochondrial pre-tRNAs are not bound tightly by *A. thaliana* PRORP1 and PRORP2, therefore we sought to address whether cleavage catalyzed by PRORP1 and 2, as measured by single turnover reaction rates, is also slow for these substrates. In good agreement with our binding data, PRORP1 and PRORP2 processed most human (mt)pre-tRNAs with single turnover rates more than 10-fold slower than that of mtRNase P, except for pre-tRNA^{SerUCN} (Figure 3D, Supplement Table 1). pre-tRNA^{SerUCN} is not processed efficiently by the mtRNase P but is cleaved by PRORP1 and 2 with single turnover rate constants comparable to that of their native substrates (~0.005-0.012 sec^{-1}) (Figure 3D, Supplement Table 1.). Together with our binding data this suggests that human mitochondrial pre-tRNAs are recognized differently by *A. thaliana* PRORPs and human mtRNase P.

MRPP3 can enhance the methylation activity of the MRPP1/2 sub-complex

The MRPP1/2 sub-complex was previously shown to methylate *in vitro* transcribed human (mt)pre-tRNAs [28, 34]. Here we aimed to measure the single turnover rate constants for MRPP1/2 catalyzing methylation of (mt)pre-tRNAs containing potential m1A9/m1G9 modification sites ((mt)pre-tRNA^{Ile}, (mt)pre-tRNA^{Leu} and (mt)pre-tRNA^{Val}) (Figure 1, Figure 4A). To determine the rate of methylation we developed fluorescent primer extension assays for the mtRNase P complex (described in materials and methods, Figure 4B). Additionally, we also assessed if the presence of MRPP3 modulates MRPP1/2 methylation activity. Our

data demonstrate that the single turnover rate constants ($k_{obs,meth}$) for methylation of (mt)pre-tRNA^{Ile} are 0.0022 ± 0.0003 sec^{-1} catalyzed by saturating MRPP1/2 concentrations and that the addition of MRPP3 does not alter the $k_{obs,meth}$ value for this substrate (Figure 4C and F). In contrast, methylation rates for (mt)pre-tRNA$^{Leu\ (UUR)}$ are a modest 2-fold higher when MRPP3 is present (Figure 4D and F) (0.0013 ± 0.0002 sec^{-1} in the absence and 0.0025 ± 0.0005 sec^{-1} in the presence of MRPP3). This indicates that MRRP3 may also affect the methylation rates of other mitochondrial substrates. MRPP1/2 also catalyzed methylation of (mt)-pre-tRNA^{Val}, however the rates are significantly slower ($k_{obs,meth}$ < 0.00008 sec^{-1}) compared to the other two pre-tRNA substrates suggesting that there are differences in how MRPP1/2 binds and methylates each pre-tRNA substrate (Figure 4E).

SAM is required for mtRNase P to efficiently bind and process some human mitochondrial pre-tRNAs

As discussed above, we found that some human mitochondrial pre-tRNAs are not efficient substrates for the reconstituted mtRNase P complex *in vitro*. However, *in vivo* RNA sequencing experiments suggest that most mitochondrial tRNAs are processed by the mtRNase P complex, including (mt)pre-tRNA^{Val} and (mt)pre-tRNASer^{UCN} [16]. This led us to consider whether some substrates, such as (mt)pre-tRNA^{Val} and (mt)pre-tRNASer^{UCN}, might require either additional modification steps prior to mtRNase P cleavage, or additional co-factors, such as a protein or small molecule.

As a first step, we investigated if the presence of the methyl donor, SAM, affects the binding affinity of the six (mt)pre-tRNAs used in this study (Figure 1.) We added a high concentration of SAM (25 μM) to our fluorescent anisotropy binding assays and measured (mt)pre-tRNAs binding affinities for the MRPP1/2 and mtRNase P complexes. We find that the presence of SAM enhances the binding affinity of (mt)pre-tRNA^{Val} for both the MRPP1/2 and the mtRNase P complexes by 15-fold (Figure 5A and B, Supplement table 2). Next, we

determined if this effect is due to the presence of SAM or methylation of the m1A9 site of (mt)pre-tRNA^{Val}. We first measured the (mt)pre-tRNA^{Val} binding affinities for MRPP1/2 and mtRNase P in the presence of the SAM analog, SAH, demonstrating an ~6-fold decrease in $K_{D,app}$ (Figure 5A and B, Supplement table 2). To further examine whether methylation is required for the increased binding affinity, we generated and measured the $K_{D,app}$ of MRPP1/2 and mtRNase P for a methylation site mutant of (mt)pre-tRNA^{Val} ((mt)pre-tRNA$^{Val/C9}$). The addition of either SAM or SAH enhance the binding affinity of the (mt)pre-tRNA$^{Val/C9}$ mutant to the same extent as the wild-type substrate (Figure 5A and B, Supplement table 2). This suggests that the presence of SAM, but not methylation, is important for (mt)pre-tRNA^{Val} substrate recognition.

In addition, we find that (mt)pre-tRNA$^{Leu(UUR)}$ binds the MRPP1/2 complex ~4-5-times tighter in the presence of SAM and SAH (Figure 5A), similar to (mt)pre-tRNA^{Val}. However, binding affinities for mtRNase P or MRPP1/2 sub-complex for the remaining four substrates are not significantly altered in the presence of SAM (Supplement Figure 3).

We next investigated if the presence of SAM and SAH impact the ability of mtRNase P to cleave the 5' end of (mt)pre-tRNAs. We find that the single turnover rate constants for the 5' end cleavage of (mt)pre-tRNA^{Val} by mtRNase P is increased by 3 to 7-fold in the presence of SAH or SAM, respectively (Figure 5C, Supplement Table 2). Moreover, the single turnover methylation rates for (mt)pre-tRNA$^{Val/C9}$ catalyzed by mtRNase P exhibit a similar pattern (Figure 5C, Supplement Table 2). Despite this rate enhancement, it is noteworthy that the rate constant for the processing of (mt)pre-tRNA^{Val} is still 4 times slower than the other investigated (mt)pre-tRNAs. Addition of SAM or SAH did not enhance the single-turnover rate constants for any of the other (mt)pre-tRNAs that we investigated (Supplemental table 3). Our results demonstrate that SAM increases the binding efficiency and 5' end processing catalyzed by mtRNase P for a subset of (mt)pre-tRNAs.

Discussion

Given the essential nature of human mtRNase P and its direct link to disease it is important to understand how this protein complex functions. Despite its importance it is mostly unclear how mtRNase P binds and processes its (mt)pre-tRNA substrates. Significantly, how the three required components of the mtRNase P interact remains a major question. Here we directly address these critical knowledge gaps by investigating how human mtRNase P binds, cleaves and methylates representative human mitochondrial pre-tRNAs. Our data demonstrate that there is extensive interplay between the mtRNase P components (MRPP1/2/3 and the MRPP1 cofactor SAM) required to recognize, process and methylate human mitochondrial pre-tRNAs. We found that mtRNase P exhibits distinct modes of substrate recognition for individual human mitochondrial pre-tRNAs, in contrast to the homologous single protein component PRORPs that bind and cleave their substrates uniformly.

The mitochondrial genome encodes 22 tRNAs that fall into four different types (0-III) based on their predicted secondary structures. The secondary structures of type 0 (mt)tRNAs are similar to those of canonical nuclear tRNAs, while types I-III vary distinctly. Type I-III (mt)tRNAs differ in the length of their anticodon stems, D- and T-loops, or lack the D-loop entirely ((mt)pre-tRNA$^{Ser(AGY)}$ [16])[35]. In our study we investigated the processing of pre-tRNAs representative of all four categories of mitochondrial pre-tRNAs; (mt)pre-tRNA^{Leu} (type 0), (mt)pre-tRNA$^{Ser(UCN)}$ (type I), (mt)pre-tRNA^{Ile} (type II), (mt)pre-tRNA^{Met} (type II), (mt)pre-tRNA^{Val} (type II) and (mt)pre-tRNA$^{Ser(AGY)}$ (type III). Most of these pre-tRNAs are of significant interest because all are hot spots for mutations responsible for a plethora of human mitochondrial diseases [17, 19, 36, 37]. Additionally, (mt)pre-tRNA^{Val} is of note because it is transcribed between the two mitochondrial rRNAs and is proposed to play an unusual structural role as part of the human mitochondrial ribosome [38, 39].

Using our selected substrates, we determined both how individual components of the mtRNase P (MRPP3 and MRPP1/2) and the mtRNase P complex bind type 0-III (mt)pre-tRNAs. We find that MRPP3 and MRPP1/2 individually bind most (mt)pre-tRNAs with low affinity ($K_{D,app}$ values in μM range). However, for (mt)pre-tRNA^{Leu}, (mt)pre-tRNA^{Ile}, (mt)pre-tRNA^{Met} binding affinities are significantly ($K_{D,app}$ values in nM range) enhanced when the entire complex is present. This suggests that the different components in the mtRNase complex depend on each other to recognize some substrates. This is in agreement with studies utilizing a model *B.subtilis* (pre-tRNA^{Asp}) substrate as a surrogate for binding by mtRNase P, indicating that protein components are all required for substrate recognition independently of the nature of the substrate (Liu et al, submitted in conjunction with this manuscript). The substrates that bind weakly to mtRNase P include a variety of types (type I (mt)pre-tRNASer$^{(UCN)}$, type II (mt)pre-tRNA^{Val}, and type III (mt)pre-tRNASer$^{(AGY)}$). The inability of the complex to bind (mt)pre-tRNA$^{Ser(AGY)}$ was not surprising because this substrate lacks the entire D- loop and stem (Figure 1) and is not predicted to be a substrate of mtRNase P *in vivo* [31]. However, the weaker binding of (mt)pre-tRNA^{Val} and (mt)pre-tRNASer$^{(UCN)}$ was unexpected since there are no obvious structural or sequence differences that allow rationalization of the low affinity with mtRNase P.

The efficiency of mtRNase P catalyzing the 5' end cleavage of particular (mt)pre-tRNAs follows the same pattern as substrate binding; (mt)pre-RNAs that associate tightly are processed 8-20 times faster (single turnover k_{obs}=0.007-0.015 min^{-1}) than substrates that bind weakly (k_{obs} ~0.0008 min^{-1}). The correlation between weak binding and slow cleavage rates at saturating enzyme suggests that these pre-tRNA substrates do not bind in a position optimal for cleavage. Notably, all (mt)pre-tRNAs that are recognized and processed efficiently by human mtRNase P are type 0 or II substrates. However, not all type II pre-tRNAs are efficiently processed by mtRNase P, such as pre-tRNA^{Val}, suggesting that the 'type' of

(mt)pre-tRNA structure is insufficient to predict how mtRNase P will recognize any given substrate. Our data indicate that the recombinant mtRNase P does not recognize all substrates equally, leading us to posit that additional factors beyond MRPP1/2 and MRPP3 may be required to ensure that all (mt)pre-tRNAs are efficiently processed in cells.

In order to gain further insight into the interplay between 5' end pre-tRNA processing and methylation activities of mtRNase P, we measured the single turnover methylation rates of MRPP1/2 in the presence and absence of MRPP3. These assays were performed using the (mt)pre-tRNAs that possess m1A9/m1G9 methylation sites ((mt)pre-tRNA^{Ile}, (mt)pre-tRNA^{Leu}, (mt)pre-tRNA^{Val}). We find that single turnover rates for methylation were at least 5 times slower than 5' end processing, suggesting that cleavage may occur prior to methylation. This finding is in agreement with previous studies that assessed (mt)pre-tRNA^{Ile} methylation catalyzed by mtRNase P [40]. Recent work indicated that 5' end processing and methylation of (mt)pre-tRNA^{Ile} catalyzed by mtRNase P are carried out by the components of mtRNase P independently, and do not affect one another [28]. While our results with (mt)pre-tRNA^{Ile} and (mt)pre-tRNA^{Val} corroborate this suggestion, we find that the presence of MRPP3 modestly increases the rate constant for methylation of (mt)pre-tRNA^{Leu} by MRPP1/2. This implies that the two functions of mtRNase P are not entirely de-coupled, and that there may be cooperation between the 5' end tRNA processing and methyltransferase functions of mtRNase P for some substrates.

Based on *in vivo* experiments [16], (mt)pre-tRNA^{Val} is predicted to be substrate of mtRNase P. However, we show that this substrate is not recognized and processed efficiently by recombinant mtRNase P *in vitro*. It has been previously demonstrated that (mt)tRNA^{Lys} requires methylation at the 9th base in order to fully adopt the clover-leaf secondary structure [41-43]. This result suggested that methylation of (mt)pre-tRNA^{Val} at the 9th position might be necessary for this substrate to fold (and subsequently be processed by mtRNase P), akin to

(mt)tRNA^{Lys}. Consistent with this model, we observed that the binding and cleavage of (mt)pre-tRNA^{Val} by mtRNase P is significantly enhanced by the addition of SAM (Figure 5). However, similar effects are observed upon addition of SAH, a SAM analogue that does not function as a cofactor for methylation catalyzed by MRPP1/2, or using m1A9 methylation site mutation of (mt)pre-tRNA^{Val} (Figure 5). These results suggest that the SAM-mediated effect on (mt)pre-tRNA^{Leu} and (mt)pre-tRNA^{Val} binding affinity and processing by mtRNase P is linked to binding to MRPP1/2 rather than pre-tRNA methylation. There are several examples in the literature where SAM acts an effector molecule affecting protein function and activity; SAM is an allosteric regulator of human cystathione-β-synthase, and histidine trimethylase EgtD from *M. segmatis* [44-46]. Furthermore, in the presence of SAM, a bifunctional restriction enzyme harboring a methyltransferase domain, RM.BpuSI, had increased processing activity without significant methylation activity [47], similarly to mtRNase P for (mt)pre-tRNA^{Val}. Based on our data, we propose that the presence of SAM bound to MRPP1 enhances the ability of MRPP1 to bind some pre-tRNA substrates.

In non-metazoan eukaryotes the MRPP3 homologue PRORP enzymes are stand-alone proteins able to cleave a wide variety of substrates from different organisms [3, 7, 48]. To gain insight into potential differences in how single-protein PRORPs and complex-forming MRPP3 enzymes select and cleave their substrates we assessed the ability of *A. thaliana* PRORP1 and PRORP2 to recognize and process human (mt)pre-tRNAs. The *A. thaliana* PRORPs do not bind or cleave most human (mt)pre-tRNAs. However, PRORPs do effectively process (mt)pre-tRNASer$^{(UCN)}$, which is not an efficient *in vitro* substrate for mtRNase P. This suggests that complex-forming protein only RNase Ps recognize their substrates differently than single enzyme PRORPs. Since *A. thaliana* PRORPs recognize the L-shaped tertiary structure of pre-tRNAs [49], we propose that mtRNase P may interact with pre-tRNAs by recognizing local structural elements or specific bases within the (mt)pre-

tRNAs. Some human mitochondrial tRNAs are known to adopt alternate secondary structures [50] and mtRNase P may have conformed to be able to recognize these non-canonical structures.

Taken together, our *in vitro* studies demonstrate that different human mitochondrial pre-tRNAs interact distinctly with mtRNase P and this recognition is potentially an important determinant for 5' tRNA processing. Additionally, we found that some substrates are not efficiently bound and processed by mtRNase P suggesting a role of other factors in mitochondrial 5'end tRNA processing. In line with this, we found that SAM, the cofactor of MRPP1, can enhance substrate recognition and 5' processing by mtRNAse P. Our data reveal that single subunit PRORPs have a distinct substrate binding pattern than the human mitochondrial RNase P suggesting that single subunit and complex PRORPs may possess different mode of pre-tRNA recognition. In addition, our data provide the first evidence that there is an interplay between the 5' end (mt)pre-tRNA processing and methylation functions of mtRNase P. Together, this work builds on the understanding of the role of MRPP1/2 developed previously (Liu et al, submitted in conjunction with this manuscript) and provides the first framework how the different components of mtRNase P work together to bind, process and methylate mitochondrial pre-tRNAs.

ACKNOWLEDGEMENTS

We thank Dr. Aranganathan Shamuganathan for supplying some of the MRPP1/2 enzyme preparation. We are grateful for Dr. Bradley Klemm for helpful comments and for Dr. Kristin Koutmou for reading the manuscript. We also thank Dr. Xin Liu for providing great help in developing methods to prepare mtRNase P.

FUNDING

This work was supported by the National Institutes of Health [R01 GM117141 to M.K.] and [R01 GM55387 to C.A.F]. and by American Heart Association pre-doctoral fellowship [16PRE29890011 to A.K.].

Conflict of interest

None.

Tables

Table 1. Human mtRNase P binds and processes a subset of mitochondrial pre-tRNA substrates efficiently.

human (mt) pre-tRNA	$K_{D,\ MRPP3}$ (μM)	$K_{Dapp,\ MRPP1/MRPP2}$ (nM)	$K_{Dapp,\ mtRNase\ P*}$ (nM)
(mt)pre-tRNA$^{Leu(UUR)}$	9.2 ± 1.6	> 2000	50.6 ± 5.3
(mt)pre-tRNA^{Ile}	4.4 ± 0.6	104 ± 24	13.5 ± 2.3
(mt)pre-tRNA^{Val}	21.7 ± 2.6	>2000	4124 ± 560
(mt)pre-tRNA^{Met}	19.3 ± 5.5	> 2000	707 ± 168
(mt)pre-tRNA$^{Ser(UCN)}$	12.2 ± 2.2	730 ± 196	3556 ± 540
(mt)pre-tRNA$^{Ser(AGY)}$	43.9 ± 7.9	> 2000	12660 ± 1312

All fluorescent binding measurements were carried out in 30 mM MOPS pH=7.8, 150 mM NaCl, 1 mM DTT and 20 nM Fl pre-tRNAs. K_D values were calculated from a fit of a binding isotherm to the concentration dependence of the anisotropy data.
*Measurements for mtRNAse P were performed as following; first folded pre-tRNA was incubated with 150 nM MRPP1/2 for 5 minutes then varying amount of MRPP3 was added. Fluorescent anisotropy values were read after 5 minutes further incubation.

Table 2. 5' end cleavage of mitochondrial pre-tRNAs by the mtRNase P complex.

human (mt) pre-tRNA	$K_{1/2}^{MRPP3}$ (nM)	$k_{max,c}$ (sec^{-1})
(mt)pre-tRNA$^{Leu(UUR)}$	423 ± 107	0.0068 ± 0.0007
(mt)pre-tRNA^{Ile}	389 ± 85	0.013 ± 0.001
(mt)pre-tRNA^{Val}	-	0.0008 ± 0.00002
(mt)pre-tRNA^{Met}	933 ± 299	0.0075 ± 0.0012
(mt)pre-tRNA$^{Ser(UCN)}$	-	0.0001 ± 0.00002
(mt)pre-tRNA$^{Ser(AGY)}$	-	0.0001 ± 0.00002

Figures

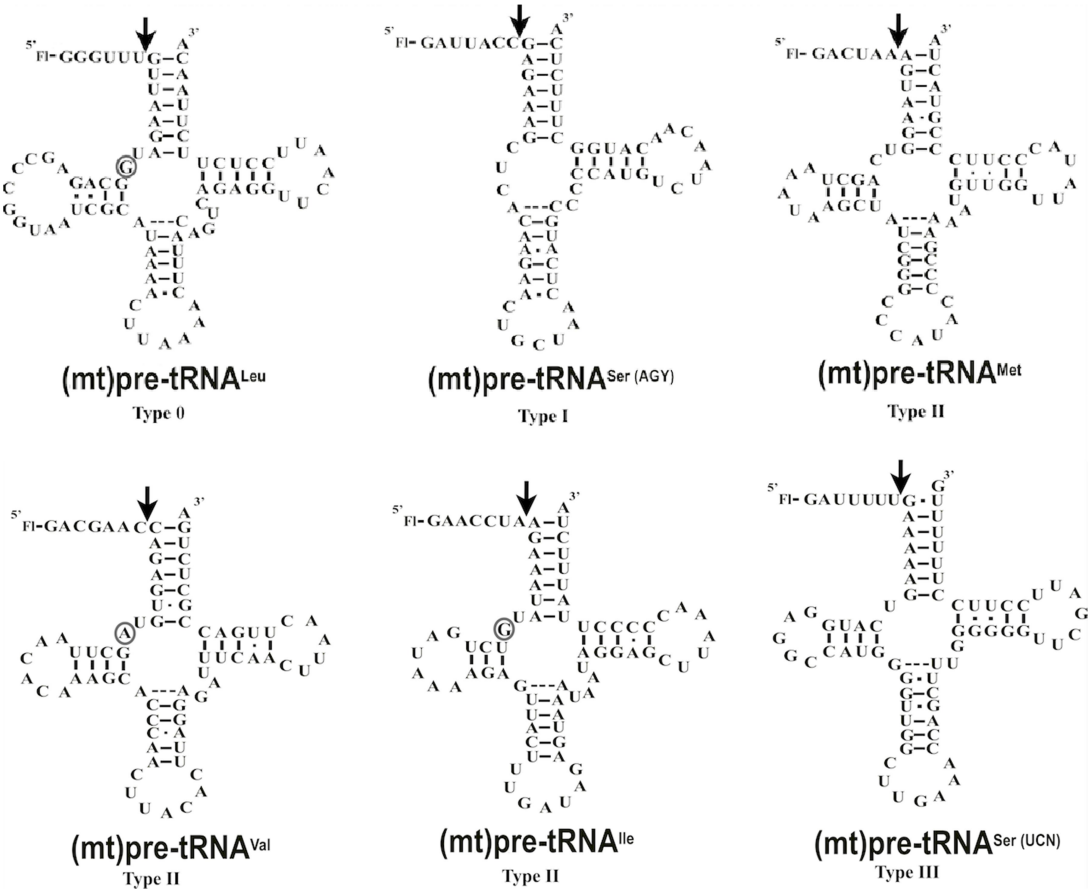


Figure 1. Proposed secondary structures of different types of human mitochondrial pre-tRNAs used in this study.
Black arrows indicate the 5' cleavage site and ellipses mark the m1A9/m1G9 methylation sites for MRPP1/2.

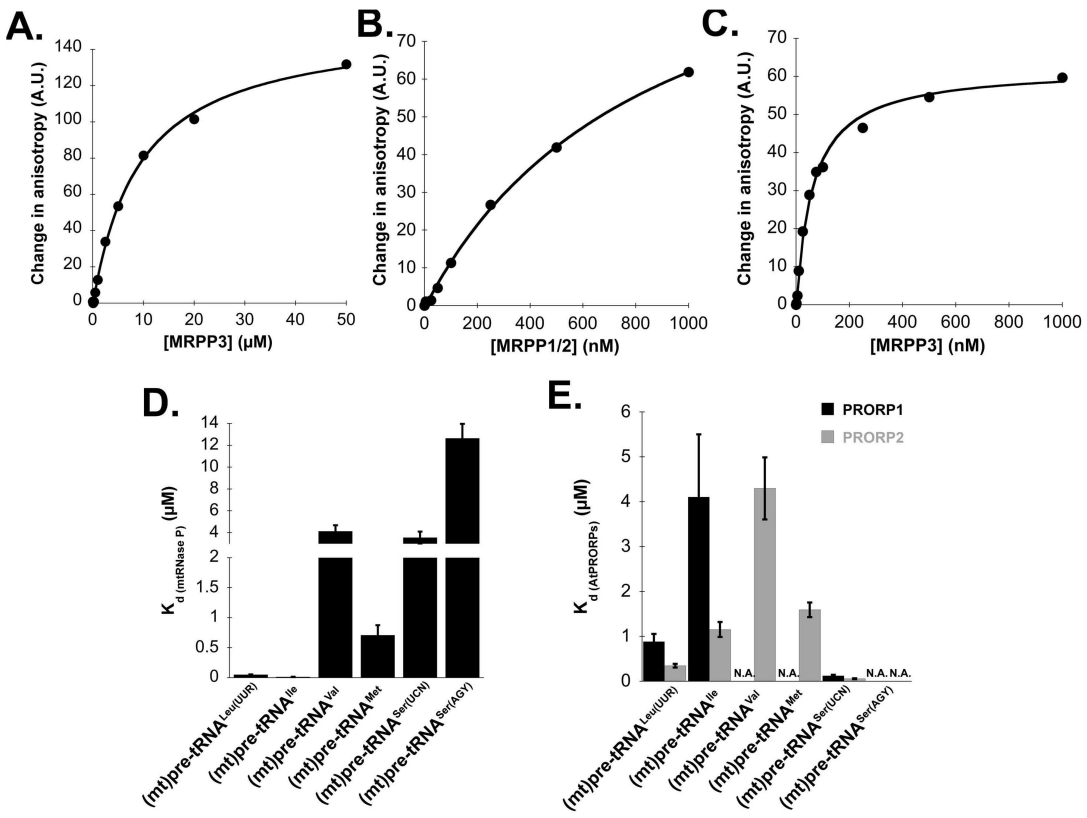


Figure 2. Presence of MRPP1/2 is required for efficient recognition of mitochondrial pre-tRNAs.

A. Representative figure of pre-tRNA binding to MRPP3 measured by changes in fluorescent polarization. 20 nM Fl-(mt)pre-tRNA$^{Leu(UUR)}$ was titrated against increasing concentrations of MRPP3 (0-50 μM) using standard binding conditions. **B.** Representative figure of pre-tRNA binding to MRPP1/2 measured by changes in fluorescent polarization. 20 nM Fl-(mt)pre-tRNA$^{Leu(UUR)}$ was titrated against increasing concentrations of MRPP1/2 (0-1 μM) using standard binding conditions. **C.** Representative figure of pre-tRNA binding to MRPP3 in the presence of 150 nM MRPP1/2 measured by changes in fluorescent polarization. 20 nM Fl-pre-(mt)tRNA$^{Leu(UUR)}$ was titrated against increasing amount of MRPP3 (0-1 μM) using standard binding conditions. **D.** Average dissociation constants for the mtRNase P complex and investigated pre-tRNAs, measured as described in C. **E.** Average dissociation constants for PRORP1 and 2 and investigated human pre-tRNAs in fluorescent binding assays using standard reaction conditions. For some pre-tRNAs dissociation constants were out of the measured range (N.A.).

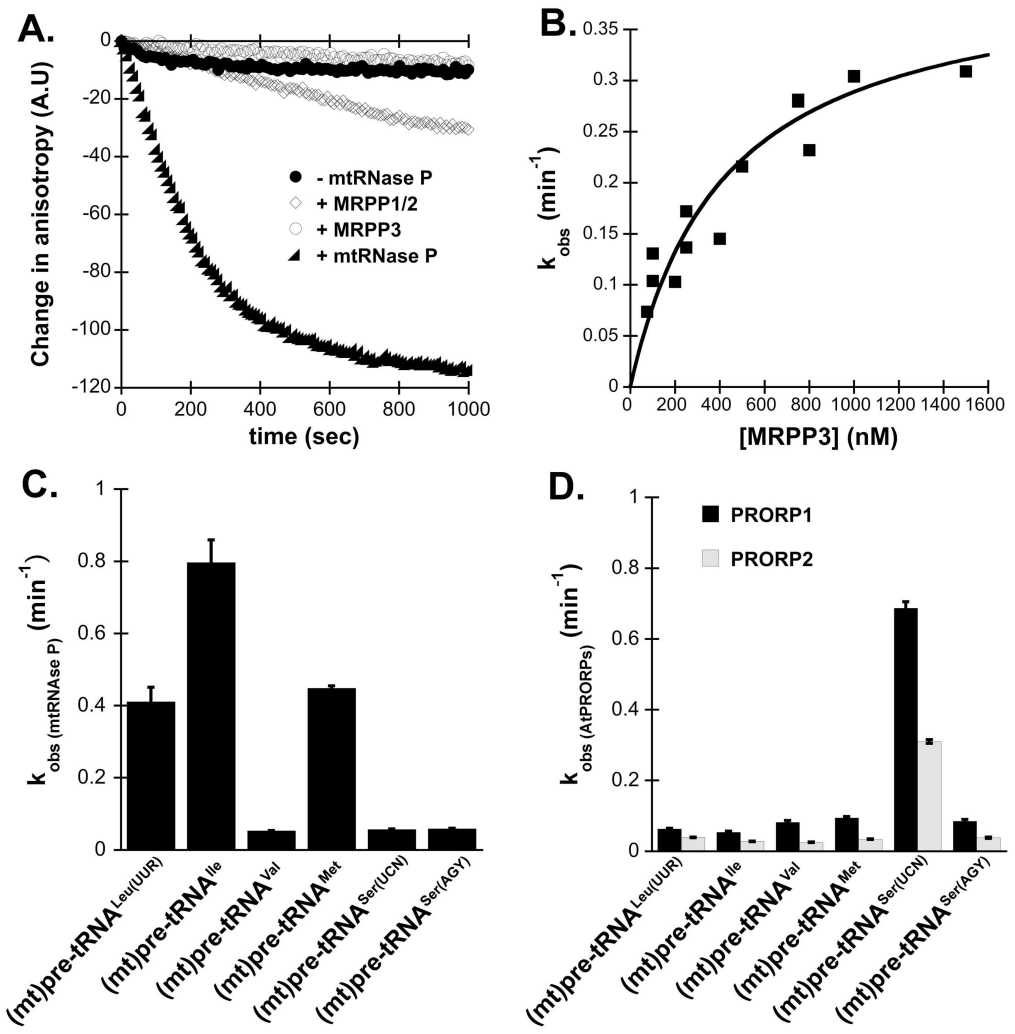


Figure 3. Some human mitochondrial pre-tRNAs are efficiently cleaved by the mtRNase P complex *in vitro*.

A. Representative figure of single turnover cleavage of 20 nM (mt)pre-tRNA$^{Leu(UUR)}$ measured using changes in fluorescent polarization in the presence of the mtRNase P complex (closed triangles), MRPP3 only (open circles), MRPP1/2 only (open diamonds). Control reaction containing only Fl- (mt)pre-tRNA$^{Leu(UUR)}$ is marked by closed circles. **B.** Dependence of single turnover rate constant, k_{obs}, for cleavage of (mt)pre-tRNA$^{Leu(UUR)}$ on the concentration of MRPP3 in the presence of 0.4 μM MRPP1/2. **C.** Average single turnover cleavage rates at saturating MRPP3 in the presence of 0.4 μM MRPP1/2 for investigated pre-tRNAs. **D.** Average observed single turnover cleavage rates catalyzed by saturating concentrations of PRORP1 and 2 for investigated human pre-tRNAs.

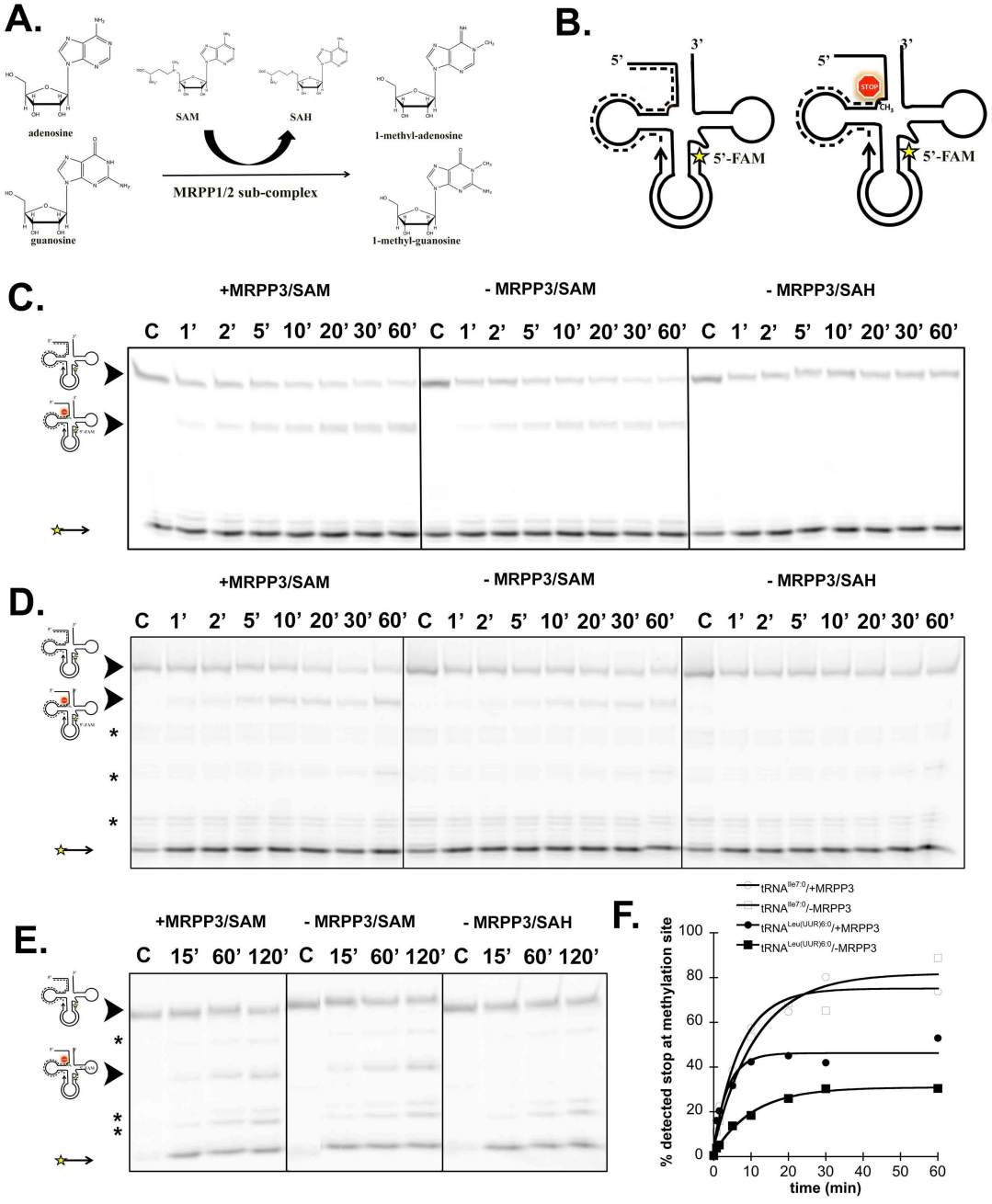


Figure 4. MRPP1/2 methylates human mitochondrial pre-tRNAs.

A. Schematic representation of m1A9/m1G9 methylation catalyzed by MRPP1/2 in the presence of S-adenosyl methionine (SAM). SAH=S-adenosyl homocysteine **B.** Scheme for primer extension methylation assays. 5' fluorescein (5-FAM) labeled primers (black arrow) were designed to base pair with the anticodon loop. In the absence of m1A9/m1G9 methylation, reverse transcriptase (RT) reads all the way to the 5' end of pre-tRNA (dashed line). When pre-tRNA is methylated at m1A9 or m1G9 position, RT stops at this modification site. **C.-E.** Representative gels for methylation of (mt)pre-tRNA^{Ile}, (mt)pre-tRNA^{Leu} and (mt)pre-tRNA^{Val} in the presence (first panel) and absence (second panel) of MRPP3. Substitution of SAH for SAM was used as a negative control for methylation (third panel). Black arrows

indicate the full-length and methylation stop primer extension products. Asterisks indicate non-specific bands. **F.** Example quantification of the gel-based primer extension methylation assays for (mt)pre-tRNA^{Ile} (open symbols) and (mt) pre-tRNA^{Leu} (closed symbols) in the presence (circles) and absence (squares) of MRPP3.

Figure 5.

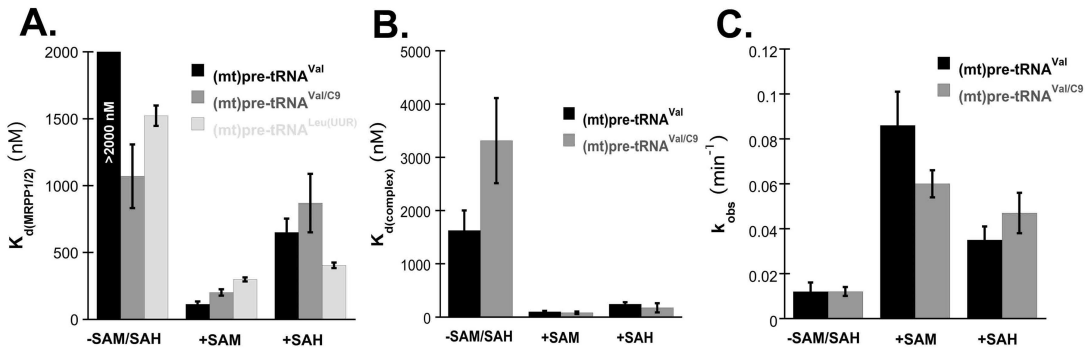


Figure 5. Presence of SAM enhances recognition and 5' end processing of some mitochondrial pre-tRNAs by mtRNase P.
A. Average dissociation constants for (mt)pre-tRNA^{Val} and (mt)pre-tRNA$^{Leu(UUR)}$ for MRPP1/2 in the absence or presence of 25 μM SAM or SAH. **B.** Average dissociation constants for mtRNase P and (mt)pre-tRNA^{Val} in the absence or presence of 25 μM SAM or SAH. **C.** Average observed single turnover cleavage rates for the mtRNase P complex and (mt)pre-tRNA^{Val}. Reaction was measured by gel based cleavage assay in the presence of 625 nM MRPP1/2, 1875 nM MRPP3 and 80 nM labeled pre-tRNA.

Supplemental Material

Supplemental Table 1. *A.thaliana* PRORP1 and PRORP2 do not bind and process most human mitochondrial pre-tRNAs efficiently.

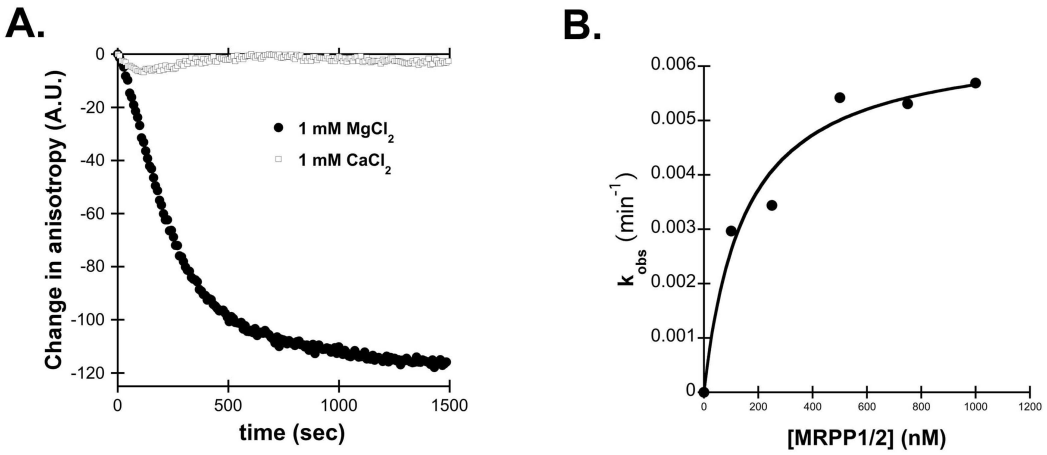
human (mt)pre-tRNA	$K_{D,\ \mathbf{PRORP1}}$ **(nM)**	$k_{obs,PRORP1}$ **(sec^{-1})**	$K_{D\ \mathbf{PRORP2}}$ **(nM)**	$k_{obs,PRORP2}$ **(sec^{-1})**
(mt)pre-tRNA$^{Leu(UUR)}$	883 ±174	0.0010 ± 0.00003	349 ± 40	0.0007 ± 0.00002
(mt)pre-tRNA^{Ile}	4105 ± 1400	0.0008 ± 0.00005	1155 ± 167	0.0005 ± 0.00002
(mt)pre-tRNA^{Val}	>> 10000	0.0013 ± 0.00008	4300 ± 690	0.0005 ± 0.00002
(mt)pre-tRNA^{Met}	> 5000	0.0015 ± 0.00007	1596 ± 163	0.0005 ± 0.00002
(mt)pre-tRNA$^{Ser(UCN)}$	123 ±23	0.0115 ± 0.00033	59 ± 10	0.0052 ± 0.00008
(mt)pre-tRNA$^{Ser(AGY)}$	>> 10000	0.0015 ± 0.00008	> 5000	0.0007 ± 0.00003

Supplemental Table 2. Summary of binding and single turnover cleavage experiments for wild type and methylation site mutant tRNA$^{Val7:0}$.

	pre-tRNA$^{Val\ 7:0}$			**pre-tRNA $^{Val\ 7:0/C9}$**		
	$K_{D,app,\mathbf{MRPP1/MRPP2}}$ **(nM)**	$K_{Dapp,\ \mathbf{mtRNase\ P}}$ **(nM)**	$k_{obs,c}$ **(sec^{-1})&**	$K_{D,app,\mathbf{MRPP1/MRPP2}}$ **(nM)**	$K_{D,\mathbf{app\ mtRNase\ P}}$ **(nM)**	$k_{obs,c}$ **(sec^{-1})&**
No SAM/SAH	>2000	1626 ± 375	0.0002 ± 0.00007	1070 ± 238	3313 ± 800	0.0002 ± 0.00003
25 µM SAM	114 ± 20	101 ± 13	0.0014 ± 0.00015	201 ± 24	80 ± 23	0.0010 ± 0.00010
25 µM SAH	650 ± 103	243 ± 34	0.0006 ± 0.00010	869 ± 219	273 ± 87	0.0008 ± 0.00015

Supplemental Table 3. Binding and 5' end cleavage of human pre-tRNAs by mtRNase P in the presence of excess SAM.

human (mt) pre-tRNA	$K_{D,\mathbf{app\ MRPP1/MRPP2}}$ **(nM)**	$K_{Dapp,\ \mathbf{mtRNase\ P}}$ **(nM)**	$k_{obs,\ c}$ **(sec^{-1})**
(mt)pre-tRNA$^{Leu(UUR)}$	298 ± 53	36.6 ± 7.11	0.0024 ± 0.0002
(mt)pre-tRNA^{Ile}	124 ± 18*	15.3 ± 2.1	0.0083 ± 0.0002
(mt)pre-tRNA^{Met}	>2000	1024 ± 335	0.0048 ± 0.0001
(mt)pre-tRNA$^{Ser(UCN)}$	733 ± 170	>2000	<0.0008
(mt)pre-tRNA$^{Ser(AGY)}$	>2000	>2000	<0.0008



Supplemental Figure 1.

A. mtRNase P cleaves the 5' end of (mt)pre-tRNA$^{Ile7:0}$ in 1 mM $MgCl_2$, but there is no significant cleavage in 1 mM $CaCl_2$. **B.** Single turnover cleavage rate constants for (mt)pre-tRNA^{Leu} as a function of the MRPP1/2 concentration in the presence of 1 μM MRPP3.

REFERENCES

1. Holzmann, J., et al., *RNase P without RNA: identification and functional reconstitution of the human mitochondrial tRNA processing enzyme.* Cell, 2008. **135**(3): p. 462-74.
2. Taschner, A., et al., *Nuclear RNase P of Trypanosoma brucei: a single protein in place of the multicomponent RNA-protein complex.* Cell Rep, 2012. **2**(1): p. 19-25.
3. Gobert, A., et al., *A single Arabidopsis organellar protein has RNase P activity.* Nat Struct Mol Biol, 2010. **17**(6): p. 740-4.
4. Gutmann, B., A. Gobert, and P. Giege, *PRORP proteins support RNase P activity in both organelles and the nucleus in Arabidopsis.* Genes Dev, 2012. **26**(10): p. 1022-7.
5. Pinker, F., et al., *Biophysical analysis of Arabidopsis protein-only RNase P alone and in complex with tRNA provides a refined model of tRNA binding.* J Biol Chem, 2017.
6. Gobert, A., et al., *Structural insights into protein-only RNase P complexed with tRNA.* Nat Commun, 2013. **4**: p. 1353.
7. Karasik, A., et al., *Nuclear Protein-Only Ribonuclease P2 Structure and Biochemical Characterization Provide Insight into the Conserved Properties of tRNA 5′ End Processing Enzymes.* J Mol Biol, 2016. **428**(1): p. 26-40.
8. Howard, M.J., et al., *RNase P enzymes: divergent scaffolds for a conserved biological reaction.* RNA Biol, 2013. **10**(6): p. 909-14.
9. Howard, M.J., et al., *Mitochondrial ribonuclease P structure provides insight into the evolution of catalytic strategies for precursor-tRNA 5′ processing.* Proc Natl Acad Sci U S A, 2012. **109**(40): p. 16149-54.
10. Howard, M.J., et al., *Differential substrate recognition by isozymes of plant protein-only Ribonuclease P.* Rna, 2016. **22**(5): p. 782-92.
11. Ojala, D., J. Montoya, and G. Attardi, *tRNA punctuation model of RNA processing in human mitochondria.* Nature, 1981. **290**(5806): p. 470-4.
12. Sanchez, M.I., et al., *RNA processing in human mitochondria.* Cell Cycle, 2011. **10**(17): p. 2904-16.
13. Reinhard, L., S. Sridhara, and B.M. Hallberg, *The MRPP1/MRPP2 complex is a tRNA-maturation platform in human mitochondria.* Nucleic Acids Res, 2017.
14. Abbott, J.A., C.S. Francklyn, and S.M. Robey-Bond, *Transfer RNA and human disease.* Front Genet, 2014. **5**: p. 158.
15. Sen, A., et al., *Loss of the mitochondrial protein-only ribonuclease P complex causes aberrant tRNA processing and lethality in Drosophila.* Nucleic Acids Res, 2016. **44**(13): p. 6409-22.
16. Rackham, O., et al., *Hierarchical RNA Processing Is Required for Mitochondrial Ribosome Assembly.* Cell Rep, 2016. **16**(7): p. 1874-90.
17. Wang, S., et al., *Maternally inherited essential hypertension is associated with the novel 4263A>G mutation in the mitochondrial tRNAIle gene in a large Han Chinese family.* Circ Res, 2011. **108**(7): p. 862-70.
18. Bindoff, L.A., et al., *Abnormal RNA processing associated with a novel tRNA mutation in mitochondrial DNA. A potential disease mechanism.* J Biol Chem, 1993. **268**(26): p. 19559-64.
19. Rossmanith, W. and R.M. Karwan, *Impairment of tRNA processing by point mutations in mitochondrial tRNA(Leu)(UUR) associated with mitochondrial diseases.* FEBS Lett, 1998. **433**(3): p. 269-74.

20. Li, R. and M.X. Guan, *Human mitochondrial leucyl-tRNA synthetase corrects mitochondrial dysfunctions due to the tRNALeu(UUR) A3243G mutation, associated with mitochondrial encephalomyopathy, lactic acidosis, and stroke-like symptoms and diabetes.* Mol Cell Biol, 2010. **30**(9): p. 2147-54.
21. Deutschmann, A.J., et al., *Mutation or knock-down of 17beta-hydroxysteroid dehydrogenase type 10 cause loss of MRPP1 and impaired processing of mitochondrial heavy strand transcripts.* Hum Mol Genet, 2014.
22. Chatfield, K.C., et al., *Mitochondrial energy failure in HSD10 disease is due to defective mtDNA transcript processing.* Mitochondrion, 2015.
23. Chatfield, K.C., et al., *Mitochondrial energy failure in HSD10 disease is due to defective mtDNA transcript processing.* Mitochondrion, 2015.
24. Deutschmann, A.J., et al., *Mutation or knock-down of 17beta-hydroxysteroid dehydrogenase type 10 cause loss of MRPP1 and impaired processing of mitochondrial heavy strand transcripts.* Hum Mol Genet, 2014. **23**(13): p. 3618-28.
25. Hodgkinson, A., et al., *High-resolution genomic analysis of human mitochondrial RNA sequence variation.* Science, 2014. **344**(6182): p. 413-5.
26. Reinhard, L., S. Sridhara, and B.M. Hallberg, *Structure of the nuclease subunit of human mitochondrial RNase P.* Nucleic Acids Res, 2015. **43**(11): p. 5664-72.
27. Li, F., et al., *Auto-inhibitory Mechanism of the Human Mitochondrial RNase P Protein Complex.* Sci Rep, 2015. **5**: p. 9878.
28. Vilardo, E., et al., *A subcomplex of human mitochondrial RNase P is a bifunctional methyltransferase--extensive moonlighting in mitochondrial tRNA biogenesis.* Nucleic Acids Res, 2012. **40**(22): p. 11583-93.
29. Helm, M., et al., *Search for characteristic structural features of mammalian mitochondrial tRNAs.* Rna, 2000. **6**(10): p. 1356-79.
30. Suzuki, T., A. Nagao, and T. Suzuki, *Human mitochondrial tRNAs: biogenesis, function, structural aspects, and diseases.* Annu Rev Genet, 2011. **45**: p. 299-329.
31. Rossmanith, W., *Processing of human mitochondrial tRNA(Ser(AGY))GCU: a novel pathway in tRNA biosynthesis.* J Mol Biol, 1997. **265**(4): p. 365-71.
32. Liu, X., Y. Chen, and C.A. Fierke, *A real-time fluorescence polarization activity assay to screen for inhibitors of bacterial ribonuclease P.* Nucleic Acids Res, 2014. **42**(20): p. e159.
33. Brillante, N., et al., *Substrate recognition and cleavage-site selection by a single-subunit protein-only RNase P.* Nucleic Acids Res, 2016. **44**(5): p. 2323-36.
34. Falk, M.J., et al., *A novel HSD17B10 mutation impairing the activities of the mitochondrial RNase P complex causes X-linked intractable epilepsy and neurodevelopmental regression.* RNA Biol, 2016. **13**(5): p. 477-85.
35. Watanabe, Y., T. Suematsu, and T. Ohtsuki, *Losing the stem-loop structure from metazoan mitochondrial tRNAs and co-evolution of interacting factors.* Front Genet, 2014. **5**: p. 109.
36. Wortmann, S.B., et al., *Mitochondrial DNA m.3242G > A mutation, an under diagnosed cause of hypertrophic cardiomyopathy and renal tubular dysfunction?* Eur J Med Genet, 2012. **55**(10): p. 552-6.
37. Yan, H., N. Zareen, and L. Levinger, *Naturally occurring mutations in human mitochondrial pre-tRNASer(UCN) can affect the transfer ribonuclease Z cleavage site, processing kinetics, and substrate secondary structure.* J Biol Chem, 2006. **281**(7): p. 3926-35.
38. Amunts, A., et al., *Ribosome. The structure of the human mitochondrial ribosome.* Science, 2015. **348**(6230): p. 95-98.

39. Greber, B.J., et al., *Ribosome. The complete structure of the 55S mammalian mitochondrial ribosome.* Science, 2015. **348**(6232): p. 303-8.
40. Vilardo, E. and W. Rossmanith, *Molecular insights into HSD10 disease: impact of SDR5C1 mutations on the human mitochondrial RNase P complex.* Nucleic Acids Res, 2015. **43**(13): p. 6649.
41. Helm, M., et al., *The presence of modified nucleotides is required for cloverleaf folding of a human mitochondrial tRNA.* Nucleic Acids Res, 1998. **26**(7): p. 1636-43.
42. Sissler, M., et al., *Aminoacylation properties of pathology-related human mitochondrial tRNA(Lys) variants.* Rna, 2004. **10**(5): p. 841-53.
43. Motorin, Y. and M. Helm, *tRNA stabilization by modified nucleotides.* Biochemistry, 2010. **49**(24): p. 4934-44.
44. McCorvie, T.J., et al., *Inter-domain communication of human cystathionine beta-synthase: structural basis of S-adenosyl-L-methionine activation.* J Biol Chem, 2014. **289**(52): p. 36018-30.
45. Jeong, J.H., et al., *Structural insights into the histidine trimethylation activity of EgtD from Mycobacterium smegmatis.* Biochem Biophys Res Commun, 2014. **452**(4): p. 1098-103.
46. Lin, Y., et al., *Detecting S-adenosyl-L-methionine-induced conformational change of a histone methyltransferase using a homogeneous time-resolved fluorescence-based binding assay.* Anal Biochem, 2012. **423**(1): p. 171-7.
47. Sarrade-Loucheur, A., S.Y. Xu, and S.H. Chan, *The role of the methyltransferase domain of bifunctional restriction enzyme RM.BpuSI in cleavage activity.* PLoS One, 2013. **8**(11): p. e80967.
48. Howard, M.J., B.P. Klemm, and C.A. Fierke, *Mechanistic Studies Reveal Similar Catalytic Strategies for Phosphodiester Bond Hydrolysis by Protein-only and RNA-dependent Ribonuclease P.* J Biol Chem, 2015.
49. Klemm, B.P., et al., *Molecular recognition of pre-tRNA by Arabidopsis protein-only Ribonuclease P.* Rna, 2017.
50. Lorenz, C., C.E. Lunse, and M. Morl, *tRNA Modifications: Impact on Structure and Thermal Adaptation.* Biomolecules, 2017. **7**(2).

MANUSCRIPT 2: DISEASE ASSOCIATED MUTATIONS IN PRECURSOR TRNAS AFFECT BINDING, M1R9 METHYLATION AND 5' END PRECURSOR TRNA PROCESSING BY MTRNASE P IN HUMAN MITOCHONDRIA

Agnes Karasik[1], Carol A. Fierke[2], Markos Koutmos[3*]

[1]Department of Biochemistry and Molecular Biology, Uniformed Services University of the Health Sciences, Bethesda, MD, 20814, USA

[2]Department of Chemistry, Department of Biological Chemistry, University of Michigan, Ann Arbor, MI 48109, USA

[3]Department of Chemistry, Program in Biophysics, University of Michigan, Ann Arbor, MI, 48109, USA

*Corresponding author (mkoutmos@umich.edu, Tel: 734 936-2678)

Keywords: RNase P, PRORP, pre-tRNA, mitochondria, tRNA processing, mitochondrial diseases, tRNA mutations

Author contributions: A.K. designed and executed all experiments and therefore A.K. generated data for all figures and tables. A.K., C.A.F and M.K. wrote and edited the manuscript.

Abstract

Mitochondrial diseases linked to mutations in mitochondrial (mt)tRNA sequences are abundant. However, how these tRNA mutations contribute to the development of diseases is mostly unknown. Mutations may affect interactions with (mt)tRNA maturation enzymes or affect translation directly that subsequently lead to the lack of mature RNAs, decreased mitochondrial translation and mitochondrial dysfunction. In human mitochondria the first step of tRNA maturation is the removal of the 5'end of precursor tRNAs (pre-tRNA) catalyzed by the three-component enzyme, mtRNase P. Additionally, the sub-component of mtRNase P, mitochondrial RNase P protein 1 (MRPP1) methylates the R9 base in pre-tRNAs. Despite the central role of 5' end processing in the mitochondria the link between mtRNase P and diseases is mostly unexplored. Here we have *in vitro* transcribed (mt)pre-tRNAs containing 11 different human disease linked mutations and investigated how these affected activities of mtRNase P. While we have found that only some mutations result in pre-tRNAs weakened binding, most of them affected 5' end processing and methylation activity of mtRNase P. In addition, all investigated mutations in pre-tRNA$^{Leu(UUR)}$ exhibited structural changes that may contribute to the reduced function of mtRNase P. Overall, we have found that selected mutations in (mt)pre-tRNAs impair early steps of tRNA maturation suggesting a potential etiological link between mtRNase P and mitochondrial diseases

Introduction

Mitochondria serves as the powerhouse for the eukaryotic cell by synthetizing most of its energy currency, the ATP molecules. Due to the endosymbiotic origin of mitochondria it possesses its own circular genome (mtDNA) encoding for 2 rRNAs, 22 tRNAs and 13 mRNAs essential in mitochondrial function. Similarly to the nuclear genome, mutations in the human mtDNA can lead to the development of diseases [1-6]. Though one out of every

4,000 children is born with a mitochondrial disease in the US, their pathogenesis is not clearly understood and treatment is very limited [1, 2, 5]. Interestingly, the majority (>50%) of mitochondrial disease-associated mtDNA mutations are located in mitochondrial transfer RNAs (tRNA) genes that occupy only ~10% of the mtDNA [4, 7, 8]. tRNAs are essential elements required for protein synthesis and undergo several maturation steps before they become fully functional [9]. A link between mitochondrial diseases and impaired tRNA maturation in the mitochondria is beginning to emerge [7, 10-12]. The human mitochondrial genome encodes for three polycistronic units where tRNAs genes are interspersed between rRNAs and mRNAs sequences [13]. Since encoded polycistronic units contain no or only short extra spaces between tRNA genes and other coding regions, 3' and 5' end tRNA processing contributes also to the maturation rRNAs and mRNAs. As a consequence, improper tRNA processing can influence maturation of other essential RNAs in the mitochondria [7, 8]. When RNA maturation is disturbed, the amount of mature RNAs available for normal function, such as protein translation, is decreased potentially leading to mitochondrial dysfunction. Since mitochondria are the major source of energy of the cell, decrease in their function contributes to failure of physiological functions that require high amounts of ATP and therefore to development of disease.

In human mitochondria the first step of pre-tRNA maturation is the removal of the 5' end of precursor tRNAs (pre-tRNA) [14]. This early step is catalyzed by the three-component enzyme mitochondrial ribonuclease P (mtRNaseP) [15]. In this complex, human MRPP3 (Mitochondrial RNase P Protein 3 or Protein Only RNase P, PRORP) harbors the catalytic core for 5' end cleavage, however, it is only active in the presence of the sub-complex consisting of MRPP1 and MRPP2 (Mitochondrial RNase P Protein 1 and 2)[15]. The MRPP1/2 sub-complex catalyzes the methyl transfer to the ninth base (m1A9/m1G9) of human mitochondrial tRNAs independently from 5' end cleavage function of mtRNase P

[16]. In this sub-complex, MRPP2 (17β-hydroxysteroid dehydrogenase type 1, SDR5C1) is likely to serve as a scaffold protein supporting MRPP1's (TRM10C) S-adenosyl-methionine (SAM) dependent methyltransferase function [16].

mtRNase P is essential and plays a central role in mitochondria [14, 17-19]. In agreement with its vital function, disturbance of 5' end pre-tRNA processing is indicated in several mitochondrial diseases, such us maternally inherited essential hypertension, mitochondrial myopathy, MELAS and HSD10 disease [10, 20-26]. Mitochondrial diseases can be inherited in two ways; by mendelian mutations in the nuclear genome or mutations in the mitochondrial genome. In particular, mutations in the nuclear encoded MRPP2 are linked to HSD10 disease [26-29]. Strikingly, most patient mutations in MRPP2 do not affect the dehydrogenase activity of MRPP2 but the methyltransferase and 5' end cleavage activity of mtRNase P due to improper mtRNase P complex formation [25, 28, 29]. In addition, a single nucleotide polymorphism in the MRPP3 gene can influence mitochondrial tRNA methylation pattern and potentially differences in metabolism amongst individuals [30]. Besides mutations in the components of mtRNase P, disease linked mutations in human (mt)pre-tRNAs can also impair 5' end pre-tRNA processing, although such studies are limited. In the most comprehensive study so far, it has been shown that the A4263G (mt)tRNA^{Ile} mutation linked to maternally inherited essential hypertension can affect 5' end cleavage and methyltransferase activity of the human mtRNase P [10]. This mutation decreases mature mitochondrial tRNA^{Ile} levels in patient cell lines suggesting that the perturbed processing of tRNA^{Ile} is likely an underlying cause of this disease.

Despite the potential link between mtRNase P and some other mitochondrial diseases there are very few studies addressing the direct role of mtRNase P in disease. Hence, here we have *in vitro* transcribed 11 pre-tRNAs containing disease linked mutations and investigated their effects on binding, methylation and nuclease activity of human mtRNase P. We found

that most investigated mitochondrial pre-tRNA mutations negatively affected the methylation and nuclease activity of the mtRNase P complex. Additionally, we have shown that a subset of these pre-tRNA mutations influenced proper tRNA folding and tertiary structure that may account for the decrease in mtRNase P activity. Taken together, our study reveals that pathological mutations in (mt)tRNAs result in reduced mtRNase P activity in vitro and suggests that the pathogenicity of these mutations in vivo may be related to modulated and disrupted mtRNase P function.

Materials and Methods

***In vitro* transcription and 5' end labeling of pre-tRNAs.** Wild-type pre-tRNAs were prepared as previously described (Karasik et al, submitted to NAR) [31, 32]. Wild type and mutant pre-tRNA DNA templates for *in vitro* transcription were commercially synthesized by Integrated DNA Technologies. The concentrations of total and labeled pre-tRNA were measured with absorbance using a Nanodrop (Thermo Scientific) spectrophotometer and calculated by using the following extinction coefficients: 909,100 cm^{-1} M^{-1} for (mt)pre-$tRNA^{Ile7:0}$, 927,300 cm^{-1} M^{-1} for (mt)pre-$tRNA^{Leu6:0}$, 838,200 cm^{-1} M^{-1} for (mt)pre-$tRNA^{Met6:0}$.

Protein expression and purification. Full length MRPP2 and His_6-Δ40 MRPP1 lacking the predicted mitochondrial targeting sequences were cloned into pCDFDuet-1 (Novagen) vector (Liu et al, submitted to NAR). MRPP1 and 2 were co-expressed and purified together from *E.coli* (BL21 or Rossetta). First, expression was induced by addition of 200 μM IPTG (Isopropyl β-D-1-thiogalactopyranoside) in transfected bacteria and overnight bacterial cultures were collected and lysed as described before [31]. Then the complex was purified using a nickel affinity column (GE Healthcare) and His-tag was removed by TEV protease from MRPP1 (Liu et al, submitted to NAR). MRPP1 and 2 appeared to form a stable complex

of ~150 kDa that was further purified by gel-filtration (Superdex 200, GE Healthcare). His_{6}-Δ95 MRPP3 cDNA lacking the N-terminal disordered region was cloned into pMCSG7 vector and expressed and purified MRPP3 as previously described (Karasik et al., submitted to NAR). In brief, MRPP3 expression was induced by addition of 200 μM IPTG (Isopropyl β-D-1-thiogalactopyranoside) to transfected *E.coli* BL21. Cells were harvested and lysed after overnight incubation similarly to the MRPP1/2 sub-complex. MRPP3 was purified by nickel affinity column and His-tag was removed by TEV-protease. Purity of the co-expressed MRPP1/2 sub-complex and MRPP3 was evaluated by SDS-PAGE (Sodium-dodecyl-sulfate polyacrylamide gel electrophoresis) and coomassie staining. Protein concentrations were measured by Nano spectrophotometer (Thermo scientific) using 56.4 kDa as molecular weight (MRPP3 $\varepsilon = 82{,}500 cm^{-1} M^{-1}$). The ratio of MRPP1/2 sub-complex as prepared is 1:4 based on analytical ultracentrifugation experiments (Liu et al, submitted to NAR). Therefore, the MRPP1/2 protein concentration was measured using 149 kDa as the molecular weight and extinction coefficient of 79 520 cm^{-1} mol^{-1}.

5' end cleavage single turnover cleavage assays. Pre-tRNA substrates were re-folded before each 5' pre-tRNA cleavage reaction. First, pre-tRNAs were heated up to 95 ˚C for 3 minutes, cooled down to room temperature (~10-15 minutes), then folded by adding "cleavage reaction buffer" (30 mM MOPS pH 7.8, 150 mM NaCl, 1 mM $MgCl_{2,}$ 1 mM DTT) containing 1 mM Mg^{2+}. All single turnover reactions were conducted as previously reported (Karasik et al, submitted to NAR) at 28 ˚C. To initiate the reaction, a mixture of 500 nM Δ40 MRPP1/MRPP2 complex and 100 nM- 2 μM Δ95 MRPP3 in cleavage reaction buffer were added to 20 nM fluorescently labeled pre-tRNA substrates. Changes in fluorescent polarization was followed at 28 ˚C using the ClarioStar plate reader (BMG LabTech). Data from at least three independent experiments were analyzed using Kaleidagraph 4.1.3. Eq 1.

was fit to the data, as described in Howard et al, 2012 to calculate the observed rate constant ($k_{obs,\ cleavage}$) and the standard error.

Eq 1. $$\text{Fraction cleaved} = 1 - e^{-kt}$$

Fluorescent polarization binding assays. Pre-tRNAs used in these experiments were folded as described above, but in Ca^{2+} containing reaction buffers. All binding assays were performed in 30 mM MOPS pH 7.8, 150 mM NaCl, 6 mM $CaCl_2$, 1 mM DTT ("binding reaction buffer") at 28 ˚C (as described in Karasik et al, submitted in NAR). First, we pre-incubated 20 nM fluorescently labeled and folded pre-tRNAs with recombinant 150 nM Δ40MRPP1/2 to reach equilibria. Then we added increasing amounts of Δ95MRPP3 (0- 5 μM) and read fluorescent anisotropy values after an additional 5 minutes incubation time. Data were corrected with the anisotropy measured in the absence of the protein but presence of 20 nM Fl-pre-tRNA. The binding isotherm (Eq. 2) was fit to the fluorescence polarization data from at least three independent experiments. Kaleidagraph 4.1.3 software was used to analyze data, such as to calculate the dissociation constant (K_d) and the standard error. In Eq 2. A is the observed anisotropy, A_o is the initial anisotropy, ΔA is the total change in anisotropy, P is the concentration of MRPP3, and K_D is the apparent dissociation constant.

Eq 2. $$A = A_0 + \frac{\Delta A\ [P]}{[P]+[K_{D,app}]}$$

Primer extension methylation assays. Unlabeled pre-tRNAs were prepared by *in vitro* transcription and gel-based purification. Before each experiment pre-tRNAs were folded in 1 mM Ca^{2+} containing "binding reaction buffer". Primer extension methylation assays were carried out as described before (Karasik et al, submitted to NAR). Sequences for primers against the anticodon loop were the following for wild type and mutant $tRNA^{Ile}$, $tRNA^{Leu(UUR)}$ and $tRNA^{Met}$ respectively: 6-FAM-CTATTATTTACTCTATC; 6-FAM-

CCTCTGACTGTAAAG; 6-FAM-CGGGGTATGGGCCCG. Data from at least three independent experiments were analyzed using Kaleidagraph 4.1.3. Eq 1. was fit to the data to calculate the single turnover rate constants ($k_{obs,\ meth}$) and the standard error.

UV melting experiments. Pre-tRNAs were folded as described above before each experiment using a "UV melting buffer" of final concentration of 10 mM PIPES pH=7, 150 mM NaCl, 1 mM $MgCl_2$ and 1 μM pre-tRNA. Thermodynamic curves were obtained by heating up the samples 1 ˚C/min from 15 ˚C to 95 ˚C while absorbance at 260 nm was monitored at every 0.5 or 1 ˚C using Cary 300 spectrophotometer. Data were corrected with data from blank measurements and analyzed with fitUVData.py and Global Melt Fit [33, 34]. Most pre-tRNA showed three or four transitions in agreement with previous findings [33]. Average T_Ms and standard errors were calculated from at least three independent experiments and bootstrapping analysis was performed to ensure the robustness of the data where it was applicable.

Results

Disease-related mutations in human mitochondrial pre-tRNAs affect substrate binding of mtRNase P

Pre-tRNA 5' end cleavage is the first tRNA modification step in human mitochondria [14, 17, 35], thus proper substrate recognition by mtRNase P is crucial for efficient RNA processing. It has been long proposed that human mitochondrial tRNA mutations contribute to diseases by altering the structure of immature tRNAs and impairing recognition by processing and modification enzymes [4, 7, 8, 22, 33, 36-39]. However, how (mt)tRNA gene mutations affect substrate binding by mtRNase P has not been evaluated thus far. Therefore, in order to address this question we measured binding affinities ($K_{D,app}$) of by mtRNase P for

pre-tRNAs containing a variety of disease–linked mutations through *in vitro* fluorescent binding assays.

We previously found that pre-tRNA^{Ile}, pre-tRNA$^{Leu(UUR)}$ and pre-tRNA^{Met} are efficient substrates for mtRNase P when *in vitro* transcribed and unmodified (Karasik et al, submitted to NAR). Since these pre-tRNAs are also hotspots for mitochondrial disease mutations [10, 20, 40-42] we aimed to investigate *in vitro* binding of their mutant versions to mtRNase P. The representative set of mitochondrial disease tRNA mutations that we have chosen for our study is shown in Figure 1. The majority of the selected mutations are located in D- and T-loop and stem (tRNA elbow region; Figure 1D) while one maps in the acceptor stem and another one is found in the leader sequence and specifically in the first position in the 5' end of the tRNA leader (N_{-1} position).

We have *in vitro* transcribed and 5' fluorescently labeled all wild type and mutant pre-tRNAs and measured their binding affinity ($K_{d,\ app,\ mtRNase\ P}$) to mtRNase P based on fluorescent polarization binding assays (Karasik et al, Liu et al, submitted to NAR)). We found that only four of the pre-tRNA mutations moderately increase the $K_{d,\ app,\ mtRNase\ P}$ values by ~2-6 fold relative to the wild type pre-tRNA sequences (mutations A3243G G3249A, A4317G and C4320U) (Figure 2A, Supplement Table 1.). On the other hand, several of the mutant pre-tRNAs (G3242A, G3250C, A3288G, U3290C, A4269G, A4401G) did not have any apparent effect on human mtRNase P binding affinity.

Taken together, while our data indicate that many of the selected mutations weaken the interactions between pre-tRNAs and the human mtRNase P, some mutations did not have impact on it suggesting a different way of influencing mitochondrial function, such as affecting other activities of mtRNase P or influencing downstream mitochondrial functions (e.g. ribosome function or activities of other mitochondrial tRNA modification enzymes).

Mitochondrial pre-tRNA mutations decrease 5' end cleavage activity of mtRNase P

A mutation associated with inherited hypertension in mitochondrial pre-tRNA^{Ile} affected 5' tRNA processing by the mtRNase P [10]. Notably, even as little as 20% decrease in mtRNase P activity can manifest in mitochondrial disease [10]. Despite the connection of 5' end tRNA processing and diseases in human mitochondria, studies of how mutant forms of mitochondrial tRNAs are processed by mtRNase P are limited. Thus here we investigated the effect of selected disease-associated mutations (Figure 1) in human mitochondrial pre-tRNAs on mtRNase P's 5' end cleavage activity. We employed a previously optimized fluorescent polarization based single turnover assay for mtRNase P (Karasik et al, submitted to NAR). We found that single turnover activity, as represented by the observed kinetic rate ($k_{obs,cleavage}$), was affected for all investigated tRNA mutants by 10% to 55% as compared to wild type (Figure 2B). The greatest impact on mtRNase P's nuclease activity was caused by pre-tRNA mutations G3249A, A3288G in pre-tRNA ^{Leu} and 4401G in pre-tRNA^{Met} (more than or close to 50% decrease in activity). Additionally we have also observed a modest decrease (30-50%) in mtRNase P activity for mutations A3243A, G3242A, G3250C, U3251C in pre-tRNA^{Leu} and A4269G in pre-tRNA^{Ile}. However, some tRNA mutations, such as U3290C in pre-tRNA^{Leu} and A3269A and A4317G in pre-tRNA^{Ile}, only slightly affected (~10%) of mtRNase P's 5' pre-tRNA processing activity. Taken together, we found that several investigated mutations affected 5' tRNA cleavage efficiency modestly and some significantly of human mtRNase P.

Disease-linked pre-tRNA$^{Leu(UUR)}$ mutations severely affect m1G9 methylation activity in the mitochondria.

The MRPP1/2 sub-complex is predicted to methylate the m1A9/m1G9 position of most mitochondrial tRNAs, however it is unknown if disease-linked mutations in pre-tRNAs

can affect MRPP1/2's activity. We have previously shown that both tRNA$^{Leu(UUR)}$ and pre-tRNA^{Ile} are methylated at their N9 position by mtRNase P (Karasik et al, submitted to NAR). We therefore wanted to test whether disease-linked mutations alter the methylation efficiency of MRPP1/2 for the various mutant versions of these two pre-tRNAs. Initially, we tested the methylation efficiency of MRPP1/2 for the selected mutant pre-tRNA^{Ile}s using our previously developed single turnover primer extension methylation assays. Since the presence of human MRPP3 in methylation assays does not change the single turnover rate for pre-tRNA^{Ile} [16](Karasik et al, submitted to NAR), we assessed the effects of mitochondrial pre-tRNA mutations using the MRPP1/MRPP2 sub-complex without the presence of MRPP3 in the assays. We observed a differential effect of mutations in pre-tRNA^{Ile} on MRPP1/2 methylation activity. Specifically, MRPP1/2 single turnover methylation rates ($k_{obs,meth}$) of both C4320U and A4317G pre-tRNA^{Ile} mutants displayed negligible differences as compared to the wild-type pre-tRNA^{Ile} (Figure 3A). In contrast, the presence of A4269G mutation in pre-tRNA^{Ile} increased the MRPP1/2 single turnover methylation rate by ~2.5 fold (Figure 3A). Next, we investigated single turnover methylation rates for pre-tRNA$^{Leu(UUR)}$ variants and mtRNase P. We have previously found that presence of MRPP3 in methylation assays enhances single turnover methylation rates of the MRPP1/2 sub-complex for the wild type pre-tRNA$^{Leu(UUR)}$ and therefore we used equimolar amount of MRPP3 and the MRPP1/2 sub-complex in our methylation assays (Karasik et al, submitted to NAR). Most mutations in pre-tRNA^{Leu} slowed down single turnover kinetics as compared to the wild type pre-tRNA, and therefore determining single turnover methylation rates were challenging. Therefore we measured single turnover methylation rates at 1 hour and compared to that of the wild type pre-tRNA$^{Leu(UUR)}$. We found that all disease-linked pre-tRNA$^{Leu(UUR)}$ mutants reduced methyltransferase activity significantly for mtRNase P (~65-95 %). Overall, our results

suggest that investigated disease-related tRNA mutations can disrupt methyltransferase and cleavage activity of human mitochondrial mtRNase P.

Mutations in mitochondrial pre-tRNAs can alter their folding and structure.

Mutations in some mitochondrial tRNAs were shown to alter their structure which in turn may lead to decreased recognition by mitochondrial tRNA binding enzymes (such as the 3' end cleavage enzyme RNase Z) [7, 12]. Therefore, we also assessed the potential contribution of selected disease related mutations in inducing tRNA structural changes by UV melting experiments. In general, tRNAs exhibit several structural transitions while unfolding as a function of increasing temperature, manifesting as hyperchromicity that can be monitored at 260 nM [33]. The first major transition is traditionally assigned to the melting of the L-shaped tertiary structure [33]. Therefore, we focused only on dissecting the first transition of wild type and mutant pre-tRNAs (Figure 4).

Analyzing the UV melting temperature of the wild type pre-tRNA^{Ile} we found that it exhibited two major transitions with melting temperature 47.7 ˚C of the first transition (Figure 4A). Then we measured the UV melting profiles for mutant pre-tRNA^{Ile}s and compared it to wild type. We found that disease-associated tRNA mutations in pre-tRNA^{Ile} caused slight changes in the first observed transition as reflected by lower maximum derivates compared to that of the wild type (Figure 4A). In addition, while we observed one pronounced first transition for wild type pre-tRNA^{Ile} in the UV melting curve, the mutants appeared to have at least two separate transitions at lower temperatures (Supplement Table 2). Although these transitions were overlapping and not well resolved, it is consistent with previous UV melting experiments carried out on wild type tRNA^{Ser} and its disease-causing mutations where introducing mutations into tRNA^{Ser} caused the separation of the pronounced first melting transition into two transitions with lower maximum derivates and unfolding

enthalpy [33]. These slight changes in the UV melting curves of pre-tRNA^{Ile}s could represent disruption of interactions with Mg^{2+} or loss of H-bonding.

UV melting curves of wild type pre-tRNA$^{Leu(UUR)}$ and pre-tRNA^{Met} exhibited at least two but most four folding transitions similarly to previous findings for other tRNAs, such as human mitochondrial tRNA^{Ser} [33]. Notably, we also observed that the first transitions displayed lower melting temperature (28 ˚C and 32.6 ˚C, respectively) than the physiological temperature (37˚C) for these pre-tRNAs (Supplemental Figure 1). This indicates that at a physiological temperature these two mitochondrial tRNAs as transcribed and without any modifications may not be fully folded. Since most reported 5' end pre-tRNA cleavage reactions by mtRNaseP have been performed at 28 ˚C, we sought to address the effect of an increased temperature closer to physiological levels on mtRNase P nuclease activity. At 37˚C we observed no 5' end cleavage of pre-tRNA$^{Leu(UUR)}$ and pre-tRNA^{Met} by mtRNase P (Supplemental Figure 1B and C). This indicates that at physiological temperatures some pre-tRNAs may be lacking the proper tertiary structure, such as integrity of the elbow region, that would be required for their in vitro binding to and processing by mtRNase P. We have excluded the possibility that mtRNase is out of its optimal temperature range at 37 ˚C since it is able to bind and cleave *B.subtilis* pre-tRNA^{Asp} efficiently at this temperature (Liu et al, submitted to NAR). Our findings suggest that some *in vitro* transcribed human mitochondrial pre-tRNAs at physiological temperatures have reduced thermostability and that their i*n vivo* processing by mt RNase P may require either additional factors or modifications. However, our UV melting experiment conditions may not reflect fully that of mitochondria.

After analyzing the UV melting curve of wild type pre-tRNA^{Leu} and pre-tRNA^{Met} we also investigated that of their mutant versions. In contrast to UV melting profiles of pre-tRNA^{Ile}, we found that all mutant pre-tRNA$^{Leu(UUR)}$s almost entirely lack the first transition observed for wild type (Figure 2B). This suggests that introducing a mutation into pre-

tRNA$^{Leu(UUR)}$ can severely affect folding and disrupt tertiary structural elements, such as interaction between the D- or T-loop. We have also examined wild type and A4401G pre-tRNA^{Met} in UV melting experiments. Since the mutation is in the 5' leader of the tRNA we did not expect to observe major differences in the UV melting profile between the two pre-tRNAs. In agreement with this the mutant pre-tRNA^{Met} exhibited similar first transition and melting temperature as wild type (T_{mA401G}=33.8 ± 1.1˚C, $T_{m\ wild\ type}$= 32.6 ± 1.1˚C). Overall, we found that majority mitochondrial tRNA mutations affected UV melting curve of the investigated pre-tRNAs implying changes in their structure.

Discussion

Reduced 5' end processing by mtRNase P in the human mitochondria is linked to disease-related mutations in tRNA genes [10, 25, 26, 29]. While mitochondrial tRNA mutations leading to diseases are numerous, there are only few *in vitro* studies investigating the connection between those and mtRNase P [10]. Thus we speculated that many more tRNA mutations in mtDNA linked to different diseases could affect mtRNase P function in the mitochondria. Here, we show that eleven mutations associated with different mitochondrial diseases in pre-tRNAs significantly reduce binding, methylation and 5' end processing activity of mtRNase P. It is also known that mitochondrial tRNA mutations can cause changes in the structure of the tRNAs [8] that impair proper substrate recognition by maturation enzymes [7, 12, 36]. We also find that a sub-set of investigated pre-tRNA mutations influence the UV melting profile and therefore potentially the structure of pre-tRNAs that may account some of the decreased enzymatic activities of mtRNase P.

In the pool of our investigated pre-tRNA mutants, outcomes and severity of associated diseases is in a wide range from infantile onset and early death to mild symptoms appearing later in adulthood. A4269G and A4317G mutations are associated with fatal

infantile cardiomyopathy (FICP) that manifests in neonates and infants resulting in severe disease and early termination of life [38, 43, 44]. Furthermore, early-onset severe encephalomiopathy is associated with C4320U mutation [45]. Among the investigated tRNA mutations, G3250C, U3251G and A3288G cause mitochondrial myopathies and G3249A is associated with Kearns-Sayre syndrome, a condition that causes blindness and cardiac dysfunction [40, 46-48]. Patients with these mutations usually survive into teenager hood or adulthood, however manifestations of these diseases often impair their health and quality of living. In the contrary, A4401G and U3290C mutations are possible hypertension factors, a condition that influences health of individuals later in their life [42, 49]. Many mutations in mitochondrial pre-tRNAs are associated with several diseases, such as A3242G, which is indicated in cardiomyopathy and ineffective hematopoiesis [50, 51] and A3243G mutation with MELAS (mitochondrial encephalomyopathy, lactic-acidose and stroke-like episodes) and diabetes with deafness [20, 52, 53]. It is likely that manifestations of these diseases are dependent on other factors in the patients, such as genetic background.

Seven of the eleven selected mitochondrial tRNA mutations are located near or in the elbow region of human mitochondrial pre-tRNA$^{Leu(UUR)}$ (Figure 1). These mutations have the potential to directly impair specific tRNA-mtRNAse P interactions (such as mutations A3243G, A4317G) or influence the structural integrity of the elbow region (disrupting predicted interactions between the T- and D-loop, e.g. A3243G and G3249A) of the pre-tRNA and therefore disable proper binding or substrate orientation by mtRNase P. We found that all investigated pre-tRNA^{Leu} mutations severely impacted single turnover rates for m1G9 methylation (~65-5% as compared to wild type) and decreased single turnover 5' end cleavage rates of mtRNase P by ~10-55%. Consistently with this finding, all mutant pre-tRNA$^{Leu(UUR)}$s show significantly altered UV melting profile as compared to the wild type referring to the affected folding and structure of these mutant pre-tRNAs. We find that

melting temperature of the wild type pre-tRNA$^{Leu(UUR)}$ is significantly lower than physiological temperature (T_m=~28˚C) suggesting that this pre-tRNA is structurally instable. It is possible that investigated mutations cause slight disturbances in folding and tertiary structure that is overall enough to disrupt the tertiary interactions of pre-tRNA$^{Leu(UUR)}$s and consequently significantly affect the first transition observed in UV melting experiments. The severely affected folding and structure of investigated pre-tRNA$^{Leu(UUR)}$s can explain the observed reduced 5' end cleavage and methylation single turnover rates for mtRNase P. However, we found that binding of these mutant pre-tRNA$^{Leu(UUR)}$s to mtRNase P (titrated for PRORP) was not altered significantly, except for A3243G pre-tRNA$^{Leu(UUR)}$. This suggests that elimination of some of the structural elements of tRNA$^{Leu(UUR)}$ only partially affects substrate recognition. We propose that although most of these mutants still bind to mtRNase P, they are not presented properly to the active sites of MRPP1 and PRORP resulting in reduced methyltransferase and cleavage activity. Overall, our data suggest that these disease-related mutations in pre-tRNA$^{Leu(UUR)}$ can affect several functions of mtRNase P and potentially influence mitochondrial tRNA maturation pathway *in vivo*, however this needs further testing.

Mitochondrial tRNA^{Ile} gene is also a hotspot for mutations. Thus, we have also investigated three pre-tRNA^{Ile}s containing disease-associated mutations located near or in the elbow region of the pre-tRNA. It has been previously shown that the A4269G mutation in mature tRNA^{Ile}, associated with the mitochondrial disease FICP, reduces aminoacylation, half-life *in vivo* and melting temperature *in vitro* [38]. In agreement with these findings, we have observed that this mutation slightly affected the folding and structure of pre-tRNA^{Ile} in UV melting experiments and significantly reduced 5' end pre-tRNA cleavage however it did not influence substrate recognition by mtRNase P. The A4269G mutation is expected to disrupt local secondary tRNA structure by eliminating base pairing at the base of the acceptor

stem and consequently cause changes in the structure of this region. Therefore, integrity in this area may play a role in proper orientation of the substrate for 5' end cleavage. On the other hand, single turnover methylation rates for this mutant pre-tRNA were enhanced (~2.5 fold). This can be potentially explained with better access to the methylation site by MRPP1 due to more relaxed structure in the acceptor stem. We have also found that A4317G and C4320U mutant pre-tRNA^{Ile}s were bound less tightly to mtRNase P and had slightly altered UV melting profile compared to the wild type pre-tRNA^{Ile}. However, these mutations did not influence single turnover methylation rates and decreased 5'end cleavage activity of mtRNAs P with only about ~10%. This suggests that these mutations may affect different functions in the mitochondria than 5' end processing or R9 methylation of pre-tRNAs. Nevertheless, we note that previous studies only found ~ 20% decrease in single turnover activity of mtRNase P *in vitro* for A4263G pre-tRNA^{Ile} mutant, but significant accumulation of 5' uncleaved mitochondrial pre-tRNAs *in vivo* [10]. Therefore, the possible role of mtRNAs P in diseases linked to A4317G and C4320U tRNA mutations cannot be excluded.

Plant homologs of MRPP3 have been shown to interact with the N_{-1} base in the 5' end leader of pre-tRNAs [54, 55]. Therefore, we hypothesized that disease-linked mutations in this position could influence 5'end tRNA cleavage in the mitochondria that could contribute to the development of diseases. Hence we also investigated the effects of mutation in mitochondrial pre-tRNA^{Met} (A4401G, found at the N_{-1} position) on mtRNase P activities. We found that this mutation affected 5'end cleavage, but not binding of mtRNase P and it did not alter the melting temperature of pre-tRNA^{Met}. We speculate that this mutation may influence the interaction between the 5' end leader and PRORP by disrupting the proper orientation of the 5' end leader to the active site of MRPP3, subsequently causing decreased 5' end processing rates by mtRNase P. Since folding and structure of this mutant pre-tRNA seems to be unaffected based on our data, subsequent steps after 5' end cleavage in the

mitochondrial tRNA maturation pathway are also unlikely to be impaired. Therefore, reduced 5' end pre-tRNA processing could be the one of the factors leading to development of hypertension in patients carrying A4401G mutation, however this needs further testing.

Freshly transcribed mitochondrial polycistronic units punctuated by tRNAs are expected to be subject to a hierarchical cascade of processing and modifications with the 5' end pre-tRNA processing and methylation by mtRNase P shown to be the first in line after transcription and required for downstream processes [14, 35]. Therefore, many pre-tRNA mutations could affect and decrease impact mtRNase P function first despite on the potential effect on other downstream processes. Additional negative effects of these mutations in downstream processes and enzymes are possible and the impact on the latter may compound the initial effect on mtRNase P activity multiplying the adverse consequences of these mutations. In support, there are accumulating evidences that downstream enzymes from mtRNase P in the mitochondrial tRNA maturation pathway also have reduced activities with pre-tRNAs containing disease-linked mutations [7, 12, 36, 41, 56, 57]. In particular, some of the investigated mutations (such as A4317G in pre-tRNA^{Ile} [57]) have been previously shown to have inhibitory effect on 3' tRNA maturation by human mitochondrial ELAC2 [41, 57]. We also observed effects on different enzyme activities (5' end processing and methylation) of the same pre-tRNA mutation. Therefore, it is likely that tRNA mutations in the mtDNA affect several steps of pre-tRNA maturation and development of diseases could be the consequence of these additive sequential effects on enzyme activity. There is a wide range of manifestation of mitochondrial diseases associated with tRNA mutations that may arise from differences in how severely these mutations affect the different steps in the tRNA maturation pathway. However, *in vivo* studies are needed to investigate the exact role of mtRNase P in human mitochondrial diseases and the potential of the additive effects on the mitochondrial tRNA maturation pathway.

Taken together, we have found that the *in vitro* activities of mtRNase P are decreased by many pre-tRNAs with human disease-linked mutations suggesting the potential connection of this enzyme complex with the development of several mitochondrial diseases.

ACKNOWLEDGEMENTS

We thank Dr. Aranganathan Shamuganathan for supplying some of the MRPP1/2 enzyme preparation. We also thank Dr. Adrian Ferre-D'Amare, Dr. Robert Trachman and Dr. Xin Liu for providing great help for UV melting experiments.

FUNDING

This work was supported by the National Institutes of Health [R01 GM117141 to M.K.] and by American Heart Association pre-doctoral fellowship [16PRE29890011 to A.K.].

Conflict of interest

None.

Figures

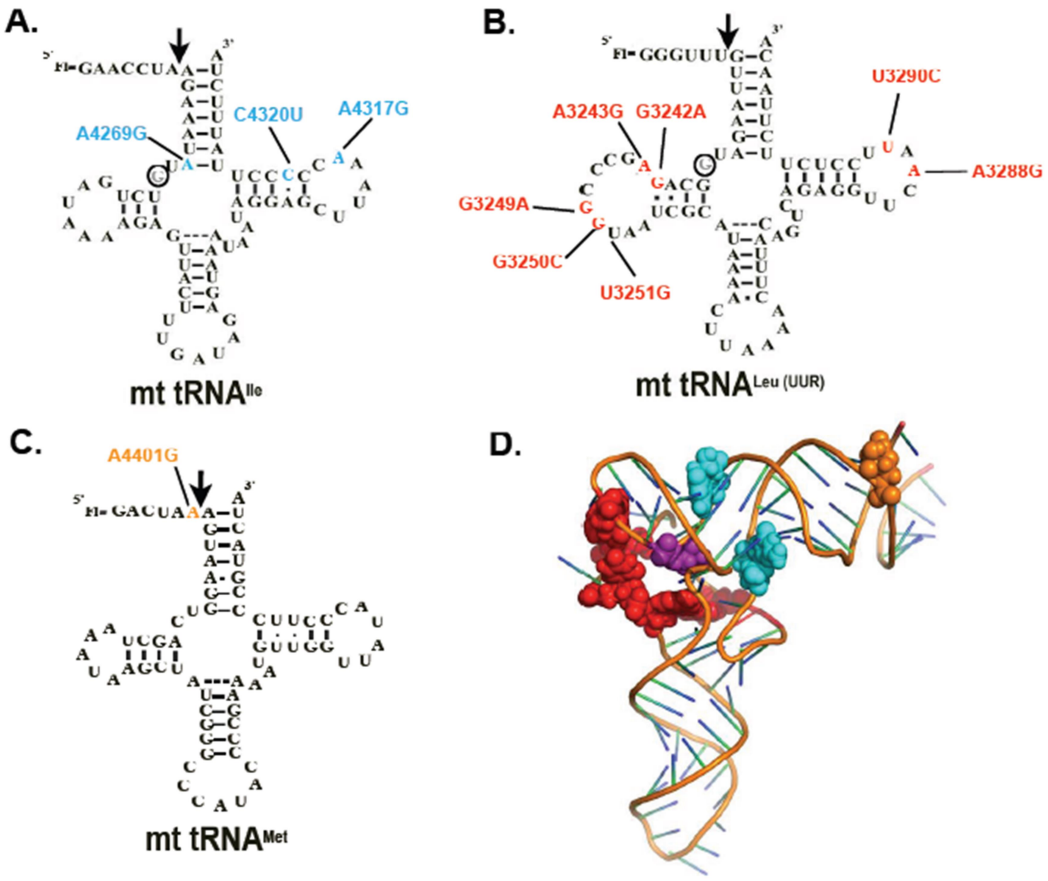


Figure 1. Locations of the investigated mitochondrial tRNA mutations in the predicted secondary structure of **A.** pre-tRNA^{Ile}, **B.** pre-tRNA$^{Leu(UUR)}$ and **C.** pre-tRNA^{Met}. Circles indicate methylation sites for the MRPP1/2 sub-complex. **D.** Location of the mutations in the L-shaped tertiary structure of tRNAs. High-resolution structure of the investigated tRNAs are not available therefore we have used a conserved eukaryotic tRNA with known structure (PDB ID: 1ehz) for generating the figure. Mutations are color coded according to the colors shown in Figure A., B. and C. Purple represents mutation at the same position in pre-tRNA^{Leu} (U3290C) and pre-tRNA^{Ile} (A4317G).

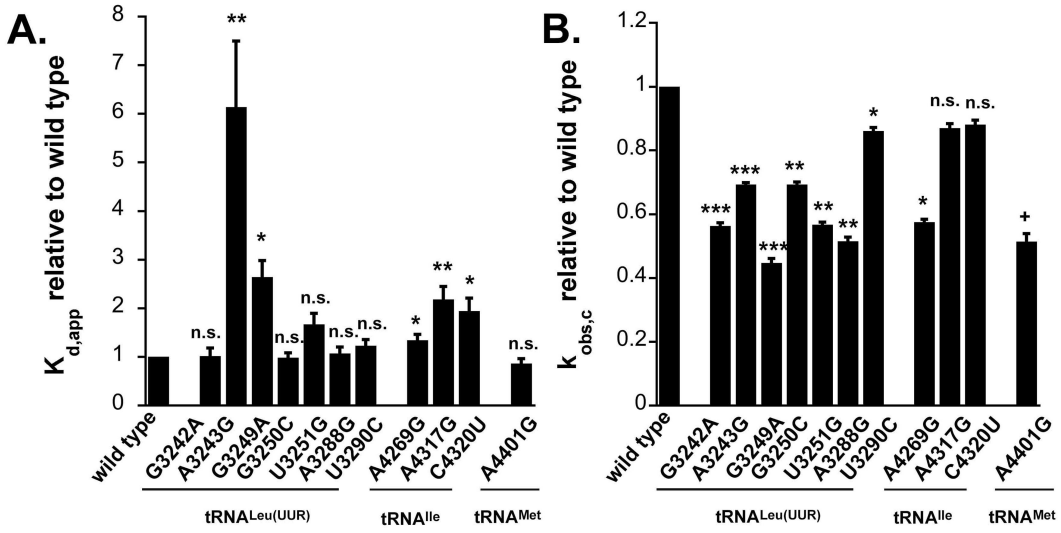


Figure 2. Disease-related tRNA mutations affect binding and 5' end pre-tRNA processing by the mtRNase P.

A. Average binding affinities of mitochondrial pre-tRNAs containing mutations for mtRNase P using standard binding conditions. 20 nM fluorescently labeled substrates were pre-incubated with 150 nM MRPP1/2 for 5 minutes and then titrated with 0-5 μM MRPP3. Data was collected when binding reached equilibria. **B.** Average single turnover cleavage rates of mitochondrial pre-tRNAs containing mutations for mtRNase P using standard cleavage conditions. Reactions contained 20 nM fluorescently labeled substrate, 1 μM MRPP3 and 0.4 μM MRPP1/2. For both Figure A. and B. paired t-test were performed assessing if observed differences were significant between $K_{d,\ app}$s and $k_{obs,\ c}$ of mutant and wild type pre-tRNAs. Significant differences were labeled with asterisks (* p value <0.05, ** p value <0.01, *** p value <0.001, + p value =0.07) or columns were labeled as n.s. (not significant) where no significant differences were found.

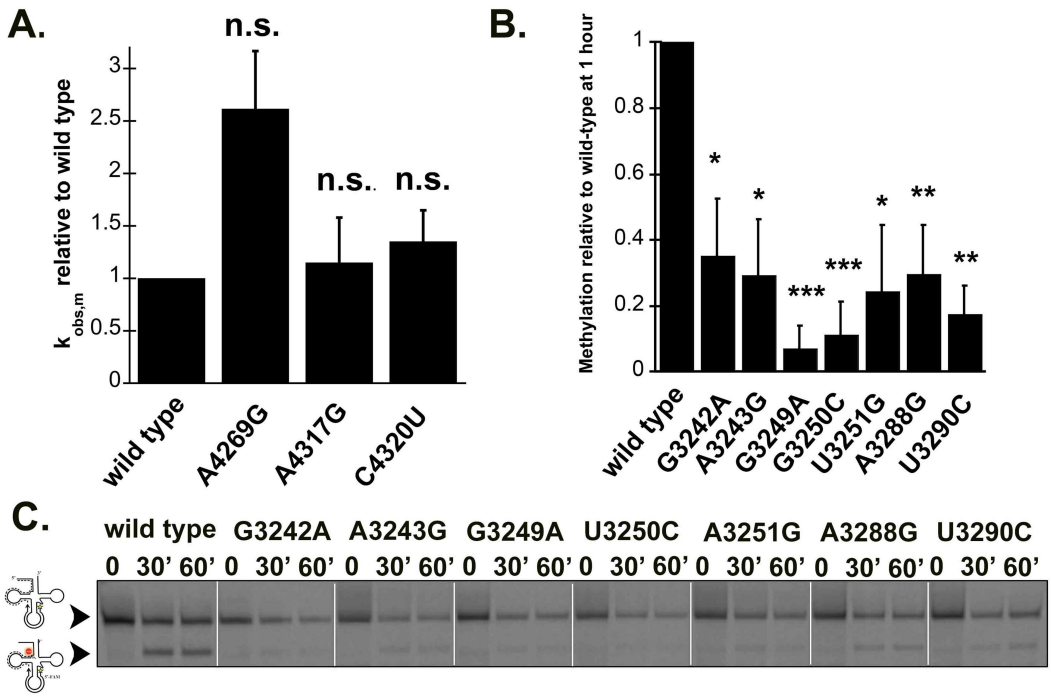


Figure 3. Disease-linked mutations in human mitochondrial pre-tRNA$^{Leu(UUR)}$ decrease methylation efficiency of the human mtRNase P complex.
A. Average single turnover methylation rates of mitochondrial mutant pre-tRNA^{Ile} relative to that of the wild type pre-tRNA^{Ile} and the MRPP1/2 sub-complex using standard reaction conditions. Reaction contained 800 nM unlabeled pre-tRNA and 5 µM MRPP1/2. **B.** Quantification of methylation efficiency of mutant pre-tRNA$^{Leu(UUR)}$s relative to wild type after 60 minutes incubation with mtRNase P. Reaction contained 800 nM unlabeled pre-tRNA and 5 µM MRPP1/2 and MRPP3. **C.** Representative gel showing methylation efficiencies of wild type and mutant pre-l$^{(UUR)}$ by human mtRNase P at 30 and 60 minutes using standard reaction conditions. Black arrows indicate two products of primer extension reactions; the read through and the stop at the methylation sites. For both Figure A. and B. paired t-test were performed assessing if observed differences were significant between $k_{obs,m}$ and relative methylation of mutant and wild type pre-tRNAs. Significant differences were labeled with asterisks (* p value <0.05, ** p value <0.01, *** p value <0.001) or columns were labeled as n.s. (not significant) where no significant differences were found.

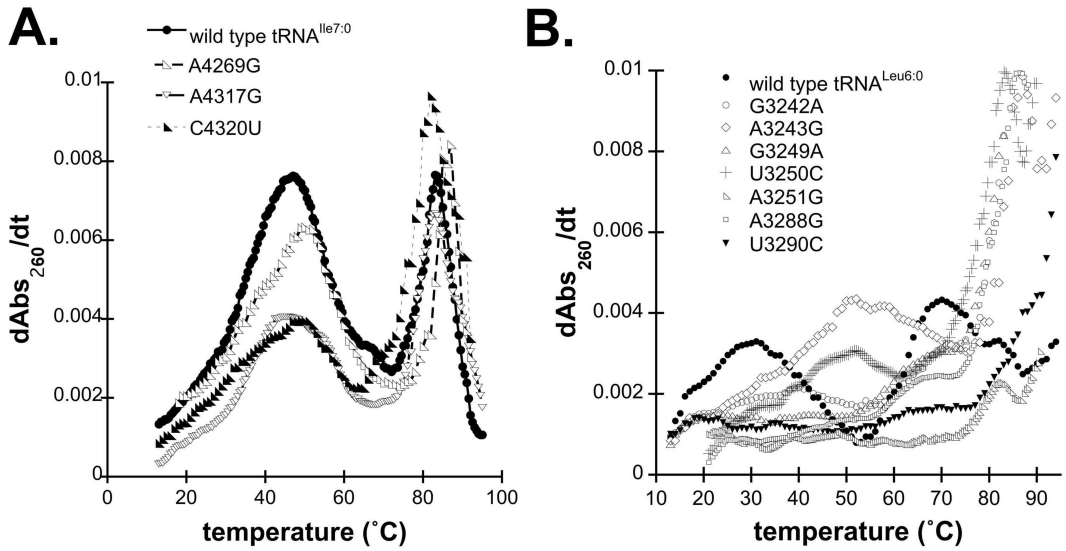


Figure 4. Disease-associated tRNA mutations alter the structure of pre-tRNAs.
A. Representative UV melting profile curves for the wild type and mutant $tRNA^{Ile}$s.
B. Representative UV melting profile curves of wild type and mutant $tRNA^{Leu}_{(UUR)}$s.

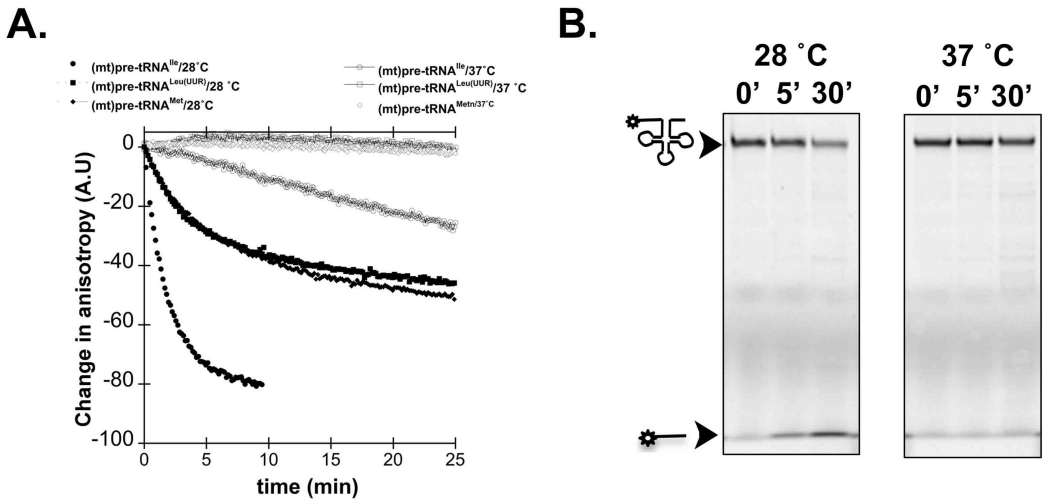
Supplemental material

Supplement Table 1. Disease-linked tRNA mutations affect binding and cleavage rates of mtRNase P.

human mitochondrial pre-tRNA	$K_{d,\ app,\ mtRNase\ P}$ (nM)	$k_{obs,cleavage}$ (min^{-1})
$tRNA^{Leu\ (UUR)}$	50.6 ± 5.3	0.309 ± 0.002
G3242A	51.3 ± 8.3	0.174 ± 0.002
A3243G	310.4 ± 69.0	0.214 ± 0.003
G3249A	133.3 ± 17.5	0.138 ± 0.004
G3250C	49.6 ± 4.9	0.214 ± 0.003
U3251G	84.2 ± 11.5	0.175 ± 0.003
A3288G	53.9 ± 6.9	0.159 ± 0.004
U3290C	62.0 ± 6.5	0.266 ± 0.003
$tRNA^{Ile}$	13.5 ± 2.33	0.573 ± 0.008
A4269G	19.4 ± 1.8	0.326 ± 0.005
A4317G	31.6 ± 3.9	0.493 ± 0.008
C4320U	28.1 ± 3.9	0.499 ± 0.008
$tRNA^{Met}$	707 ± 168	0.286 ± 0.006
A4401G	606.7 ± 72.8	0.147 ± 0.007

Supplement Table 2. Melting temperature values for first transitions for wild type pre-tRNAs and pre-$tRNA^{Ile\ 7:0}$ mutants.

human mitochondrial pre-tRNA	T_M1 (°C)	T_M2 (°C)
$tRNA^{Leu(UUR)}$	28.7 ± 0.1	-
$tRNA^{Met}$	32.6 ± 1.1	
$tRNA^{Ile}$	47.7 ± 1.6	
A4317G	42.5 ± 0.9	56.2 ± 0.5
C4320T	27.7 ± 3.7	47.5 ± 0.4



Supplemental Figure 1. Human mtRNase Ps do not process some pre-tRNAs at physiological temperatures.
A. The mtRNase P-complex processes the 5’ end of tRNA$^{Leu(UUR)}$, tRNA^{Ile} and tRNA^{Met} at 28 ˚C but not at 37˚C using fluorescent polarization cleavage assays. **B.** The mtRNase P-complex processes the 5’ end of pre-tRNA$^{Leu(UUR)}$ at 28 ˚C but not at 37˚C shown by gel-based cleavage assay.

REFERENCES

1. Lightowlers, R.N., R.W. Taylor, and D.M. Turnbull, *Mutations causing mitochondrial disease: What is new and what challenges remain?* Science, 2015. **349**(6255): p. 1494-9.
2. Chinnery, P.F., *Mitochondrial disease in adults: what's old and what's new?* EMBO Mol Med, 2015. **7**(12): p. 1503-12.
3. Finsterer, J. and S. Kothari, *Cardiac manifestations of primary mitochondrial disorders.* Int J Cardiol, 2014. **177**(3): p. 754-763.
4. Abbott, J.A., C.S. Francklyn, and S.M. Robey-Bond, *Transfer RNA and human disease.* Front Genet, 2014. **5**: p. 158.
5. Schapira, A.H., *Mitochondrial diseases.* Lancet, 2012. **379**(9828): p. 1825-34.
6. Suzuki, T., A. Nagao, and T. Suzuki, *Human mitochondrial tRNAs: biogenesis, function, structural aspects, and diseases.* Annu Rev Genet, 2011. **45**: p. 299-329.
7. Levinger, L., M. Morl, and C. Florentz, *Mitochondrial tRNA 3' end metabolism and human disease.* Nucleic Acids Res, 2004. **32**(18): p. 5430-41.
8. Wittenhagen, L.M. and S.O. Kelley, *Impact of disease-related mitochondrial mutations on tRNA structure and function.* Trends Biochem Sci, 2003. **28**(11): p. 605-11.
9. Phizicky, E.M. and A.K. Hopper, *tRNA biology charges to the front.* Genes Dev, 2010. **24**(17): p. 1832-60.
10. Wang, S., et al., *Maternally inherited essential hypertension is associated with the novel 4263A>G mutation in the mitochondrial tRNAIle gene in a large Han Chinese family.* Circ Res, 2011. **108**(7): p. 862-70.
11. Chatfield, K.C., et al., *Mitochondrial energy failure in HSD10 disease is due to defective mtDNA transcript processing.* Mitochondrion, 2015.
12. Levinger, L. and D. Serjanov, *Pathogenesis-related mutations in the T-loops of human mitochondrial tRNAs affect 3' end processing and tRNA structure.* RNA Biol, 2012. **9**(3): p. 283-91.
13. Ojala, D., J. Montoya, and G. Attardi, *tRNA punctuation model of RNA processing in human mitochondria.* Nature, 1981. **290**(5806): p. 470-4.
14. Sanchez, M.I., et al., *RNA processing in human mitochondria.* Cell Cycle, 2011. **10**(17): p. 2904-16.
15. Holzmann, J., et al., *RNase P without RNA: identification and functional reconstitution of the human mitochondrial tRNA processing enzyme.* Cell, 2008. **135**(3): p. 462-74.
16. Vilardo, E., et al., *A subcomplex of human mitochondrial RNase P is a bifunctional methyltransferase--extensive moonlighting in mitochondrial tRNA biogenesis.* Nucleic Acids Res, 2012. **40**(22): p. 11583-93.
17. Rackham, O., et al., *Hierarchical RNA Processing Is Required for Mitochondrial Ribosome Assembly.* Cell Rep, 2016. **16**(7): p. 1874-90.
18. Sen, A., et al., *Loss of the mitochondrial protein-only ribonuclease P complex causes aberrant tRNA processing and lethality in Drosophila.* Nucleic Acids Res, 2016. **44**(13): p. 6409-22.
19. Munch, C. and J.W. Harper, *Mitochondrial unfolded protein response controls matrix pre-RNA processing and translation.* Nature, 2016. **534**(7609): p. 710-3.
20. Li, R. and M.X. Guan, *Human mitochondrial leucyl-tRNA synthetase corrects mitochondrial dysfunctions due to the tRNALeu(UUR) A3243G mutation, associated*

with mitochondrial encephalomyopathy, lactic acidosis, and stroke-like symptoms and diabetes. Mol Cell Biol, 2010. **30**(9): p. 2147-54.
21. Bindoff, L.A., et al., *Abnormal RNA processing associated with a novel tRNA mutation in mitochondrial DNA. A potential disease mechanism.* J Biol Chem, 1993. **268**(26): p. 19559-64.
22. Rossmanith, W. and R.M. Karwan, *Impairment of tRNA processing by point mutations in mitochondrial tRNA(Leu)(UUR) associated with mitochondrial diseases.* FEBS Lett, 1998. **433**(3): p. 269-74.
23. Deutschmann, A.J., et al., *Mutation or knock-down of 17beta-hydroxysteroid dehydrogenase type 10 cause loss of MRPP1 and impaired processing of mitochondrial heavy strand transcripts.* Hum Mol Genet, 2014.
24. Chatfield, K.C., et al., *Mitochondrial energy failure in HSD10 disease is due to defective mtDNA transcript processing.* Mitochondrion, 2015.
25. Falk, M.J., et al., *A novel HSD17B10 mutation impairing the activities of the mitochondrial RNase P complex causes X-linked intractable epilepsy and neurodevelopmental regression.* RNA Biol, 2016. **13**(5): p. 477-85.
26. Vilardo, E. and W. Rossmanith, *Molecular insights into HSD10 disease: impact of SDR5C1 mutations on the human mitochondrial RNase P complex.* Nucleic Acids Res, 2015. **43**(13): p. 6649.
27. Amberger, A., et al., *17beta-Hydroxysteroid dehydrogenase type 10 predicts survival of patients with colorectal cancer and affects mitochondrial DNA content.* Cancer Lett, 2016. **374**(1): p. 149-55.
28. Chatfield, K.C., et al., *Mitochondrial energy failure in HSD10 disease is due to defective mtDNA transcript processing.* Mitochondrion, 2015.
29. Deutschmann, A.J., et al., *Mutation or knock-down of 17beta-hydroxysteroid dehydrogenase type 10 cause loss of MRPP1 and impaired processing of mitochondrial heavy strand transcripts.* Hum Mol Genet, 2014. **23**(13): p. 3618-28.
30. Hodgkinson, A., et al., *High-resolution genomic analysis of human mitochondrial RNA sequence variation.* Science, 2014. **344**(6182): p. 413-5.
31. Karasik, A., et al., *Nuclear Protein-Only Ribonuclease P2 Structure and Biochemical Characterization Provide Insight into the Conserved Properties of tRNA 5′ End Processing Enzymes.* J Mol Biol, 2016. **428**(1): p. 26-40.
32. Howard, M.J., et al., *Mitochondrial ribonuclease P structure provides insight into the evolution of catalytic strategies for precursor-tRNA 5′ processing.* Proc Natl Acad Sci U S A, 2012. **109**(40): p. 16149-54.
33. Mustoe, A.M., et al., *Noncanonical secondary structure stabilizes mitochondrial tRNA(Ser(UCN)) by reducing the entropic cost of tertiary folding.* J Am Chem Soc, 2015. **137**(10): p. 3592-9.
34. Draper, D.E., Bukhman, Y. V., and Gluick, T. C., *Thermal Methods for the Analysis of RNA Folding Pathways, Current Protocols in Nucleic Acid Chemistry.* John Wiley & Sons, New York, 2000: p. section 11.13.
35. Reinhard, L., S. Sridhara, and B.M. Hallberg, *The MRPP1/MRPP2 complex is a tRNA-maturation platform in human mitochondria.* Nucleic Acids Res, 2017.
36. Yan, H., N. Zareen, and L. Levinger, *Naturally occurring mutations in human mitochondrial pre-tRNASer(UCN) can affect the transfer ribonuclease Z cleavage site, processing kinetics, and substrate secondary structure.* J Biol Chem, 2006. **281**(7): p. 3926-35.
37. Kelley, S.O., S.V. Steinberg, and P. Schimmel, *Fragile T-stem in disease-associated human mitochondrial tRNA sensitizes structure to local and distant mutations.* J Biol Chem, 2001. **276**(14): p. 10607-11.

38. Yasukawa, T., et al., *A pathogenic point mutation reduces stability of mitochondrial mutant tRNA(Ile).* Nucleic Acids Res, 2000. **28**(19): p. 3779-84.
39. Kelley, S.O., S.V. Steinberg, and P. Schimmel, *Functional defects of pathogenic human mitochondrial tRNAs related to structural fragility.* Nat Struct Biol, 2000. **7**(10): p. 862-5.
40. Wang, M., et al., *Multilevel functional and structural defects induced by two pathogenic mitochondrial tRNA mutations.* Biochem J, 2013. **453**(3): p. 455-65.
41. Levinger, L., et al., *A pathogenesis-associated mutation in human mitochondrial tRNALeu(UUR) leads to reduced 3'-end processing and CCA addition.* J Mol Biol, 2004. **337**(3): p. 535-44.
42. Li, R., et al., *Failures in mitochondrial tRNAMet and tRNAGln metabolism caused by the novel 4401A>G mutation are involved in essential hypertension in a Han Chinese Family.* Hypertension, 2009. **54**(2): p. 329-37.
43. Hino, N., et al., *The pathogenic A4269G mutation in human mitochondrial tRNA(Ile) alters the T-stem structure and decreases the binding affinity for elongation factor Tu.* Genes Cells, 2004. **9**(3): p. 243-52.
44. Taniike, M., et al., *Mitochondrial tRNA(Ile) mutation in fatal cardiomyopathy.* Biochem Biophys Res Commun, 1992. **186**(1): p. 47-53.
45. Santorelli, F.M., et al., *A novel mitochondrial DNA point mutation associated with mitochondrial encephalocardiomyopathy.* Biochem Biophys Res Commun, 1995. **216**(3): p. 835-40.
46. Seneca, S., et al., *A new mitochondrial point mutation in the transfer RNA(Leu) gene in a patient with a clinical phenotype resembling Kearns-Sayre syndrome.* Arch Neurol, 2001. **58**(7): p. 1113-8.
47. Goto, Y., et al., *A novel point mutation in the mitochondrial tRNA(Leu)(UUR) gene in a family with mitochondrial myopathy.* Ann Neurol, 1992. **31**(6): p. 672-5.
48. Sweeney, M.G., et al., *Mitochondrial myopathy associated with sudden death in young adults and a novel mutation in the mitochondrial DNA leucine transfer RNA(UUR) gene.* Q J Med, 1993. **86**(11): p. 709-13.
49. Zhu, H.Y., et al., *A mitochondrial mutation A4401G is involved in the pathogenesis of left ventricular hypertrophy in Chinese hypertensives.* Eur J Hum Genet, 2009. **17**(2): p. 172-8.
50. Wortmann, S.B., et al., *Mitochondrial DNA m.3242G > A mutation, an under diagnosed cause of hypertrophic cardiomyopathy and renal tubular dysfunction?* Eur J Med Genet, 2012. **55**(10): p. 552-6.
51. Gattermann, N., et al., *Ineffective hematopoiesis linked with a mitochondrial tRNA mutation (G3242A) in a patient with myelodysplastic syndrome.* Blood, 2004. **103**(4): p. 1499-502.
52. Gerber, B., et al., *A family with diabetes and heart failure.* BMJ Case Rep, 2010. **2010**.
53. Goto, Y., I. Nonaka, and S. Horai, *A mutation in the tRNA(Leu)(UUR) gene associated with the MELAS subgroup of mitochondrial encephalomyopathies.* Nature, 1990. **348**(6302): p. 651-3.
54. Klemm, B.P., et al., *Molecular recognition of pre-tRNA by Arabidopsis protein-only Ribonuclease P.* Rna, 2017.
55. Howard, M.J., Karasik, A., Klemm, B., Mei C., Shanmuganathan, A., Fierke C.A., Koutmos, M., *Kinetic characterization of plant protein-only RNase P isozymes reveals overlapping substrate specificities and varying cleavage fidelities.* Submitted, 2015.

56. Sissler, M., et al., *Aminoacylation properties of pathology-related human mitochondrial tRNA(Lys) variants.* Rna, 2004. **10**(5): p. 841-53.
57. Levinger, L., R. Giege, and C. Florentz, *Pathology-related substitutions in human mitochondrial tRNA(Ile) reduce precursor 3' end processing efficiency in vitro.* Nucleic Acids Res, 2003. **31**(7): p. 1904-12.

CHAPTER 4: CONCLUSIONS

PRORPs were discovered a decade ago in human mitochondria [1]. Although their relation to human health and disease was becoming evident, there were only limited studies on this novel group of enzymes. Therefore, throughout my research I focused on uncovering structural and functional characteristics of PRORPs, with a specific focus on single unit nuclear *A.thaliana* PRORP2 and multi-subunit human mitochondrial mtRNase P that contains MRPP3, the human PRORP nuclease homologue.

4.1 SINGLE UNIT PRORPS

4.1.1 *A.thaliana* PRORPs are structurally and functionally conserved

While initial characterization of organellar PRORPs had begun, there was limited knowledge on the structure and function of nuclear PRORPs, including metal dependency, substrate specificity, mechanism and length of pre-tRNA trailer and leader sequences optimal for 5' end processing. Thus, I have investigated these questions using a single unit nuclear PRORP as an *in vitro* model, *A.thaliana* PRORP2.

I have shown that nuclear PRORP2 shares many structural and functional characteristics, albeit few minor differences, with paralog PRORPs. Moreover, I have demonstrated that Mg^{2+} is its most likely physiological metal, similarly to PRORP1. Furthermore, in our structural studies, we found that PRORP2 has the same overall V-shape and domain structure as PRORP1. PRORP2 however has a more open conformation since it displays a wider angle between the metallonuclease and substrate binding domains with minor local structural differences. My mutagenesis studies also pointed out that PRORP2's active site is highly conserved. It is noteworthy that the structure and metal dependency of PRORP2 were also studied simultaneously by an independent group, whose paper followed

mine, recapitulating the same conclusions [2]. Moreover, I have found that PRORP2 prefers to bind substrates with short trailer and leader sequences, however it cleaves them with comparable single turnover rate constant similarly to PRORP1 (collaborator's work included in Chapter 2 Paper 2) and PRORP3 (work based on a more recent publication by another group [3]). In addition, in order to evaluate the substrate specificity of PRORPs paralogs we compared (in collaboration) binding affinities and single and multiple turnover kinetic values for all *A.thaliana* PRORPs with four different *A.thaliana* pre-tRNAs of diverse origin (two nuclear, one mitochondrial and one chloroplast pre-tRNA). We concluded that there is little or no difference in substrate specificity between the three *A.thaliana* PRORPs. On the other hand, I have shown that nad6-t-element, a mitochondrial RNA and therefore a substrate expected to be specific to PRORP1, is cleaved ~10 times less efficiently by nuclear PRORP2 than PRORP1. Overall, this suggests that these PRORPs recognize and cleave their substrates in a similar manner, although they show some specificity towards localization specific substrates, such as t-elements.

4.1.2 PRORPs employ a different substrate recognition and cleavage mechanism than ribozyme RNase P

Since the discovery of PRORPs the question arose of how two remarkably different molecules, the protein PRORP and the ribozyme RNase P, that catalyze the exact same reaction compare in terms of substrate recognition and chemistry strategies. The rate-limiting step for ribozyme RNase P was shown to be the product release [4]. By comparing single and multiple turnover kinetic values for PRORP2 and various substrates I demonstrated that the rate-limiting step for PRORP2 is not the product release in contrast to ribozyme RNase P. Likewise the same conclusion was reached for PRORP1 and 3 (collaborator's data). This suggests that there are differences in the catalytic mechanism of the two distinct nucleases.

Despite the availability of PRORP structures, it was hard to predict with a molecular level detail how PRORP binds pre-tRNAs due to the absence of high resolution structures of PRORP-RNA complexes. Therefore, to uncover the PRORP-substrate interactions I have performed an extensive mutagenesis study on PRORP2 and characterized the potential ionic and non-ionic interactions between pre-tRNAs and PRORP2 in binding assays. As a result, I have identified several residues likely to be involved in substrate binding that map in PRORP2's 2^{nd}-4^{th} PPR motifs. Based on these data I constructed a model of a PRORP-pre-tRNA complex. Parallel studies from an independent lab (published around the same time with our work) based on mutagenesis and SAXS PRORP2 data confirmed and reinforced our own conclusions [2].

4.1.3 The PRORP inhibitor juglone covalently modifies surface cysteine residues

Juglone, a naturally occurring protein inhibitor, was identified also as a PRORP inhibitor by our collaborators based on *in vitro* high-throughput assays. However, the molecular mechanism of inhibition and the inhibition sites in PRORPs were elusive. To investigate the mode of juglone inhibition, I solved a PRORP-inhibitor structure. First, I have crystallized PRORP1 and then soaked the resulting crystal with juglone containing solutions for different time intervals. I have then collected X-ray diffraction data of these soaked crystals and solved the structures of multiple enzyme-inhibitor complexes. Based on these crystal structures I have identified four surface PRORP1 cysteine residues (C222, C346, C353 and C373) as potential inhibition sites. Although juglone is a known inhibitor of other enzymes [5, 6] and it is proposed to covalently modify cysteine residues, this is the first crystal structure to describe such interaction.

4.1.4 Limitations of study: co-crystallization of PRORP and pre-tRNA

To confirm the details of the proposed PRORP and pre-tRNA binding model I attempted to co-crystallize different PRORPs with cognate substrates. Since PRORPs are activated by several divalent cations frequently present in crystallization solutions, I have used catalytic mutant PRORPs (D440A in PRORP2 and D493A in PRORP1) that bind but do not process their substrates. In order to facilitate crystal packing and crystal formation, I have employed different strategies. First, I have used several *in vitro* transcribed pre-tRNAs derived from different organisms, such as *B.subtilis*, *A.thaliana* and thermophilic bacteria (*T.maritima* and *T.thermophilus*). tRNAs of thermophiles are expected to be more thermostable than tRNAs of mesophiles and therefore could potentially be advantageous to crystallization. Second, I have designed several engineered variations of pre-tRNAs. Substrates without an anticodon loop and stem are bound by PRORPs [3, 7, 8] and were expected to facilitate crystal packing [9]. In addition, substrates with sticky "kissing" loops could also enhance crystallization by artificially dimerizing the pre-tRNA-PRORP complex. Third, I have also used a PRORP inhibitor, gambodic acid in crystallization conditions, since it is proposed to stabilize the pre-tRNA-PRORP complex (collaborator's data). Although I had hits in many (>100) crystallization conditions I ran into the following limitations. (i) It is difficult to determine if both, protein and RNA are present in the obtained crystals. In most cases, crystals were small and limited in number. Therefore, I used sensitive methods to detect the presence of protein (SDS-PAGE followed by staining with krypton dye) and pre-tRNA (urea gel electrophoresis coupled with Et-Br staining). Additionally, I have washed crystals three times in the reservoir solution to eliminate protein or pre-tRNA contaminations

from the original crystallization solutions for SDS or urea gel analysis. However, in many cases the crystals were small and not enough to detect any of the components. Since these crystals were also frequently fragile, washing the crystals often resulted in breaking or completely destroying them. (ii) Examining the composition of the crystals, I have noticed that many crystals missed the protein moiety suggesting that the complex could fall apart over time while in the crystallization trays. (iii) In general, diffraction of crystals was very poor (up to 4.7 Å).

Overall, this high-risk project yielded initial experience in crystallizing PRORPs together with their pre-tRNA substrate. In the future, other methods, such as engineering PRORP or crosslinking the pre-tRNA to the protein, should be considered.

4.1.5 Future directions

My and other's work on characterizing PRORPs yielded many insights into their structure and function. However, several questions remain to be answered. There are no crystal structures of PRORPs from any other organisms besides *A.thaliana* and human. In order to gain insight into the evolution and mechanism of action of PRORPs, structures of other PRORPs from different model eukaryotes should be determined, such as *T.bruceii*, *O.tauri* or *D.melanogaster*. Additionally, the structure of a novel set of bacterial protein only RNase Ps, termed HARPs is completely unknown [10]. Since HARPs lack the PPR domain, it would be interesting to address how they bind and orient their substrate compared to canonical PRORPs. Therefore, there is a need to confirm the substrate-binding model of PRORPs and determine the differences between PRORPs, ribonuclease RNase P and HARPs.

Furthermore, specific details of the PRORP kinetic mechanism are still unknown. More precisely, it is uncovered what is the rate-limiting step in the kinetic cycle of PRORPs, which needs to be further dissected by *in vitro* kinetic assays. It is also a question if there is

any additional kinetic step in the mechanism of PRORPs besides the currently proposed ones. For instance, stop-flow measurements could potentially determine whether the PRORP-pre-tRNA complex also goes through a conformational change before 5' end cleavage, similarly to the ribozyme RNase P.

4.2 MULTI-SUBUNIT PRORPS.

4.2.1 Proper substrate recognition is the determinant of mtRNase P 5' pre-tRNA processing activity

Despite the human health and disease relevance of mtRNase P it is largely unknown how it processes its native human mitochondrial substrates. I have shown that when human mitochondrial MRPP3 is recombinantly expressed, purified and reconstituted with its auxiliary proteins, MRPP1 and 2 it binds, processes and methylates a group of human mitochondrial pre-tRNAs efficiently. However, I found that some pre-tRNAs were not effective mtRNase P substrates based on binding and single turnover assays. Such substrates include (mt)pre-tRNA$^{Ser(AGY)}$, (mt)pre-tRNA$^{Ser(UCN)}$ and (mt)pre-tRNA^{Val}. This indicates that weakly binding substrates may not be presented properly to the active site of mtRNase P. (mt)pre-tRNA$^{Ser(AGY)}$ lacks the entire D-loop and stem and therefore I speculate that this missing feature disables its proper recognition by mtRNase P [7]. Whereas (mt)pre-tRNA$^{Ser(AGY)}$ is not predicted to be an *in vivo* substrate for mtRNase P [11], (mt)pre-tRNA$^{Ser(UCN)}$ and (mt)pre-tRNA^{Val} are expected to be substrates for this complex *in vivo* [12]. Therefore, I speculate that other factors may be required for recognition of (mt)pre-tRNA$^{Ser(UCN)}$ and (mt)pre-tRNA^{Val} by mtRNase P. Interestingly, I observed that (mt)pre-tRNA^{Val} was bound with higher affinities and processed faster with a significant increase in

single turnover kinetic values by mtRNase P upon addition of the MRPP1 cofactor (SAM) to my assays. Since this effect was not due to methylation of this pre-tRNA I propose that SAM induces conformational changes through MRRP1 that allows for better accommodation of the pre-tRNA substrate to the active site.

4.2.2 Interplay between the pre-tRNA processing and methylation functions of mtRNase P

Since the components of mtRNase P are fulfilling at least two functions in the cell, I was interested in studying how these two functions are related to each other. While it was clear that MRPP1 and 2 are strictly required for 5' end processing by MRPP3, it was less obvious what the effect of MRPP3 on methylation function of MRPP1 and 2. I found that methylation of some substrates ((mt)pre-tRNA$^{Leu(UUR)}$) by MRPP1/2 is modestly enhanced by the presence of PRORP, suggesting that the distinct catalytic functions of mtRNase P may not be fully de-coupled from each other.

4.2.3 Single unit and multi-subunit PRORPs employ different substrate recognition mechanism

It is intriguing and still unknown why complex forming PRORPs, such as MRPP3 in metazoan mitochondria, need auxiliary proteins for function, while in other organisms are stand-alone. Therefore, I investigated how single unit and multi-subunit PRORPs bound and processed the same substrates. I have found that *A.thaliana* PRORPs show a distinct substrate binding and processing pattern from human mtRNase P. In particular, substrates that were efficiently bound and cleaved by mtRNase P were poor substrates for *A.thaliana* PRORPs and *vice versa*. This suggests that mtRNase P recognizes its substrates differently than single

unit PRORPs. While *A.thaliana* PRORPs is proposed to recognize the tRNA body, in contrast, mtRNase P may bind local structural elements in the pre-tRNA. Since metazoan (mt)pre-tRNAs have distinct structural features than their nuclear counterparts, human MRPP3 may have acquired additional accessory protein partners in order to recognize these non-canonical structural elements.

4.2.4 Physiological mutations in human mitochondrial pre-tRNAs have negative effects on mtRNase P functions

It has been proposed that pathological mutations in mitochondrial tRNAs could affect the substrate recognition and processing of mtRNase P [13, 14]. Therefore, in order to test this hypothesis, I have studied binding, 5' end processing and methylation of 11 *in vitro* transcribed human mitochondrial pre-tRNAs containing mutations related to a wide variety of diseases. I have found that most mutations affected mtRNase P activity. Specifically, mutations in (mt)tRNA^{Leu} had the most detrimental effect on the methylation activity of the MRPP1/2 sub-complex. This methylation defect most likely is associated with loss of tertiary structure features in (mt)tRNA^{Leu}. My related work, is the first comprehensive study looking at direct effects of mutations on mtRNase P activity that further reinforces the important role of this enzyme in human health and disease.

4.2.5 Loss of mtRNase complex leads to accumulation of mitochondrial RNA precursors in *D.melanogaster*

Knock-down of and mutations in components of mtRNase P in *D.melanogaster* mitochondria resulted in larval lethality suggesting that mtRNase P is essential in metazoans (collaborator's work). However, whether this observed phenotype is directly linked to the

loss of function of mtRNase P was not known. I have shown that larvae of mutant or silenced mtRNase P individual components accumulated unprocessed RNA transcripts in their mitochondria, indicating that the observed lethal phenotype most likely arises from loss of 5' end pre-tRNA processing. Later, in good agreement with our findings, an independent research group has reported that MRPP3 is vital and loss of it also resulted in accumulated unprocessed RNA transcripts in the mitochondria in mice [12]. These results further confirm the importance of 5' end processing and the essential function of mtRNase P in metazoan mitochondria.

4.2.5 Limitations of study – pre-tRNA$^{Ser(UCN)}$ is not an efficient substrate for mtRNase P

Pre-tRNA$^{Ser(UCN)}$ has been predicted to be a substrate for human mitochondrial mtRNase P *in vivo* [12]. However, I have found that this pre-tRNA is bound with low affinity and processed slowly by mtRNase P *in vitro*. tRNA$^{Ser\ (UCN)}$ possesses several unusual secondary structure features (shorter D-, variable loop and connector, longer anticodon stem) that could potentially contribute to the inefficient recognition by mtRNase P. Therefore, I have modified these regions of pre-tRNA$^{Ser\ (UCN)}$ one by one to introduce a more canonical secondary structural elements in this pre-tRNA. Nevertheless, these modifications in pre-tRNA$^{Ser\ (UCN)}$ did not enhance binding or 5'end processing by mtRNase P. It is possible that several regions need to be modified in this pre-tRNA in order for it to be recognizable by mtRNase P. My results suggests that pre-tRNA$^{Ser(UCN)}$ recognition by mtRNase P in human mitochondria may require additional factors, such as interactions with chaperons that have yet to be discovered.

4.2.6 Future directions

My *in vitro* work on mtRNase P is the first comprehensive study on how mtRNase P recognizes, processes and methylates its substrates and the potential interplay between different functions of this enzyme. These results indicate that this complex recognizes distinct human mitochondrial substrates differently. Therefore, other mitochondrial mtRNase P substrates should also be tested in *in vitro* binding assays in the future in order to further clarify differences in pre-tRNA recognition. Furthermore, my data also indicate that the functions of human mtRNase P may not be fully uncoupled as previously proposed. However, how the different activities of mtRNase P influence each other still needs to be elucidated in *in vitro* functional assays. In addition, there are no available structures with or without substrate of mtRNase P. Obtaining the crystal or cryo-EM structure of such a complex is challenging, but it could give us an important detailed insight on how the complex work together to recognize pre-tRNAs.

During my work, I have shown that a variety of pathogenic mutations influence functions of mtRNase P. The obvious next step would be to confirm my findings *in vivo* in cell cultures or in model organisms by artificially mutating tRNA genes in the mitochondria. Although this is currently technically challenging, it is possible that in the near future new methods will allow these studies, such as CRISPR-Cas9 mediated mutagenesis targeted to the mitochondrial genome.

REFERENCES

1. Holzmann, J., et al., *RNase P without RNA: identification and functional reconstitution of the human mitochondrial tRNA processing enzyme.* Cell, 2008. **135**(3): p. 462-74.
2. Pinker, F., et al., *Biophysical analysis of Arabidopsis protein-only RNase P alone and in complex with tRNA provides a refined model of tRNA binding.* J Biol Chem, 2017.
3. Brillante, N., et al., *Substrate recognition and cleavage-site selection by a single-subunit protein-only RNase P.* Nucleic Acids Res, 2016. **44**(5): p. 2323-36.
4. Hsieh, J., et al., *Pre-tRNA turnover catalyzed by the yeast nuclear RNase P holoenzyme is limited by product release.* RNA, 2009. **15**(2): p. 224-34.
5. Fila, C., C. Metz, and P. van der Sluijs, *Juglone inactivates cysteine-rich proteins required for progression through mitosis.* J Biol Chem, 2008. **283**(31): p. 21714-24.
6. Chao, S.H., A.L. Greenleaf, and D.H. Price, *Juglone, an inhibitor of the peptidyl-prolyl isomerase Pin1, also directly blocks transcription.* Nucleic Acids Res, 2001. **29**(3): p. 767-73.
7. Gobert, A., et al., *Structural insights into protein-only RNase P complexed with tRNA.* Nat Commun, 2013. **4**: p. 1353.
8. Mao, G., et al., *Cleavage of Model Substrates by Arabidopsis thaliana PRORP1 Reveals New Insights into Its Substrate Requirements.* PLoS One, 2016. **11**(8): p. e0160246.
9. Ferre-D'Amare, A.R. and J.A. Doudna, *Methods to crystallize RNA.* Curr Protoc Nucleic Acid Chem, 2001. **Chapter 7**: p. Unit 7 6.
10. Nickel, A.I., et al., *Minimal and RNA-free RNase P in Aquifex aeolicus.* Proc Natl Acad Sci U S A, 2017. **114**(42): p. 11121-11126.
11. Rossmanith, W., *Processing of human mitochondrial tRNA(Ser(AGY))GCU: a novel pathway in tRNA biosynthesis.* J Mol Biol, 1997. **265**(4): p. 365-71.
12. Rackham, O., et al., *Hierarchical RNA Processing Is Required for Mitochondrial Ribosome Assembly.* Cell Rep, 2016. **16**(7): p. 1874-90.
13. Wang, S., et al., *Maternally inherited essential hypertension is associated with the novel 4263A>G mutation in the mitochondrial tRNAIle gene in a large Han Chinese family.* Circ Res, 2011. **108**(7): p. 862-70.
14. Abbott, J.A., C.S. Francklyn, and S.M. Robey-Bond, *Transfer RNA and human disease.* Front Genet, 2014. **5**: p. 158.

APPENDIX

PAPER 2: DIFFERENTIAL SUBSTRATE RECOGNITION BY ISOZYMES OF PLANT PROTEIN-ONLY RIBONUCLEASE P

Michael J. Howard[1], Agnes Karasik[2], Bradley P. Klemm[1], Christine Mei[3], Aranganathan Shanmuganathan[2], Carol A. Fierke[1,4,*] and Markos Koutmos[2,*]

[1]Department of Biological Chemistry, University of Michigan, Ann Arbor, MI, 48109, USA

[2]Department of Biochemistry and Molecular Biology, Uniformed Services University of the Health Sciences, Bethesda, MD, 20814, USA

[3]Department of Microbiology and Immunology, University of Michigan, Ann Arbor, MI, 48109, USA

[4]Department of Chemistry, University of Michigan, Ann Arbor, MI, 48109, USA

* To whom correspondence should be addressed. Tel: [+1 734 936 2678]; Fax: [+1 734 647 4865]; Email: [fierke@umich.edu]. Correspondence may also be addressed to Tel: [+1 301 295 9419]; Fax: [+1 301 295 3512]; Email: [markos.koutmos@usuhs.edu].

Author contributions: M.H., A.K. , B.P.K., C.A.F and M.K. designed experiments. M.H., A.K., and B.P.K. performed PRORP comparison experiments. M.H. executed all other experiments. C.M. expressed and purified PRORP3. M.H., A.K. , B.P.K., C.A.F

and M.K. analyzed data. All authors were involved in writing or editing the manuscript. A.K. contributed to data in Table 2, Table 3, Figure 4 and 5.

Abstract

Ribonuclease P (RNase P) catalyzes the cleavage of leader sequences from precursor tRNA (pre-tRNA). Typically, these enzymes are ribonucleic protein complexes that are found in all domains of life. However, a new class of RNase P has been discovered that is composed entirely of protein, termed protein-only RNase P (PRORP). To investigate the molecular determinants of PRORP substrate recognition, we measured the binding affinities and cleavage kinetics of *Arabidopsis* PRORP1 for varied pre-tRNA substrates. This analysis revealed that PRORP1 does not make significant contacts within the trailer or beyond N_{-1} of the leader, indicating that this enzyme recognizes primarily the tRNA body. PRORP1 activity with model substrates confirms the importance of the D-arm for substrate recognition and indicates no interaction with the anti-codon stem-loop of tRNA. To determine the extent to which sequence variation within the tRNA body modulates substrate selectivity and to provide insight into the evolution and function of PRORP enzymes, we measured the reactivity of the three *Arabidopsis* PRORP isozymes (PRORP1-3) with four pre-tRNA substrates. A 13-fold range in catalytic efficiencies (10^4 - 10^5 M^{-1} s^{-1}) was observed demonstrating moderate selectivity for pre-tRNA substrates. Although PRORPs bind the different pre-tRNA species with affinities varying by as much as 100-fold, the three isozymes have similar affinities for a given pre-tRNA, suggesting similar binding modes. However, PRORP isozymes have varying degrees of cleavage fidelity, which is dependent on the pre-tRNA species and the presence of a 3'-discriminator base. This work defines molecular determinants of PRORP substrate recognition that provides insight into this new class of RNA processing enzymes.

Introduction

Transfer RNAs (tRNAs) are transcribed as precursors (pre-tRNA) that contain extra nucleotides flanking the 5' and 3' ends. Removal of these extraneous sequences is critical for tRNA function, thus the enzymes responsible for tRNA maturation are essential. RNase P is the endonuclease responsible for catalyzing the 5' end maturation of pre-tRNA and is found in all domains of life [1]. RNase P enzymes are extremely diverse with regards to their macromolecular composition [2]. In Bacteria, Archaea, and some eukaryotic lineages, pre-tRNA cleavage is catalyzed by a conserved RNA-based RNase P (ribozyme) that associates with a number of different protein cofactors (1-10, depending on the Domain) [3]. However, the majority of eukaryotic lineages are predicted to use a protein-only form of RNase P (PRORP) to catalyze pre-tRNA maturation within organelles (mitochondria and chloroplast) and, depending on the lineage, within the nucleus [3, 4]. PRORPs were first discovered in human mitochondria, where they process mitochondrial encoded pre-tRNAs [5]. Human mitochondrial RNase P requires three protein subunits for efficient catalysis: a nuclease (MRPP3/human PRORP), a tRNA methyltransferase (TRMT10C/MRPP1), and a dehydrogenase (SDR5C1/MRPP2). SDR5C1 and TRMT10C form a complex and are proposed to play a scaffolding role in pre-tRNA maturation catalyzed by human PRORP [6, 7]. In contrast to the mammalian enzyme, the recombinant PRORPs from plants, some protists, and algae do not require additional proteins for efficient catalysis, offering a simpler model system to understand the function of this new class of nuclease [4, 8, 9].

While mammals retain an RNA-based RNase P in their nucleus, bioinformatic studies suggested that land plants lack a catalytic RNA component for RNase P activity [10]. Consistent with this, the prototypical land plant *Arabidopsis thaliana* possesses three nuclear encoded PRORP enzymes (PRORP1, 2, and 3) (Figure 1A) [11, 12]. PRORP1 is essential and is localized to the mitochondria and chloroplasts [4, 11]. PRORP2 and 3 are localized to the nucleus where they play essential but redundant roles; knockout of both PRORP2 and PRORP3 is lethal, however knockout of either one is not [4, 11, 13]. Similar to *Arabidopsis*, the moss *Physcomitrella patens* contains three PRORP isozymes and no apparent catalytic RNA component for the RNA-dependent RNase P [14]. In contrast to *Arabidopsis*, *P. patens* localizes two PRORP enzymes to the mitochondria and chloroplast and one to the nucleus [14]. Thus, PRORP enzymes may have replaced the ancient RNA-based RNase P in *A. thaliana* and *P. patens,* processing tRNA transcripts in the chloroplast, mitochondria, and nucleus. However, the extent to which these isozymes vary in substrate specificity and the molecular interactions that confer substrate specificity of these important enzymes remain largely unknown.

PRORP enzymes contain three domains: an N-terminal pentatricopeptide repeat (PPR) domain, a central Zn-binding domain, and a Nedd4-BP1, YacP nuclease (NYN) domain (Figure 1) [15]. The PPR domain contains five PPR or PPR-like motifs, which are helix-turn-helix motifs found in tandem. This domain has been proposed to interact with pre-tRNA and enhance binding affinity [15-17]. The largest sequence variation among the PRORPs is found in the PPR domains and thus differences in substrate recognition may lie within this region. The central domain binds a Zn^{2+} ion and structurally links the PPR and metallonuclease domains. The NYN-metallonuclease

domain catalyzes phosphodiester bond hydrolysis and contains four conserved aspartates important for binding catalytic metal ions and catalysis [15, 18]. Both the protein and RNA-based RNase P enzymes are proposed to use a two-metal ion mechanism for catalysis [18, 19]. Despite this similarity, RNA-based RNase P enzymes have higher catalytic efficiency under *in vitro* conditions than PRORP enzymes [2]. The sequence identity among the *A. thaliana* PRORPs is highest in the metallonuclease domain. PRORP2 and 3 are most similar (80% identity and 88% similarity); the percent identity and similarity between PRORP1 and 2 are 48% and 65% and between PRORP1 and 3 are 49% and 65%, respectively.

To provide insight into the evolution and function of PRORP enzymes we measured substrate specificities, equilibrium binding affinities, and cleavage fidelities for varied pre-tRNA substrates. Previous studies have identified the importance of the elbow region of tRNA for PRORP1 substrate recognition [16, 20]. However, recognition of the tRNA leader and trailer by PRORP is largely unknown. Our data demonstrate no dependence on the trailer or leader length beyond the first nucleotide (N_{-1}). This is in contrast to bacterial RNA-based RNase P that makes significant interactions with the leader and trailer sequences of pre-tRNA [21-24]. However, the pre-tRNA sequence alters the binding affinity (≤40-fold) and, hence, the catalytic efficiency of PRORP cleavage. The three PRORP isozymes have comparable catalytic efficiencies for a given pre-tRNA suggesting similar, but not identical, substrate selectivity. However, PRORP isozymes have varying degrees of cleavage fidelity, which is dependent on the pre-tRNA species and the presence of a 3'-discriminator base. This work defines molecular

determinants of PRORP substrate recognition that provides insight into this new class of RNA processing enzymes.

Results

PRORP1 substrate recognition has little dependence on leader and trailer length

The binding affinity of *B. subtilis* RNase P for pre-tRNA has a significant dependence on pre-tRNA leader length, with the pre-tRNA affinity increasing ~50-fold when the leader length is increased from one to five nucleotides [25]. To determine if PRORP1 shares a similar dependence on leader length, we measured the binding affinity and single-turnover (STO) cleavage rate constant for *B. subtilis* pre-tRNA^{Asp} lacking the 3'-CCA sequence. This substrate was previously used to interrogate both the mechanism of PRORP [18] and leader interactions with *B. subtilis* RNase P [23, 25, 26]. This allows a direct comparison between the recognition modes of PRORP1 and bacterial RNase P.

A fluorescence anisotropy binding assay was used to measure the equilibrium dissociation constant (K_D) of PRORP1 binding to 5' fluorescein-labeled *B. subtilis* pre-tRNAs with varying leader lengths while maintaining a discriminator base on the 3' end (Figure 2A). Increasing the pre-tRNA leader length from 1 to 14 nts has little effect on PRORP1 binding affinity (Figure 2B and Table 1), with K_D values ranging between 100 – 310 nM. The observed binding trend is independent of the presence of the 5'-fluorescein label on the 5' end of pre-tRNA (Figure S1). In contrast, the binding affinity of the mature tRNA product (0 nt leader) is ~30-fold weaker than for pre-tRNA. These data

suggest that PRORP1 does not significantly recognize the leader past the first nucleotide (N_{-1}).

To examine the effect of leader length on PRORP1 cleavage activity, the STO rate constant (k_{obs}) was measured using a gel-based assay. The observed rate constant under these conditions is proposed to mainly reflect the chemical cleavage step [18]. In all cases, the leader length was consistent with cleavage at the correct site. The STO rate constant for *B. subtilis* pre-tRNA with varying leader lengths was generally uniform (Figure 2C and Table 1), with the exception of the 1 and 2 nt leader substrates, which have ~4- and 8-fold increased STO rate constant compared to 14:1 (leader nt length: trailer nt length) pre-tRNA, respectively. This increased reactivity may be due to catalytic enhancement imparted by the positioning of the 5' guanosine and fluorescein. The cleavage rate constant of the 1:1 pre-tRNA may depend on the sequence at both the -1 nt and the discriminatory base, as suggested by the slower STO cleavage rate of an unmodified U-tRNA (Figure S3). Nonetheless, these data indicate that PRORP1 can efficiently bind and catalyze removal of 1 nt leader *B. subtilis* pre-tRNA, further demonstrating that PRORP1 does not significantly contact the leader sequence beyond N_{-1}.

To determine whether the trailer is an important determinant for PRORP1 recognition, we assayed the STO activity and binding affinity of PRORP1 with *A. thaliana* mitochondrial encoded Cys-Mito pre-tRNA (Figure 3) containing a 24 nt long trailer and a 5 nt long leader (5:24). A Cys-Mito pre-tRNA substrate was used for these studies because extension of the *B. subtilis* pre-tRNA trailer to 20 nt resulted in significant STO biphasic kinetics (data not shown), potentially as a result of the pre-

tRNA adopting an alternative structure [27]. Variation of the Cys-Mito trailer length does not alter the binding affinity (K_D = 65 ± 5 and 70 ± 10 nM for 5:1 and 5:24, respectively, under standard binding conditions with the exception of 100 mM NaCl) or STO cleavage rate constant (k_{obs} = 0.037 ± 0.002 and 0.033 ± 0.001 for 5:1 and 5:24, respectively), suggesting that PRORP1 does not make significant contacts with the 3' trailer. Taken together, these data suggest that the leader (past N_{-1}) and trailer sequences are not important determinants of molecular recognition by PRORP1, therefore PRORP1 mainly recognizes the tRNA body.

PRORP reactivity with model substrates reveals the importance of the D-arm in recognition

To determine the regions within the tRNA body that are important for PRORP recognition, we created two truncated versions of pre-tRNA Cys-Mito. These model substrates include an RNA lacking an anticodon arm (ΔAC), and an RNA that connects the acceptor arm and TψC-arm to form a stem-loop (SL), thereby removing the D- and anticodon arms (Figure 3). Both were labeled at the 5' end with fluorescein and cleavage catalyzed by PRORP1 was assessed under STO conditions. PRORP1 catalyzed removal of the 5' leader from the ΔAC substrate with an observed rate constant similar to wild type pre-tRNA, k_{obs} = 0.037 ± 0.002 and 0.023 ± 0.005 s^{-1} for Cys-Mito pre-tRNA and ΔAC, respectively. PRORP1 binding affinity for the ΔAC and pre-tRNA substrates are similar: K_D = 70 ± 10 and 65 ± 5 nM, respectively (under standard binding conditions with the exception of 100 mM NaCl). This result is consistent with a previous observation that PRORPs can cleave t-element RNA, tRNA-like structures that lack an anticodon stem-loop [4, 11]. The SL RNA was cleaved > 1000-fold slower than Cys-

Mito pre-tRNA ($k_{obs} < 3.3 \times 10^{-5}$ s^{-1}). This result indicates that the D-arm of pre-tRNA is critical for substrate binding and/or cleavage by PRORP1.

Arabidopsis PRORP isozymes display differential catalytic efficiencies with four pre-tRNAs

Given that the PRORP1 substrate recognition relies on interactions with the tRNA body, differences in the nucleotide sequence of tRNA species could potentially alter recognition and catalytic efficiencies. To explore the range of reactivity, we measured the steady-state (multiple-turnover, MTO) kinetic parameters of the three *A. thaliana* PRORPs with four pre-tRNAs. The pre-tRNAs assayed are: two nuclear-encoded pre-tRNAs (Cys-Nuc and Phe-Nuc) and two organellar-encoded pre-tRNAs (Cys-Mito and Phe-Chlor) (Figure 3). We used a real-time fluorescence anisotropy assay to measure the steady-state kinetic parameters for PRORP-catalyzed pre-tRNA hydrolysis (Figure 4A; Table 2) [28]. A comparison of the catalytic efficiencies (k_{cat}/K_M values) reveals that PRORP1 has the highest activity, with values 2- to 13-fold higher for a given substrate than PRORP2 and 3 (Figure 4B). The kinetic parameter k_{cat}/K_M is a measure of the productive associations between enzyme and substrate and sets a lower limit for the second-order rate constant for substrate binding (k_{on}). PRORP1 is most selective for the Phe-Chlor substrate ($k_{cat}/K_M = 4.1 \times 10^5$ M^{-1} s^{-1}) relative to PRORP2 and 3, representing a 9- and 13-fold enhancement, respectively. Each isozyme reacts fastest with a different pre-tRNA: PRORP1 with Phe-Chlor, PRORP2 with Phe-Nuc, and PRORP3 with Cys-Mito. The values of the turnover number (k_{cat}) for cleavage catalyzed by PRORP1 and 2 vary little (~2-fold) between substrates. However, PRORP3 catalyzes cleavage of the Cys-Nuc substrate nearly 8-fold slower than Phe-Nuc pre-tRNA. These data indicate that

sequence variation within the tRNA body can modulate substrate specificity, albeit within a range of 10^4-10^5 M^{-1} s^{-1}.

PRORPs bind individual pre-tRNAs similarly

To further explore determinants of substrate recognition, we measured the dissociation constants (K_D) of PRORP1, 2, and 3 for the four *A. thaliana* pre-tRNA substrates using the fluorescence anisotropy binding assay (Figure 5A) [28]. The affinity of the PRORPs for these substrates varies by as much as 100-fold (60 nM to 6000 nM) (Figure 5B and Table 3), demonstrating significant discrimination between the substrates. However, comparison of the dissociation constants reveals that all three PRORPs have comparable binding affinities for a given substrate (< 4-fold difference). All three PRORPs demonstrate the weakest affinity for the Cys-Nuc pre-tRNA and the highest affinity for the Phe-Chlor pre-tRNA. Thus, the PRORP enzymes use similar binding modes for pre-tRNA substrate recognition.

Product release is not rate-limiting for MTO catalysis by PRORP

The kinetic parameters measured under MTO conditions include all steps in the PRORP kinetic mechanism. To begin dissecting the contribution of discrete steps in the mechanism (e.g. substrate cleavage, product release, etc.) to the progression of the reaction, we measured the STO kinetics of PRORP1, 2, and 3 for catalysis of pre-tRNA cleavage. In contrast to the MTO k_{cat}, the STO rate constant k_{obs} includes only the steps in the kinetic mechanism prior to and including substrate cleavage. For all three PRORPs, the observed STO rate constants (k_{obs}) range between 0.02- 0.07 s^{-1} (Table 2), regardless

of the substrate assayed. The observed rate constant for total product formation (C_0 + M_{-1}) is reported for pre-tRNA substrates that are significantly miscleaved (see following section).

For *B. subtilis* RNase P, a significant difference (~300-fold) between the STO and MTO rate constants previously revealed that product release is the rate-limiting step in the reaction [29]. However, the PRORP MTO k_{cat} values are within 2-fold of the STO k_{obs} values, suggesting that the rate-limiting step at saturating PRORP is a step prior to product dissociation. The one exception is the difference between the k_{obs} and k_{cat} values for PRORP3 catalyzing cleavage of Cys-Nuc pre-tRNA (k_{obs} is 3.6-fold greater than k_{cat}), suggesting that product release is partially rate limiting for this enzyme/substrate pair.

PRORPs have varying cleavage fidelities

Gel analysis of the STO cleavage assays indicate two distinct product bands in all PRORP-catalyzed reactions with the Phe-Nuc substrate, and for PRORP2 and 3 reactions with the Cys-Mito and Cys-Nuc substrates (Figure 6 and Figure S2). To further investigate the miscleavage, assay products were separated by high resolution urea-PAGE and compared to *B. subtilis* RNase P-catalyzed cleavage of pre-tRNAs (Figure 6). This analysis revealed that the products represent the correct (5 nt, C_0) and incorrect (4 nt, M_{-1}) cleavage products (Figure 6). Additionally, all enzymes cleave *B. subtilis* pre-$tRNA^{Asp}$ correctly, indicating that the miscleavage observed with other substrates is not a result of nuclease contamination. *B. subtilis* RNase P cleaves all four *A. thaliana* pre-tRNAs correctly; only a distinct 5 nt product band (< 5% miscleaved product) is observed. In contrast, the PRORP enzymes have variable cleavage fidelities, with

PRORP3 displaying the lowest cleavage fidelity among the PRORPs (Figure 6 and Table S1). Furthermore, the nuclear-localized PRORP2 and PRORP3 significantly miscleaved the Cys-Mito and Cys-Nuc substrates whereas the organellar PRORP1 did not (< 5%), demonstrating differences in cleavage site selection between the nuclear and organellar PRORPs (Figure 6 and Table S1).

PRORP-catalyzed miscleavage of pre-tRNA between the -2/-1 nts (M_{-1}) generates a product with a 1 nt leader, a potential substrate for PRORP. Since we are assaying cleavage using a 5' labeled pre-tRNAs, we cannot determine whether the miscleaved product is further processed by PRORP. Thus, we performed primer extension assays on tRNA at various time-points taken during STO cleavage reactions catalyzed by PRORP1 and 3 of Phe-Nuc pre-tRNA (the substrate miscleaved by all isozymes) (Figure S3). These data demonstrate that the miscleaved product is further processed by PRORP to generate mature tRNA (Figure S3). However, the observed rate constant for PRORP catalyzed removal of the 1 nt leader is decreased (~0.0006-0.001 s^{-1}) (Figure S3).

3' discriminator base can contribute to PRORP cleavage fidelity

One feature of the Phe-Nuc substrate that could lead to the observed miscleavage by all three PRORP enzymes is the formation of a base pair between the adenine discriminator base and the uridine base in the N_{-1} position of the leader (Figure 3), which would extend the acceptor stem helix creating a 4 nt leader. Consistent with this hypothesis, the three pre-tRNA substrates that can form an extra base pair (U/A) between the discriminator base and the N_{-1} leader position (Phe-Nuc, Cys-Mito, and Cys-Nuc) exhibit miscleavage, albeit to varying extents depending on the PRORP (Figure 6). To

test this hypothesis, we assessed the ability of PRORPs to correctly cleave three different Phe-Nuc pre-tRNAs variants possessing 5 nt leaders and variable 3' ends: with (5:1) or without (5:0) a 3' discriminator base and with an extended 20 nt trailer sequence (5:20) (Figure 7). Removal of the discriminator base (5:0) from Phe-Nuc pre-tRNA eliminated the miscleavage catalyzed by all of the PRORP enzymes, whereas addition of a longer trailer sequence had no significant effect on miscleavage (Figure 7). Similarly, removal of the discriminator base from the Cys-Mito pre-tRNA, to delete a potential A-U base pair with N_{-1}, significantly reduced miscleavage catalyzed by PRORP3 (Figure S4).

Taken together, these data provide evidence that the presence of a base pair between N_{-1} and the discriminator base can engender miscleavage by PRORPs, possibly due to extension of the acceptor stem. However, the potential to form this base pair does not guarantee miscleavage; the Cys-Mito and Phe-Chlor substrates, which contain a potential base pair between the N_{-1} and the discriminator base, are not significantly miscleaved by PRORP1 or 2. Thus, other determinants including sequence context, stability of the pre-tRNA structure, and differences in PRORP substrate recognition must also influence cleavage fidelity.

Discussion

To define the molecular determinants of PRORP recognition, we examined the reactivity of PRORP1 with model substrates and pre-tRNAs with varying leader and trailer lengths. This analysis revealed that PRORP1 makes little or no catalytically important interactions with the trailer or with the leader past the first nucleotide (Figure 2 and Table 1). This is in contrast to bacterial RNase P where pre-tRNA binding affinity

increases ~50-fold upon increasing the leader from one to five nts [25]. Thus, PRORP enzymes do not share a major determinant of molecular recognition utilized by bacterial RNase P. Furthermore, PRORP1 and *B. subtilis* RNase P bind mature tRNA ~30 and 400-fold weaker than pre-tRNA (leader length ≥ 4 nts), respectively [23]. This is consistent with PRORP1 making fewer interactions with the leader than *B. subtilis* RNase P. Similar to PRORP1, recent binding studies with *A. thaliana* nuclear pre-tRNA^{Gly} suggest PRORP2 does not require long leader (≤ 8 nts) and trailer (1 nt) lengths for tight binding [30]. PRORPs efficiently catalyze removal of leader sequences from Cys-Mito tRNA lacking an anti-codon stem-loop (ΔAC) but not from a model substrate lacking the anticodon stem-loop and D-arm (SL substrate). However, Bacterial RNase P can catalyze processing of minimal stem-loop model substrates [31], demonstrating a more important role for the interaction between the D-arm and PRORP compared to bacterial RNase P. Thus far, the available data reveal that the molecular determinants of PRORP1 substrate recognition lie within the elbow of the tRNA body and the N_{-1} nucleotide of the leader. Given the similarities in binding affinities and kinetic parameters of the PRORP isozymes for pre-tRNAs, it is likely that PRORP2 and 3 also share these determinants.

The detailed kinetic comparison of *A. thaliana* PRORP enzymes reveals both similarities and differences. In general, the three *A. thaliana* PRORPs catalyze 5' end cleavage with comparable catalytic efficiencies (10^4 -10^5 M^{-1} s^{-1}) and pre-tRNA binding affinity. This suggests that the differentially localized PRORP isozymes are not selective for pre-tRNAs of different organellar origin. The STO cleavage rate constants among the PRORP isozymes are consistent with a previous study using a bacterial pre-tRNA^{Gly} substrate, where the observed rate constants vary between 0.04 – 0.13 s^{-1} [32]. Despite

these similarities, our data indicate that there is a subset of pre-tRNAs that are more efficiently processed by specific PRORP isozymes. For example, PRORP1 has a ~10-fold higher k_{cat}/K_M value for cleaving Phe-Chlor pre-tRNA compared to PRORP2 and 3. Nucleotide variations in the D- and TψC –loops may contribute to preferential cleavage and recognition by PRORP1. However, more detailed studies are needed to determine the molecular interactions that confer this enhanced reactivity.

While PRORPs bind and cleave substrates with similar K_D values and cleavage rate-constants, they exhibit unexpected differences in cleavage fidelity. For instance, PRORP3 catalyzes the miscleavage of Cys-Mito, Cys-Nuc, and Phe-Nuc pre-tRNA to a greater extent than PRORP1 and PRORP2 (Figure 6). Removal of the discriminator base from Cys-Mito or Phe-Nuc pre-tRNAs results in increased fidelity for all three enzymes, suggesting that the discriminator base engenders miscleavage (Figure 7). Base-pairing between the discriminator nucleotide and the N_{-1} nucleotide of the leader, extending the acceptor stem by one base pair, could account for the observed miscleavage. The greater fidelity observed with PRORP1 could originate from specific interactions with the N_{-1} of the leader and/or interactions with the discriminator base. These data suggest a difference in substrate recognition among the PRORPs with regards to cleavage site selection. While the frequency of PRORP-catalyzed pre-tRNA miscleavage *in vivo* is unknown, PRORP catalyzes phosphodiester bond hydrolysis between -1 nt/+1 nt (correct) and -2 nt/-1 nt (miscleavage) both *in vivo* and *in vitro* with the atypically processed plant mitochondrial pre-tRNA^{His} [33]. Furthermore, PRORPs can correct miscleavage by catalyzing the removal of the miscleaved 1 nt leader, albeit slower than the rate constant for the initial cleavage step (Figure S3). This step is likely slow due to base pairing

between the -1 nt and the discriminator base. Cleavage fidelity *in vivo* could be enhanced by RNA binding proteins that decrease incorrect base pairing or that stabilize RNA structure.

While all three PRORP enzymes catalyze miscleavage of the Phe-Nuc pre-tRNA (Figure 6), *B. subtilis* RNase P catalyzes only the correct product from the same substrate. This observation suggests that PRORP enzymes use different criteria to recognize the substrate cleavage site than bacterial RNase P. Bacterial RNase P interacts with the elbow of tRNA, (nucleotides within the TψC and D-loops), the acceptor stem, nucleotides within the leader sequence, and the CCA of the 3' end of pre-tRNA, though all are not required for accurate cleavage [24, 34]. Interactions that could increase fidelity of bacterial RNase P compared to PRORP in cleavage of the Phe-Nuc substrate are the base pairing between the RNA component and both the N_{-1} uridine and the 3' end of pre-tRNA, leading to splaying of the 3' and 5' ends in the bound complex [24, 35]. Future experiments examining the nucleotide identity near the cleavage site, including the discriminator base, 1 nt/72 nt base pair, and 3'-CCA, will further define PRORP cleavage site selection.

Based on the kinetic characterization performed here, the substrate selectivity of PRORP2 and 3 are more similar to one another than to PRORP1, consistent with their higher sequence similarity and knockout data that suggest a redundant function for PRORP2 and 3 within the nucleus [11]. Furthermore, the fidelity of PRORP2 is more similar to PRORP3 and, interestingly, both enzymes share higher activity toward the SL substrate than PRORP1 (k_{obs} > 12-fold) (Table S2). This suggests that the nuclear PRORPs have subtle but distinct differences in substrate recognition as compared to the

organellar PRORP1. The overlapping substrate specificities of *Arabidopsis* PRORP enzymes suggest that they are in the early stages of diversification, which may be the result of relatively recent gene duplication events [4, 36]. It is interesting to note that *Arabidopsis* encodes four variants of the nuclease that catalyzes 3' end pre-tRNA maturation, tRNase Z [37]. These enzymes are differentially localized, but only the chloroplast-localized tRNase Z knockout is lethal, suggesting several isozymes have a redundant function, as with PRORP2 and 3. The abundance of tRNase Z enzymes in *Arabidopsis* is attributed to differential cellular compartmental localization, differential expression, and/or tissue specific expression [37]. The data available suggest that this is also the case with PRORP enzymes.

Material and Methods

Enzyme and substrate preparation

PRORP constructs (Δ76PRORP1, full-length PRORP2, and Δ68PRORP3) were cloned, expressed and purified from *E. coli* as previously described [15]. The concentrations of PRORP1, 2 and 3 were determined by absorbance using extinction coefficients in the native state at 280 nm of 84,630 M^{-1} cm^{-1}, 91,300 M^{-1} cm^{-1}, and 84,700 M^{-1} cm^{-1}, respectively. Purified enzymes were aliquoted, flash-frozen, and stored at -80 °C in 20 mM MOPS pH 7.8, 100 mM NaCl, and 1 mM TCEP. Truncation of PRORP1 and 3 was required to obtain soluble protein. However, full-length PRORP2 expressed in *E. coli* is observed mainly in the soluble fraction. A Δ20 amino acid truncation of PRORP2 a the N-terminus (the comparable truncation to Δ76 PRORP1) has comparable activity to full-length PRORP2 [30].

Pre-tRNA substrates were prepared by *in vitro* transcription catalyzed by T7 polymerase [38, 39]. Substrate sequences were retrieved from the *A. thaliana* genomic tRNA database [40]. The DNA template for transcription was created by PCR amplification of DNA purchased from Life Technologies GeneArt. To generate fluorescein-labeled pre-tRNA substrates, transcription reactions were performed in the presence of guanosine monophosphorothioate and the 5' phosphorothioate was reacted with 5-(iodoacetamido)fluorescein to label the 5' end, as previously described [26]. The pre-tRNA substrates were purified by denaturing PAGE (12%). The discriminator base on the SL substrate was removed to mitigate miscleavage products catalyzed by PRORP2 and 3. The proposed tRNA secondary structures were generated with tRNAscan-SE 1.21 [41].

Multiple turnover assays

Multiple-turnover (MTO) reactions were performed in a 96-well plate format using a fluorescence anisotropy (FA) assay (as described in [28]). Standard reaction conditions (25 °C, 30 mM MOPS pH 7.8, 150 mM NaCl, 1 mM TCEP, and 1 mM $MgCl_2$) were used with an enzyme concentration of 20 nM (PRORP1 and PRORP3) or 80 nM (PRORP2). Higher concentrations of PRORP2 were required to obtain consistent v_0/[E] values at a given substrate concentration. The concentration of fluorescently labeled pre-tRNA was held constant at 40 nM in the reactions while the concentration of unlabeled pre-tRNA substrate was varied. The ratio of labeled to unlabeled substrate did not alter the measured initial rates (data not shown). Black Corning half-area 96-well plates were used with a final reaction volume of 40 μL per well. Initial rates were

calculated from the linear decrease in anisotropy [28]. The steady state kinetic parameters were calculated from a fit of the Michaelis-Menten equation (1) to the concentration-dependence of the initial rates using KaleidaGraph (Synergy Software). These kinetic parameters encompass both incorrect and correct cleavage product formation. The reported kinetic parameters and standard error were determined by fitting equation 1 to the concentration-dependence of the initial rates.

$$(1)\quad \frac{v_o}{[\mathrm{E}]} = \frac{k_{\mathrm{cat}}[\mathrm{S}]}{K_{\mathrm{M}} + [\mathrm{S}]}$$

Anisotropy Binding Assays

Binding assays were performed as described previously [15]. Briefly, the concentration of fluorescein-labeled pre-tRNA was maintained at 20 nM, while the concentration of PRORP was varied (0.005 – 20 μM). Binding experiments were performed in 20 mM MOPS pH 7.8, 300 mM NaCl, 1 mM TCEP, and 1 mM $CaCl_2$ in a 96-well plate format. PRORP1 can bind but not cleave substrates in $CaCl_2$ [15]. Fluorescence anisotropy was measured at an excitation wavelength of 488 nm and an emission wavelength of 535 nm. The observed anisotropies in binding assays where the total fluorescence intensity increased greater than 15% upon PRORP addition (*B. subtilis* substrates containing 1, 2, 3, and 4 nt leaders) were corrected [42]. Equation 2 was fit to the dependence of the anisotropy on the protein concentration where A is the observed anisotropy, A_o is the initial anisotropy, ΔA is the total change in anisotropy, [P] is the concentration of PRORP, and K_D is the apparent dissociation constant.

$$(2)\quad \mathrm{A} = \mathrm{A_o} + \frac{\Delta\mathrm{A}\,[\mathrm{P}]}{[\mathrm{P}] + K_{\mathrm{D}}}$$

Single-Turnover Assays

For single-turnover (STO) reactions, the enzyme and pre-tRNA concentrations were 5 μM and 30 nM, respectively, unless otherwise noted. Reactions were performed in standard conditions (see MTO), initiated by addition of enzyme, and quenched at specified time points (0 – 1200 sec) with an equal volume of 100 mM EDTA, 6 M urea, 0.1 % bromophenol blue, 0.1 % xylene cyanol, and 2 μg/μl yeast tRNA. The fluorescently labeled 5' leader product was separated from pre-tRNA by electrophoresis on 20 or 22.5% denaturing PAGE gel. Gels were visualized using a Typhoon 9410 scanner and the fraction product quantified using ImageQuant 5.2 software. The observed single-turnover rate constant was calculated from a fit of a first order exponential equation to the data using KaleidaGraph fitting software (equation 3), where A is the end point, B is the amplitude, *k* is the observed rate constant, and *t* is time. The STO assays with *Bacillus subtilis* RNase P were performed at 25 °C with 1.8 μM bacterial RNase P, 50 mM Tris pH 7.4, 100 mM KCl, 75 mM NaCl, 10 mM DTT, and 3 mM $MgCl_2$. The *B. subtilis* RNase P was prepared as previously described [25]. The alkaline ladder was produced by the incubation of a given pre-tRNA in 10 mM NaOH and 1 mM EDTA at 95°C for 2 mins. Free fluorescein runs as a blur near the second nt (Figure 6). The miscleavage product (4 nts) does not align with the 4 nt ladder product (Figure 6). This may be a result of running near the gel front in combination with differences in the alkaline cleavage products (3' Phosphate) and RNase P products (3' hydroxyl). STO miscleavage kinetics catalyzed by the PRORPs were analyzed as described in [34, 43]. Briefly, the observed rate constants for both correct and miscleaved product are obtained from a single-exponential fit to the data (equation 3). The resulting amplitude (A_c or A_m)

for each respective fit is multiplied by the observed rate constant ($k_{obs,c}$ or $k_{obs,m}$) to obtain k_c and k_m (equations 4 and 5).

$$(3) \quad Fraction\ Product = \mathrm{A} - \mathrm{B}(\mathrm{e}^{-kt}(3)\mathrm{FractionProduct} = \mathrm{A\text{-}B}(\mathrm{e}^{\text{-}\mathrm{kt}})$$

$$(4) \quad k_c = k_{obs,c}\,(A_c)(5)\mathrm{k_c} = \mathrm{k_{obs,c}(A_c)}(4)\mathrm{k_c} = \mathrm{k_{obs,c}(A_c)}$$

$$(5) \quad k_m = k_{obs,m}\,(A_m)$$

Primer Extension

Processing of the Phe-Nuc miscleavage product catalyzed by PRORP1 and PRORP3 was measured by primer extension using Omniscript (Qiagen) reverse transcriptase (RTase). Substrate was incubated with the PRORPs under standard conditions. Time points were mixed 1:1 with a quench solution containing 10 mM Tris pH 8.0, 50 mM EDTA, and 8 M urea. RNA was re-purified by phenol/chloroform extraction and ethanol precipitation. The ladder was generated by alkaline hydrolysis of substrate in 10 mM NaOH and 1 mM EDTA at 95°C for 10 minutes, then quenched with HCl. The time points, ladder, and substrate were each used to template reverse transcription (RT) reactions. Each template was melted in the presence of an oligo-dNTP primer (IDT, 5'-FAM-CCCAACTGAGCTATCC-3') at 95°C for 3 minutes, then cooled to 37°C. The primed-RNA was then mixed 1:1 with a master mix containing Omniscript RT buffer, dNTPs, SUPERase•In (Thermo Fisher), and Omniscript RTase, and incubated at 37°C for 60 minutes. Glycerol was added for gel loading and products were separated using denaturing PAGE (22.5%) and then fluorescence of the fluorescein label was imaged with a Typhoon 9410 scanner. The substrate and product bands were quantified using ImageQuant 5.2 software. The fraction miscleaved was calculated with (M-

$_1$/(C_0+M$_{-1}$+Substrate)). As has been previously reported, some non-templated nucleotide addition by the RTase was observed [44].

ACKNOWLEDGEMENT

We thank Yu Chen, Xin Liu, and Nancy Wu for providing *B. subtilis* RNase P and for critical discussions. We also thank Xin Liu for deriving an equation for K_D^{app} used to obtain $K_{D,Un}$ in Figure S1.

FUNDING

This work was supported by the National Institutes of Health [R01 GM055387 to C.A.F]; in part by the Molecular Biophysics Training Grant [T32 GM8270-25 to M.J.H.]; and by Uniformed Services University of the Health Sciences start-up funds [R071KB to M.K.].

Tables

Table 1. Dissociation constant (K_D) and STO observed rate constant (k_{obs}) for PRORP1 with *B. subtilis* pre-tRNA containing varying leader lengths

pre-tRNA	K_D (nM)[a]	Fold[b]	k_{obs} (s^{-1})[c]	Fold[b]
0	3,400 ± 400	34	--	--
1	150 ± 60	1.5	0.078 ± 0.003	3.9
2	310 ± 20	3.1	0.15 ± 0.02	7.8
3	140 ± 40	1.4	0.032 ± 0.001	1.6
4	150 ± 40	1.5	0.025 ± 0.001	1.3
5	190 ± 60	1.9	0.025 ± 0.001	1.3
10	100 ± 50	1	0.025 ± 0.001	1.3
14	100 ± 30	1	0.02 ± 0.001	1

[a]Measured as described in the legend of Figure 2 and Materials and Methods. The mean and standard deviation is reported from two independent determinations.
[b]As compared to pre-tRNA with a 14 nt leader
[c]Measured as described in the legend of Figure 2 and Materials and Methods. The standard error from fitting is reported.

Table 2. Kinetic parameters for pre-tRNA cleavage catalyzed by *A. thaliana* PRORP1, 2 and 3

		Single-turnover[a]	*Multiple-turnover*[b]		
Enzyme	Pre-tRNA	k_{obs} (s^{-1})[c]	k_{cat} (s^{-1})	K_M (nM)	k_{cat}/K_M ($mM^{-1}s^{-1}$)
PRORP1	Cys-Mito	0.037 ± 0.002	0.062 ± 0.005	670 ± 230	96 ±10
	Phe-Chlor	0.035 ± 0.002	0.042 ± 0.005	140 ± 50	410 ± 60
	Cys-Nuc	0.037 ± 0.003	0.040 ± 0.002	550 ± 50	73 ± 5
	Phe-Nuc	0.078 ± 0.003	0.035 ± 0.003	160 ± 50	220 ± 60
PRORP2	Cys-Mito	0.013 ± 0.003	0.013 ± 0.002	340 ± 60	37 ± 6
	Phe-Chlor	0.018 ± 0.003	0.015 ± 0.002	340 ± 100	45 ± 10
	Cys-Nuc	0.027 ± 0.002	0.030 ± 0.002	940 ± 130	32 ± 3

	Phe-Nuc	0.035 ± 0.002	0.023 ± 0.002	250 ± 50	95 ± 16
PRORP3	Cys-Mito	0.023 ± 0.002	0.022 ± 0.002	430 ± 30	53 ± 3
	Phe-Chlor	0.023 ± 0.002	0.013 ± 0.002	440 ± 50	32 ± 3
	Cys-Nuc	0.030 ± 0.002	0.008 ± 0.002	420 ±100	17 ± 4
	Phe-Nuc	0.072 ± 0.003	0.062 ± 0.023	2000 ± 850	37 ± 8

[a]Reactions contained 5 μM PRORP, 30 nM pre-tRNA, 30 mM MOPS pH 7.8, 150 mM NaCl, 1 mM TCEP, and 1 mM $MgCl_2$ at 25 ºC. The standard error from fitting is reported.
[b]As described in the legend of Figure 4 and Materials and Methods. The standard error from
fitting is reported.
[c] Because both correct and incorrect cleavage products are catalyzed with some substrates (See Figures 6, S2), k_{max} represents the single-exponential fit to the time course of total product ($C_0 + M_{-1}$) formation. The multiple turnover kinetics similarly reflect total product formation.

Table 3. Dissociation constants (K_D in nM) for PRORP1, 2, and 3 binding to pre-tRNAs[a]

	Pre-tRNA			
Enzyme	Cys-Mito	Phe-Chlor	Cys-Nuc	Phe-Nuc
PRORP1	510 ± 120	60 ± 10	2300 ± 300	330 ± 60
PRORP2	350 ± 70	140 ± 10	6100 ± 2100	350 ± 40
PRORP3	300 ± 70	220 ± 30	1500 ± 200	380 ± 50

[a]Measured as described in the legend of Figure 5 and Materials and Methods. The standard error from fitting is reported.

Figures

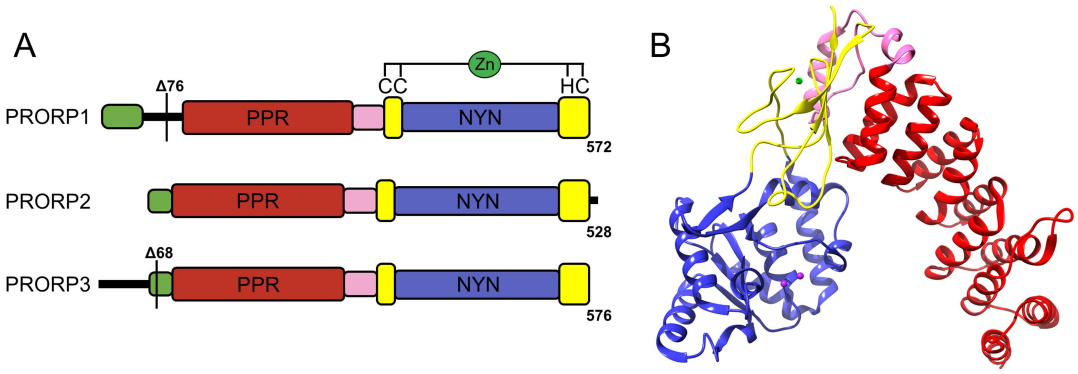


Figure 1. A. *A. thaliana* encodes three PRORP enzymes, PRORP1, 2 and 3. N-terminal truncations of PRORP1 (Δ76) and PRORP3 (Δ68) were used in this study. PRORP enzymes contain three domains: PPR (red), central-Zn binding (yellow), and NYN (blue) domains. The N-terminal green region represents the proposed localization sequences: PRORP1 contains a mitochondrial targeting peptide (1-48, predicted by the TargetP 1.1 algorithm [45]), while PRORP2 and 3 contain canonical bipartite nuclear localization signals (H/R-RSR-R/H-X_9-K-K-K-K) [46]. The pink region represents a plant-specific insert in the gene sequence. B. The crystal structure of PRORP1 (PDB 4G24) with the domains colored as in A.

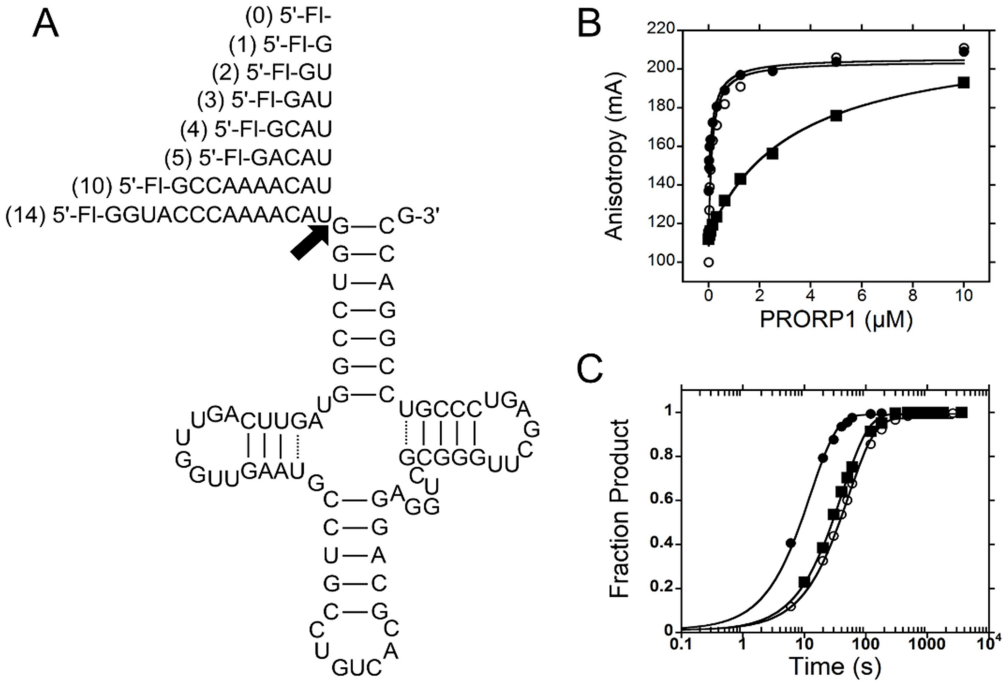


Figure 2. Binding affinity and STO activity of PRORP1 for varying leader lengths of *B. subtilis* pre-tRNA.

A. Predicted secondary structures of *B. subtilis* pre-tRNAs with varying leader lengths used in this study. All substrates were prepared using *in vitro* transcription. The 5' end is labeled with fluorescein (Fl). The arrow indicates the RNase P cleavage site. B. Representative binding isotherms for 0:1 (mature tRNA with a discriminator base at the 3' end) (closed square), 1:1 (closed circle), and 14:1 (open circle). Values for STO rate constants and K_Ds are reported in Table 1. C. Representative STO timecourses for PRORP1 catalyzed *B. subtilis* pre-tRNA cleavage under standard reaction conditions; 1:1 (closed circle), 5:1 (closed square), and 14:1 (open circle).

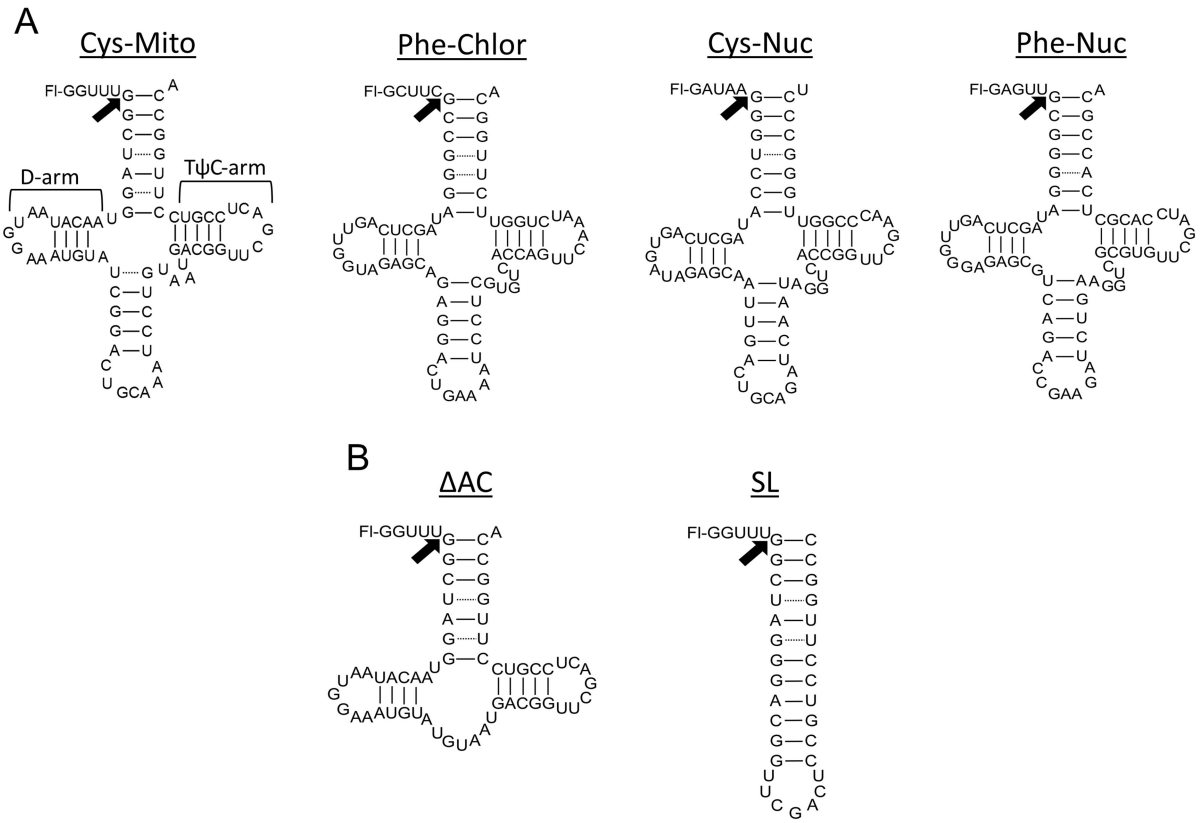


Figure 3. A. Predicted secondary structures of *A. thaliana* pre-tRNA substrates used in this study.
All substrates were prepared using *in vitro* transcription. Cys-Mito and Phe-Chlor substrates are derived from the organellar genomes (Cys-mitochondrial and Phe-chloroplast), and Cys-nuclear and Phe-nuclear are from the nuclear genome. The pre-tRNAs contain 5 nt leaders labeled with fluorescein at the 5' end and a discriminator base at the 3' end. B. Model substrates. Predicted secondary structures of two model substrates, ΔAC and SL, derived from the mitochondrial pre-tRNA^{Cys} sequence. The SL substrate connects the acceptor stem helix and TψC -arm.

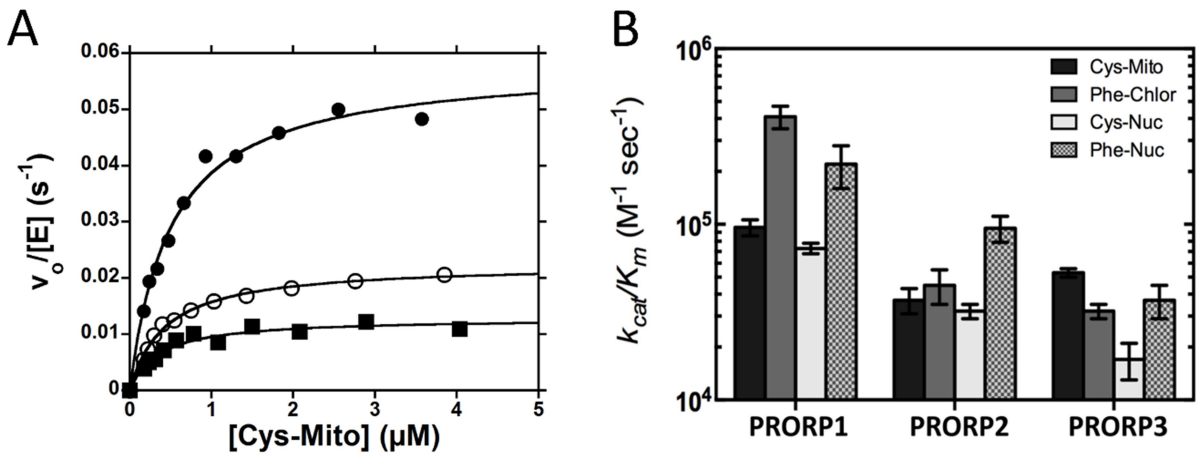


Figure 4. Multiple-turnover cleavage of pre-tRNA catalyzed by PRORPs.
A. The substrate dependence of the initial velocity (v_o/[E]) for cleavage of Cys-Mito pre-tRNA catalyzed by PRORP1 (closed circle), PRORP2 (closed square), and PRORP3 (open circle). Reactions were performed under standard reaction conditions. B. Bar graph comparing the catalytic efficiencies (k_{cat}/K_M) of the three PRORP enzymes with the four pre-tRNA substrates. The error bars represent the standard error from fitting.

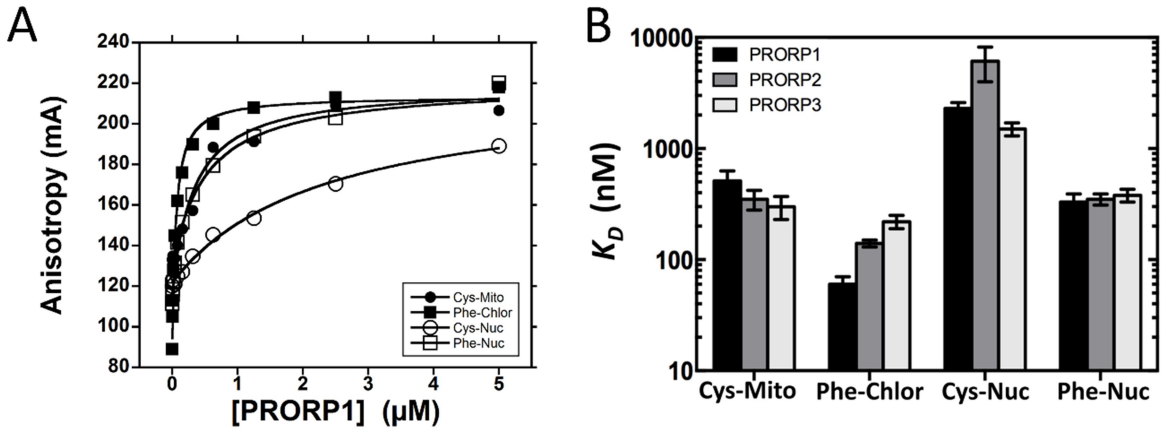


Figure 5.

A. Representative fluorescence anisotropy binding isotherms for varying concentrations of PRORP1 and 20 nM fluorescein-labeled pre-tRNA [Cys-Mito (closed circle), Phe-Chlor (closed square), Cys-Nuc (open circle) and Phe-Nuc (open square)] in 20 mM MOPS pH 7.8, 300 mM NaCl, 1 mM TCEP, and 1 mM $CaCl_2$. B. Bar graph comparing the binding affinity (K_D) of the PRORP isozymes for four pre-tRNAs. The error bars represent the standard error from fitting.

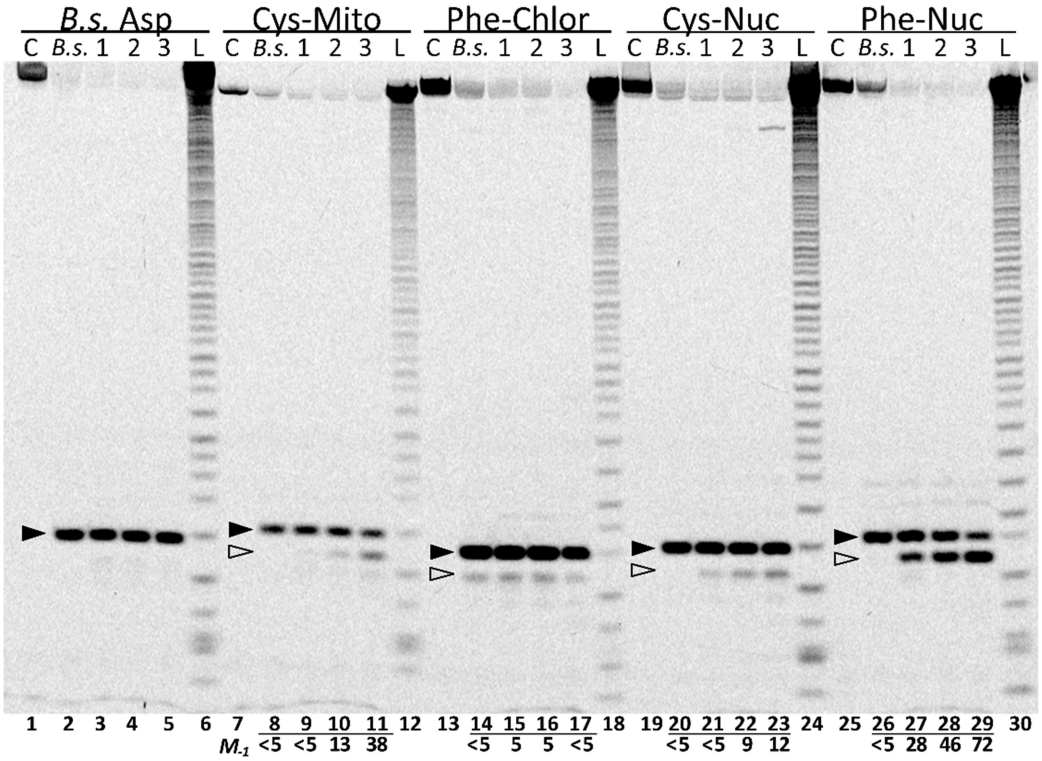


Figure 6. PAGE analysis of reaction products from RNase P-catalyzed STO cleavage of pre-tRNA.

30 nM pre-tRNA substrate was incubated with either 5 μM PRORP for 30 mins under standard assay conditions or 1.8 μM *B. subtilis* RNase P for 60 mins under conditions described in Materials and Methods. The pre-tRNA substrate in each reaction is indicated above the wells. The enzyme in each lane is indicated by: C: No enzyme control, *B.s.*: *B. subtilis* RNase P, 1: PRORP1, 2: PRORP2, 3: PRORP3, and L: alkaline hydrolysis ladder. The normalized percent miscleaved (% M_{-1}) is indicated below the lane number at the bottom of the gel. Closed arrows indicate the correct cleavage product (5 nts, C_0) and open arrows indicate miscleaved product (4 nts, M_{-1}).

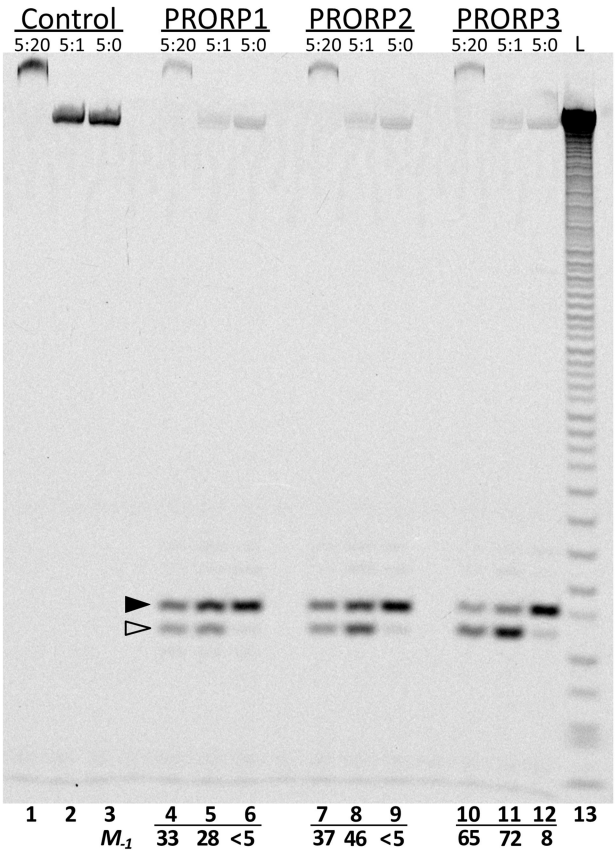


Figure 7. Miscleavage of pre-tRNA catalyzed by PRORP is alleviated by removal of the discriminator base.

30 nM Phe-Nuc pre-tRNA substrates (5:20, 5:1, and 5:0) were incubated with 5 μM PRORP1, 2, or 3 for 30 mins under standard reaction conditions. Products were resolved on a 20% gel. Closed arrows indicate the correct cleavage product (5 nts, C_0) and open arrows indicates miscleaved product (4 nts, M_{-1}). The normalized percent miscleaved (% M_{-1}) is indicated below the lane number at the bottom of the gel. In each case, miscleavage is decreased for the substrate lacking the discriminator base (5:0).

Table S1. STO miscleavage kinetics catalyzed by PRORP1, 2, and 3[a]

Phe-Nuc Pre-tRNA

Enzyme	$k_{obs,c}$ (s^{-1})[b]	A_c[c]	$k_{obs,m}$ (s^{-1})[d]	A_m[e]	k_c (s^{-1})[f]	k_m (s^{-1})[f]	k_c/k_m
PRORP1	0.067	0.70	0.083	0.30	0.047	0.025	1.9
PRORP2	0.035	0.49	0.035	0.41	0.017	0.014	1.2
PRORP3	0.048	0.25	0.050	0.69	0.012	0.045	0.3

Cys-Nuc Pre-tRNA

Enzyme	$k_{obs,c}$ (s^{-1})	A_c	$k_{obs,m}$ (s^{-1})	A_m	k_c (s^{-1})	k_m (s^{-1})	k_c/k_m
PRORP2	0.027	0.77	0.025	0.1	0.021	0.003	7
PRORP3	0.025	0.82	0.020	0.12	0.021	0.002	10.5

Cys-Mito Pre-tRNA

Enzyme	$k_{obs,c}$ (s^{-1})	A_c	$k_{obs,m}$ (s^{-1})	A_m	k_c (s^{-1})	k_m (s^{-1})	k_c/k_m
PRORP2	0.014	0.77	0.009	0.12	0.011	0.001	11
PRORP3	0.023	0.58	0.022	0.36	0.013	0.008	1.6

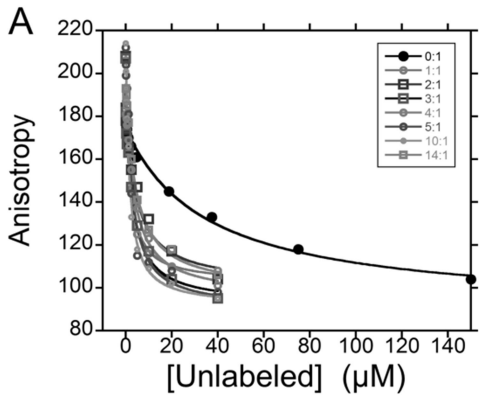
[a]Measured under standard reaction conditions. Error from fitting less than 20%, omitted for clarity.
[b]The observed rate constant for correct product formation (C_o)
[c]Corresponding amplitude of $k_{obs,c}$
[d]The observed rate constant for miscleavage (M_{-1})
[e]Corresponding amplitude of $k_{obs,m}$
[f]Rate constants calculated as described in methods

Table S2. Single-turnover observed rate constants (k_{obs}) for cleavage of model substrates

	RNA		
Enzyme	Cys-Mito (s^{-1})[a]	Cys-Mito ΔAC (s^{-1})[b]	Cys-Mito SL (s^{-1})[c]
PRORP1	0.037 ± 0.002	0.023 ± 0.005	$< 3.3 \times 10^{-5}$
PRORP2[d]	0.013 ± 0.003	0.012 ± 0.003	$4.2 \pm 0.5 \times 10^{-4}$
PRORP3[d]	0.023 ± 0.002	0.012 ± 0.002	$3.5 \pm 0.2 \times 10^{-4}$

[a]values from Table 2 shown for comparison
[b]Measured under standard reaction conditions using gel-based assay.
[c]Measured under standard assay conditions except with 10 μM enzyme using gel-based assay.

[d] k_{obs} calculated from total product (C_0 + M_{-1}) formation. PRORP2 and 3 catalyzed miscleavage of the ΔAC and to a lesser extent the SL substrate because it lacks a discriminator base.



B

Leader	Direct Measurement $K_{D,Fl}$ (nM)[a]	Competition K_D^{app} (μM)[b]	Calculated $K_{D,Un}$ (nM)[c]
0	3400 ± 400	36	5600
1	150 ± 60	2	180
2	310 ± 20	4.3	550
3	140 ± 40	2.8	310
4	150 ± 40	3.5	420
5	190 ± 60	2.3	230
10	100 ± 50	1.7	130
14	100 ± 30	4.2	530

[a] Data from Table 1 shown for comparison.
[b] Obtained by fitting a hyperbola to the data in panel A
[c] Calculated using Equation S1 as in the figure legend.

Figure S1. Competition binding assays using unlabeled pre-tRNAs.
A. ES complex was formed in the presence of 1 mM Ca^{2+} with 5 nM 5:1 *B. subtilis* pre-tRNA and 1 μM PRORP1 (final concentrations). Then unlabeled pre-tRNA was titrated into the reaction and the anisotropy was measured. A hyperbola was fit to the resulting data to obtain an apparent K_D (K_D^{app}) for the unlabeled substrate. B. Affinities for the fluorescein labeled substrate ($K_{D,Fl}$) were measured directly using the anisotropy assay (taken from Table 1). The apparent affinity for unlabeled substrate was measured using the competition assay in panel A (K_D^{app}). The resulting values overestimate the true K_D ($K_{D,Un}$) for the unlabeled substrate. Equation S1 was used to calculate $K_{D,Un}$ using the values of the $K_{D,Fl}$ of the 5:1 pre-tRNA and the K_D^{app} of each unlabeled pre-tRNA. In Eq. S1 K_D^{app} is the apparent affinity obtained by the competition assay; $K_{D,Un}$ is the calculated affinity for the unlabeled substrate or tRNA product (S); $K_{D,Fl}$ is the affinity for the 5:1 labeled substrate (S_{Fl}); [S_{Fl}] is the concentration of the 5:1 labeled substrate; f is the bound/free ratio for S_{Fl} at [S]=0, calculated from equation S2. In Eq S2 f_0 is the fraction of S_{Fl} bound at [S]=0, calculated using equation S3. In Eq. S3 [E] is the concentration of PRORP1.
Equation S1:

$$K_{D,Un} = \frac{K_D{}^{app}}{\left[1 + f + \frac{[S_{Fl}] \times (2+f)}{2 \times K_{D,Fl} \times (1+f)}\right]} - K_{D,Fl} \times \left(\frac{f}{2+f}\right)$$

Equation S2: $f = \frac{f_0}{1-f_0}$

Equation S3: $f_0 = \frac{([E]+[S_{Fl}]+K_{D,Fl})-\sqrt{([E]+[S_{Fl}]+K_{D,Fl})^2-4\times[E]\times[S_{Fl}]}}{2\times[S_{Fl}]}$

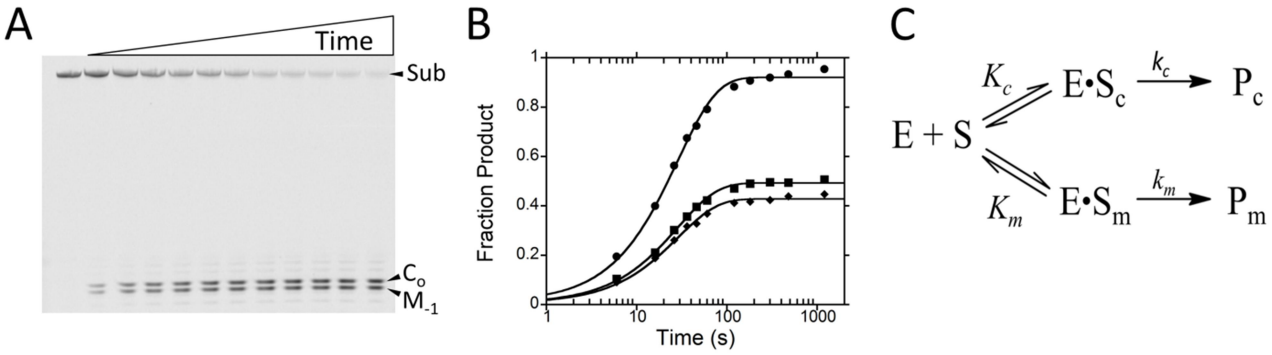


Figure S2. STO cleavage kinetics of Phe-nuc pre-tRNA catalyzed by PRORP. A. Representative urea-PAGE of STO cleavage of the Phe-Nuc pre-tRNA catalyzed by saturating PRORP2 under standard reaction conditions. Reactions were quenched at specific time points and resolved on a 22.5% urea-PAGE. C_0 indicates the correct 5 nt product and M_{-1} indicates the miscleaved 4 nt product. B. A plot of the timecourse for product formation. Circles represent the total product formation ((C_0 + M_{-1})/(C_0 + M_{-1} + Substrate)), squares represent correct product formation (C_0 / (C_0 + M_{-1} + Substrate)), and diamonds represent incorrect cleavage (M_{-1} / (C_0 + M_{-1} + Substrate)). A single-exponential equation was fit to the timecourses resulting in values for $k_{obs,t}$, $k_{obs,c}$, and $k_{obs,m}$. C. Scheme for miscleavage, assuming rapid equilibrium binding of pre-tRNA. K_c and K_m represent the equilibrium constants for the respective complex formation, k_c and k_m represent the rate constants for correct cleavage and for miscleavage, respectively. Kinetic parameters for miscleavage are summarized in Table S1.

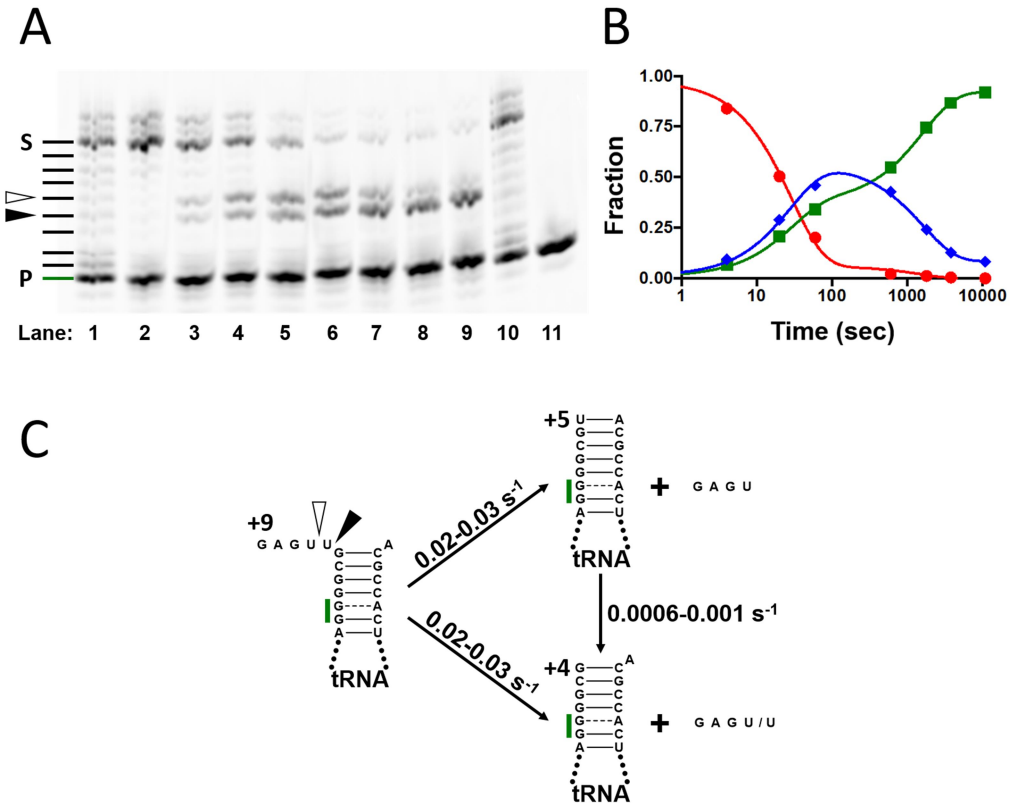


Figure S3. STO cleavage kinetics of phe-nuc pre-tRNA catalyzed by PRORP analyzed by reverse transcription.

A. Representative gel of a primer extension assay of the time course of the 5:1 Phe-Nuc pre-tRNA processed by PRORP1 under standard single turnover conditions. Fluorescence of the fluorescein label on the primer is imaged using a Typhoon 9410 scanner. Substrate (S) and primer (P) are indicated, in addition to the correct (+4, closed arrow) and -1 miscleavage (+5, open arrow) products. Lanes are: 1 & 10, ladder; 2, Phe-Nuc pre-tRNA alone; 3-9, cleavage time points of 4 sec, 20 sec, 1 min, 10 min, 30 min, 1 hr, and 3 hr; 11, primer. B. Quantification of the PRORP1 reaction represented as the fraction substrate (circles), product (squares), and miscleavage product (diamonds) at each time point. A double exponential equation was globally fit to the data using GraphPad Prism. Rate constants are $k_{obs,1}$ = 0.03 ± 0.002 s^{-1} and $k_{obs,2}$ = 0.0006 ± 0.00005 s^{-1} (PRORP1) and $k_{obs,1}$ = 0.1 ± 0.008 s^{-1} and $k_{obs,2}$ = 0.001 ± 0.00007 s^{-1} (PRORP3). C. Scheme for processing Phe-Nuc pre-tRNA (left) with miscleavage (top right) and correct (bottom right) products. For clarity, a minimal structure is shown with the acceptor stem and an abbreviated tRNA body. Canonical RNase P cleavage site (closed arrow) and -1 miscleavage site (open arrow) are indicated. Green bars represent the binding site for the 3' end of the oligo-dNTP primer. Expected primer extension lengths are given for each molecule. Rate constants k_c and k_m, calculated as described in the methods, are given for the initial cleavage steps.



Figure S4. Miscleavage of pre-tRNA Cys-mito catalyzed by PRORP3 is reduced by removal of the discriminator base.
Reactions were performed as described in the legend of Figure 6. Closed arrows indicate the correct cleavage product (5 nts, C_0) and open arrows indicate the miscleaved product (4 nts, M_{-1}). The normalized percent miscleaved (% M_{-1}) is indicated below the lane number at the bottom of the gel.

REFERENCES

1. Walker, S.C. and D.R. Engelke, *Ribonuclease P: the evolution of an ancient RNA enzyme.* Crit Rev Biochem Mol Biol, 2006. **41**(2): p. 77-102.
2. Howard, M.J., et al., *RNase P enzymes: divergent scaffolds for a conserved biological reaction.* RNA Biol, 2013. **10**(6): p. 909-14.
3. Lechner, M., et al., *Distribution of Ribonucleoprotein and Protein-only RNase P in Eukarya.* Molecular biology and evolution, 2015.
4. Gobert, A., et al., *A single Arabidopsis organellar protein has RNase P activity.* Nat Struct Mol Biol, 2010. **17**(6): p. 740-4.
5. Holzmann, J., et al., *RNase P without RNA: identification and functional reconstitution of the human mitochondrial tRNA processing enzyme.* Cell, 2008. **135**(3): p. 462-74.
6. Vilardo, E., et al., *A subcomplex of human mitochondrial RNase P is a bifunctional methyltransferase--extensive moonlighting in mitochondrial tRNA biogenesis.* Nucleic Acids Res, 2012. **40**(22): p. 11583-93.
7. Vilardo, E. and W. Rossmanith, *Molecular insights into HSD10 disease: impact of SDR5C1 mutations on the human mitochondrial RNase P complex.* Nucleic Acids Res, 2015.
8. Taschner, A., et al., *Nuclear RNase P of Trypanosoma brucei: a single protein in place of the multicomponent RNA-protein complex.* Cell Rep, 2012. **2**(1): p. 19-25.
9. Lai, L.B., et al., *A functional RNase P protein subunit of bacterial origin in some eukaryotes.* Mol Genet Genomics, 2011. **286**(5-6): p. 359-69.
10. Hartmann, E. and R.K. Hartmann, *The enigma of ribonuclease P evolution.* Trends Genet, 2003. **19**(10): p. 561-9.
11. Gutmann, B., A. Gobert, and P. Giege, *PRORP proteins support RNase P activity in both organelles and the nucleus in Arabidopsis.* Genes Dev, 2012. **26**(10): p. 1022-7.
12. Goldfarb, K.C., S. Borah, and T.R. Cech, *RNase P branches out from RNP to protein: organelle-triggered diversification?* Genes Dev, 2012. **26**(10): p. 1005-9.
13. Zhou, W., et al., *Multiple RNA processing defects and impaired chloroplast function in plants deficient in the organellar protein-only RNase P enzyme.* PLoS One, 2015. **10**(3): p. e0120533.
14. Sugita, C., et al., *Molecular Characterization of Three PRORP Proteins in the Moss Physcomitrella patens: Nuclear PRORP Protein Is Not Essential for Moss Viability.* PLoS One, 2014. **9**(10): p. e108962.
15. Howard, M.J., et al., *Mitochondrial ribonuclease P structure provides insight into the evolution of catalytic strategies for precursor-tRNA 5′ processing.* Proc Natl Acad Sci U S A, 2012. **109**(40): p. 16149-54.
16. Gobert, A., et al., *Structural insights into protein-only RNase P complexed with tRNA.* Nat Commun, 2013. **4**: p. 1353.
17. Imai, T., et al., *Pentatricopeptide repeat motifs in the processing enzyme PRORP1 in Arabidopsis thaliana play a crucial role in recognition of nucleotide bases at T*

ψC loop in precursor tRNAs. Biochem Biophys Res Commun, 2014. **450**(4): p. 1541-6.
18. Howard, M.J., B.P. Klemm, and C.A. Fierke, *Mechanistic Studies Reveal Similar Catalytic Strategies for Phosphodiester Bond Hydrolysis by Protein-only and RNA-dependent Ribonuclease P.* J Biol Chem, 2015.
19. Steitz, T.A. and J.A. Steitz, *A general two-metal-ion mechanism for catalytic RNA.* Proc Natl Acad Sci U S A, 1993. **90**(14): p. 6498-502.
20. Imai, T., et al., *Pentatricopeptide repeat motifs in the processing enzyme PRORP1 in Arabidopsis thaliana play a crucial role in recognition of nucleotide bases at T ψC loop in precursor tRNAs.* Biochem Biophys Res Commun, 2014. **450**(4): p. 1541-6.
21. Niranjanakumari, S., et al., *Protein component of the ribozyme ribonuclease P alters substrate recognition by directly contacting precursor tRNA.* Proc Natl Acad Sci U S A, 1998. **95**(26): p. 15212-7.
22. Sun, L., et al., *Binding of C5 protein to P RNA enhances the rate constant for catalysis for P RNA processing of pre-tRNAs lacking a consensus (+ 1)/C(+ 72) pair.* J Mol Biol, 2010. **395**(5): p. 1019-37.
23. Crary, S.M., S. Niranjanakumari, and C.A. Fierke, *The protein component of Bacillus subtilis ribonuclease P increases catalytic efficiency by enhancing interactions with the 5′ leader sequence of pre-tRNAAsp.* Biochemistry, 1998. **37**(26): p. 9409-16.
24. Reiter, N.J., et al., *Structure of a bacterial ribonuclease P holoenzyme in complex with tRNA.* Nature, 2010. **468**(7325): p. 784-9.
25. Hsieh, J. and C.A. Fierke, *Conformational change in the Bacillus subtilis RNase P holoenzyme--pre-tRNA complex enhances substrate affinity and limits cleavage rate.* RNA, 2009. **15**(8): p. 1565-77.
26. Rueda, D., et al., *The 5′ leader of precursor tRNAAsp bound to the Bacillus subtilis RNase P holoenzyme has an extended conformation.* Biochemistry, 2005. **44**(49): p. 16130-16139.
27. Bhaskaran, H., et al., *Structural dynamics of a mitochondrial tRNA possessing weak thermodynamic stability.* Biochemistry, 2014. **53**(9): p. 1456-65.
28. Liu, X., Y. Chen, and C.A. Fierke, *A real-time fluorescence polarization activity assay to screen for inhibitors of bacterial ribonuclease P.* Nucleic Acids Res, 2014. **42**(20): p. e159.
29. Beebe, J.A. and C.A. Fierke, *A kinetic mechanism for cleavage of precursor tRNA(Asp) catalyzed by the RNA component of Bacillus subtilis ribonuclease P.* Biochemistry, 1994. **33**(34): p. 10294-304.
30. Karasik, A., et al., *Nuclear Protein-Only Ribonuclease P2 Structure and Biochemical Characterization Provide Insight into the Conserved Properties of tRNA 5′ End Processing Enzymes.* J Mol Biol, 2015.
31. Brannvall, M., et al., *Evidence for induced fit in bacterial RNase P RNA-mediated cleavage.* J Mol Biol, 2007. **372**(5): p. 1149-64.
32. Pavlova, L.V., et al., *tRNA processing by protein-only versus RNA-based RNase P: kinetic analysis reveals mechanistic differences.* Chembiochem, 2012. **13**(15): p. 2270-6.

33. Placido, A., et al., *Plant mitochondria use two pathways for the biogenesis of tRNAHis.* Nucleic Acids Res, 2010. **38**(21): p. 7711-7.
34. Zahler, N.H., et al., *The pre-tRNA nucleotide base and 2'-hydroxyl at N(-1) contribute to fidelity in tRNA processing by RNase P.* J Mol Biol, 2005. **345**(5): p. 969-85.
35. Zahler, N.H., E.L. Christian, and M.E. Harris, *Recognition of the 5' leader of pre-tRNA substrates by the active site of ribonuclease P.* RNA, 2003. **9**(6): p. 734-45.
36. Lynch, M. and J.S. Conery, *The evolutionary fate and consequences of duplicate genes.* Science, 2000. **290**(5494): p. 1151-5.
37. Canino, G., et al., *Arabidopsis encodes four tRNase Z enzymes.* Plant Physiol, 2009. **150**(3): p. 1494-502.
38. Milligan, J.F. and O.C. Uhlenbeck, *Synthesis of small RNAs using T7 RNA polymerase.* Methods Enzymol, 1989. **180**: p. 51-62.
39. Brunelle, J.L. and R. Green, *In vitro transcription from plasmid or PCR-amplified DNA.* Methods Enzymol, 2013. **530**: p. 101-14.
40. Michaud, M., et al., *A global picture of tRNA genes in plant genomes.* Plant J, 2011. **66**(1): p. 80-93.
41. Schattner, P., A.N. Brooks, and T.M. Lowe, *The tRNAscan-SE, snoscan and snoGPS web servers for the detection of tRNAs and snoRNAs.* Nucleic Acids Res, 2005. **33**(Web Server issue): p. W686-9.
42. Lakowicz, R.J., *Principles of fluorescence spectroscopy*. 3rd ed. 2006: Springer.
43. Loria, A. and T. Pan, *Recognition of the 5' leader and the acceptor stem of a pre-tRNA substrate by the ribozyme from Bacillus subtilis RNase P.* Biochemistry, 1998. **37**(28): p. 10126-33.
44. Chen, D. and J.T. Patton, *Reverse transcriptase adds nontemplated nucleotides to cDNAs during 5'-RACE and primer extension.* Biotechniques, 2001. **30**(3): p. 574-80, 582.
45. Emanuelsson, O., et al., *Locating proteins in the cell using TargetP, SignalP and related tools.* Nat Protoc, 2007. **2**(4): p. 953-71.
46. Lange, A., et al., *Classical nuclear localization signals: definition, function, and interaction with importin alpha.* J Biol Chem, 2007. **282**(8): p. 5101-5.

PAPER 3: MOLECULAR RECOGNITION OF PRE-TRNA BY *ARABIDOPSIS* PROTEIN-ONLY RIBONUCLEASE P

Bradley P. Klemm,[1] Agnes Karasik,[2] Kipchumba J. Kaitany,[1] Aranganathan Shanmuganathan,[2] Matthew J. Henley,[4] Adam Z. Thelen,[1] Allison J.L. Dewar,[3] Nathaniel D. Jackson,[2] Markos Koutmos,[2,*] Carol A. Fierke[1,3,4,*]

[1]Department of Biological Chemistry, University of Michigan, Ann Arbor, MI, 48109, USA

[2]Department of Biochemistry and Molecular Biology, Uniformed Services University of the Health Sciences, Bethesda, MD, 20814, USA

[3]Department of Chemistry, University of Michigan, Ann Arbor, MI, 48109, USA

[4]Program in Chemical Biology, University of Michigan, Ann Arbor, MI, 48109, USA

*Corresponding authors: markos.koutmos@usuhs.edu; fierke@umich.edu.

Running title: Plant RNase P pre-tRNA molecular recognition

Keywords: RNase P, PRORP, PPR, pre-tRNA, molecular recognition

Author Contributions: B.P.K., A.K., M.K., and C.A.F. designed experiments. B.P.K., A.K., K.J.K., A.J.L.D., A.Z.T., A.S., N.J., and M.J.H. purified mutants and performed assays. A.K. and M.K. performed the modeling experiments. All authors were involved

in writing or editing the manuscript. A.K. contributed with data to Table 1, Table S2, Figure 2 and Figure 7.

Abstract

Protein-only ribonuclease P (PRORP) is an enzyme responsible for catalyzing the 5' end maturation of precursor transfer ribonucleic acids (pre-tRNAs) encoded by various cellular compartments in many eukaryotes. PRORPs from plants act as single-subunit enzymes and have been used as a model system for analyzing the function of the metazoan PRORP nuclease subunit, which requires two additional proteins for efficient catalysis. There are currently few molecular details known about the PRORP-pre-tRNA complex. Here, we characterize the determinants of substrate recognition by the single subunit *Arabidopsis* thaliana PRORP1 and PRORP2 using kinetic and thermodynamic experiments. The salt dependence of binding affinity suggests 4–5 contacts with backbone phosphodiester bonds on substrates, including a single phosphodiester contact with the pre-tRNA 5' leader, consistent with prior reports of short leader requirements. PRORPs contain an N-terminal pentatricopeptide repeat (PPR) domain, truncation of which results in > 30-fold decrease in substrate affinity. While most PPR-containing proteins have been implicated in single-stranded sequence specific RNA recognition, we find that the PPR motifs of PRORPs recognize pre-tRNA substrates differently. Notably, the PPR domain residues most important for substrate binding in PRORPs do not correspond to positions involved in base recognition in other PPR proteins. Several of these residues are highly conserved in PRORPs from algae, plants, and metazoans, suggesting a conserved strategy for substrate recognition by the PRORP PPR domain. Furthermore, there is no evidence for sequence specific interactions. This work clarifies molecular determinants of PRORP-substrate recognition and provides a new predictive model for the PRORP-substrate complex.

Introduction

Ribonuclease P (RNase P) enzymes are essential endonucleases with diverse macromolecular composition that are responsible for catalyzing the maturation of the 5' end of pre-tRNA [1]. In many biological settings, RNase P is a ribonucleoprotein complex containing a large catalytic RNA capable of processing pre-tRNAs *in vitro* [2]. Additionally, one or more associated protein components are required for function *in vivo* [3, 4]. In bacterial RNase P, the protein subunits increase substrate affinity and the ability of divalent metal ions to bind at specific sites [5-8].

In many eukaryotic species, including protists, algae, land plants, and metazoans, protein-only RNase Ps (PRORPs) have been identified [9-12]. Human mitochondrial RNase P (mtRNase P) was the first PRORP described and it requires 2 additional protein subunits for activity [9]. These subunits are an m^1G/A_9 tRNA-methyltransferase (TRMT10C, also MRPP1) and a hydroxysteroid dehydrogenase/reductase (HSD17B10, also MRPP2), which form a sub-complex [9, 13]. MRPP1 and MRPP2 are proposed to contribute primarily to substrate recognition.

In contrast to the metazoan PRORP, the PRORPs from algae, protists, and plants do not require additional subunits for efficient catalysis *in vitro* [10-12, 14-17], suggesting differences in substrate recognition. The three PRORPs from A. thaliana are designated PRORP1–3. AtPRORP1 localizes to the mitochondria and chloroplasts where it is responsible for catalyzing pre-tRNA maturation [10], while AtPRORP2 and AtPRORP3 co-localize to the nucleus and are not fully redundant in nuclear pre-tRNA processing [14]. AtPRORP1 utilizes a metal ion-dependent mechanism similar to the mechanism of the ribozyme, relying on ionization of metal-bound waters for nucleophile

activation in catalysis [16, 18]. Given the additional mechanistic information and the relative simplicity of the AtPRORPs, they have been used as a model system to study PRORP-substrate molecular recognition.

PRORPs contain a unique three domain architecture (Figure 1A). An N-terminal pentatricopeptide repeat (PPR) domain significantly enhances the affinity for substrate and truncation of the first 3–4 repeats abolishes catalytic activity [19-21]. Thus, the PPR domain is proposed to both bind and orient substrate with respect to the metallonuclease domain [19]. In addition, the nuclease domain is a member of the Nedd4-BP1, YacP nuclease (NYN) family [22]. Lastly, a bipartite CC/HC Zn^{2+}-binding domain flanks the NYN domain [19]. Our current understanding of how each domain, in particular the PPR domain (Figure 1B, Figure S1), contributes to PRORP substrate recognition is limited.

Previous results suggest differences in substrate recognition between the bacterial RNA-dependent RNase P and PRORP. Unlike the ribozyme, the PRORP active site metal ions apparently do not contact the pro-R_P oxygen [23], but rather contact the pro-S_P oxygen of the scissile phosphodiester bond [24]. Furthermore, while the 3'-CCA is specifically recognized by bacterial RNase P RNA, it is either inhibitory or immaterial to AtPRORP activity [25-27]. Additionally, AtPRORP1 and AtPRORP3 do not significantly contact either the 5' leader sequence beyond N_{-2} or the 3' trailer (Figure 2A); these regions do not alter substrate affinity or catalytic activity [26, 28]. The minimal 5' and 3' end interactions indicate that PRORP substrate recognition lies primarily within the tRNA body.

Previously, a nuclease footprinting assay demonstrated that there was significant protection of bases in the D- and TψC-loops (Figure 2A) by AtPRORP1 [25]. Given

these data and the likelihood that the NYN domain binds at the scissile phosphodiester bond, it was proposed that the PPRs recognized the pre-tRNA elbow, the structure formed by interaction between the D- and TψC-loops [25]. However, this proposal remains to be tested. Recent attempts to alter base specificity of the PPR domain in AtPRORP3 were unsuccessful [26]. Furthermore, while the TψC-arm is sufficient for recognition and catalysis by plant PRORPs, the presence of a D-arm increases the affinity significantly [26, 28]. These data provide a basis for examining the features of PRORP that contribute to recognition of pre-tRNA.

A model of substrate-bound AtPRORP1 was previously generated using molecular dynamics and includes the PPR domain docked to the TψC-loop [20]. The authors assumed that PRORPs use the recognition strategy employed by several single-stranded RNA binding PPR proteins. The ssRNA-binding PPR proteins recognize nucleobases utilizing residues in two tandem repeats at positions 6 and 1' (Figure 1B, Figure S1), as well as hydrophobic amino acids at position 3 that contribute to binding affinity by van der Waals or stacking interactions [29, 30]. Cleavage assays catalyzed by AtPRORP1 indicated that mutations to position 6 of PPR motifs 2, 3, and 4 reduce activity modestly (≤ 70% reduction) [20]. However, the full suite of PPR residues important for PRORP substrate recognition remains to be identified.

Here, we characterize the mode of substrate binding and recognition by the highly conserved AtPRORP1 and 2 using a variety of biochemical techniques. The salt-dependence of pre-tRNA affinity indicate that AtPRORP1 and AtPRORP2 make at least four direct contacts to substrate backbone phosphodiester bonds, including a single phosphodiester bond contact with the pre-tRNA leader. Importantly, these interactions

with the backbone are not sequence specific. However, the salt-dependence of affinity for mature tRNA also demonstrates that a significant portion of the affinity for substrate stems from interactions with the sugars and/or bases in the body of the substrate, in contrast to the bacterial ribozyme, which makes more contacts with the 5' leader and 3' CCA. To test whether AtPRORP1 uses canonical PPR-nucleobase interactions, we mutated residues in both the PRORP PPR domain and nucleotides in a pre-tRNA substrate and assessed how the mutations impact the PRORP-pre-tRNA affinity. In contrast to other known PPR proteins, PRORP does not exhibit demonstrable sequence selectivity for substrate affinity, suggesting that substrate recognition relies instead on the three-dimensional structure of pre-tRNA. These experiments provide a biochemical framework for understanding molecular recognition of complex RNA structures by the non-canonical PPRs of plant PRORPs.

Results

AtPRORP-substrate recognition mode

To begin characterizing how AtPRORPs recognize their cognate substrates, we set out to determine the general mode of substrate binding. We first measured the dependence of the protein-nucleic acid interaction on the concentration and identity of ions in solution. These data parse the dependence of affinity on ionic interactions with backbone phosphodiester bonds, compared to that of non-ionic interactions. Monovalent and divalent cations directly interact with backbone phosphodiester bonds on nucleic acids. These ions must be released for a protein to directly contact those sites, thus affinity depends on the cation concentration [31, 32]. Cations associate with nucleic acids

through an ionic atmosphere also containing anions, which inhibits protein-nucleic acid interactions through a related screening mechanism [31].

We measured the dependence of the substrate binding affinity of AtPRORP1 and AtPRORP2 on ions in solution to estimate the number of backbone phosphodiester bond contacts. We determined dissociation constants (K_D) for AtPRORP1 and 2 by fluorescence anisotropy (FA) assays using three substrates: a B. subtilis pre-tRNA^{Asp} (AtPRORP1 and 2), an A. thaliana mitochondrial pre-tRNA^{Cys} (AtPRORP1), each with 5-nt leaders, and an A. thaliana nuclear pre-tRNA^{Gly} (AtPRORP2) with a 6-nt leader; all substrates have a fluorescein label at the 5' end (Figure 2A). The pre-tRNA^{Asp} substrate has been used extensively with the bacterial ribozyme, allowing us to make direct comparisons to PRORPs, while the pre-tRNA^{Cys} is a cognate substrate for AtPRORP1 and the pre-tRNA^{Gly} is a cognate substrate for AtPRORP2. We obtained thermodynamic affinities (K_D) by fitting a hyperbola (Equation 1, Materials and Methods) to the data (Figure 2B).

The Na^+-dependence of K_D shows a linear dependence in a log-log plot (Figure 2C), as described by Equation S1 (Supporting Methods), which was adapted from Equation 18 of deHaseth, et al. [33]. Divalent cations are required to fold the pre-tRNA, so $CaCl_2$, which does not activate AtPRORP1 or AtPRORP2 [19, 21], was supplied at a constant value for each measurement. The primary effect of Ca^{2+} in our assays is to increase the anisotropy of free pre-tRNA (see the next section), while the affinity we measure at different $CaCl_2$ concentrations varied ≤ 65% at a given NaCl concentration. Thus, we selected $CaCl_2$ concentrations that allowed us to best measure the affinity under high concentrations of NaCl (20 or 6 mM $CaCl_2$ for AtPRORP1 or AtPRORP2,

respectively). We observe minimal competition between Ca^{2+} and Na^{+} for the RNA substrate under the concentrations used for the binding assays for AtPRORP1, as evidenced by the relatively linear Na^{+}-dependence in the log-log plot (Figure 2C). We maintained constant pH during the experiments and anion effects are precluded based on the $CaCl_2$-alone and Na_2SO_4 data described below. In the absence of these effects, Equation S1 can be reduced to Equation 4 (Materials and Methods), which was fit to the data.

The slope of a $-\log(K_D)$ versus $-\log[Na^{+}]$ plot is given by $Z\varphi$ (Equation 4), represented as $Z\phi$ for divalent cations, where φ^{Na} is the fraction of Na^{+} associated thermodynamically with each backbone phosphodiester bond and Z is the number of cations (M^{+}) that are released from the nucleic acid upon binding to the protein, which approximates the number of protein-phosphodiester bond contacts. Previous data suggest that the value of φ^{Na} for dsRNA and structured RNAs, such as pre-tRNA, are comparable to the φ^{Na} for dsDNA [34, 35]. Thus, we used the value for dsDNA, $\varphi^{Na} = 0.88$, in fitting Equation 4 to the data (Table 1). The Z values for AtPRORP1 suggest the formation of four protein-phosphodiester bond contacts upon binding pre-tRNA. The values for AtPRORP2 are higher, possibly suggesting contacts with five phosphodiester groups. Furthermore, these Z values do not have a high dependence on the estimated value of φ^{Na}. Specifically, the Z value for AtPRORP2 binding to pre-$tRNA^{Gly}$ increases to 6 if $\varphi^{Na} < 0.85$. However, Z remains ≤ 5 for the other PRORP/pre-tRNA pairs until $\varphi^{Na} < 0.75$ and is ≤ 6 until $\varphi^{Na} < 0.6$, which is likely to be well below the actual value.

The extrapolated substrate affinity at 1 M NaCl has been used to estimate the contribution of non-ionic interactions to affinity in model systems, using normal Gibbs

free energy definitions (Equation 5) [36]. For AtPRORP1 at 27°C, the $-\log(K_D)$ at 1 M NaCl indicates values of –6.9 ± 0.1 and –6.0 ± 0.3 kcal/mol for pre-tRNA^{Asp} and pre-tRNA^{Cys}, respectively (Figure 2C). For AtPRORP2, the values are –6.9 ± 0.2 and –5.9 ± 0.4 kcal/mol for pre-tRNA^{Asp} and pre-tRNA^{Gly}, respectively (Figure 2C). The reduced affinity for pre-tRNA^{Cys} or pre-tRNA^{Gly} compared to pre-tRNA^{Asp} represents only a minor loss of non-ionic interactions.

AtPRORP1 does not have specific anion binding sites that compete with substrate binding

Specific anion binding sites on proteins can decrease the binding affinity of nucleic acids, in an ion-dependent manner similar to the effect of cations binding to nucleic acids. We screened the AtPRORP1 affinity for pre-tRNA^{Asp} in several Na^+ salts at a single Na^+ concentration; the data largely follow the lyotropic series (Supplementary methods, Table S1). This trend suggests that the primary effect of the anions is to alter protein stability, as opposed to directly binding to the pre-tRNA binding sites on AtPRORP1 to inhibit pre-tRNA binding. Anion sites on proteins have also been probed by comparing the dependence of binding affinity on the concentrations of monovalent (M^+) and divalent (M^{2+}) cations for a given anion [32, 33].

For a protein binding to dsDNA in the absence of specific anion binding sites, the theoretical ϕ^{Mg}/φ^{Na} is 0.53, which corresponds to the difference in the cations' occupancy on the phosphodiester bonds in the backbone [33]. To further test whether anion binding to AtPRORP1 contributes to the salt dependence of binding affinity, we measured dissociation constants in the presence of varying concentrations of $CaCl_2$ (alone) or Na_2SO_4 (Figure 3B). Fitting Equation 4 to the $CaCl_2$ data with Z = 4, we obtained ϕ^{Ca} =

0.51 ± 0.04. This value is in relatively good agreement with $\phi^{Mg} = 0.47$ for dsDNA [33]. For the PRORP/pre-tRNA complex, the ratio of the slopes (Ca^{2+}/Na^{+}) for the dependence of log K_D on log concentration is 0.54, similar to the Mg^{2+}/Na^{+} ratio of 0.53 for protein/DNA [33]. Thus, the salt-dependence of PRORP binding affinity can be explained using only the occupancies of the cations on backbone phosphodiester bonds and excluding anions.

The slope of $-\log(K_D)$ as a function of $\log[Na_2SO_4]$ is smaller than the slope of the NaCl data, resulting in tighter binding at higher Na^{+} concentrations in Na_2SO_4 (Figure 3B). However, when $-\log(K_D)$ is plotted against ionic strength ($-\log[I]$), the NaCl and Na_2SO_4 data nearly overlay, while the $CaCl_2$ data remains distinct (Figure 3C). Thus, the modest differences in affinity observed in NaCl compared to Na_2SO_4 are most likely due mainly to non-specific screening by the ionic atmosphere, to which Na_2SO_4 contributes less due to the lower concentration of SO_4^{2+} at a given concentration of Na^{+}. Given these data, we exclude the term for specific anion binding sites from our fits. The 1 M NaCl, 1 M Na_2SO_4, and 1 M $CaCl_2$ ionic strength intercepts are within error (Figure 3C), confirming that the non-ionic contributions to binding are ion-independent.

AtPRORP1 makes fewer contacts to substrate leader than the bacterial ribozyme

Varying the leader length of pre-tRNA substrates beyond 1-nt [28] or 2-nt [26] was previously shown to have little effect on the single-turnover activity and binding affinity with AtPRORPs. From these data, it is apparent that AtPRORPs can process a substrate with short 1- and 2-nt leaders, and that AtPRORP1 discriminates against binding the tRNA product (> 30-fold lower affinity for tRNA than pre-tRNA). In

contrast, the B. subtilis RNA-based RNase P relies on extensive contacts with the leader and trailer sequences for substrate recognition and displays a significant dependence on leader length beyond 2 nt [8, 37].

We determined the Na^+-dependence of affinity for the fluorescein-labeled 1-nt pre-$tRNA^{Asp}$ and $tRNA^{Asp}$ product to evaluate the nature of the AtPRORP1 interactions with the leader (Table 1, Figure 4). For the 1-nt substrate, the main effect is a value for K_0 that is increased 2-fold compared to the 5-nt substrate, suggesting a 0.5 kcal/mol reduction in non-ionic interactions with the shorter leader. The value of Z is also reduced modestly, although not enough to indicate the full loss of a phosphodiester contact. In contrast, the Z value for $tRNA^{Asp}$ is reduced to 2.8 ± 0.5, consistent with the loss of one full phosphodiester bond contact. Interaction between PRORP and a phosphodiester bond in the 5' leader is a feature of recognition in common with bacterial RNase P, which contacts the N_{-3}/N_{-2} phosphodiester bond [38]. The value of K_0 for $tRNA^{Asp}$ also increases significantly compared with pre-$tRNA^{Asp}$ containing either a 5 nt or 1 nt leader, equivalent to a loss of 2.1 and 1.6 kcal/mol, respectively, indicative of non-ionic interactions with the leader. Apart from the interactions in the leader, the data also demonstrate that non-ionic interactions with the tRNA body are important determinants of binding affinity, contributing 4.8 kcal/mol, or ~ 70% of the non-ionic binding energy (Table 1).

The PRORP PPR domain recognizes tRNAs using non-canonical positions

Previous work demonstrated that mutations of N136T, T180N, and G215N, each at position 6 of an AtPRORP1 PPR motif, resulted in minor pre-tRNA processing defects [20]. Likewise, T113S and T113N mutations in AtPRORP2, equivalent to T180 in AtPRORP1, resulted in little or no processing defects [26]. To further characterize substrate recognition by the PRORP PPR domain we measured the pre-tRNA binding affinity and salt-dependence for variants of seven residues in AtPRORP1. The targeted side chains: (1) are highly- or fully-conserved among plant PRORPs, as judged from alignment of PRORPs from 16 species; (2) are located on the PPR surface facing the NYN domain; and (3) have the potential to make hydrogen bonding, ionic, or base-stacking interactions (Figure 5). In addition to the residues at the 1, 3, and 6 positions that have been shown to be involved in base selection in other PPR domains [29, 30], we also targeted residues at position 10, which was not identified in the canonical base-selection motifs [39]. While residues at position 3 in ssRNA binding PPR proteins are typically hydrophobic (i.e. Leu, Phe), in PRORPs the residues at this position are mostly small or hydrophilic. Figure 5A shows the position of the residues that we targeted: Y133 (position 3; PPR2), N136 (position 6; PPR2), Y140 (position 10; PPR2), N175 (position 1; PPR3), T180 (position 6; PPR3), R184 (position 10; PPR3), and R212 (position 3; PPR4). We examined the effects of alanine mutations at each position, as well as more conservative mutations including Y133F, T180S, and R184K.

We measured the binding affinities of the AtPRORP1 mutants for the B. subtilis 5-nt pre-tRNA^{Asp} substrate using the FA assay at 330 mM NaCl; these data are summarized in Table 2. We observed the largest reductions in binding affinity for the Y140A and R184A variants with decreases of > 190- and 67-fold, respectively, as well as

for the R212A mutant (see below). Representative binding data for Y140A and R184A at 330 mM NaCl are shown in Figure S2. T180 was the only residue in a canonical PPR base-selection position that we tested with a strong effect on binding; T180A reduces the binding affinity by approximately 20-fold compared to WT AtPRORP1. The other canonical base-selecting residues that we mutated led to modest decreases in binding affinity: N136A had a 6.3-fold effect and N175A had a 9-fold effect. Finally, R212A eliminated binding as measured with the anisotropy assay ($K_D > 30$ μM) (Figure S3B). Additionally, the enzymatic activity of this mutant in an STO assay remained lower than the wild-type value even with > 35 μM enzyme and high Mg^{2+} concentrations and several significant miscleavage bands were observed (Figure S3A).

We parsed the determinants of substrate binding by AtPRORP1 in more detail by analyzing the salt dependence of the mutants. In general, the mutations had little effect on the Z value for the Na^+-dependence of binding affinity, but they affected the intercept value, K_0 (Table 2). These results indicate that the mutated side chains do not form ionic interactions with the phosphodiester backbone of pre-tRNA, rather mediating non-ionic interactions with the substrate. The largest measurable reduction in affinity (> 190-fold) was observed for the Y140A variant, corresponding to a loss of 2.8 kcal/mol of non-ionic binding energy. However, the Y140F mutation only increased K_0 by 6.5-fold, corresponding to a loss of approximately 1 kcal/mol in non-ionic interactions compared to WT AtPRORP1. These results are consistent with PRORP interacting with pre-tRNA with both the tyrosine hydroxyl and the phenyl ring [40]. For the R184A mutant, the 67-fold reduced affinity corresponds to a reduction of 2.5 kcal/mol compared to WT, while

the R184K mutation increased the K_0 by 10-fold, corresponding to a loss of 1.4 kcal/mol of binding energy compared to WT.

The Y133 variants reveal a relationship different from that of the Y140 variants. The Y133F and Y133A variants reduce pre-tRNA affinity by comparable values, 1.8 kcal/mol and 1.6 kcal/mol, respectively. These data suggest that the hydroxyl group, but not the phenyl ring of Y133, contributes to substrate affinity. The N136A and N175A mutations reduce the value of the intercept (K_0) corresponding to approximately the loss of 1 kcal/mol in non-ionic binding energy apiece. We estimated comparable free energy losses for T180A and T180S variants, 1.7 and 1.5 kcal/mol, respectively, compared to that of WT.

The AtPRORP2 PPR domain recognizes tRNAs using a similar binding surface

To determine whether this binding surface is shared among *Arabidopsis* PRORPs and whether additional PRORP PPR side chains are important for substrate binding, we screened the pre-tRNA binding affinity of 22 alanine variants in AtPRORP2 (Figure 5B). Previously, we and others proposed that the 1st, 3rd, 6th and 10th residues (numbered as in Barkan, et al. 2012) in each PPR motif could periodically contribute to substrate binding in AtPRORPs (Figure S1) [21, 29, 39, 41]. Therefore, we systematically targeted residues in these positions for all five PPR motifs and the PPR C-terminal helix (α11) for alanine mutagenesis. This analysis necessarily excludes three alanine residues (A110, A150, and A182).

We examined the binding affinity of the alanine mutants with A. thaliana nuclear 6-nt pre-tRNA^{Gly} and B. subtilis 5-nt pre-tRNA^{Asp} substrates. The residues that we

identified with alanine scanning mutagenesis of AtPRORP2 are consistent with the binding surface identified in AtPRORP1, although the effects on binding affinity are smaller. The largest decreases in binding affinity compared to wild type AtPRORP2 were observed for Q67A (position 3; PPR2), N108A (position 1; PPR3), T113A (position 6; PPR3), and R145A (position 1; PPR4), which increased the K_D values for pre-tRNA by at least 1.5-fold (in the highest fold-increase that we observed, Table S2). Importantly, these residues (excluding R145) correspond to three of the seven positions we identified in the AtPRORP1 PPR domain. This analysis also identified additional residues that decrease pre-tRNA binding affinity beyond those evaluated in AtPRORP1, all of which fall primarily within the nearby PPR surface. These include N38A (position 10; PPR1), S65A (position 1; PPR2), T31A (position 3; PPR1), and K220A (position 6; α11), each of which increased the K_D by at least 2-fold compared to wild type AtPRORP2 (in the highest fold-increase that we observed, Table S2). Four AtPRORP2 alanine mutants – Q70A (position 6; PPR2), Y74A (position 10; PPR2), R117A (position 10; PPR3), R147A (position 3; PPR4) – did not express as soluble proteins, suggesting that mutation of these residues may affect the stability of AtPRORP2. These residues are all located on the proposed substrate binding surface, and include four of the seven residues that alter substrate affinity in AtPRORP1.

Given the importance of Y140 in AtPRORP1 for pre-tRNA affinity, we further investigated the interaction between this amino acid and pre-tRNA by analyzing the Y74S and Y74F mutants in AtPRORP2. We found that these mutations significantly decrease substrate affinity (Table S2), as observed for AtPRORP1. These results further demonstrate that Y140 interacts with substrate using both the phenyl ring and the

hydroxyl group. Taken together, the above results suggest that surface we identified in AtPRORP1, primarily in PPR2 and PPR3, generalizes as the major surface involved in PRORP substrate binding.

PRORP PPR domain appears not to recognize tRNAs with base-specificity

To investigate whether AtPRORPs recognize pre-tRNA in a base-specific manner, we mutated residues that the previously established PPR recognition codes suggest should recognize pyrimidines [29, 30]. AtPRORP1 contains amino acids located between PPR motifs 2 and 3 (Y133/N136/N175) that should recognize pyrimidines [29, 30]. For this analysis, we examined pyrimidines in pre-tRNA that would likely interact with PRORPs. The D- and TψC-loops (tRNA elbow) in pre-tRNA have been proposed to interact with the PPR domain [25]. We assumed that the pyrimidines should not be in secondary/tertiary contacts or otherwise buried and inaccessible in the unbound tRNA structure, limiting the proposed interaction to uridines at positions 16, 17, 20, and 21 in pre-tRNA^{Asp} (Figure 2A). Mutation to adenosine at each of these positions altered the affinity by at most 2-fold (Table S3), demonstrating a lack of sequence-specific interaction at these sites. In combination with the previous data regarding the effects of tRNA mutations on PRORP binding/catalysis [20, 26], these data reinforce the hypothesis that PRORPs utilize a mode of substrate recognition different from the previously described PPR base-selection determined in ssRNA binding proteins. However, the possibility remains that there are other sites in pre-tRNA that interact with PRORP PPRs in a sequence-specific manner.

Na^+ screening inhibits AtPRORP1 single-turnover activity

While it is possible that the ionic strength affects only the binding affinity, it might also affect other aspects of PRORP catalysis. To determine whether the NaCl concentration affects cleavage catalyzed by PRORP, we performed single-turnover (STO) activity assays with 5 μM AtPRORP1, which is saturating under low NaCl conditions, and limiting (30 nM) B. subtilis pre-$tRNA^{Asp}$. We used concentrations of $MgCl_2$ that we previously determined to be either saturating (20 mM) or sub-saturating (1.25 mM) for catalysis [16]. The observed rate constant (k_{obs}) is independent of the NaCl concentration between 25 mM and 200 mM, but is reduced at higher NaCl concentrations (Figure 6). The concentration dependence of NaCl inhibition above 400 mM is similar for saturating and sub-saturating $MgCl_2$. Fitting a general inhibition model (Equation 3, weighted fit, Materials and Methods) with a variable Hill Coefficient (n^{Na}) to the data yields similar IC_{50} (310 ± 70 mM for 20 mM $MgCl_2$ and 360 ± 70 mM for 1.25 mM $MgCl_2$) and n^{Na} values (4.5 ± 1.3 for 20 mM $MgCl_2$ and 5.0 ± 1.3 for 1.25 mM $MgCl_2$) for both $MgCl_2$ conditions (Figure 6). The Hill coefficients for STO inhibition (4.5–5) by sodium are in good agreement with the cooperativity we observe for inhibition of pre-tRNA binding.

If the observed inhibition is due to decreased affinity of AtPRORP1, the activity should begin to decrease at NaCl ~ 530 mM (the point at which K_D reaches > 1 μM; thus, [E] becomes < 5 times the K_D, as measured in Ca^{2+}), assuming that the binding affinity is equivalent in Ca^{2+} and Mg^{2+}. However, the activity is inhibited at lower NaCl concentrations (~ 300 mM). To test whether this observation is only due to an effect of NaCl on binding affinity, as opposed to NaCl affecting other steps in catalysis, we measured the STO k_{obs} at 20 mM $MgCl_2$ and 350 mM NaCl with varying enzyme

concentration (data not shown). The STO k_{obs} is strongly dependent on enzyme concentration under these conditions, indicating that 5 μM PRORP1 is sub-saturating, thus requiring that the STO $K_{1/2}$ in $MgCl_2$ is > 30-fold higher than the thermodynamic K_D (155 ± 20 nM) in $CaCl_2$. These data also indicate that PRORP-substrate affinity is reduced in $MgCl_2$ as compared to $CaCl_2$. This cation-dependent decrease in affinity is consistent with an EcoRV catalytic mutant that binds its cognate DNA ≈ 40-fold weaker in Mg^{2+} than in Ca^{2+} [42]. In summary, the STO data are consistent with NaCl disrupting PRORP-substrate binding, but not other kinetic steps.

Discussion

The goal of this work was to characterize the molecular interactions between AtPRORPs and pre-tRNA using the ion-dependence of binding, catalysis and mutations in the PPR domain. The NaCl-dependence of pre-tRNA affinity of AtPRORPs revealed 4–5 interactions with phosphodiester bonds in pre-tRNA and approximately 6 to 7 kcal/mol of non-ionic binding energy. These narrow ranges support previous observations that pre-tRNA recognition by AtPRORPs is similar across paralogs and largely independent of sequence. Depending on the context, biological hydrogen bonds can supply 0.5–3 kcal/mol of free energy [43], while van der Waals interactions such as base stacking can supply 0.5–2 kcal/mol [40]. AtPRORPs likely form a combination of hydrogen bonds and van der Waals interactions with pre-tRNA.

Comparison of the Na-dependence and mutation of residues in the substrate binding domain in both AtPRORP1 and 2 indicate a similar binding surface with modest differences in substrate recognition, as previously evaluated [21]. In general, alanine

mutations affect the substrate affinity of AtPRORP1 to a greater extent than AtPRORP2. This might be due to the lower $CaCl_2$ conditions used for affinity measurements with AtPRORP2, which also reduced the differences between wild type and mutant AtPRORP1 binding affinity (Table S4). The variety of ion-dependent effects on PRORP binding affinity that we observe can be synthesized as follows.

Cations such as Na^+ and Ca^{2+} inhibit PRORP/pre-tRNA binding by interacting with and competing for phosphodiester bonds on pre-tRNA. We observe a log-linear decrease in PRORP/pre-tRNA binding affinity with respect to [Na^+] above 180 mM NaCl (Figures 2C, 3B, 3C, and 4). The PPR mutations we generated (described in further detail below), do not affect the slope of the Na^+-dependence of binding at high [Na^+] (Table 2). However, we observe lesser effects from these mutations on binding affinity below 180 mM NaCl (Tables S2 and S4). Overall, these data are most informative with respect to the differences we observe between WT and variant PRORPs and pre-tRNAs, which allow us to parse the interactions between various aspects of each.

PRORP PPR domain

Our extensive mutagenesis data in the PPR domain allow us to contrast PRORP-RNA binding with previously-described PPR proteins. PPR-containing proteins are a large family with the structurally-conserved ≈ 35 residue helix-turn-helix motif found in tandem repeats that have been implicated in RNA metabolism [44, 45]. PPR proteins are found broadly in eukaryotes, with land plants having the largest set of PPR proteins. Some PPR proteins bind target RNAs in a sequence-specific manner, with recognition of a nucleobase achieved primarily by residues 6 and 1’ (also numbered 4 and ii by Yagi, et

al., or 5 and 35 by Yin, et al.) on the A helices of two tandem PPR motifs (Figure 1B, Figure S1; A helices colored dark green) [29, 30, 41]. In some cases, the binding sites have been identified in the UTRs of mRNAs, where the PPR proteins are proposed to regulate splicing, translation and/or stability of the mature transcript [45, 46]. In contrast, our mutagenesis experiments indicate that PRORP PPRs use a different mode of RNA recognition. The PPR domains of AtPRORP1 and AtPRORP2 do not rely on interactions with a limited number of residues from every repeat, but rather a more extensive surface primarily located in PPR2 and PPR3, which is consistent with previous data indicating impaired activity for ΔPPR2 and ΔPPR3 AtPRORP1 variants [20].

We initially hypothesized that PRORP PPRs would not recognize RNA using base selection as observed with ssRNA-binding PPR proteins because the base-specifying residues in the five tandem PPR repeats in PRORPs are frequently noncanonical (e.g. 6 and 1' are not often asparagine, aspartate, or threonine, Figure S1). Several substrate binding residues that we identified, such as Y140 and R184, are conserved in metazoan PRORPs (Y183 and R218 in humans). Thus, even though the metazoan PRORPs require additional subunits for catalysis, pre-tRNA recognition by the human PRORP PPR domain could use the same interaction surface as plant PRORP PPRs.

The alanine mutations most detrimental to B. subtilis pre-tRNA^{Asp} affinity were Y140A in AtPRORP1 PPR2 (> 190-fold), R184A in AtPRORP1 PPR3 (67-fold) and R212A in AtPRORP1 PPR4; the equivalent mutations in AtPRORP2 (Y74A, R117A and R147A) rendered the protein insoluble. Despite these insoluble variants, we find no evidence that the soluble AtPRORP1 mutants are less stable than the WT enzyme. The melting temperatures (T_m) [47] for Y140A, R184A and R212 AtPRORP1 are not

significantly different from WT (Figure S2C; data not shown) and the CD spectrum for Y74S AtPRORP2 does not reveal a significantly different secondary structure from WT (Figure S2D). Furthermore, R184A catalyzes STO cleavage at high concentrations (Figure S2E), with no apparent miscleavage (Figure S2F). These data support the conclusion that the PPR mutations primarily reduce the affinity for pre-tRNA.

Y140A and R184A AtPRORP1 mutations similarly bind the A. thaliana pre-tRNA^{Cys} substrate weaker than WT in 20 mM $CaCl_2$ and 330 mM NaCl conditions (> 93-fold and > 3.8-fold, respectively). Unexpectedly, the effects of the AtPRORP1 mutations are greater than the 34-fold decrease in binding affinity reported for a Δ245 AtPRORP1, which fully lacks the first 4 PPR motifs [19]. However, this measurement was carried out at 1 mM $CaCl_2$ and 100 mM NaCl with the A. thaliana mitochondrial pre-tRNA^{Cys} substrate. Under these conditions, the individual mutations have little effect on binding affinity (Table S4). This effect is likely explained by the increased proportion of the PRORP-substrate affinity on ionic interactions under lower ionic strength, such that individual non-ionic interactions we identify contribute less significantly to the overall affinity.

The loss of 1 kcal/mol that we observe for the Y140F is consistent with Y140 interacting through a hydrogen bond to substrate with the tyrosine hydroxyl. The additional 1.8 kcal/mol loss observed with the alanine substitution is consistent with the energy supplied by stacking a phenyl ring with a nucleic acid base [40]. For the R184A mutant, the 67-fold reduced affinity corresponds to a loss of 2.5 kcal/mol in non-ionic binding energy compared to WT, which could indicate loss of 1–3 hydrogen bonds with the guanidinium group and/or hydrophobic interactions with the arginine methylene

groups. By comparison, the R184K mutation increased the K_0 by 10-fold, corresponding to a loss of 1.4 kcal/mol compared to WT, consistent with the loss of a hydrogen bond. In AtPRORP1, Y140 and R184 are located at position 10 of neighboring helices forming a non-sequential, structural pair. This YR pair is widely conserved in PRORP PPRs, including metazoan PRORPs (Figure S1).

The C-terminal La domain of the telomerase protein p65 also contains a conserved YR structural pair (Y407 and R465), situated on neighboring β-strands, that are important for recognition of the conserved GA bulge in stem IV of the telomerase RNA [48]. Given the significant contribution of the phenyl ring and the guanidinium group revealed by the Y140A/F and R184A/K mutations in AtPRORP1 and Y74S/F in AtPRORP2, we propose that these residues make similar interactions with the tRNA elbow, the conserved structural feature that results from the interaction of the D- and TψC-loops, which were previously proposed to interact with PRORPs [25]. These interactions do not need to be sequence specific, but like the p65 YR pair [48], they could favor purines such as the conserved $G_{18}G_{19}$ in the D-loop. Consistent with this, mutation of these resides to adenine in a canonical pre-$tRNA^{Gly}$ leads to a ≈ 4.5-fold (G_{18}) or ≈ 1.5-fold (G_{19}) increase in the STO $K_{1/2}$ [26].

In contrast to our Y140 data, the data for Y133 indicate that the hydroxyl group, but not the phenyl ring, contributes to substrate affinity. Mutation of N136 and N175 in PRORP1 results in the loss of approximately 1 kcal/mol apiece, consistent with a hydrogen bond from the amide side chain of each. The T180A and T180S mutations in PRORP1 lead to a 1.5–1.7 kcal/mol loss while the homologous T113A in PRORP2 had at most a 3.5-fold effect on binding affinity. However, substitutions of T113S and T113N in

PRORP2 were not sufficient for significant processing defects [26]. These data suggest that the threonine methyl group is required to sterically position the hydroxyl for substrate interaction or to make a hydrophobic contact to substrate.

While AtPRORP1 T180 (T113 in AtPRORP2) is at a base-selecting position 6, its corresponding 1' partner in the putative base-selection position would be R210 (R145 in AtPRORP2). Arginine residues have not previously been identified as base-selecting residues for PPRs [29, 30]. Furthermore, the potential nucleobase binding cleft is occluded by an interaction between T180 (T113) and R212 (R147), as visualized in the AtPRORP1 and AtPRORP2 crystal structures (PDB 4g24 and 5diz) [19, 21]. Taken together, the mutagenesis data for AtPRORP1 and AtPRORP2 indicate that the PRORP PPR domain does not interact with pre-tRNA in the same manner as ssRNA-binding PPR proteins.

An alternative recognition mode could include structural recognition, like the tRNA elbow recognition employed by the specificity (S) domain of the P RNA subunit in the bacterial ribozyme. The S-domain makes stacking interactions with the conserved G_{19}–C_{56} tertiary interaction between the D- and TψC-loops, and sugar face interactions with the conserved G_{53}–C_{61} pair at the end of the TψC arm [49]. These interactions recognize conserved pre-tRNA structural elements and allow P RNA to recognize the entire set of pre-tRNA transcripts without specificity for the tRNA body sequence. Likewise, we propose that the PPRs of PRORPs recognize tRNA using structure-specific interactions. A similar mode of recognition has been proposed previously [25]. However, our data does not completely rule out base-recognition strategies such as those employed by canonical PPR proteins.

PRORP-substrate recognition model

Combining our data with published data [20, 25], we propose a new, predictive model to describe how AtPRORP1 and AtPRORP2 bind their substrates. A previous model of the complex utilized AtPRORP1 bound to tRNA with base-specifying interactions between a TψC-loop cytosine and PPR motifs 3 and 4 [20]. The tRNA coordinates were derived from the bacterial RNase P holoenzyme in complex with a tRNA product [49] and tRNA bound to a pseudouridine synthetase [50], which has significant alterations to the TψC-loop bases and backbone. While this paper was under review, a similar model was published that largely supports our model [51].

For constructing our model, we employed the crystal structures of AtPRORP1 (PDB 4g24) and AtPRORP2 (PDB 5diz) [19, 21]. The two structures are highly conserved, yet there is a significant difference in the angle between specific PPR motifs and between the central domain and the metallonuclease domain; as a consequence, AtPRORP2 is in a more "open" conformation. We propose that the two distinct structural snapshots may represent two different conformations that potentially play a role in substrate binding [21]. The more "open" AtPRORP2 conformation can more readily accommodate tRNA, since the distance between the active site and the proposed substrate binding region in the PPR domain is ~ 50 Å. Therefore, we used the AtPRORP2 structure to generate a tRNA interaction model and used this model as a template to generate a model for AtPRORP1-tRNA recognition. There are no crystal structures available for any of the tRNAs used in this study. However, since the 3D structure of tRNAs is highly conserved, we used a canonical eukaryotic tRNA, yeast $tRNA^{Phe}$, with high resolution

crystal structure (PDB 1ehz) [52] with only slight modifications to bases predicted to interact with the protein.

The tRNA substrate can be accommodated well between the metallonuclease and PPR domains in our model (Figure 7), with one exception. There is a short PRORP helix (α21) and part of the loop that precedes it near the active site that sterically clashes with the 3' strand of the tRNA acceptor stem. We posit that this NYN helix will adopt a different conformation upon pre-tRNA binding and may be directly involved in recognition. This region could serve as a hinge that allows or blocks substrate binding to the metallonuclease domain. Interestingly, the invariant and solvent exposed R496 (R443 in PRORP2) and H498 (H445 in PRORP2) residues in this region are ideally placed for interaction with the phosphodiester backbone in the acceptor stem. Mutational analysis of the residues H498 (H498A/H498Q, AtPRORP1) and H445 (H445A, AtPRORP2) demonstrate that these mutations reduce the STO k_{obs} without significantly affecting the K_D [16, 21]. We proposed that these residues are involved in positioning the substrate and our model provides potential contacts with substrate for testing this hypothesis.

Our model suggests an exit groove for the 5' leader that would place the N_{-3}/N_{-2} phosphodiester bond and N_{-3} nucleoside outside the bounds of the NYN domain. This is consistent with data suggesting few contacts with the leader beyond the N_{-2} nucleoside. Moreover, our model places the N_{-2}/N_{-1} phosphodiester bond near the invariant H438 (H386 in PRORP2) and R441 (R389 in PRORP2), implicating these residues for interactions with the negatively charged backbone. This aspect of our model is congruent with our data indicating that PRORPs form one non-base-specific phosphodiester backbone contact with the tRNA leader. Furthermore, the α16–α17 loop is positioned to

separate the 5' leader and 3' trailer. Interestingly, AtPRORP1 has 4 fewer amino acids in the loop than AtPRORP2/3. These loop differences might explain the variations in 5' end discrimination observed previously, in which AtPRORP2/3 had a stronger propensity to miscleave at the N_{-1} position when an N_{-1}/N_{73} base pair was possible [26, 28].

The elbow region of tRNAs are highly structured and numerous tRNA binding enzymes recognize this part of the tRNA using a variety of interaction motifs [53]. Importantly, our model predicts that: (i) R210 (R145 in AtPRORP2) and R212 (R147 in PRORP2) contact TψC stem phosphodiester bonds; (ii) Asp 105 (N38 in PRORP2), N136 (Q70 in PRORP2), and N175 (N108 in PRORP2) are positioned to hydrogen bond with bases of the D loop (first residue) or the TψC (last two nucleotides) loop respectively; and (iii) Y140 (Y74 in PRORP2) is capable of both base stacking and hydrogen bonding with bases of the TψC loop. Although our proposed model needs to be further tested, it provides insight into the details of precursor tRNA binding of PRORPs in the absence of crystal structures of PRORP-tRNA complexes and a rough framework for the design of future experiments.

Conclusions

The data we present herein support a novel model for PRORP-pre-tRNA recognition that shares similarities with the mode of substrate recognition by the RNase P ribozyme. The salt-dependence of PRORP-substrate binding parses the ionic and non-ionic contributions to PRORP-substrate binding affinity. The data reveal that AtPRORPs make at least four contacts with pre-tRNA phosphodiester bonds. Only one of these is contained in the leader sequence, most likely at the N_{-2}/N_{-1} phosphodiester bond.

Additionally, we identified an extended surface on the PPR domains of AtPRORP1 and AtPRORP2 that interacts with substrate. Mutations on this surface suggested a mode of binding different from that of sequence specific ssRNA-binding PPR proteins. The biochemical and modeling data we have presented will facilitate the development of additional hypotheses for single-subunit PRORP substrate recognition. Given that metazoan PRORPs require two additional proteins for catalysis, there are likely differences that will need to be determined.

Materials and methods

Reagents

A full list of reagents used in this manuscript is detailed in the Supporting Information.

Enzyme preparation. Variants of Δ76 AtPRORP1 and full length AtPRORP2 were generated by site directed mutagenesis [54]. Sequences were verified at the University of Michigan DNA Sequencing Core facility. Variants were expressed in Rosetta™, Rosetta 2™ or BL21(DE3) E. coli (Novagen/EMD Millipore) from the T7 promoter on a pETM-11 (encoding His_6-TEV-AtPRORP1) or pMCSG7 (His_6-TEV-AtPRORP2) vector in LB media with 50 μg/mL kanamycin and 33 μg/mL chloramphenicol for selection of pETM-11 and pRARE (a plasmid encoding rare-codon tRNAs in the Rosetta cell lines) or 100 μg/mL ampicillin for selection of pMCSG7. Wild type Δ76 AtPRORP1 and full length

AtPRORP2 and variants of these enzymes were purified as described previously [16, 19, 21].

Substrate preparation. Substrates were prepared as described previously [16, 19]. Briefly, substrates were synthesized by run-off transcription from restriction-digested plasmid encoding pre-tRNA, a PCR-amplified template DNA, or a commercially synthetized ultramer oligo (IDT) [55]. *In vitro* transcription was carried out in the presence of 5'-O-monophosphorothioate guanosine (GMPS) in 5:1 excess of GTP. The pre-tRNA containing a 5'-GMPS was reacted with 5-iodoacetamidofluorescein (5-IAF) to generate a 5'-fluorescein label. The pre-tRNA product was gel purified using 12% urea-PAGE and substrate was eluted from the gel using the crush-soak method [55]. The purified pre-tRNAs were washed and concentrated using 10 kDa MWCO Amicon® Ultra Centrifugal Filters, then ethanol precipitated. Substrate stocks were resuspended in 10 mM tris(hydroxymethyl)aminomethane (Tris) pH 8.0 with 1 mM EDTA, quantified by absorbance and stored at –20 or –80°C. The extinction coefficients at 260 nm for total RNA concentration are: 685000 M^{-1} cm^{-1} for Bacillus subtilis pre-tRNA^{Asp} (experimentally determined by alkaline hydrolysis), 674390 M^{-1} cm^{-1} for A. thaliana mitochondrial pre-tRNA^{Cys} (experimentally determined by alkaline hydrolysis), and 870700 M^{-1} cm^{-1} for A. thaliana nuclear pre-tRNA^{Gly} (calculated). The fluorescein concentration was measured at 492 nm (extinction coefficient = 78000 M^{-1} cm^{-1}). Variants of pre-tRNA^{Asp} were generated by site-directed mutagenesis [54]. Immediately before initiating an assay, substrates were thawed, diluted with H_2O, and heated at 95°C

for 60–90 seconds. Substrates were re-folded by cooling to 25°C for ≥ 10 min, then incubating with buffer (as specified for each assay) for ≥ 10 min.

Anisotropy binding assays. Thermodynamic binding assays were performed in a 96-well plate format as previously described [16, 19]. Briefly, WT AtPRORP1 was serially diluted and mixed 1:1 with a concentration of pre-folded pre-tRNA containing a 5-fluorescein. In all experiments, the maximum enzyme concentration ([P]) was at least three times greater than the K_D and the pre-tRNA concentration at least five times lower than the K_D. In all cases, the data were well-described by a hyperbolic binding curve (Equation 1). Reactions were incubated at 28 ± 1°C in 30 mM MOPS pH 7.8, and 1 mM TCEP (AtPRORP1) or 1 mM DTT (AtPRORP2). The NaCl concentration was varied between 0.025–1.0 M. Unless otherwise specified, assays contained 20 or 6 mM $CaCl_2$ for AtPRORP1 and AtPRORP2, respectively. The $CaCl_2$ concentrations were chosen to maintain the K_D values in the measurable range. For AtPRORP1, decreasing the $CaCl_2$ concentration to 6 mM increased the K_D values (65%) but altered the slope of the Na^+-dependence < 10% (data not shown). When varying the Na^+ salt, we maintained constant Na^+ at 330 mM (see Supplemental Methods). Changes in anisotropy of the 5'-fluorescein-pre-tRNA was measured with a Tecan Ultra plate reader with polarizing filters using excitation and emission wavelengths of 485 and 535 nm, respectively. Readings were taken 3–5 times over the course of 15–20 minutes to ensure that the reading was stable.

$$FA = FA_0 + \frac{\Delta FA \bullet [P]}{[P] + K_D} \quad (1)$$

Single-turnover assays. Single-turnover kinetic assays for AtPRORP1 were performed in a stopped-format as previously described [16, 19]. Briefly, enzyme was mixed with pre-folded B. subtilis pre-$tRNA^{Asp}$ with a 5-nt leader and a 5'-fluorescein to final concentrations of 5 μM and 30 nM, respectively. For R184A assays, 30 nM substrate was incubated with 1–50 μM enzyme. Reactions were incubated at 25°C in 30 mM MOPS pH 7.8, 1 mM TCEP, with $MgCl_2$ and NaCl varied as indicated for a given assay. Aliquots were removed at various times and mixed 1:1 with a 2x quench dye (6 M urea (MP Biochemicals), 100 mM EDTA (Acros Organics), 0.1% bromophenol blue (BPB; Fisher Scientific), 0.1% xylene cyanol (XC; United States Biochemical Corporation), and 2 μg/μL bulk yeast tRNA (Fisher Scientific)). Products were resolved from substrate by fractionation on a ≥ 20% urea-PAGE and the gels were scanned using a Typhoon 9410 (GE Life Sciences) in fluorescence mode with a 532 nm green laser and fluorescein emission filter. Assays for AtPRORP2 were carried out using the same conditions, but changes in polarization upon cleavage were detected by ClarioStar (BMG Labtech) in 96-well plate format. The observed rate constants (k_{obs}) were determined by quantifying the fraction product using ImageQuant 5.2 software and fitting a single exponential (Equation 2, where A is the endpoint, B is the amplitude, and t is the time) to the data using KaleidaGraph 4.0 software. At low concentrations of NaCl (below ≈ 90 mM), the 5' leader product degraded after it appeared and did not accumulate to 100%. A double exponential was fit to these data and the k_{obs} from the phase with increasing product is reported. The IC_{50} for inhibition of AtPRORP1 by NaCl was determined by fitting Equation 3 to the dependence of the STO k_{obs} on the NaCl concentration (as described in the Results section).

$$\text{Fraction Product} = A - B(e^{-k_{obs} * t}) \quad (2)$$

$$k_{obs} = \frac{k_{max}}{\left(1 + \left(\frac{[Na^+]}{IC_{50}}\right)^n\right)} \quad (3)$$

Sodium dependence. Equation 4 is an approximation of Equation S1 (shown in the supporting methods) that describes the dependence of the affinity on cations when effects from pH, anions, and divalent ions are negligible or can otherwise be precluded by maintaining constant pH and divalent ions and observing the log-linear region of the decreasing affinity. The dependent variable is the monovalent cation concentration ($[M^+]$). The parameters include a "standard affinity" at 1 M M^+ (K_0), the apparent number of phosphodiester bonds on the substrate interacting with the protein (Z), and the fraction of phosphodiester bonds in the nucleic acid that thermodynamically associate with a monovalent ion (φ). When divalent cations are varied in the absence of monovalent ions, the slope is distinguished by replacing φ with ϕ. Standard affinity values were converted to energetic values using Gibbs free energy definitions and assuming equilibrium conditions (Equation 5), for which R is the gas constant (1.987 cal K^{-1} mol^{-1}) and T is the temperature (300K for our assays).

$$-\log K_D = \log K_0 - Z\varphi \bullet \log[M^+] \quad (4)$$

$$\Delta G = -RT \ln K_0 \quad (5)$$

Model building. Crystal structures of AtPRORP1 (PDB ID: 4g23) and AtPRORP2 (PDB ID: 5diz) and yeast $tRNA^{Phe}$ (PDB ID: 1ehz) were used to model the elbow region of pre-tRNA bound to the proteins. Initial models were obtained using ZDOCK server [56] and

these were processed through iterative rounds of manual adjustment by PyMOL [57]. The model amino acid or nucleotide geometry regularization and use of allowed side chain rotomers were corrected with Coot [58]. The coordinates of these models are available upon request.

SUPPLEMENTAL INFORMATION

Supporting material is available for this article.

ACKNOWLEDGEMENTS

We thank Michael J. Howard for supplying the WT AtPRORP1 enzyme preparation. We thank David R. Engelke for helpful discussions and Nancy Wu for helpful comments on this manuscript. This work was supported in part by the National Institutes of Health (R01 GM055387 to C.A.F. and R01 GM117141 to M.K.); the Endowment for the Basic Sciences – Endowment for the Development of Graduate Education (EBS–EDGE) Award to B.P.K. and by American Heart Association pre-doctoral fellowship (16PRE29890011 to A.K.).

Tables

Table 1. Na^+-dependence of binding affinity.

Enzyme	Pre-tRNA Substrate	Leader	K_D (nM)[a]	Z[b]	–log(K_0)[b]	ΔG_0 (kcal/mol)[c]
*At*PRORP1	Asp	5-nt	155 ± 20	4.3 ± 0.3	5.0 ± 0.1	–6.9 ± 0.1
		1-nt	600 ± 50	3.7 ± 0.2	4.66 ± 0.06	–6.4 ± 0.1
		0-nt	25400 ± 6100	2.8 ± 0.5	3.5 ± 0.2	–4.8 ± 0.3
	Cys	5-nt	1330 ± 120	3.7 ± 0.5	4.4 ± 0.2	–6.0 ± 0.3
*At*PRORP2	Asp	5-nt	80 ± 9	4.4 ± 0.6	5.0 ± 0.3	–6.9 ± 0.4
		0-nt	17200 ± 1100	3.2 ± 0.3	3.5 ± 0.2	–4.8 ± 0.3
	Gly	6-nt	470 ± 50	5.0 ± 0.5	4.3 ± 0.2	–5.9 ± 0.3

a: Value and error reported are from fitting a hyperbola to the results of two independent experiments in 330 mM NaCl plotted together.
b: Value and error from fitting Equation 4 to the data from Figures 2C and 4 using φ^{Na}= 0.88, as described in the Materials and Methods.
c: Calculated using $\Delta G_0 = -RT \times \ln K_0$.

Table 2. Na^+-dependence of *At*PRORP1 variants affinity for *B. subtilis* pre-$tRNA^{Asp}$.

***At*PRORP2 residue**[a]	***At*PRORP1 Variant**	K_D **(nM)**[b]	**Fold-WT**	Z[c]	**–log(K_0)**[c]	**ΔG_0 (kcal/mol)**[d]
–	WT	155 ± 20	1.0	4.3 ± 0.3	5.0 ± 0.1	–6.9 ± 0.1
Q67	Y133A	2600 ± 200	17	4.4 ± 0.3	3.8 ± 0.2	–5.2 ± 0.3
	Y133F	4600 ± 300	30	4.2 ± 0.2	3.7 ± 0.1	–5.1 ± 0.1
Q70	N136A	980 ± 180	6.3	3.9 ± 0.2	4.3 ± 0.1	–6.0 ± 0.1
Y74	Y140A	29700 ± 7000	192	4.2 ± 0.4	3.0 ± 0.3	–4.1 ± 0.4
	Y140F	1000 ± 200	6.5	4.1 ± 0.6	4.3 ± 0.3	–5.9 ± 0.4
N108	N175A	1400 ± 400	9.0	3.8 ± 0.2	4.4 ± 0.2	–5.9 ± 0.3
T113	T180A	3300 ± 1500	22	4.0 ± 0.2	3.8 ± 0.1	–5.2 ± 0.1
	T180S	1700 ± 300	11	4.6 ± 0.4	3.9 ± 0.2	–5.4 ± 0.3
R117	R184A	10400 ± 2400	67	4.5 ± 0.5	3.2 ± 0.3	–4.4 ± 0.3
	R184K	1900 ± 300	12	4.6 ± 0.5	4.0 ± 0.3	–5.5 ± 0.4
R147	R212A[e]	> 30000	> 194	ND[f]	ND	ND

a: Amino acid in *At*PRORP2 that is in the homologous position to the side chain in *At*PRORP1.
b: Value and error reported are from fitting a hyperbola to the results of two independent experiments in 330 mM NaCl plotted together.
c: Value and error from fitting Equation 4 to the log-log plot of the Na^+-dependence data using φ^{Na} = 0.88 as described in the Materials and Methods.
d: Calculated using $\Delta G_0 = -RT \times \ln K_0$.
e: Affinity for the R212A mutant was not measurable; little change in anisotropy was observed at 25 μM *At*PRORP1 (Figure S3B).
f: Not determined (ND).

Figures

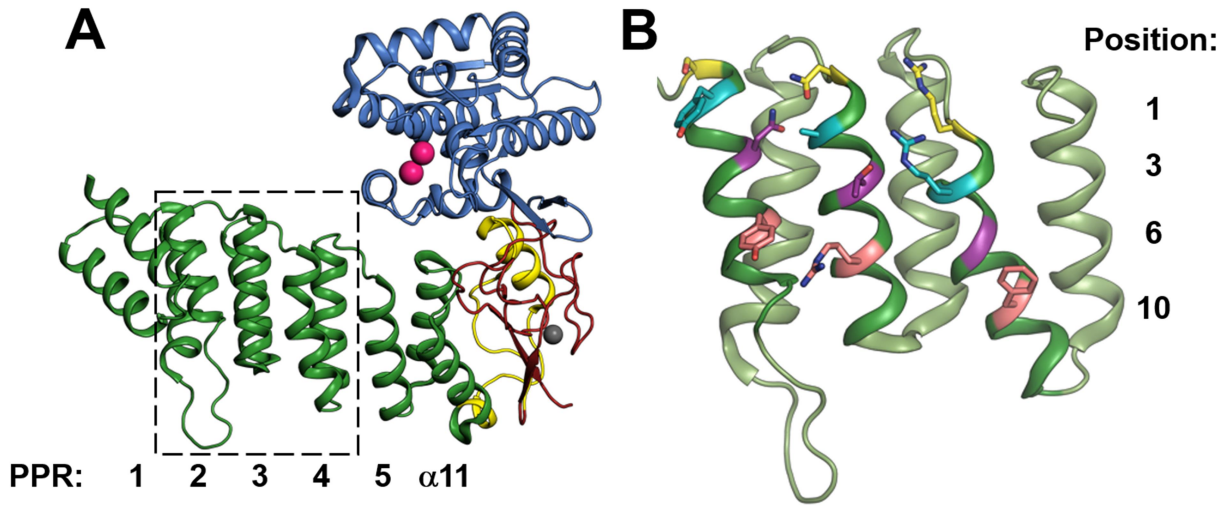


Figure 1. Structure of *Arabidopsis thaliana* PRORP1 (PDB 4g24), generated in PyMOL [57].
(**A**) Overall architecture of *At*PRORP1. PPR motifs are in green and numbered from the N-terminal end, a plant-specific helical insertion in yellow (α12–13), central domain in red, and NYN domain in blue. Mn^{2+} ions displayed as pink spheres and Zn^{2+} ion displayed as a gray sphere. The region marked by the dashed box is expanded in panel B. (**B**) *At*PRORP1 PPR domain motifs 2–4, generated in PyMOL. For each PPR motif, position 1 is colored yellow, position 3 is colored cyan, position 6 is colored purple, and position 10 is colored pink.

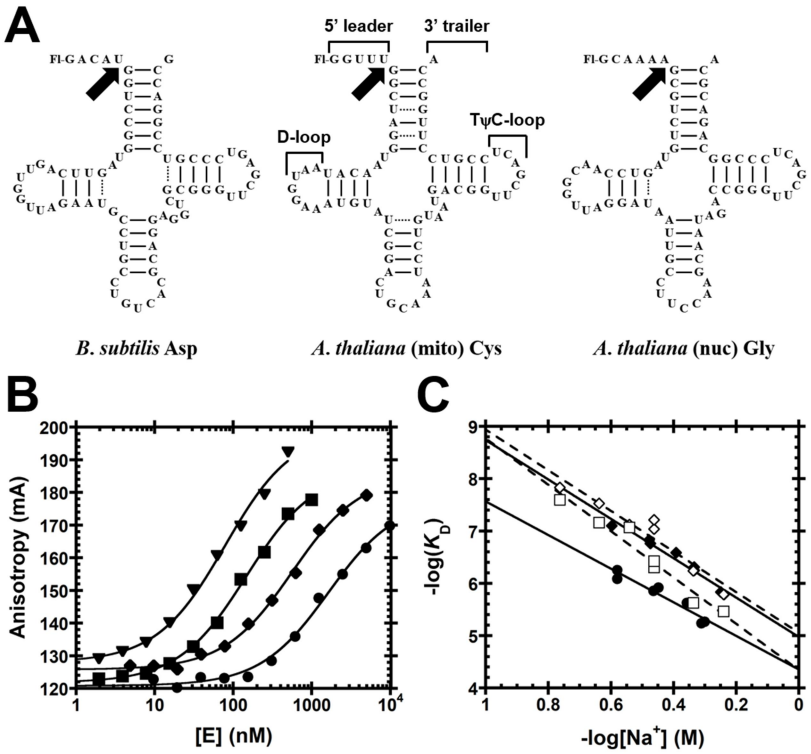


Figure 2. Substrates used for functional assays.

(**A**) Substrates containing a 5'-fluorescein label include pre-tRNA^{Asp} from *Bacillus subtilis* and *Arabidopsis thaliana* pre-tRNA^{Cys} and pre-tRNA^{Gly} from the mitochondrial and nuclear genomes, respectively. Structural features of pre-tRNA are detailed on pre-tRNA^{Cys}, including the 5' leader, 3' trailer, and the D- and TψC-loops. Black arrows indicate canonical RNase P cleavage site. (**B**) Fluorescence anisotropy binding curves for *At*PRORP1 binding to *B. subtilis* pre-tRNA^{Asp} (log scale). A hyperbola (Equation 1, Materials and Methods) was fit to the data. Data were measured in 30 mM MOPS pH 7.8, 1 mM TCEP, and 20 mM $CaCl_2$ with 250 mM (▼), 330 mM (■), 450 mM (♦), and 550 mM NaCl (●). (**C**) Na^+-dependence of *At*PRORP affinity. Equation 4 (Materials and Methods) was fit to the data. The slope of the line (Z) reports on the apparent number of ionic interactions with substrate phosphodiester bonds, while the intercept [$-\log(K_0)$] reports on the non-ionic contributions to affinity. Data include *At*PRORP1 binding to pre-tRNA^{Asp} (♦) and pre-tRNA^{Cys} (●) in 20 mM Ca^{2+}, as well as *At*PRORP2 in 6 mM Ca^{2+} binding to pre-tRNA^{Asp} (◊) and pre-tRNA^{Gly} (□).

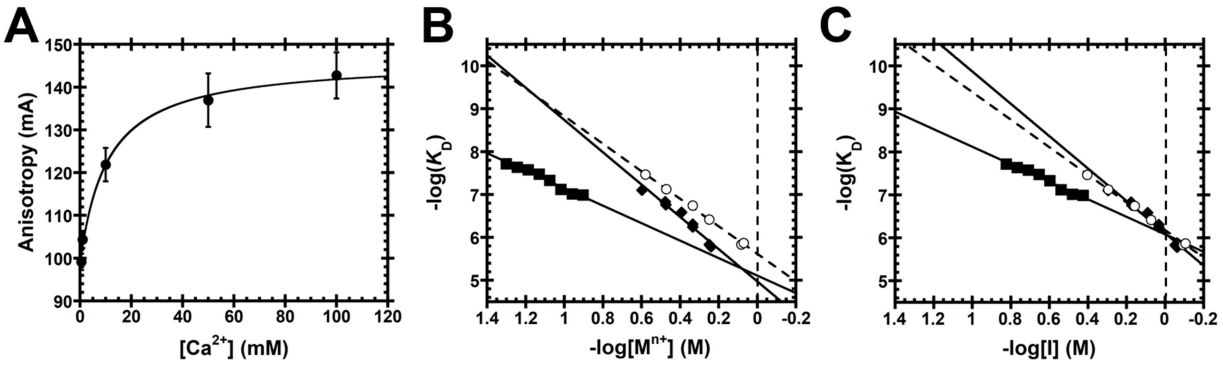


Figure 3: Cation (M^{n+}) dependence of dissociation constants for *At*PRORP1 binding to *B. subtilis* fluorescein-labeled pre-$tRNA^{Asp}$.
(**A**) Anisotropy of *Bacillus subtilis* pre-$tRNA^{Asp}$ in the absence of PRORP is dependent on $CaCl_2$ concentration. Data reported as the mean and standard deviation of four independent experiments. A hyperbola (Equation 1, Materials and Methods) was fit to the data ($K_{D,app}$ = 11 ± 3 mM). (**B**) Equation 4 (Materials and Methods) was fit to the data with the dsDNA φ^{Na} = 0.88 or ϕ^{Mg} = 0.47. Data include the dependence of *At*PRORP1 affinity on: NaCl (♦, Z = 4.3 ± 0.3, –log(K_0) = 5.0 ± 0.1), Na_2SO_4 (○, Z = 3.6 ± 0.1, –log(K_0) = 5.62 ± 0.03), and $CaCl_2$ (■, Z = 4.3 ± 0.3, –log(K_0) = 5.1 ± 0.2). The slope of the line ($Z\varphi$ or $Z\phi$) reports on the apparent number of ionic interactions made to substrate phosphodiester bonds, while the intercept [–log(K_0)] reports on the non-ionic contributions to affinity. (**C**) Ionic strength (I) dependence of *At*PRORP1 binding to pre-$tRNA^{Asp}$, plotted as the –log(K_D) versus –log[I]. Equation 4 (Materials and Methods) was fit to the data with φ^{Na} = 0.88 or ϕ^{Ca} = 0.47. Data include *At*PRORP1 binding in NaCl (♦; –log(K_0) = 6.11 ± 0.04), Na_2SO_4 (○; –log(K_0) = 6.18 ± 0.02), and $CaCl_2$ (■; –log(K_0) = 6.08 ± 0.09).

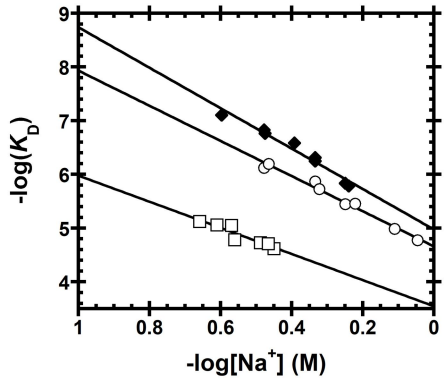


Figure 4. Sodium dependence of *At*PRORP1 affinity for substrates with varied leader lengths.

Data include *At*PRORP1 binding to 5' fluorescein-labeled substrates, including: 5-nt pre-tRNA^{Asp} (♦, $Z = 4.3 \pm 0.3$, $-\log(K_0) = 5.0 \pm 0.1$), 1-nt pre-tRNA^{Asp} (○, $Z = 3.7 \pm 0.2$, $-\log(K_0) = 4.7 \pm 0.1$), and tRNA^{Asp} (□, $Z = 2.8 \pm 0.5$, $-\log(K_0) = 3.5 \pm 0.2$). Equation 4 (Materials and Methods) was fit to the data. The slope of the line (Z) reports on the apparent number of ionic interactions made to substrate phosphodiester bonds, while the intercept [$-\log(K_0)$] reports on the non-ionic contributions to affinity.

Figure 5

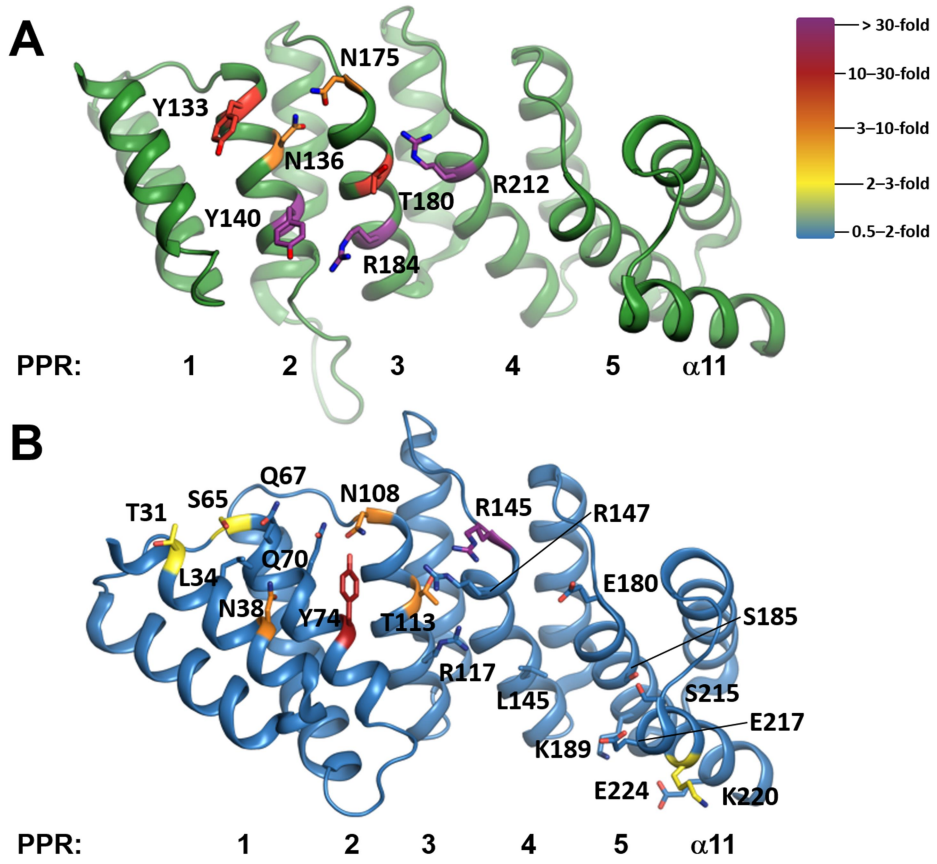


Figure 5: Residues selected for mutation in the PPRs of *At*PRORPs, generated in PyMOL [57].
(**A**) *At*PRORP1 (PDB 4g24) PPRs are numbered left (PPR1) to right (helix α11). Residues that were targeted for mutation are numbered. Carbon atoms are color-coded by the largest effect on binding as indicated by the color ramp. (**B**) *At*PRORP2 (PDB 5diz) PPRs are numbered left (PPR1) to right (helix α11). Residues that were targeted for mutation are numbered. Carbon atoms are color-coded as in **A**. Alanine mutants were not soluble for Q70, R117, and R147, so no data were collected for these variants.

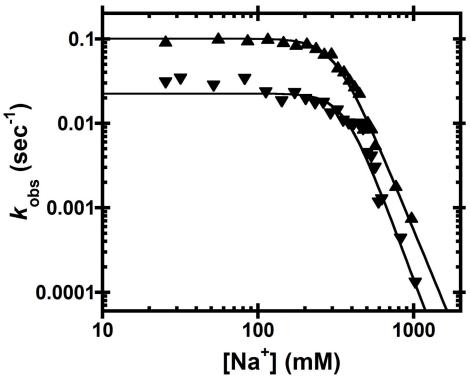


Figure 6. Na^+-dependence of *At*PRORP1 cleavage activity.
The dependence of the *At*PRORP1-catalyzed cleavage of fluorescein-labeled pre-$tRNA^{Asp}$ on the [NaCl] was measured under single turnover conditions (k_{obs}). Data include *At*PRORP1-catalyzed cleavage in 20 mM (▲) or 1.25 mM (▼) $MgCl_2$. Equation 3 (Materials and Methods, weighted fit) was fit to the data. For 20 mM $MgCl_2$, IC_{50} = 310 ± 70, n^{Na} = 4.5 ± 1.3. For 1.25 mM $MgCl_2$, IC_{50} = 360 ± 70, n^{Na} = 5.0 ± 1.3.

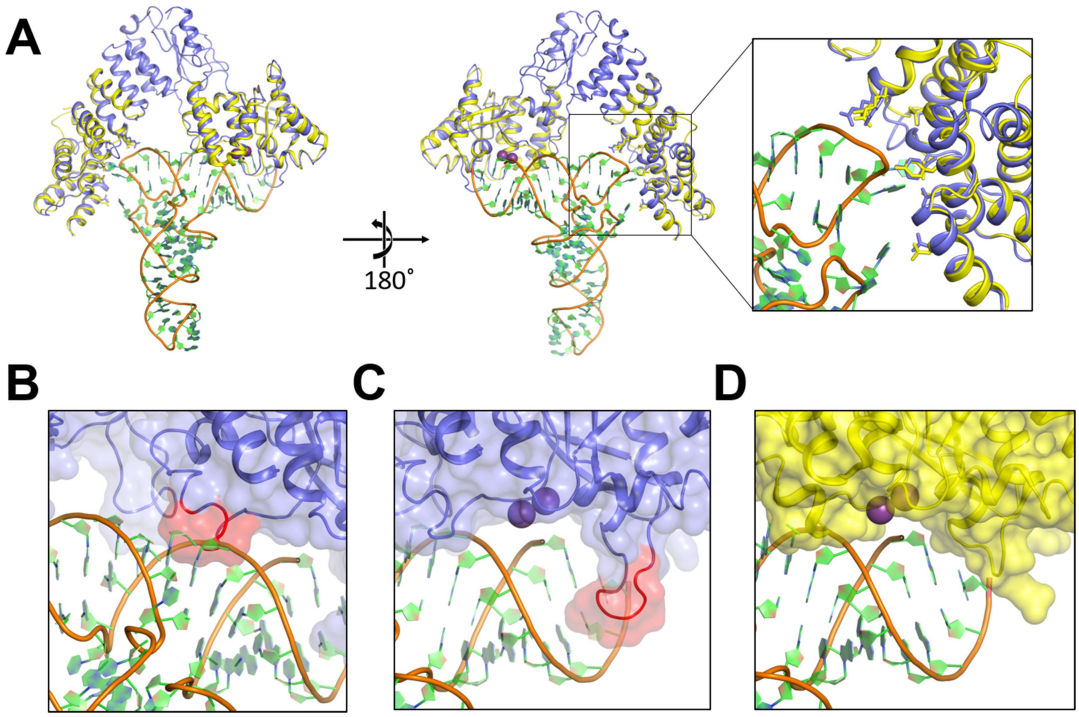


Figure 7: Model of the PRORP-substrate complex.
(**A**) Overall view of the modeled complex. *At*PRORP2 (PDB 5diz, blue) is bound to tRNA (PDB 1ehz, orange backbone with green and blue rings). The *At*PRORP1 (PDB 4g24, yellow) NYN and PPR domains are aligned to the corresponding residues domains in *At*PRORP2. Purple spheres are the Mn^{2+} ions bound to the *At*PRORP1 active site. Close-up view of the PPR domain highlights the positions of residues for which mutation affected binding affinity (> 3-fold), including D105/N38, N136/Q70, Y140/Y74, N175/N108, T180/T113, R210/R145, and R212/R147 in *At*PRORP1/*At*PRORP2, respectively. (**B**) Close-up of the *At*PRORP2-tRNA complex with a potential steric clash between NYN helix α21 (red) and the 3' side of the tRNA acceptor stem. (**C–D**) Close-up of the *At*PRORP2- (C) or *At*PRORP1-substrate complex (D) showing the NYN active site. The loop for which *At*PRORP2–3 have a 4 residue insertion is highlighted in red (C). In both structures, the 5' leader of pre-tRNA would extend forward from the panel, while the 3' trailer would extend behind the NYN domain.

Supplemental Methods

Reagents. Reagents used in this manuscript include 3-morpholinopropane-1-sulfonic acid (MOPS; Acros Organics), tris (2-carboxyethyl)phosphine (TCEP; Gold Biotechnology, Inc.), 1,4-dithio-D-threitol (DTT; Gold Biotechnology, Inc.) 5-iodoacetamidofluorescein (5-IAF; Life Technologies), ethylenediaminetetraacetic acid (EDTA; Acros Organics), tris(hydroxymethyl)aminomethane (Tris; Fisher Scientific), magnesium chloride ($MgCl_2$; Fisher Scientific), calcium chloride ($CaCl_2$; Sigma-Aldrich), sodium chloride (NaCl; Sigma-Aldrich), sodium acetate (NaAc; Fisher Scientific), sodium bromide (NaBr; Sigma-Aldrich), sodium iodide (NaI; Sigma-Aldrich), sodium nitrate ($NaNO_3$; Sigma-Aldrich), sodium sulfate (Na_2SO_4; Fisher Scientific), 5'-O-monophosphorothioate guanosine (GMPS, synthesized), nucleoside triphosphates (NTPs; Sigma-Aldrich), kanamycin (Acros Organics), chloramphenicol (Acros Organics), urea (MP Biochemicals), bromophenol blue (BPB; Fisher Scientific), xylene cyanol (XC; United States Biochemical Corporation), SYPRO® Orange Protein Gel Stain (Invitrogen), bulk yeast tRNA (Fisher Scientific), and the SequaGel UreaGel system (National Diagnostics).

Protein-nucleic acid interactions. Equation S1 was adapted from Equation 18 of deHaseth, *et al*. 1977 and describes the effects of solution ions on the binding affinity between proteins and nucleic acids [33]. Variables potentially affecting the measured affinity include pH ($K_H[H^+]$), anion concentration ($K_X[X^-]$), monovalent cation concentration ($[M^+]$), and divalent cation concentration ($[S]/[S_0]$). Parameters include a "standard affinity" under 1 M M^+ (K_0), the number of proton donating groups on the protein directly interacting with substrate phosphates (r), the number of specifically-occupied anion binding sites on the protein (a), the number of phosphates on the substrate

directly interacting with the protein (Z), the fraction of phosphates in the nucleic acid that thermodynamically associate with a monovalent ion (φ), and the competition of M^+ with M^{2+} for occupancy on backbone phosphates given by the total concentration of nucleotides [S] and the concentration of nucleotides that are bound as they would with no M^{2+} in solution [S_0]. The term [S]/[S_0] is described by Equation S2.

$$-log\, K_{\mathrm{D}} = log\, K_0 - r \bullet log\left(\frac{1+K_H[H^+]}{K_H[H^+]}\right) - a \bullet log(1 + K_X[X^-]) - Z\varphi \bullet log[M^+] - Z \bullet log\left(\frac{[S]}{[S_0]}\right) \quad \text{(S1)}$$

$$\frac{[S]}{[S_0]} = \frac{1}{2}\left(1 + \sqrt{1 + 4K_A^M[M^{2+}]}\right) \quad \text{(S2)}$$

Anion variation. Binding affinity was measured in various sodium salts at 330 mM Na^+ (Table S1). Binding affinity was also measured with varying $CaCl_2$ (alone) and Na_2SO_4. The pre-tRNA^{Asp} anisotropy in the absence of PRORP and Na^+ displays a hyperbolic dependence on $CaCl_2$ ($K_{D,app}$ = 11 ± 3 mM, Figure 3A). This behavior is likely due to stabilization of the tRNA structure upon addition of divalent cations [59], as the 5'-fluorescein likely has less rotational freedom when the tRNA structure is compact [60]. The anisotropy of free pre-tRNA increased less than 20% above 50 mM Ca^{2+}, so $CaCl_2$ was varied from 50 to 125 mM.

Thermofluor assays. Melting curves for each variant at 5 μM enzyme were measured in 30 mM MOPS, pH 7.8, 150 mM NaCl, and 1 mM TCEP, with 20X SYPRO® Orange. Fluorescence intensity (I) was monitored using λ_{Ex} = 485 nm and λ_{Em} = 625 nm. The melting temperature (T_m) was determined by fitting equation S3 was fit to the data to the maximum intensity, as previously described [61], for which A is the initial intensity, B is the maximum intensity, T is the temperature in Celsius, and C is a slope factor.

$$I = \left(A + \frac{(B-A)}{\left(1+e^{(Tm-T)/C}\right)}\right) \qquad \text{(S3)}$$

Circular dichroism assays. Far UV-CD spectra are presented as the average of 5 accumulations for 10 µM enzyme measured at 25°C in 10 mM phosphate buffer, pH 7.2. The CD measurements were carried out on a Jasco J-815 spectropolarimeter equipped with a circulating water bath and peltier temperature controller. Spectra were converted to mean molar residue ellipticity (θ) using equation S4 as previously described [62], for which M_r is the mean molar mass per residue, l is the path-length, and c is the protein concentration. Overall, the characteristic features of the far UV-CD of WT *At*PRORP2 were retained in Y74S, suggesting that there are no major conformational changes when compared to WT.

$$[\theta] = \frac{\theta \bullet M_r}{10 \bullet l \bullet c} \qquad \text{(S4)}$$

Supplemental Tables

Table S1. Effects of anion identity on affinity for pre-tRNA^{Asp}.

Na^+ Salt[a]	K_D (nM)[b]	Lyotropic series
Ac^-	32 ± 7	More kosmotropic
SO_4^{2-}	70 ± 10	
Cl^-	155 ± 20	
Br^-	450 ± 160	
NO_3^-	490 ± 60	
I^-	2900 ± 500	More chaotropic

a: Supplied as the sodium salt at 330 mM Na^+.
b: Value and error reported are from fitting a hyperbola to the results of two independent experiments plotted together.

Table S2. Effects of mutation to *At*PRORP2 PPRs on affinity for pre-tRNA.

*At*PRORP1 Residue	*At*PRORP2 Residue	Position (PPR / Residue)	pre-tRNA^{Gly}		pre-tRNA^{Asp}	Highest Fold-WT
			K_D (nM)[a,b]	K_D (nM)[a,c]	K_D (nM)[a,b]	
–	WT	–	58 ± 8	260 ± 30	24 ± 5	1.0
A98	T31A	1 / 3	60 ± 8	530 ± 50		2.0
K101	L34A	1 / 6	28 ± 6	170 ± 10		0.7
D105	N38A	1 / 10	160 ± 40	1410 ± 150	70 ± 20	5.4
S131	S65A	2 / 1	100 ± 20	590 ± 80	35 ± 8	2.3
Y133	Q67A	2 / 3	70 ± 10	390 ± 70	30 ± 5	1.5
Y140	Y74S	2 / 10	1340 ± 170		110 ± 30	23
	Y74F		170 ± 20		45 ± 9	2.9
N175	N108A	3 / 1	190 ± 30	720 ± 50	70 ± 20	3.3
T180	T113A	3 / 6	70 ± 20	900 ± 130	30 ± 3	3.5
R210	R145A[d]	4 / 1	> 2000			> 34
F119	L154A	4 / 10	60 ± 10	230 ± 20		1.0
E245	E180A	5 / 1	35 ± 4	150 ± 20		0.6
A250	S185A	5 / 6	40 ± 6	350 ± 40		1.3
K254	K189A	5 / 10	52 ± 9	350 ± 30		1.3
S280	S215A	α11 / 1	66 ± 21	360 ± 60		1.4
S282	E217A	α11 / 3	56 ± 14	260 ± 20		1.0
D285	K220A	α11 / 6	129 ± 64	250 ± 40		2.2
E289	E224A	α11 / 10	55 ± 7	310 ± 35		1.2

a: Value and error reported are from fitting a hyperbola to the results of three independent experiments plotted together.
b: Measured in 30 mM MOPS pH 7.8, 1 mM DTT, 150 mM NaCl, and 6 mM $CaCl_2$.
c: Measured in 30 mM MOPS pH 7.8, 1 mM DTT, 330 mM NaCl, and 6 mM $CaCl_2$.
d: Low protein yield for R145A limited us to two binding assays, neither of which reached saturation up to 7500 nM. A lower limit for the K_D was estimated from the available data.

Table S3. Effects of *B. subtilis* pre-tRNA^{Asp} mutants on affinity for *At*PRORP1.

Variant	K_D (nM)[a]	Fold-WT
WT	155 ± 20	1.00
U16A	140 ± 20	0.90
U17A	100 ± 10	0.65
U20A	200 ± 10	1.29
U21A	300 ± 30	1.94

a: Value and error reported are from fitting a hyperbola to the results of two independent experiments in 330 mM NaCl plotted together.

Table S4. Effects of mutations on *At*PRORP1 affinity for pre-tRNA.

Variant	pre-tRNA^{Cys}				pre-tRNA^{Asp}	
	K_D (nM)[a]	Fold-WT	K_D (nM)[b]	Fold-WT	K_D (nM)[a]	Fold-WT
WT	200 ± 40	1	1720 ± 160	1	155 ± 20	1
Y140A[c]	150 ± 20	0.75	>160000	>93	29700 ± 7000	192
R184A	170 ± 40	0.85	>6500	>3.8	10400 ± 2400	67

a: Value and error reported are from fitting a hyperbola to the results of two independent experiments plotted together in 30 mM MOPS pH 7.8, 1 mM TCEP, 100 mM NaCl, and 1 mM $CaCl_2$.
b: Value and error reported are from fitting a hyperbola to the results of two independent experiments plotted together in 30 mM MOPS pH 7.8, 1 mM TCEP, 330 mM NaCl, 20 mM $CaCl_2$.
c: We could not reach saturating enzyme conditions for Y140A binding to pre-tRNA^{Cys} in 330 mM NaCl and 20 mM $CaCl_2$. A lower limit for K_D was estimated from the available data, assuming the saturating anisotropy was the same as for WT.

Supplemental Figures

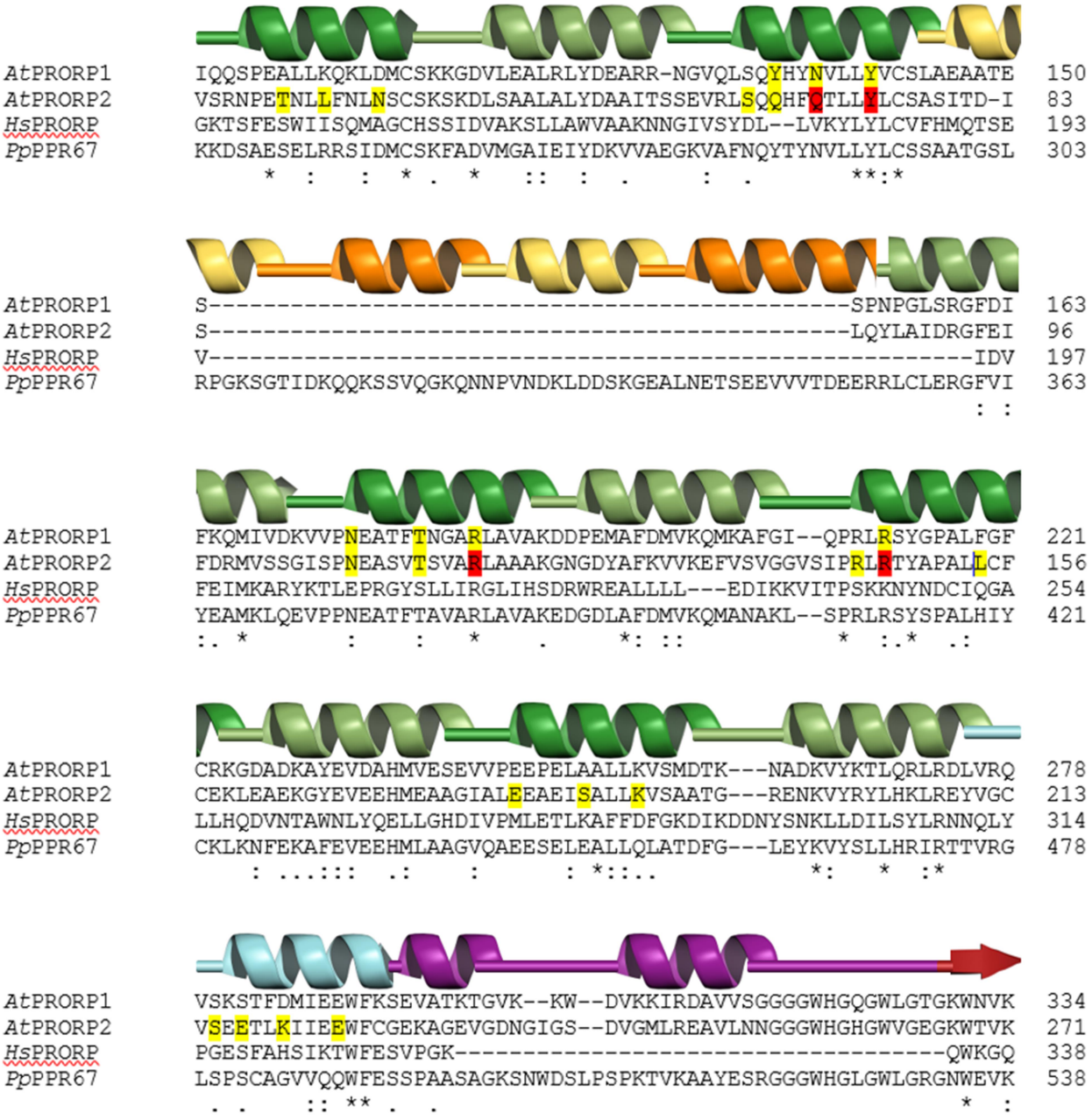


Figure S1. Alignment of PRORP PPR domains (Clustal Omega) [63, 64].
The three *Arabidopsis thaliana* PRORPs (*At*PRORP1-3) were aligned to the human PRORP (*Hs*PRORP) and PRORPs from the moss *Physcomitrella patens* (*Pp*PPR63, *Pp*PPR67, and *Pp*PPR104). For clarity, *At*PRORP3, *Pp*PPR67, and *Pp*PPR104 are excluded from the figure. The boundaries of additional PPR helices in *P. patens* PRORPs were assigned using models generated with *At*PRORP1 (PDB 4g23) and chloroplast PPR protein 10 (PDB 4m59) as templates in the SWISS-MODEL ExPASy server [65-68]. PPR A helices, which were

targeted for mutation, are colored *dark green*, while PPR B helices are colored *pale green*. Additional putative PPR A helices in *Pp*PPR67 are colored *orange*, while putative PPR B helices are colored *beige*. PPR helix 11 (numbered as in *At*PRORPs) is colored *cyan*, while a plant-specific helical insert is *purple* and the first β-strand of the central domain is *red*. *At*PRORP1 and *At*PRORP2 residues mutated in this manuscript are highlighted in yellow. *At*PRORP2 residues for which alanine mutants were insoluble are highlighted in red.

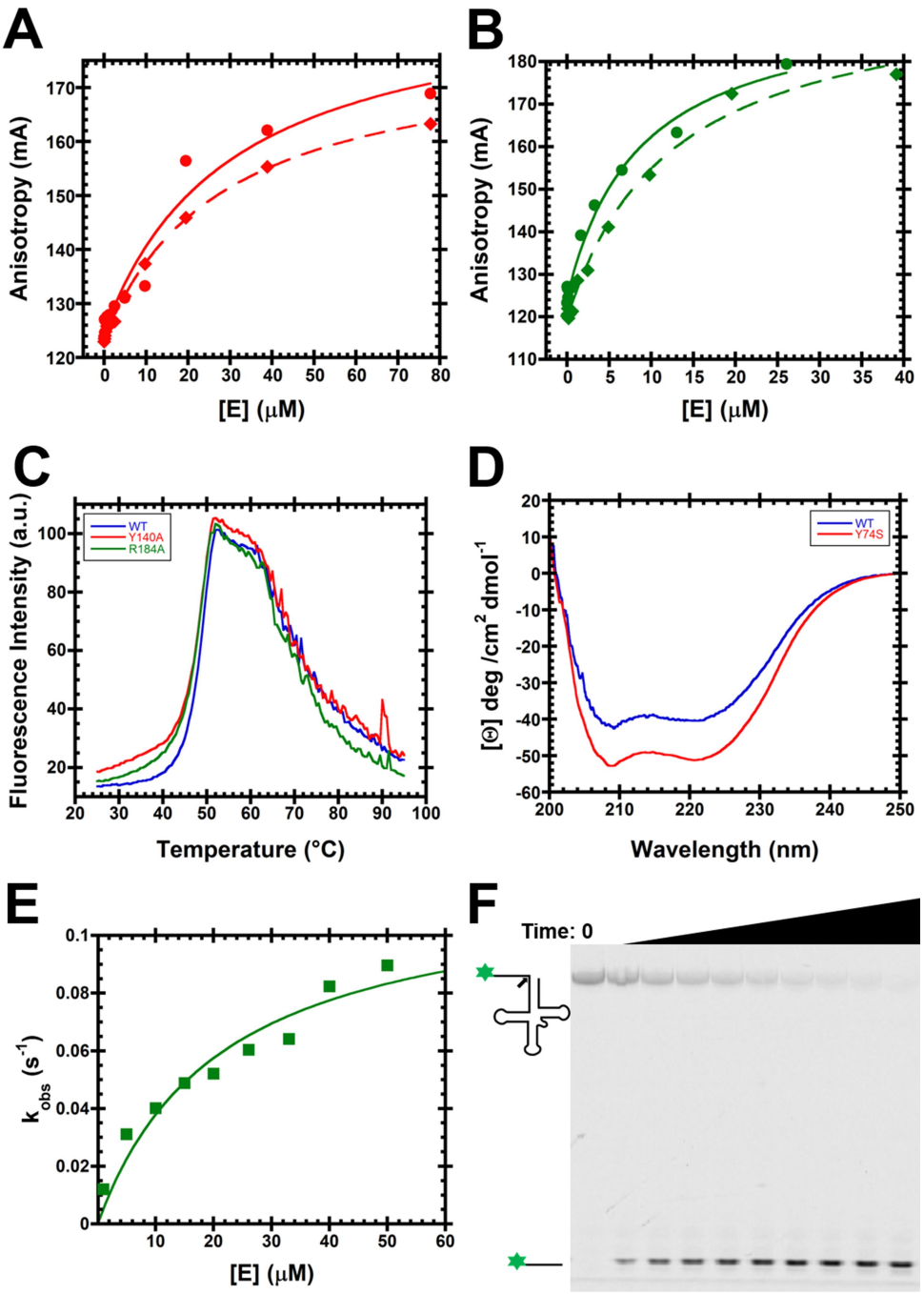


Figure S2. Stability of Y140A and R184A *At*PRORP1 or Y74S *At*PRORP2. (**A**) Binding curves for Y140A *At*PRORP1 collected at 330 mM NaCl, as described in the Materials and Methods. (**B**) Binding curves for R184A *At*PRORP1 collected at 330 mM NaCl, as described in the Materials and Methods. (**C**) Thermofluor melting curves for WT, Y140A, and R184A *At*PRORP1, collected and analyzed as described in the Supplemental Methods. The T_m values are 48.3 ± 0.1 (WT), 47.7 ± 0.2 (Y140A), and 47.4 ± 0.2 (R184A). (**D**) Circular dichroism data for WT and Y74S *At*PRORP2, collected and analyzed as described in the Supplemental Methods. (**E**) Single turnover

kinetic analysis of R184A *At*PRORP1 with *B. subtilis* pre-tRNA^{Asp}, collected at 25°C in 30 mM MOPS, pH 7.8, 150 mM NaCl, 20 mM $MgCl_2$, and 1 mM TCEP. Fitting a hyperbola to the data, we obtain $k_{max}^{E} = 0.12 \pm 0.01$ s^{-1} and $K_{1/2}^{E} = 21 \pm 7$ μM. The WT enzyme value under these conditions is ~ 0.1 s^{-1} [16]. (**F**) A representative gel from the experiments described in panel E, at 40 μM enzyme. Time points (left to right) are 0, 6 sec, 16 sec, 26 sec, 40 sec, 1 min, 2.5 min, 5 min, 10 min, and 30 min.

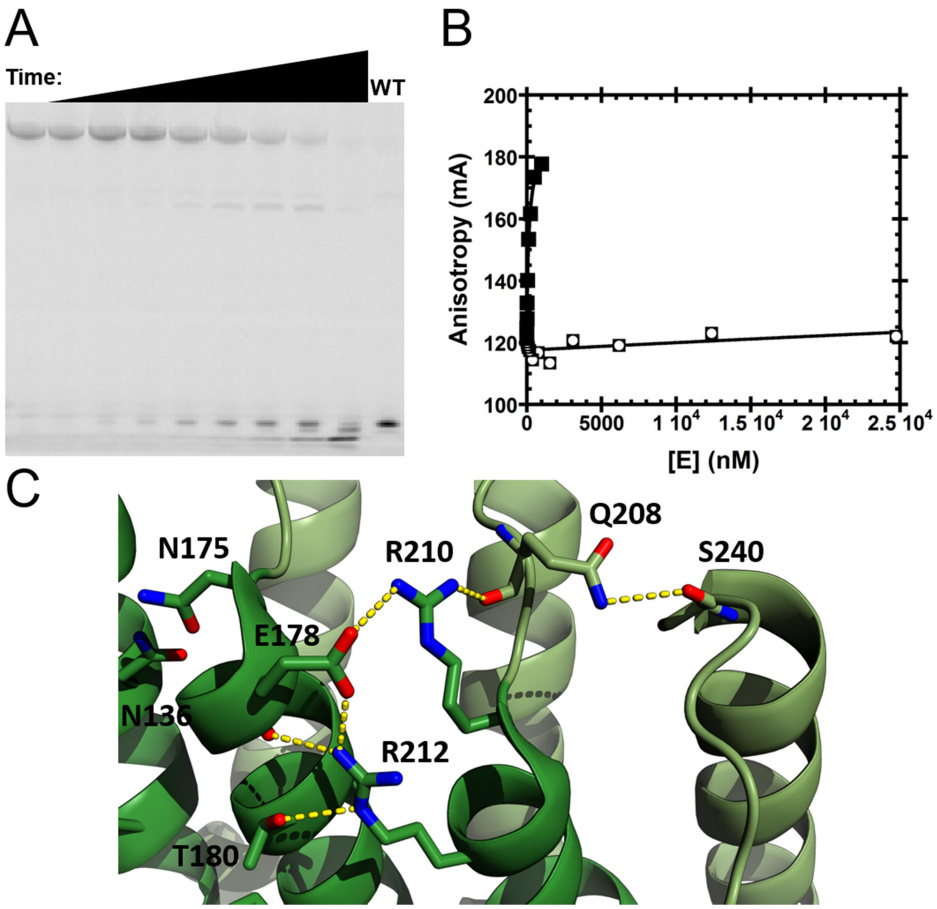


Figure S3. Defects in R212A *At*PRORP1 catalysis and substrate binding with *B. subtilis* pre-tRNA^{Asp}.

(**A**) Single turnover assay with 37 μM R212A and 30 nM substrate. Time points (left to right) are 0, 1 min, 5 min, 10 min, 30 min, 1 hr, 2 hr, 4 hr 20 min, and 20 hr 40 min. 5 μM WT enzyme at 30 minutes (at right) was included for comparison. (**B**) Anisotropy pre-tRNA^{Asp} binding to R212A (◘) or WT (■) *At*PRORP1. A hyperbola (Equation 1, Materials and Methods) was fit to the data ($K_{D,app}$ > 300000 nM; lower limit estimated assuming the change in anisotropy for fully-bound substrate is the same as WT). (**C**) Arg 212 in *At*PRORP1 takes part in an extended series of interactions involving both main chain and side chain atoms, beginning with Thr 180 (PPR 3 helix A) and terminating with Ser 240 (PPR 4 helix B). Generated in PyMOL (PDB 4g24) [57].

REFERENCES

1. Howard, M.J., et al., *RNase P enzymes: divergent scaffolds for a conserved biological reaction.* RNA Biol, 2013. **10**(6): p. 909-14.
2. Guerrier-Takada, C., et al., *The RNA moiety of ribonuclease P is the catalytic subunit of the enzyme.* Cell, 1983. **35**(3 Pt 2): p. 849-57.
3. Walker, S.C. and D.R. Engelke, *Ribonuclease P: the evolution of an ancient RNA enzyme.* Crit Rev Biochem Mol Biol, 2006. **41**(2): p. 77-102.
4. Marvin, M.C. and D.R. Engelke, *Broadening the mission of an RNA enzyme.* J Cell Biochem, 2009. **108**(6): p. 1244-51.
5. Kurz, J.C. and C.A. Fierke, *The affinity of magnesium binding sites in the Bacillus subtilis RNase P x pre-tRNA complex is enhanced by the protein subunit.* Biochemistry, 2002. **41**(30): p. 9545-58.
6. Kurz, J.C., S. Niranjanakumari, and C.A. Fierke, *Protein component of Bacillus subtilis RNase P specifically enhances the affinity for precursor-tRNAAsp.* Biochemistry, 1998. **37**(8): p. 2393-400.
7. Niranjanakumari, S., J.C. Kurz, and C.A. Fierke, *Expression, purification and characterization of the recombinant ribonuclease P protein component from Bacillus subtilis.* Nucleic Acids Res, 1998. **26**(13): p. 3090-6.
8. Crary, S.M., S. Niranjanakumari, and C.A. Fierke, *The protein component of Bacillus subtilis ribonuclease P increases catalytic efficiency by enhancing interactions with the 5' leader sequence of pre-tRNAAsp.* Biochemistry, 1998. **37**(26): p. 9409-16.
9. Holzmann, J., et al., *RNase P without RNA: identification and functional reconstitution of the human mitochondrial tRNA processing enzyme.* Cell, 2008. **135**(3): p. 462-74.
10. Gobert, A., et al., *A single Arabidopsis organellar protein has RNase P activity.* Nature Structural & Molecular Biology, 2010. **17**(6): p. 740-U113.
11. Lai, L.B., et al., *A functional RNase P protein subunit of bacterial origin in some eukaryotes.* Mol Genet Genomics, 2011. **286**(5-6): p. 359-69.
12. Taschner, A., et al., *Nuclear RNase P of Trypanosoma brucei: a single protein in place of the multicomponent RNA-protein complex.* Cell Rep, 2012. **2**(1): p. 19-25.
13. Vilardo, E., et al., *A subcomplex of human mitochondrial RNase P is a bifunctional methyltransferase--extensive moonlighting in mitochondrial tRNA biogenesis.* Nucleic Acids Res, 2012. **40**(22): p. 11583-93.
14. Gutmann, B., A. Gobert, and P. Giege, *PRORP proteins support RNase P activity in both organelles and the nucleus in Arabidopsis.* Genes & Development, 2012. **26**(10): p. 1022-1027.
15. Sugita, C., et al., *Molecular Characterization of Three PRORP Proteins in the Moss Physcomitrella patens: Nuclear PRORP Protein Is Not Essential for Moss Viability.* PLoS One, 2014. **9**(10): p. e108962.
16. Howard, M.J., B.P. Klemm, and C.A. Fierke, *Mechanistic Studies Reveal Similar Catalytic Strategies for Phosphodiester Bond Hydrolysis by Protein-only and RNA-dependent Ribonuclease P.* J Biol Chem, 2015. **290**(21): p. 13454-64.

17. Bonnard, G., et al., *Transfer RNA maturation in Chlamydomonas mitochondria, chloroplast and the nucleus by a single RNase P protein.* Plant J, 2016. **87**(3): p. 270-80.
18. Chen, Y., X. Li, and P. Gegenheimer, *Ribonuclease P catalysis requires Mg2+ coordinated to the pro-RP oxygen of the scissile bond.* Biochemistry, 1997. **36**(9): p. 2425-38.
19. Howard, M.J., et al., *Mitochondrial ribonuclease P structure provides insight into the evolution of catalytic strategies for precursor-tRNA 5 ' processing.* Proceedings of the National Academy of Sciences of the United States of America, 2012. **109**(40): p. 16149-16154.
20. Imai, T., et al., *Pentatricopeptide repeat motifs in the processing enzyme PRORP1 in Arabidopsis thaliana play a crucial role in recognition of nucleotide bases at TpsiC loop in precursor tRNAs.* Biochem Biophys Res Commun, 2014. **450**(4): p. 1541-6.
21. Karasik, A., et al., *Nuclear Protein-Only Ribonuclease P2 Structure and Biochemical Characterization Provide Insight into the Conserved Properties of tRNA 5' End Processing Enzymes.* J Mol Biol, 2016. **428**(1): p. 26-40.
22. Anantharaman, V. and L. Aravind, *The NYN Domains: Novel Predicted RNAses with a PIN Domain-like Fold.* RNA Biology, 2006. **3**(1): p. 18-27.
23. Pavlova, L.V., et al., *tRNA processing by protein-only versus RNA-based RNase P: kinetic analysis reveals mechanistic differences.* Chembiochem, 2012. **13**(15): p. 2270-6.
24. Walczyk, D., et al., *Analysis of the Cleavage Mechanism by Protein-Only RNase P Using Precursor tRNA Substrates with Modifications at the Cleavage Site.* J Mol Biol, 2016. **428**(24 Pt B): p. 4917-4928.
25. Gobert, A., et al., *Structural insights into protein-only RNase P complexed with tRNA.* Nature Communications, 2013. **4**(1353): p. 1-8.
26. Brillante, N., et al., *Substrate recognition and cleavage-site selection by a single-subunit protein-only RNase P.* Nucleic Acids Res, 2016. **44**(5): p. 2323-36.
27. Mao, G., et al., *Cleavage of Model Substrates by Arabidopsis thaliana PRORP1 Reveals New Insights into Its Substrate Requirements.* PLoS One, 2016. **11**(8): p. e0160246.
28. Howard, M.J., et al., *Differential substrate recognition by isozymes of plant protein-only Ribonuclease P.* Rna, 2016. **22**(5): p. 782-92.
29. Barkan, A., et al., *A Combinatorial Amino Acid Code for RNA Recognition by Pentatricopeptide Repeat Proteins.* PLOS Genetics, 2012. **8**(8): p. e1002910.
30. Yagi, Y., et al., *Elucidation of the RNA recognition code for pentatricopeptide repeat proteins involved in organelle RNA editing in plants.* PLoS One, 2013. **8**(3): p. e57286.
31. Record, M.T., Jr., C.F. Anderson, and T.M. Lohman, *Thermodynamic analysis of ion effects on the binding and conformational equilibria of proteins and nucleic acids: the roles of ion association or release, screening, and ion effects on water activity.* Q Rev Biophys, 1978. **11**(2): p. 103-78.
32. Barkley, M.D., P.A. Lewis, and G.E. Sullivan, *Ion effects on the lac repressor--operator equilibrium.* Biochemistry, 1981. **20**: p. 3842-51.

33. deHaseth, P.L., T.M. Lohman, and M.T. Record, Jr., *Nonspecific interaction of lac repressor with DNA: an association reaction driven by counterion release.* Biochemistry, 1977. **16**(22): p. 4783-90.
34. Day-Storms, J.J., S. Niranjanakumari, and C.A. Fierke, *Ionic interactions between PRNA and P protein in Bacillus subtilis RNase P characterized using a magnetocapture-based assay.* Rna, 2004. **10**(10): p. 1595-608.
35. Latt, S.A. and H.A. Sober, *Protein-nucleic acid interactions. II. Oligopeptide-polyribonucleotide binding studies.* Biochemistry, 1967. **6**(10): p. 3293-306.
36. Record, M.T., Jr., M.L. Lohman, and P. De Haseth, *Ion effects on ligand-nucleic acid interactions.* J Mol Biol, 1976. **107**(2): p. 145-58.
37. Rueda, D., et al., *The 5′ leader of precursor tRNAAsp bound to the Bacillus subtilis RNase P holoenzyme has an extended conformation.* Biochemistry, 2005. **44**(49): p. 16130-9.
38. Hansen, A., et al., *Exploring the minimal substrate requirements for trans-cleavage by RNase P holoenzymes from Escherichia coli and Bacillus subtilis.* Mol Microbiol, 2001. **41**(1): p. 131-43.
39. Kobayashi, K., et al., *Identification and characterization of the RNA binding surface of the pentatricopeptide repeat protein.* Nucleic Acids Res, 2012. **40**(6): p. 2712-23.
40. Guckian, K.M., et al., *Factors Contributing to Aromatic Stacking in Water: Evaluation in the Context of DNA.* J Am Chem Soc, 2000. **122**: p. 2213-2222.
41. Yin, P., et al., *Structural basis for the modular recognition of single-stranded RNA by PPR proteins.* Nature, 2013. **504**(7478): p. 168-171.
42. Martin, A.M., et al., *Divalent metal dependence of site-specific DNA binding by EcoRV endonuclease.* Biochemistry, 1999. **38**(26): p. 8430-9.
43. Fersht, A.R., et al., *Hydrogen bonding and biological specificity analysed by protein engineering.* Nature, 1985. **314**(6008): p. 235-8.
44. Small, I.D. and N. Peeterns, *The PPR motif – a TPR-related motif prevalent in plant organellar proteins.* Trends in Biochemical Sciences, 2000. **25**(2): p. 46-47.
45. Schmitz-Linneweber, C. and I. Small, *Pentatricopeptide repeat proteins: a socket set for organelle gene expression.* Trends Plant Sci, 2008. **13**: p. 663-70.
46. Chen, X., et al., *Dek35 encodes a PPR protein that affects cis-splicing of mitochondrial nad4 intron 1 and seed development in maize.* Mol Plant, 2016.
47. Pantoliano, M.W., et al., *High-density miniaturized thermal shift assays as a general strategy for drug discovery.* J Biomol Screen, 2001. **6**(6): p. 429-40.
48. Singh, M., et al., *Structural basis for telomerase RNA recognition and RNP assembly by the holoenzyme La family protein p65.* Mol Cell, 2012. **47**: p. 16-26.
49. Reiter, N.J., et al., *Structure of a bacterial ribonuclease P holoenzyme in complex with tRNA.* Nature, 2010. **468**(7325): p. 784-9.
50. Hoang, C. and A.R. Ferre-D'Amare, *Cocrystal structure of a tRNA Psi55 pseudouridine synthase: nucleotide flipping by an RNA-modifying enzyme.* Cell, 2002. **107**: p. 929-39.
51. Pinker, F., et al., *Biophysical analysis of Arabidopsis protein-only RNase P alone and in complex with tRNA provides a refined model of tRNA binding.* Journal of Biological Chemistry, 2017.

52. Shi, H. and P.B. Moore, *The crystal structure of yeast phenylalanine tRNA at 1.93 A resolution: a classic structure revisited.* Rna, 2000. **6**(8): p. 1091-105.
53. Zhang, J. and A.R. Ferre-D'Amare, *The tRNA Elbow in Structure, Recognition and Evolution.* Life (Basel), 2016. **6**(1).
54. Hutchison, C.A., 3rd, et al., *Mutagenesis at a specific position in a DNA sequence.* J Biol Chem, 1978. **253**(18): p. 6551-60.
55. Milligan, J.F. and O.C. Uhlenbeck, *Synthesis of small RNAs using T7 RNA polymerase.* Methods Enzymol, 1989. **180**: p. 51-62.
56. Pierce, B.G., et al., *ZDOCK server: interactive docking prediction of protein-protein complexes and symmetric multimers.* Bioinformatics, 2014. **30**(12): p. 1771-3.
57. Schrödinger, LLC, *PyMOL Molecular Graphics System, Version 1.5.* 2010.
58. Emsley, P., et al., *Features and development of Coot.* Acta Crystallogr D Biol Crystallogr, 2010. **66**(Pt 4): p. 486-501.
59. Leroy, J.L., et al., *Role of divalent ions in folding of tRNA.* Eur J Biochem, 1977. **74**: p. 567-74.
60. Liu, X., Y. Chen, and C.A. Fierke, *A real-time fluorescence polarization activity assay to screen for inhibitors of bacterial ribonuclease P.* Nucleic Acids Res, 2014. **42**(20): p. e159.
61. Ericsson, U.B., et al., *Thermofluor-based high-throughput stability optimization of proteins for structural studies.* Anal Biochem, 2006. **357**(2): p. 289-98.
62. Jayasimha, P., et al., *Contribution of buried aspartic acid to the stability of the PDZ2 protein.* The Journal of Chemical Thermodynamics, 2012. **52**: p. 64-68.
63. Goujon, M., et al., *A new bioinformatics analysis tools framework at EMBL-EBI.* Nucleic Acids Res, 2010. **38**(Web Server issue): p. W695-9.
64. Sievers, F., et al., *Fast, scalable generation of high-quality protein multiple sequence alignments using Clustal Omega.* Mol Syst Biol, 2011. **7**: p. 539.
65. Arnold, K., et al., *The SWISS-MODEL workspace: a web-based environment for protein structure homology modelling.* Bioinformatics, 2006. **22**(2): p. 195-201.
66. Guex, N., M.C. Peitsch, and T. Schwede, *Automated comparative protein structure modeling with SWISS-MODEL and Swiss-PdbViewer: a historical perspective.* Electrophoresis, 2009. **30 Suppl 1**: p. S162-73.
67. Kiefer, F., et al., *The SWISS-MODEL Repository and associated resources.* Nucleic Acids Res, 2009. **37**(Database issue): p. D387-92.
68. Biasini, M., et al., *SWISS-MODEL: modelling protein tertiary and quaternary structure using evolutionary information.* Nucleic Acids Res, 2014. **42**(Web Server issue): p. W252-8.

PAPER 4: LOSS OF THE MITOCHONDRIAL PROTEIN-ONLY RIBONUCLEASE P COMPLEX CAUSES ABERRANT TRNA PROCESSING AND LETHALITY IN DROSOPHILA

Published online 30 April 2016

Nucleic Acids Research, 2016, Vol. 44, No. 13 **6409–6422**
doi: 10.1093/nar/gkw338

Loss of the mitochondrial protein-only ribonuclease P complex causes aberrant tRNA processing and lethality in Drosophila

Aditya Sen[1,†], Agnes Karasik[1,†], Aranganathan Shanmuganathan[1], Elena Mirkovic[2], Markos Koutmos[1,*] and Rachel T. Cox[1,*]

[1]Department of Biochemistry and Molecular Biology, Uniformed Services University, Bethesda, MD, 20814, USA and [2]Walt Whitman High School, Bethesda, MD, 20817, USA

Received February 26, 2016; Revised April 12, 2016; Accepted April 14, 2016

ABSTRACT

Proteins encoded by mitochondrial DNA are translated using mitochondrially encoded tRNAs and rRNAs. As with nuclear encoded tRNAs, mitochondrial tRNAs must be processed to become fully functional. The mitochondrial form of ribonuclease P (mt:RNase P) is responsible for 5′-end maturation and is comprised of three proteins; mitochondrial RNase P protein (MRPP) 1 and 2 together with proteinaceous RNase P (PRORP). However, its mechanism and impact on development is not yet known. Using homology searches, we have identified the three proteins composing Drosophila mt:RNase P: Mulder (PRORP), Scully (MRPP2) and Roswell (MRPP1). Here, we show that each protein is essential and localizes with mitochondria. Furthermore, reducing levels of each causes mitochondrial deficits, which appear to be due at least in part to defective mitochondrial tRNA processing. Overexpressing two members of the complex, Mulder and Roswell, is also lethal, and in the case of Mulder, causes abnormal mitochondrial morphology. These data are the first evidence that defective mt:RNase P causes mitochondrial dysfunction, lethality and aberrant mitochondrial tRNA processing *in vivo*, underscoring its physiological importance. This *in vivo* mt:RNase P model will advance our understanding of how loss of mitochondrial tRNA processing causes tissue failure, an important aspect of human mitochondrial disease.

INTRODUCTION

Most metazoan mitochondrial genomes encode the same transcripts (1). The 13 proteins encoded by mitochondrial DNA (mtDNA) are required components of the complexes that carry out oxidative phosphorylation. In order for mitochondria to fulfill the ATP demands of the cell, each mitochondrial-encoded protein must be efficiently generated by the mitochondrial machinery. To this end, the mitochondrial ribosomes rely on the large and small ribosomal RNAs and the entire suite of tRNAs encoded by the mtDNA.

Nuclear tRNAs are transcribed as pre-tRNAs that require 5′- and 3′-end cleavage and other modifications in order to mature and become fully functional (2–4). As mitochondria have a bacterial origin, mtDNA is transcribed as polycistrons that must be processed and cleaved to create the final products (5,6). Thus, mtDNA transcription is complex and places unique demands on the mitochondrial RNA processing machinery, differing significantly from the transcription that commonly takes place in the nucleus (7). Mitochondrial tRNAs (mt:tRNAs) punctuate the mRNAs and rRNAs found in mtDNA and thus have the added complication of requiring excision from the polycistron before maturation (8). In the nucleus, the RNAse P ribozyme has long been known to be responsible for the 5′-end pre-tRNA cleavage reaction, while other endonucleases, such as RNase Z and Rex1p carrying out the 3′-end cleavage reaction (9–11). Recently, a new class of protein-only RNase Ps (proteinaceous RNase P (PRORP)) has been identified that can carry out the 5′-end cleavage in human mitochondria (12). In contrast to the RNAse P ribozyme, PRORP (also called Mitochondrial RNase P Protein 3 (MRPP3)) is a metallonuclease without an RNA component. Single protein PRORPs exist in the nucleus and organelles of land plants and unicellular eukaryotes (13,14). In contrast, human PRORP has only been identified in mitochondria and is part of a three-protein complex referred to as mt:RNase P, comprising mitochondrial RNase P Protein 1 (MRPP1/TRMT10C) and mitochondrial RNase P Protein 2 (MRPP2/SDR5C1/HSD10) (12). MRPP1 is re-

*To whom correspondence should be addressed. Tel: +1 301 295 9791; Fax: +1 301 295 3512; Email: rachel.cox@usuhs.edu
Correspondence may also be addressed to Markos Koutmos. Tel: +1 301 295 9419; Fax: +1 301 295 3512; Email: markos.koutmos@usuhs.edu
†These authors contributed equally to the paper as first authors.

Published by Oxford University Press on behalf of Nucleic Acids Research 2016.
This work is written by (a) US Government employee(s) and is in the public domain in the US.

quired for methylation of the ninth position of certain mitochondrial tRNAs, although this activity is not obligatory for mt:RNAse P function and 5′-end cleavage (15). MRPP2 is a dehydrogenase, however evidence supports that in the context of mt:RNase P it is required for the methyltransferase activity of MRPP1, as well as likely functions as a scaffold protein for the formation of an MRPP1 and 2 sub-complex (15). As such, the MRPP1 and MRPP2 subcomplex catalyzes tRNA methylation and in the context of mt:RNase P supports 5′-end processing by PRORP. The 3′-end cleavage of mt:tRNAs also uses a mitochondrially localized RNase Z, called ELAC2 in humans and RNase Z^L in Drosophila. While these two enzyme complexes are distinct, there is evidence that RNase Z/ELAC2 preferentially cleaves products that have already been processed by RNase P (16).

While this newly identified mt:RNAse P complex appears critical for tRNA processing and maturation, it is currently unknown how loss of mt:RNAse P function affects mitochondrial output and health. This is particularly relevant to human health as the majority of mitochondrial diseases caused by mutations in mtDNA are due to point mutations in mt:tRNAs (17). Based on their location, most of the mitochondrial tRNA mutations could affect mt:RNAse P function, leading to unprocessed RNA species and mitochondrial dysfunction. Specific examples include MELAS (mitochondrial encephalopathy, lactic acidosis and stroke-like episodes), mitochondrial myopathy and HSD10 disease (18–23). Highlighting the importance of mt:tRNA processing in human health, mutations in RNase Z/ELAC2 and MRPP2/SDR5C1 are associated with cardiomyopathy and neurodegeneration, and cause mis-regulated mt:tRNA cleavage in cell culture (24,25). For unknown reasons mitochondrial diseases manifest very differently in different organs and tissues and have quite different etiology, making their diagnoses and treatment difficult, therefore it is critical to understand the molecular mechanisms underlying mt:tRNA cleavage *in vivo* (17,26).

Drosophila is an excellent model system to study the effect of altered mtDNA post-transcriptional processes as Drosophila and human mtDNA genomes are arranged in a similar manner, with mt:tRNAs punctuating the mRNAs and rRNAs (27). In order to determine the developmental and physiological significance of mt:RNase P function, we have used sequence similarities to identify the Drosophila mt:RNase P complex and examined Drosophila lacking the orthologs for PRORP, MRPP2 and MRPP1, called Mulder, Scully and Roswell, respectively. Here we show that Mulder, Scully and Roswell localize to mitochondria as expected and that each can associate with the others. Importantly, reducing any one of the three causes lethality. Furthermore, flies lacking Mulder, Scully or Roswell have associated mitochondrial deficiencies, exhibiting greatly reduced levels of ATP and swollen, damaged-looking mitochondria. In addition, flies with reduced Mulder, Scully or Roswell accumulate unprocessed mt:tRNA indicating that the mitochondrial defects we observe are at least in part direct and specific for the protein complex function. Finally, we find that overexpressing either Mulder or Roswell exerts dominant negative effects on development and can also cause mitochondrial defects. These data are the first to show that loss of mt:RNase P function is detrimental in metazoans and specifically mis-regulates mt:tRNA processing. Understanding the role of the highly conserved mt:RNase P will be useful to dissect a subset of the complex mechanisms underlying mitochondrial diseases.

MATERIALS AND METHODS

Fly stocks

The following fly stocks were obtained from the Bloomington Stock Center: y^1 *w* mldr*^{B} FRT19A/FM7i, ActGFP, y^1 *w* mldr*^{C} FRT19A/FM7i, ActGFP, y^1 *w* scu*^{A} FRT19A/FM7i, ActGFP, y^1 *w* scu*^{D} FRT19A/FM7i, ActGFP, y^1 v^1; *scu*$^{TRiP.HMS02305}$, y^1 *sc** v^1; *scu*$^{TRiP.GL01079}$, y^1 *sc** v^1; *rswl*$^{TRiP.HMC02423}$, y^1 *w**; P{w[+mC] = tubP-GAL4}LL7/ TM3, P{w[+mC] = ActGFP}JMR2, Ser[1], y^1 *w**; P{w[+mC] = Act5C-GAL4}17bFO1/ TM3, P{w[+mC] = ActGFP}JMR2, Ser, *w**; P{w[+mC] = ple-GAL4.F}3, P{w[+mC] = GAL4::VP16-nos.UTR}. The following stocks were obtained from the Vienna Drosophila Research Center: *y* w^{1118}/ *mldr*^{KK108043}, w^{1118}; *rswl* ^{GD12447} (28).

Transgenic flies and constructs

The full-length Open Reading Frames for each respective gene was amplified from the following Drosophila ESTs (Drosophila Genomics Resource Center, Bloomington, IN, USA): *rswl* (LD44982), *scu* (IP05285) and *mldr* (SD17694). The two point mutations present in SD17694 were corrected (R250L and L528M) using the QuikChange method (Stratagene). For transgenic flies, *rswl*, *scu* and *mldr* were sub-cloned into pPWM, pPWF and pPWV plasmids (The Drosophila Gateway Collection, Carnegie Institution of Washington, Baltimore, MD, USA), respectively, then commercially injected (Genetic Services, Inc, Cambridge, MA, USA). For S2R+ tissue culture constructs, *rswl*, *scu* and *mldr* were sub-cloned into pAWM containing a C-terminal myc tag. *scu* and *mldr* were also cloned into pAWF containing a C-terminal FLAG tag (The Drosophila Gateway Collection, Carnegie Institution of Washington, Baltimore, MD, USA).

Northern blots

Total RNA was extracted from 5 to 10 mg of wild-type and mutant strains of Drosophila larvae using a Tissue and Insect RNA kit (Zymo Research Corporation, St. Louis, MO, USA). Five micrograms from each sample were mixed with an equal amount of 2× urea loading dye (0.05% Bromo-Phenol-Blue, 0.05% Xylene Cyanol dye, 50% m/v urea, 0.1 M EDTA) and run on 6% urea-polyacrylamide gel. Northern blot analysis was performed according to the DIG Northern Starter Kit (Sigma-Aldrich Corp. St. Louis, MO, USA) with a hybridization temperature of 50°C. The size standards of the RNA fragments were detected using DIG-labeled RNA Molecular Weight Marker I (Sigma-Aldrich Corp. St. Louis, MO, USA). Each blot was performed at least three times.

Immunofluorescence

Larval brains and ovaries from well-fattened females were dissected and fixed as previously described (29). S2R+ culture cells were fixed and mounted as described (29). In short, samples were fixed in Grace's Insect Medium (modified) (BioWhittaker, Lonza, Cologne, Germany) containing 4% paraformaldehyde and 20 mM formic acid (Sigma-Aldrich Corp. St. Louis, MO, USA). Antibody staining was performed in antibody wash buffer (1× PBS:0.1% Triton X-100:1% BSA). The following antibodies were used: rabbit anti-GFP (1:2000, Torrey Pines Biolabs, Secaucus, NJ, USA), mouse anti-myc (1:1000, Sigma-Aldrich Corp. St. Louis, MO, USA), anti-FLAG (1:1000, Sigma-Aldrich Corp. St. Louis, MO, USA), mouse anti-ATP synthase (1:1000, CVA, Mitosciences) and Phalloidin (1:250, Invitrogen). The following secondary antibodies were used: goat anti-mouse $IgG2_b$ Alexa 488, goat anti-mouse $IgG2_b$ Alexa 568, goat anti-mouse IgG_1 Alexa 488 and goat anti-rabbit Alexa 488 (Molecular Probes, Lifetechnologies, Grand Island, NY, USA). Images were collected using Zeiss 710 and Zeiss 700 confocal microscopes and 63× Plan Apo NA 1.4 lens.

Western blotting, immunoprecipitation and cell fractionation

Western blotting, immunoprecipitations (IP) and cell fractionations have been performed as described earlier (29,30). The following antibodies were used: mouse anti-myc (1:5000, Sigma-Aldrich Corp. St. Louis, MO, USA), anti-FLAG (1:10000, Sigma-Aldrich Corp. St. Louis, MO, USA), anti-CVA (1:100000, Mitosciences), mouse anti-alpha tubulin (1:5000, Developmental Studies Hybridoma Bank, University of Iowa, Iowa City, IA, USA) and anti-Mldr (1:2000, this study).

Pupation, eclosion and negative geotaxis measurements

Pupation, eclosion and negative geotaxis measurement were performed as described (29,30). *P*-values were calculated in Microsoft Excel using a two-tailed Student's *t*-test.

ATP measurements and aconitase assay

ATP measurements and aconitase assays were performed as described (29). In short, for ATP measurement, larval samples were homogenized in ATP extraction buffer (100 mM Tris-Cl, pH 8.0, 4 mM EDTA, pH 8.0; 6 M guanidine hydrochloride) and protein concentrations were measured using Bradford assay. The ATP concentration was determined using an ATP Determination Kit (Molecular Probes, Invitrogen) according to the manufacturer's directions. One hundred microliter assays were performed in a 96-well plate and the luminescence was measured using a Biotek Synergy H1 luminometer. Each sample was processed in duplicate and read in triplicate. The amount of ATP was normalized against protein concentration. For aconitase assays, larval extracts were electrophoresed on cellulose acetate membrane (Cellogel, Accurate Chemicals, Westbury, NY, USA) in running buffer [20 mM potassium phosphate (pH 7.8), 3.6 mM citrate]. Aconitase activities were detected on the membrane by incubating it in staining solution [100 mM potassium phosphate, (pH 6.5), 1 mM $NADP_1$, 25 mM $MgCl_2$, 2 mM cis-aconitic acid, 0.5 mg/ml 2,3-bis-(2-methoxy-4-nitro-5-sulfenyl)-2H-tetrazolium-5 carboxanilide disodium salt (XTT) or MTT, 0.3 mM phenazine methosulfate, 5 units/ml isocitrate dehydrogenase] for 10 min. From three membranes, the band intensities from mitochondrial aconitase activity of each sample were normalized against the respective cytoplasmic aconitase activity for comparison. Analyses were done using ImageJ (31).

Mulder antibody generation

The Drosophila EST SD17694 (Drosophila Genomics Resource Center, Bloomington, IN, USA) was cloned into pMCSG7 vector (gifted from Midwest Center for Structural Genomics, IL, USA) and transformed into BL21(DE3) expression cells (New England Biolabs, MA, USA). The culture was grown at 37°C and the protein was expressed using 200 μM of IPTG at 18°C in TB media (Sigma-Aldrich Corp. St. Louis, MO, USA). The cells were lysed using lysis buffer (8M urea, 100 mM NaH_2PO_4, 10 mM Tris and 10 mM imidiazole pH 8.0) and sonication. The lysate was centrifuged and the supernatant was passed through Ni-NTA column and washed with a denaturing wash buffer (8M urea, 100 mM NaH_2PO_4, 150 mM NaCl, 20 mM imidiazole pH 8.0). The protein samples were eluted from the column using 20 mM MOPS pH 7.8,100 mM NaCl, 1 mM TCEP, 500 mM imidazole and 6 M urea. The purity of the sample was verified by SDS PAGE gel and fractions having a single band were pooled and then commercially injected into rabbits (Covance Research Products, Princeton, NJ, USA). A 1 mg/ml protein was used for the injection and the serum was checked by ELISA test for antibody tightness.

RESULTS

Members of the protein only RNase P complex localize to mitochondria in Drosophila

Pre-tRNAs are processed through cleavage of their 5′ and 3′ ends, as well as by the covalent modification of various bases (2,3). In metazoan mitochondria, the protein in the mt:RNase P complex responsible for catalyzing the 5′-end cleavage is PRORP which contains a metallonuclease domain, as well as a pentatricopeptide repeat (PPR) domain thought to bind RNA (Figure 1A). The Drosophila ortholog contains all of the same recognizable domains, including a mitochondrial targeting signal. The Drosophila PRORP ortholog is the previously undescribed gene CG15896 that we have named *mulder* (*mldr*) (Figure 1A). MRPP2 is a member of the short-chain dehydrogenase/reductase (SDR) superfamily and is also known as Hydroxysteroid (17-Beta) Dehydrogenase 10 (HSD10 is the protein, HSD17B10 is the gene) (Figure 1A). The Drosophila ortholog Scully (Scu) is highly homologous to MRPP2, with 69% amino acid identity (Figure 1A) (32). MRPP1 is a methyltransferase and Drosophila contain two potential orthologs. However, only one has a mitochondrial targeting signal, which is encoded by the previously undescribed gene CG5190 that we have named *roswell* (*rswl*) (Figure 1A).

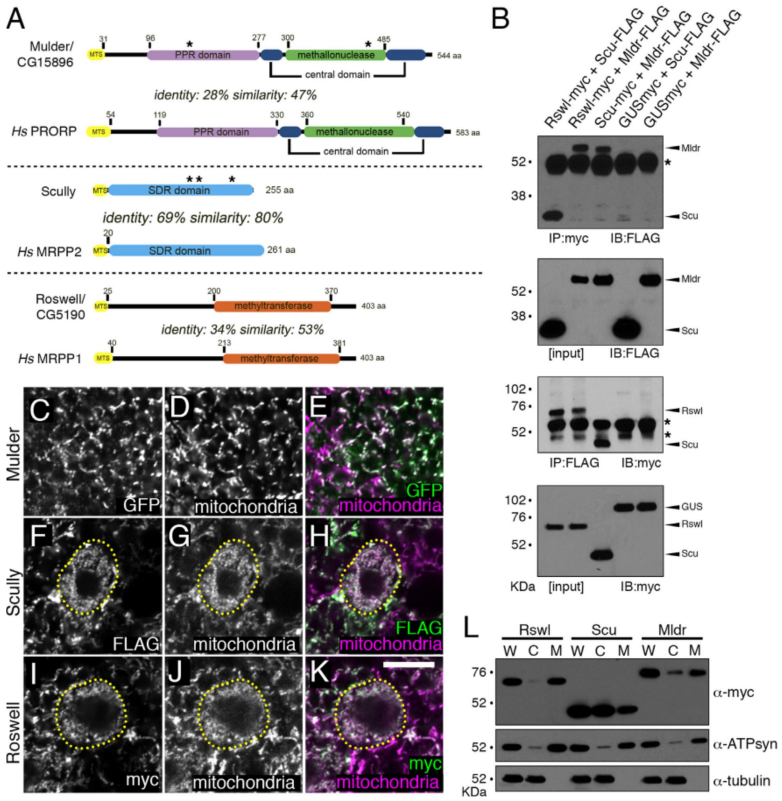


Figure 1. The Drosophila mt:RNase P proteins Mldr, Scu and Rswl localize to mitochondria. (**A**) Schematics indicating the domains of each protein and their homology to the human homologs. Asterisks indicate the approximate location of the mutations used in this study. The length of the mitochondrial targeting sequence (MTS, yellow) was predicted using the Mitoprot server. Domain boundaries of Drosophila mt:RNase P components were predicted based on alignments with human homologs (Clustal Omega). Sequence identify and similarity were determined by BLAST. (**B**) Western blots showing each mt:RNase P protein can reciprocally co-immunoprecipitate with the others. GUS = glucuronidase as a negative control. Arrowheads indicate the correct band size. Asterisks indicate the anti-mouse IgG cross-reactive bands. (**C–K**) GFP-tagged Mldr, FLAG-tagged Scu and myc-tagged Rswl (C, F, I, respectively) co-localize with mitochondria (D, G, J) in larval brains. E, H, K show the merged images. Dashed yellow lines indicate third larval instar neuroblasts. Overexpression of Mldr causes early larval lethality and it is difficult to find NBs in the very young brains, thus there is no NB indicated (C, D). (L) Western blot of fractionated S2R+ cell extract from cells transfected with myc-tagged Mldr, Scu or Rswl shows each protein is located in the mitochondrial fraction (M). Tubulin and ATP synthase are controls for cytoplasmic (C) and mitochondrial (M) fractions, respectively. W = whole cell extract. White = anti-ATP synthase (D, G, J), anti-GFP (C), anti-FLAG (F), anti-myc (I). Green = anti-GFP (E), anti-FLAG (H), anti-myc (K). Magenta = anti-ATP synthase (E, H, K). Scale bar = 10 μm in K for C–K.

For Mldr, Scu and Rswl to exert their function as the Drosophila mt:RNase P, they would have to associate with each other. To test this, we transfected S2R+ cells pairwise with myc- and FLAG-tagged constructs and performed reciprocal immunoprecipitation (IP) (Figure 1B). Rswl and Scu, Rswl and Mldr and Scu and Mldr reciprocally co-IP'd, indicating that the three were able to associate. Myc-tagged glucuronidase (GUS) served as a negative control. Furthermore, the mt:RNase P complex must localize to mitochondria in order to process mt-tRNAs. Mldr, Scu and Rswl contain putative mitochondrial targeting signals (Figure 1A; MTS), however none have been previously shown to localize to mitochondria *in vivo*. To test the localization of each protein, we developed transgenic flies using the UAS/GAL4 system to conditionally express GFP-tagged Mldr, FLAG-tagged Scu and myc-tagged Rswl (33). As evidenced by immunofluorescence, all three proteins co-localized with mitochondrial ATP synthase in the larval brain (Figure 1C–K) and germ cells (Supplementary Figure S1A–F, Figure 6D–F). S2R+ cells transfected with myc-tagged Mldr, Scu and Rswl also showed strong mitochondrial co-localization with ATP synthase (Supplementary Figure S1G–O). To confirm this localization biochemically, we transfected S2R+ cells with myc-tagged Mldr, Scu and Rswl and separated the extract into cytoplasmic and mitochondrial fractions. By probing the fractions with anti-myc antibody, we saw that each protein is detected in the mitochondrial fraction (Figure 1L). There were minimal

amounts of Mldr and Rswl in the cytoplasmic fractions which were likely due to a trace contamination from the mitochondrial fraction judging from the ATP synthase antibody. While immunofluorescence *in situ* showed predominantly mitochondrial staining, Scu was also found in the cytoplasmic fraction, which could be due to overexpression in S2R+ cells that often led to large cytoplasmic aggregates (Supplementary Figure S2, arrows). ATP synthase and tubulin served as controls for the purity of the mitochondrial and cytoplasmic fractions, respectively. Taken together, these data show that Mldr, Scu and Rswl can associate with each other, and that each is localized to mitochondria *in vivo*.

Mulder, Scully and Roswell are orthologous to PRORP, MRPP2 and MRPP1

There are no available structures for Mldr and Scu. We have, however, used known structures of homologous proteins to construct the high confidence models shown in Figure 2. Specifically, Phyre server was used to create a structure model of Mldr using the metallonuclease domain of human PRORP and the full-length structures of A. thaliana PRORP1 and PRORP2 as templates (34–36). The I-Tasser server was used to create a structure model of Scu based on structures of human MRPP2 (37,38). There are two uncharacterized publicly available alleles of *mldr* that were generated in a large-scale mutagenesis screen: $mldr^{B}$ (Y121D in the PPR domain) and $mldr^{C}$ (W465R in the metallonuclease domain) (Figure 2A, yellow circles) (39). There are three available *scu* alleles. Two of them were generated in the same genetic screen as was *mldr*: scu^{D} (S163F) is in a highly conserved residue (Figure 2B, red circle) and scu^{A} (Q159Stop) is predicted to result in a C-terminal truncation (Figure 2B, shown in yellow) (39). scu^{4058} results from a small X-ray induced deletion which causes a frameshift at E205 leading to a stop codon 60 nucleotides downstream after E236 (32). This results in a smaller truncation than scu^{A}, consisting of the last 19 residues (Figure 2B, shown in green). The putative tetrameric assembly of Scu is presented where the four monomers are differentially color-coded (Figure 2C). It is evident that S163 lies in the interface between two monomers.

Reducing Mldr, Scu and Rswl causes lethality *in vivo*

In order to study the consequences of loss of mt:RNase P *in vivo*, we examined mutants for *mldr* and *scu*, and *RNAi* knockdown for *mldr*, *scu* and *rswl*. We found the mutant alleles for *mldr* and *scu* cause lethality because flies containing mutations in either gene do not make it to the adult stage as we only saw heterozygous sibling adult flies eclose, whereas homozygous mutant adults never eclosed (Figure 2D). While $mldr^{B}$ and $mldr^{C}$ are only point mutations, the larvae contained very low protein levels as judged by western blot (Figure 2E). To determine at which stage of development the lethality occurs, we transferred 20 one-day-old mutant larvae into vials and scored how many pupated (Figure 2F–H). Under these uncrowded conditions, $mldr^{B}$ showed a delay in pupation relative to wild-type sibling controls, with all the larvae finally pupating by day 16 (Figure 2F). $mldr^{C}$ had a stronger phenotype, with a longer pupation delay and only 60% of the larvae pupating compared with sibling controls (Figure 2F). The three available *scu* alleles gave similar results. scu^{A} and scu^{D} were both lethal and experienced delayed pupation under uncrowded conditions (Figure 2G). scu^{4058} was the most severe, with a slightly longer pupation delay and only 60% of the larvae pupating (Figure 2G). Pupae mutant for *mldr* and *scu* frequently did not develop normally and had reduced spiracle eversion (Supplementary Figure S3). Expressing *UAS-rswl-RNAi* also gave a modest delay in pupation compared to control (Figure 2H).

In addition to examining both *mldr* and *scu* mutants, we ubiquitously expressed available RNAi lines using the highly expressed *tubGAL4* and lower expressed *ActGAL4* (Table 1 & Supplementary Table S1). Expressing *UAS-scu* and *UAS-mldr RNAi* using *tubGAL4* allowed larvae to pupate equally well as controls. The *scu RNAi* knockdown pupae did not develop to adulthood. Approximately 10% of the *mldr* knockdown pupae eclosed and using ActGAL4 to express the *RNAi* at lower levels allowed an even larger portion of the adults to eclose (Table 1 and Supplementary Table S1). At present, there are no available alleles for *rswl* and only one RNAi stock. Expressing *rswl-RNAi* using *ActGAL4* allowed the larvae to pupate, but not develop. While this is only one RNAi line, this result is very similar to our results with *mldr* and *scu*. Expressing *UAS-rswl* RNAi at higher levels using *tubGAL4* suppressed even pupation (Table 1).

Neurons are particularly sensitive to mitochondrial output. To determine if decreasing Mldr, Scu or Rswl caused neuronal deficits, we expressed *UAS-RNAi* for each using the tyrosine hydroxylase *pleGAL4* specific to dopaminergic neurons and examined the ability of the flies to climb at different ages (Figure 2I). Expressing neither *UAS-rswl* nor *UAS-scu* RNAi caused deficits in locomotion. However, knocking down *mldr* in dopaminergic neurons caused an age-progressive loss of locomotive function (Figure 2I). Taken together, these data support an essential role for mt:RNase P *in vivo*. Furthermore, ubiquitously knocking down each complex member caused lethality at the same developmental stage and thus gave very similar phenotypes, suggesting they function in the same pathway.

mldr and *scu* mutants and *rswl* knockdown larvae have reduced ATP levels but no apparent mitochondrial oxidative stress

In metazoans, mtDNA encodes the entire suite of tRNAs necessary for translating mtDNA encoded proteins. There are only 13 proteins encoded by mtDNA, all of which are required for the protein complexes used for oxidative phosphorylation. Since human mt:RNase P is involved in mt:tRNA processing *in vitro*, we tested whether knocking down each component caused ATP levels to decrease *in vivo*. Larvae mutant for *mldr* and *scu* showed greatly reduced ATP levels relative to wild-type control (Figure 3A). Consistent with this result, extract from larvae expressing *UAS-RNAi* for *mldr*, *scu* and *rswl* also showed low levels of ATP relative to control (Figure 3B). One of the consequences of electron transport during respiration can be the accumula-

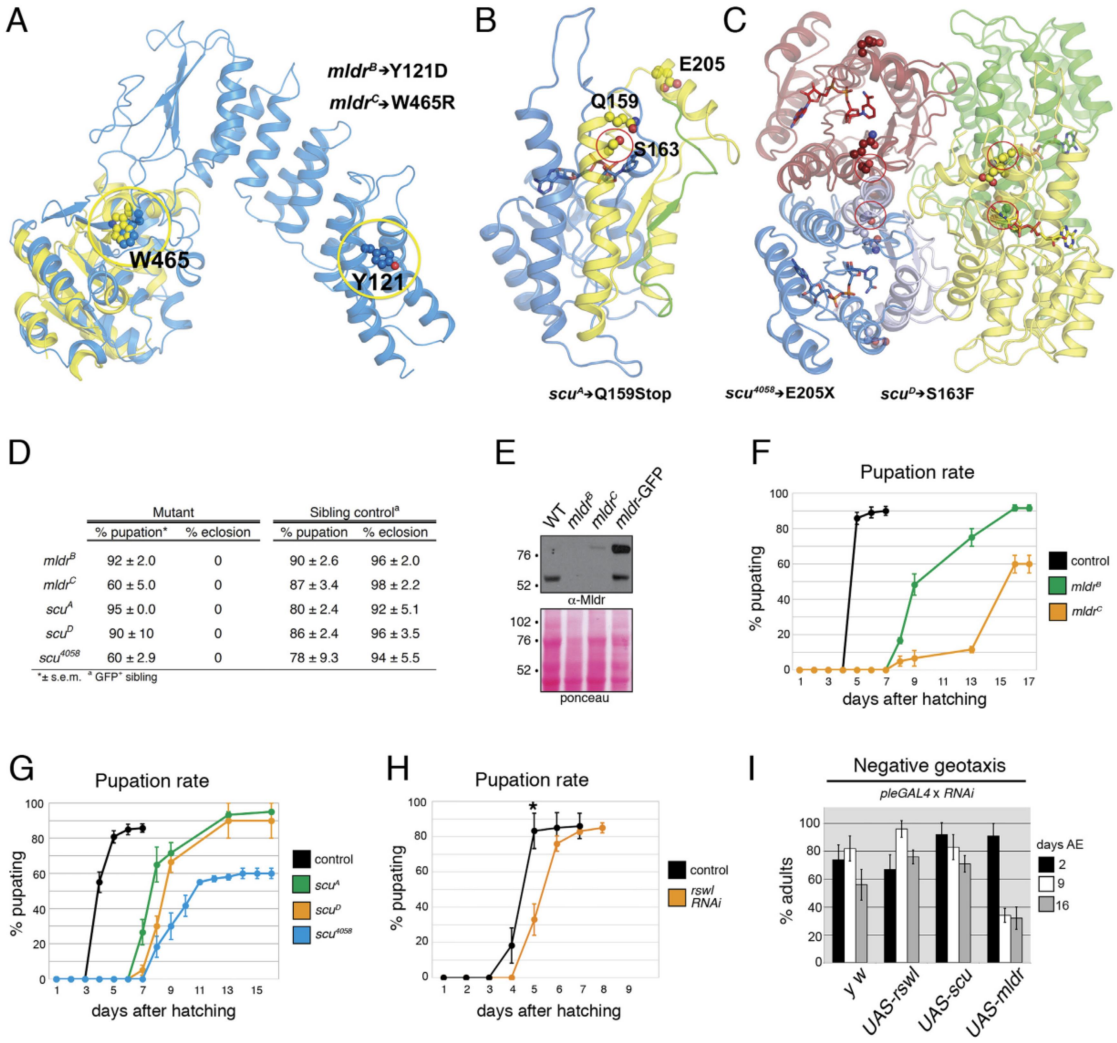


Figure 2. Loss of *mldr* and *scu* results in lethality in Drosophila. (A–C) Predicted structure of Mulder based on the Arabidopsis thaliana PRORP1, PRORP2 and the human PRORP available structures (**A**) and Scully (**B and C**) based on the available human MRPP2 structures. The modeled MRPP2 monomer is shown in blue in B whereas the expected tetrameric assembly is shown in C. The point mutations used in this study are indicated with yellow (A) and red (B, C) circles. The *scu* alleles Q159Stop and E205X result in truncations. The E205X and Q159Stop mutations result in a 19-residue truncation in yellow and an additional 87-residue truncation in green, respectively shown in B. The position of W465, Y121 in Mulder and S163, Q159 and E205 are all shown as ball and sticks. (**D**) Table summarizing percent pupation and eclosion for *mldr* and *scu* alleles. (**E**) Western blot indicating larvae mutant for $mldr^B$ and $mldr^C$ have greatly reduced protein levels. (**F–H**) Pupation rates. Both $mldr^B$ and $mldr^C$ mutant larvae have delayed pupation with 40% of $mldr^C$ mutant larvae failing to pupate (F). Larvae mutant for *scu* have delayed pupation as well. The scu^{4058} allele also fails to pupate 40% of the time (G). (H) Expressing *UAS-rswl-RNAi* using *ActGAL4* shows a modest but reproducible pupation delay. Note the different scale in the X-axis. The controls (black lines) for F–H are a representative sibling control for one of the genotypes. The lines stop because the adults eclose. (**I**) Negative geotaxis assay. Expressing *scu* or *rswl* RNAi in dopaminergic neurons using *Ple-GAL4* has no effect on adult fly locomotion, whereas expressing *mldr-RNAi* causes an age-dependent decrease in locomotion. AE = After Eclosion. Error bars = s.e.m. for F, G and s.d. for H. * $P = 0.02$, determined using a two-tailed Student's *t*-test in Microsoft Excel.

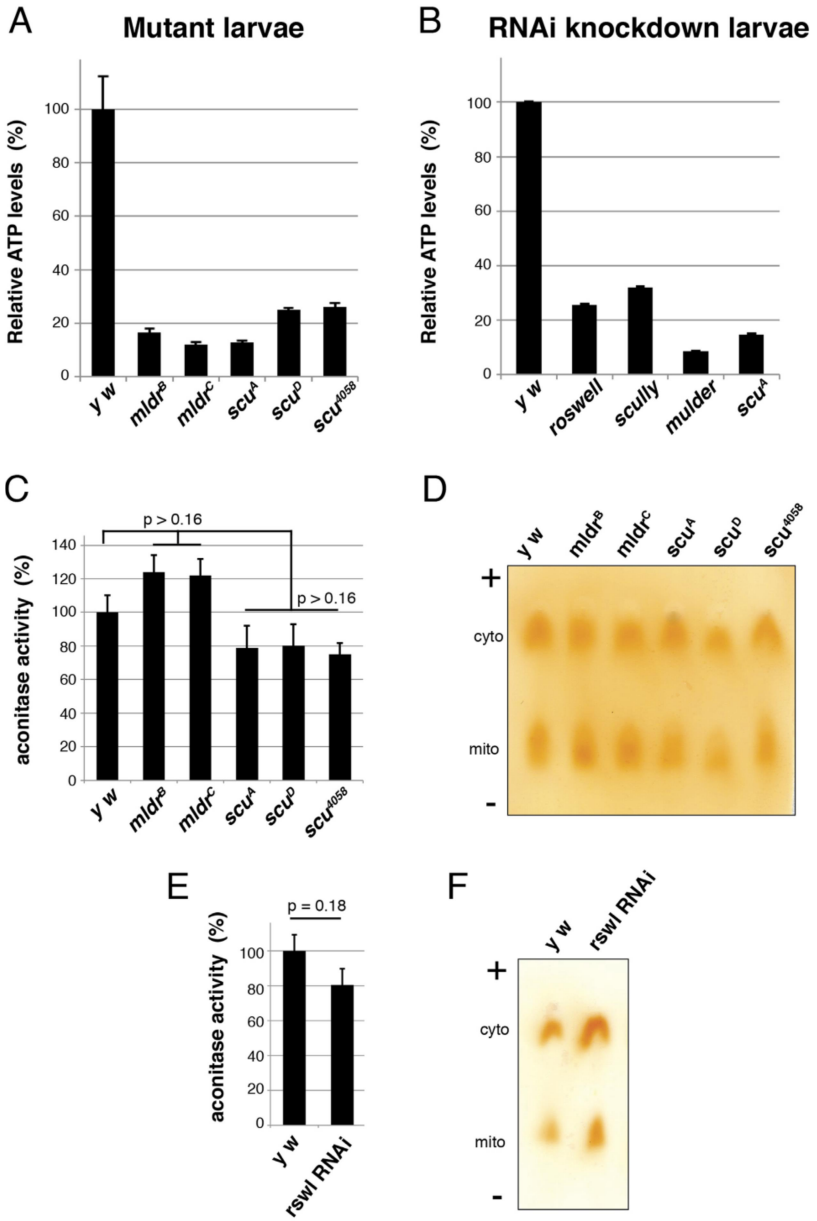


Figure 3. Loss of mt:RNase P complex proteins causes decreases in ATP *in vivo*. (**A**) Larvae mutant for *mldr* and *scu* have greatly reduced levels of ATP compared to wild-type (*y w*). (**B**) Larvae ubiquitously expressing *RNAi* for *rswl*, *scu* and *mldr* using *tubGAL4* also have reduced levels of ATP. scu^{A} mutant larvae are included as a control. (**C, E**) *mldr* and *scu* mutant larvae (C) and larvae ubiquitously expressing *rswl-RNAi* (E) do not have decreased mitochondrial aconitase activity relative to cytoplasmic aconitase activity. (**D, F**) Representative cellulose acetate membranes for C and E, respectively, showing cytoplasmic (cyto) and mitochondrial (mito) aconitase activity. '+' and '−' indicate the electrophoretic migration. Error bars represent s.e.m.. *P* -values were calculated using a two-tailed Student's *t*-test in Microsoft Excel. Information on replicates can be found in the Materials and Methods.

Table 1. mt:RNase P *RNAi* knockdown pupation and eclosion rates

	RNAi		Sibling control[b]	
	Percent pupation[a]	Percent eclosion	Percent pupation	Percent eclosion
tubGAL4/ UAS-rswl^{GD12447}	0	0	85 ± 5	98 ± 1.8
ActGAL4/ UAS-rswl^{GD12447}	92 ± 3.3	0	98 ± 1.7	98 ± 1.7
UAS-scu$^{TRiP.HMS02305}$ /+; *tubGAL4*/+	86 ± 7.2	0	98 ± 2.5	98
tubGAL4/ UAS-scu$^{TRiP.GL01079}$	92 ± 1.7	0	95 ± 2.9	97 ± 3.3
tubGAL4/ UAS-mldr^{KK108043}	83 ± 1.7	8 ± 5.1	92 ± 1.7	97 ± 3.3

[a]± s.e.m.
[b]GFP^{+} sibling larvae.

tion of reactive oxygen species. If reactive oxygen species accumulate, mitochondria can experience a reduction in ATP due to the build-up of general oxidative damage as a consequence of oxidative stress. For example, Drosophila harboring mutations for various mitochondrial proteins often suffer from mitochondrial oxidative damage and flies lacking mt:RNase Z function were shown to have increased oxidative damage (examples include (29,40–43)). One assay to assess the mitochondrial redox environment is to measure the enzymatic ability of mitochondrial aconitase, an enzyme easily rendered non-functional due to oxidation (44,45). *mldr* and *scu* mutants and *rswl RNAi* knockdown larvae did not show a decrease in mitochondrial aconitase activity relative to cytoplasmic aconitase activity (Figure 3C–F). This suggests that the drop in ATP levels is not due to general mitochondrial oxidative stress.

Mitochondria swell in the absence of Mldr and Scu

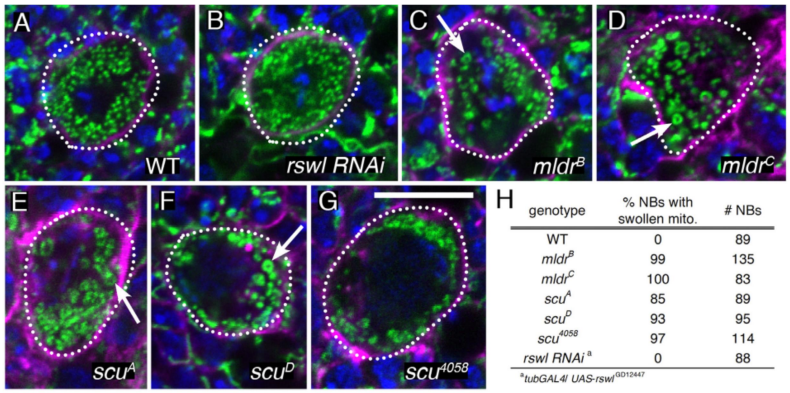
When the inner mitochondrial membrane of a mitochondrion loses its selective permeability due to damage, it osmotically swells and ruptures the outer mitochondrial membrane. This phenomenon gives rise to swollen, ring-like mitochondria when viewed by microscopy. Mldr, Scu and Rswl localized to mitochondria, and there was a decrease in ATP levels when any of the three were knocked down. The lethality we observed with *mldr* and *scu* mutants and with *UAS-rswl-RNAi* knockdown could be due to a variety of non-specific defects. To examine whether there are defects in mitochondrial size and shape with loss of mt:RNase P, we examined mitochondrial morphology using immunofluorescence. Mitochondria in larval brain neuroblasts have a stereotypical, distinctive, small spherical structure (Figure 4A) (29). When we examined neuroblasts in *mldr* and *scu* mutant larval brains, we found they were larger and swollen compared to wild-type, and often contained ring-like mitochondria (Figure 4C–G, arrows, versus A). For *scu*^{4058}, this is consistent with mitochondrial morphological changes seen using transmission electron microscopy (32). Loss of mitochondrial proteins in Drosophila does not always give rise to this phenotype (29). In contrast, the *rswl RNAi* knockdown using tubGAL4 did not show swollen or ring-like mitochondria, even though these larvae do not grow past second instars (Figure 4B).

Mitochondrial tRNA processing is altered in the absence of Mldr and Scu

Products encoded by mtDNA do not contain introns and with the exception of the A+T rich region, there are very few nucleotides that do not encode mRNA, rRNA or tRNA (Figure 5A) (27). Drosophila mtDNA is thought to be transcribed as five polycistrons (5,6). tRNAs in these polycistronic units are thought to serve as punctuation marks for 3′ and 5′ end processing of mitochondrial rRNAs and mRNAs (8). As such, most mt:mRNAs and mt:rRNAs are separated by at least one mt:tRNA (Figure 5A). Since the human mt:RNase P complex cleaves the mt:tRNA 5′-ends *in vitro*, we investigated whether mt:tRNA processing was aberrant *in vivo* in *mldr* and *scu* mutants and with *rswl RNAi* knockdown. mt:tRNAs are found in different sequence milieux. To test a variety of upstream sequence context, we chose to examine tRNAs that are found downstream of rRNA (mt:tRNA$^{Leu(CUN)}$ and mt:tRNA^{Val}), mRNA (Cytochrome c oxidase subunit III (CoIII), mt:tRNA^{Gly}) and the A+T rich region (mt:tRNA^{Ile}) (Figure 5A, asterisks). mt:tRNA processing by Arabidopsis PRORPs appears to be highly efficient and go to completion at steady-state levels *in vitro* (46); thus, normally unprocessed tRNAs would not be predicted to be observable by northern analysis. As such, wild-type larvae consistently and completely processed each of the mt:tRNAs we examined, with no evidence of unprocessed higher molecular weight RNA intermediates (Figure 5B–E, *y w*). In contrast, the mutant alleles of *mldr* and *scu*, and the larvae expressing *rswl RNAi* knockdown accumulated precursor mitochondrial RNAs (Figure 5B–E). mt:tRNA^{Ile} and mt:tRNA^{Gly} are encoded in the same polycistron. After probing for mt:tRNA^{Ile} in *mdlr* mutants, we observed three distinct bands, in contrast to *scu* mutants and *rswl RNAi* knockdown. Probing for mt:tRNA^{Gly}, however, showed only a single band (Figure 5C). mt:tRNA$^{Leu(CUN)}$ and mt:tRNA^{Val} are in the same polycistron and when probing with each gave bands at approximately the same sizes for *mldr* and *scu* mutants and *rswl* knockdown.

Overexpressing Mldr causes mitochondrial dysfunction

For multiprotein enzyme complexes, a decrease in any one protein often results in changes or loss of enzymatic function. Mutations in *mldr* and *scu*, as well as *RNAi* knockdown of *rswl*, resulted in pupal death, developmental delays and a decrease in mitochondrial function indicating each is essential *in vivo*. On the other hand, ectopically increasing enzyme levels can also lead to dominant negative effects through sequestering critical components from their normal function, or through mis-regulated activity. Using *tubGAL4* for high, global expression, we found overexpressing *UAS-mldr-GFP* and *UAS-rswl-myc* resulted in



H

genotype	% NBs with swollen mito.	# NBs
WT	0	89
mldr^{B}	99	135
mldr^{C}	100	83
scu^{A}	85	89
scu^{D}	93	95
scu^{4058}	97	114
rswl RNAi [a]	0	88

[a] *tubGAL4/ UAS-rswl*^{GD12447}

Figure 4. Larvae lacking Mldr and Scu have mitochondrial defects. (**A–G**) Larval stem cells (dashed circles) from third instar larval brains labeled for mitochondria (green), actin (magenta) and DAPI (blue). Larval stem cells in wild-type brains have small, dispersed mitochondria (A). (**C–G**) In contrast, mitochondria in the neuroblasts of *mldr* and *scu* mutants are grossly swollen with frequent ring-shaped mitochondria (arrows). (**B**) Ubiquitously expressing *rwsl*-RNAi using *tubGAL4* does not cause defects in mitochondrial morphology. (**H**) Table indicating the penetrance of neurobasts (NB) with swollen mitochondria and the number of neuroblasts examined. Green = anti-ATP synthase, magenta = phalloidin, blue = DAPI (A–G). Scale bar = 10 μm in G for A–G.

lethality (Table 2). Larvae overexpressing *mldr* could develop to second instars, but often did not develop past first instar (Figure 6A). In contrast, larvae overexpressing *rswl* were able to develop to third instars (Figure 6B). In agreement with the lethality, both genotypes exhibited low levels of ATP production (Figure 6C). Larvae overexpressing *scu* had increased ATP levels relative to *mldr* and *rswl*, albeit lower than wild-type, which did not result in lethality (Figure 6C, Table 2). To determine whether mitochondrial morphology was affected, we examined germ cells. *nanos-GAL4* (*nosGAL4*) is expressed exclusively in the germline. The *nosGAL4* stock we used does not give uniform expression in all developmental stages of the ovary, with lower expression in early germ cells and very high expression later (Figure 6J). When we examined mitochondrial morphology using immunofluorescence, we observed that in the lower expressing germ cells, mitochondria had the narrow, rod-shaped morphology characteristic of normal germ cell mitochondria (Figure 6D–F). However, mitochondria in germ cells with high expression of *UAS-mldr* had swollen, ring-shaped mitochondria indicative of a loss of selective permeability (Figure 6G–I). ATP synthase, which is found in the mitochondrial inner-membrane, labeled the outside of the ring-shaped mitochondria (Figure 6H, inset) whereas antibodies against Mldr, which is a mitochondrial matrix protein, labeled the inside of the mitochondrial rings (Figure 6G and I). Although overexpressing *UAS-rswl-myc* ubiquitously was lethal and decreased ATP levels, in contrast to *UAS-mldr*, mitochondrial morphology was normal (Figure 1I–K, Supplementary Figure S4). These results indicate that past a threshold expression level, Mldr causes dominant effects.

DISCUSSION

Each component of mt:RNase P is required *in vivo*

PRORPs represent a new class of tRNA 5′-end processing enzymes that lack a catalytic RNA component, i.e. a ribozyme. In humans, PRORP requires the obligatory presence of a sub-complex containing MRPP1 and MRPP2 to catalyze the cleavage reaction. The complex was initially identified from mitochondrial extracts and while it has been localized to mitochondria in cell culture, the physiological significance of these proteins during development has not been previously addressed *in vivo* (47). Here, we have shown that Drosophila contains orthologs of each member of the mt:RNase P complex: Mulder (PRORP), Scully (MRPP2) and Roswell (MRPP1). Each member localizes to mitochondria, and its loss causes lethality. In addition, decreasing the amount of Mldr, Scu or Rswl causes an accumulation of unprocessed mt:tRNAs, supporting that they function in the mt:tRNA processing pathway and that the mitochondrial defects seen in the mutants (loss of ATP, mitochondrial morphology defects) may be due to a decrease in mature mt:tRNAs.

Mldr levels are the most critical *in vivo*

Overall, the lethality we observed in *mldr* and *scu* mutants and *rswl RNAi* knockdown was very similar and consistent. All were pupal lethal, and *mldr* and *scu* mutants showed delayed pupation. Even though *mldr*^{B} and *mldr*^{C} are point mutations, there are low levels of protein present (Figure 2E). While both alleles cause a lack of protein, *mldr*^{C} (W465R) has a more severe developmental defect since 40% of the larvae do not pupate, suggesting that there is a difference in how any potential residual protein functions between the two alleles. The *scu* mutants we examined also showed differences in lethality, with *scu*^{4058} being the most severe

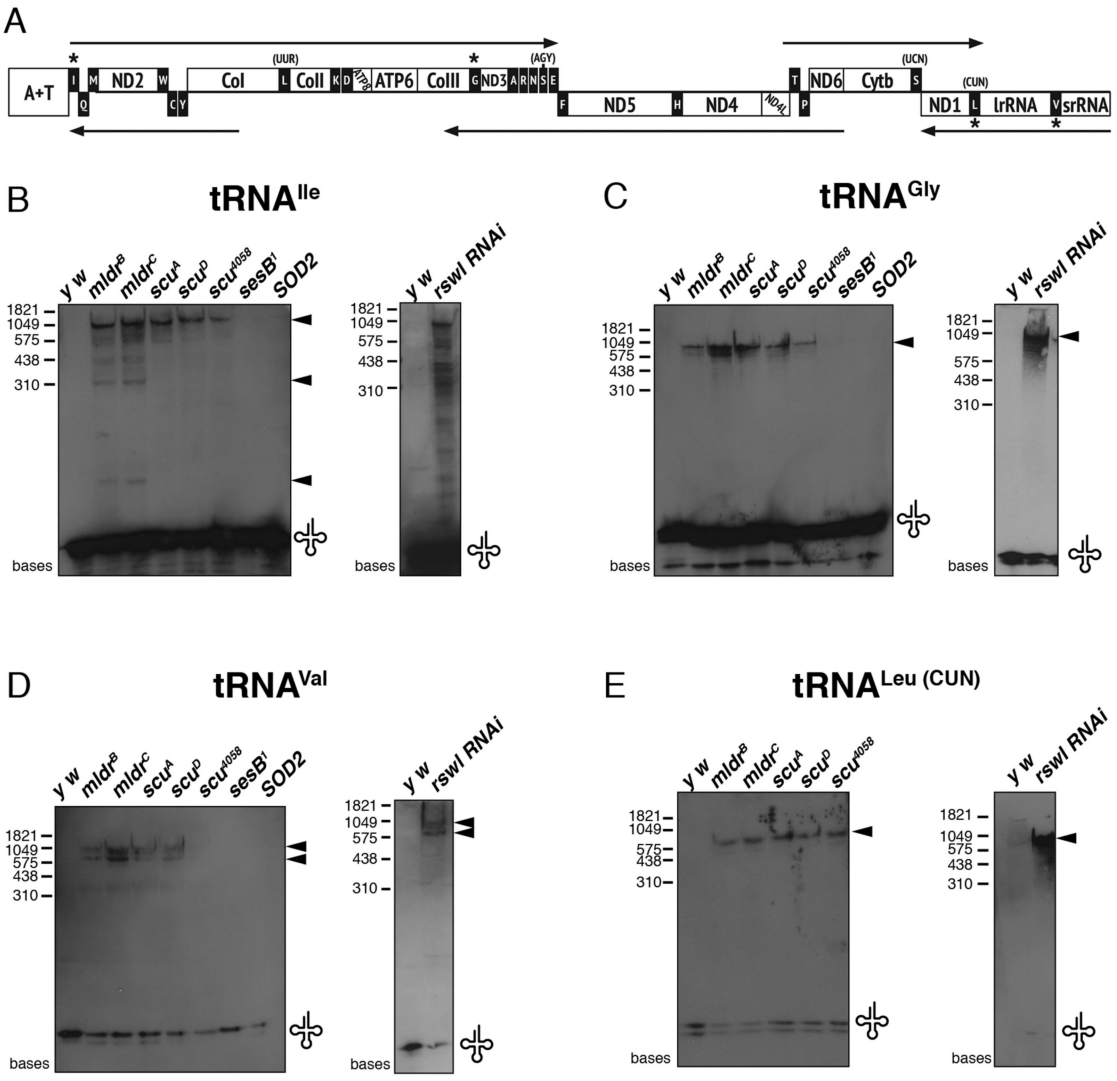


Figure 5. The mt:RNase P complex is required for mt:tRNA processing in Drosophila. (**A**) Diagram of Drosophila mitochondrial DNA structure (adapted from Xie and Dubrovsky). The five arrows indicate the predicted five transcribed polycistrons. Asterisks denote which mt:tRNAs were assayed via northern blot. ND = NADH dehydrogenase (Complex I), Cytb = ubiquinol: cytochrome c oxidoreductase (Complex III), Co = Cytochrome c oxidase (Complex IV), ATP = ATP synthase (Complex V). (B–E) Northern blots. *mldr* and *scu* mutant larvae contain unprocessed mt:tRNAs transcripts for mt:tRNA^{Ile}, mt:tRNA^{Gly}, mt:tRNA^{Val} and mt:tRNA$^{Leu(CUN)}$. Northern blots using extract from *rswl RNAi* knockdown larvae also show unprocessed, larger molecular weight species. Arrows indicate the major additional bands. *sesB^1* and *SOD2* mutant larvae are used as controls. The mature tRNAs are indicated by the tRNA symbol at the bottom of the blot.

which is surprising given that *scu^A* is a larger truncation. One potential explanation is that the additional amino acids left in *scu^{4058}* allows it to sequester other proteins, acting as a dominant negative. The human MRPP2 ortholog must form a tetramer in order to function (48,49). The truncations for *scu^{4058}* and *scu^A*, shown in only the blue monomer in Figure 2C, and color-coded with two lighter shades of blue, form the majority of the dimerization interface. It seems that even if these truncations were to result in viable coded proteins they would be unable to form a tetramer. Thus, it is likely these *scu* mutations could lead to disruption of tetramer formation with subsequent detrimental effects to the mt:RNase P function. In addition, MRPP2 (also known as HSD10 (HSD17B10 is the gene)) is known to function in the isoleucine biosynthetic pathway. However, patients suffering from HSD10 disease have symptoms that

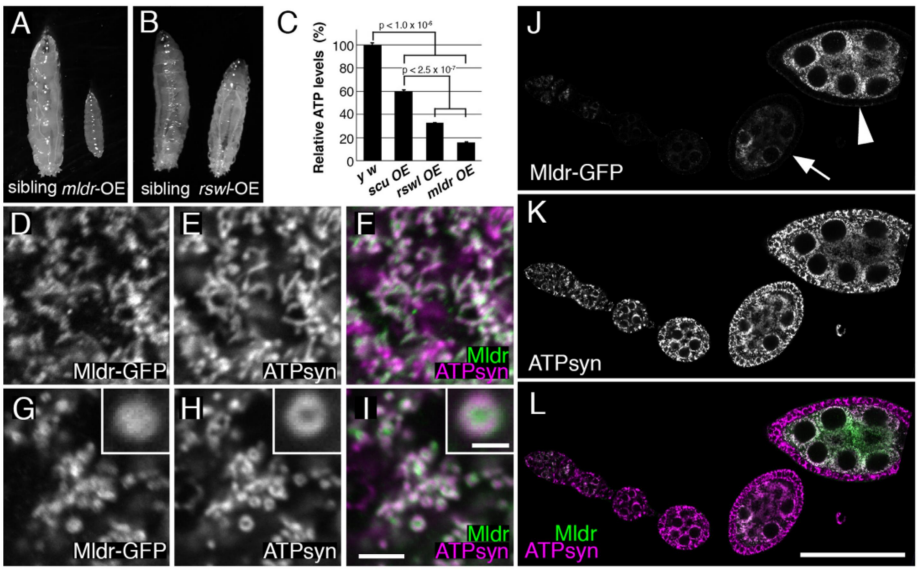


Figure 6. Overexpressing Mulder causes mitochondrial morphology defects. (**A**) *UAS-mldr-GFP* expressing larvae driven by *tubGAL4* do not develop past second instar. The sibling control larva is a third instar. (**B**) *UAS-rswl-myc* larvae, in contrast, are able to grow to the third instar stage driven by *tubGAL4*. (**C**) Graph showing relative ATP levels for *UAS-scu*, *UAS-rswl* and *UAS-mldr* larvae overexpressed using *tubGAL4*. OE = overexpression. (**D–I**) Germ cells expressing *UAS-mldr-GFP* under the control of *nosGAL4*. (D–F) Germ cells with lower Mldr expression (D) have mitochondria that are of the normal shape and size (E, F is the merge). Germ cells with high expression of UAS-Mldr-GFP (G) have swollen mitochondria (H, I is the merge). The swollen, ring-shaped mitochondria (H, inset) have Mldr-GFP concentrated in the middle (G, inset, I inset is the merge). (**J–L**) A representative ovariole expressing *UAS-mldr-GFP* under control of *nosGAL4*. Weaker expression is seen in younger germ cells (J, arrow) compared to strong Mldr-GFP expression in older ones (J, arrowhead). ATP synthase labeling shows all of the mitochondria throughout the ovariole (K). L is the merge of J and K. White = anti-GFP (D, G, J), anti-ATP synthase (E, H, K). Green = anti-GFP (F, I, L). Magenta = anti-ATP synthase (F, I, L). Scale bars = 5 μm in I for D-I, 1.5 μm in I inset for all insets, 50 μm in L for J–L. Error bars = s.e.m.. *P*-values were calculated in Microsoft Excel using a two-tailed Student's *t*-test.

Table 2. Effect of mt:RNase P overexpression

tubGAL4/ TM3 Ser ActGFP x	Number of adults	
	Balancer	non-Balancer
UAS-rswl-myc-4a/Y	299[a]	0
UAS-rswl-myc-5a/TM3 Sb	163	3
UAS-rswl-myc-1b/CyO	167	1
UAS-scu-FLAG-3a	300	327
UAS-scu-FLAG-3a/CyO[b]	168	70
UAS-scu-FLAG-4a/CyO	199	84
UAS-mldr-GFP-4b	213	0
UAS-mldr-GFP-2a/TM6b Hu Tb	125	0
UAS-mldr-GFP-4a/Y	108[a]	0

[a]includes all males.
[b]same insertion as 3a, maintained as a balanced stock.

do not correlate with an increase in toxic metabolites due to misregulated isoleucine biosynthesis. Rather, the symptoms are related to mitochondrial dysfunction and apoptotic cell death (50). Thus, while MRPP2/HSD10 has dehydrogenase activity, it is likely the loss of mitochondrial function associated with *MRPP2/HSD17B10* mutations is primarily due to its non-enzymatic function in the mt:RNase P.

In addition to the common phase of lethality, knockdown of *mldr*, *scu* and *rswl* exhibited greatly reduced ATP levels and accumulation of unprocessed mt:RNAs (Figures 3 and 5). However, our more detailed analyses of mitochondrial function revealed some critical differences between the three proteins. For example, only *mldr RNAi* caused an age-related decrease in locomotion when expressed in dopaminergic neurons (Figure 2I). In addition, *mldr* and *scu* mutants had swollen and ring-like mitochondria in neuroblasts, whereas *rswl-RNAi* did not (Figure 4). In general, when mitochondria have this morphology, it is indicative of a loss of selective permeability. Once this is lost, the mitochondrial outer membrane fragments, leading to a lack of ATP production. However, normal morphology does not necessarily mean ATP production is at appropriate levels.

These data suggest that while all three proteins are essential, cells are most sensitive to reductions in Mldr.

Interestingly, while decreasing Mldr, Scu and Rswl caused lethality, overexpressing Mldr and Rswl had the same effect (Table 2). In contrast, overexpressing *UAS-scu-FLAG* in a wild-type background resulted in the expected Mendelian ratio of adults, suggesting that too much of Scu does not appear to alter the function of the complex, cause a deleterious increase in dehydrogenase activity or sequester any critical components in a dominant negative fashion. In contrast, overexpressing Mldr was lethal, led to decreased ATP levels and also caused defects in mitochondrial morphology (Figure 6). Overexpressing Rswl was lethal, but unlike Mldr, did not appear to change mitochondrial morphology as judged by immunofluorescence (Supplementary Figure S4). One possible explanation is that too much Mldr causes indiscriminate nucleotide cleavage in the mitochondrion resulting in a more severe effect. However, while the lethal outcome of Rswl overexpression may be more specific to mt:tRNA processing, we cannot rule out there is a concomitant deleterious increase in nonselective methyltransferase activity. It could be that an increase in indiscriminate methyltransferase activity is simply not as deleterious as nucleotide cleavage while still being important. Thus, decreasing and increasing Rswl expression causes a decrease in ATP and lethality, but does not give rise to any mitochondrial morphological changes. Looking at all of the phenotypes caused by lack and overexpression of the three mt:RNase P complex members, it is apparent based on our data that Drosophila is most sensitive to alterations in the levels of Mldr.

Decreasing Drosophila mt:RNase P complex proteins does not cause oxidative stress

We saw a consistent loss of ATP for *mldr* and *scu* mutants, as well as RNAi knockdown of *mldr*, *scu* and *rswl*. The ATP loss is very striking, and is not necessarily observed in other larvae mutant for proteins involved in various mitochondrial functions (29,43). However, we observed no accompanying oxidative stress by assaying mitochondrial aconitase function. Mitochondrial aconitase is well established as being exceedingly sensitive to oxidation, and thus loss of its function is often used as an indirect assay for an increased mitochondrial oxidative environment (45,51). Mutating Drosophila proteins involved in mitochondrial function does not always lead to oxidative stress in larvae (29). One possible reason is that since mitochondria fulfill a variety of biochemical functions, lowering levels of different pathways would not necessarily cause oxidative stress. Another possible reason is that there is evidence that larvae primarily use glycolysis, and not respiration, to maintain ATP levels (52). Respiration is primarily responsible for generating reactive oxygen species in mitochondria since the electron transport chain can be 'leaky'.

RNAse Z is the enzyme responsible for 3′-end tRNA cleavage. Drosophila lacking mitochondrial RNAse Z have been reported to have cell cycle defects, as well as oxidative damage (43). In contrast, we did not observe any particularly small imaginal disks (indicative of cell cycle defects), and while larvae development showed a delay, the larval brains were of relatively normal size, as were the pupae that formed. It is still possible that mutant clones would be smaller relative to their wild-type siblings. Thus, it appears that while flies lacking either mt:RNAse Z or mt:RNase P accumulate unprocessed mitochondrial RNA species, they have different effects on ATP levels and oxidative stress (43).

Reducing Mldr, Scu and Rswl results in accumulation of unprocessed mitochondrial RNAs

Larvae mutant for *mldr* and *scu*, as well as *rswl RNAi* knockdown, accumulate unprocessed mt:RNAs (Figure 5). There are several conclusions that can be gleaned from these experiments. Wild-type larvae consistently and completely processed the four mt:tRNAs we examined, as did the *sesB*^{1} and *SOD2* mutants – two genes mutated in unrelated processes (53–55). Thus, accumulation of mt:RNAs was specific for Mldr, Scu and Rswl and not due to general mitochondrial dysfunction. For mt:tRNA^{Ile} and mt:tRNA^{Gly}, which are encoded in the polycistron downstream of the A + T rich region, the amount of processed mt:tRNA was larger compared to mt:tRNA^{Val} and mt:tRNA$^{Leu(CUN)}$, both encoded in the polycistron that also encodes the large and small mt:rRNAs. There are several possible explanations for this observation. First, both ribozyme and protein-only RNase P enzymes have differential affinities and cleavage rates for some RNA substrates *in vitro* (46,56–58). Thus the differences in the amount of processed product could be due to different cleavage efficiencies of mt:RNase P for the two polycistrons. However, given that there is more processed product for mt:tRNA^{Ile} and mt:tRNA^{Gly}, the two polycistrons would also need to be differentially transcribed, as happens in humans (59). Since the same amount of total RNA was added for all the blots, it is possible the two polycistrons are differentially transcribed. However, counterintuitively, the polycistron encoding the mt:rRNAs appears to be at lower levels than the one downstream of the A + T rich region, in contrast to what is thought to happen for human mtDNA (59). The difference in transcript levels does not appear to be due to non-specific binding of the probes to other tRNAs, as performing BLAST analysis with each full-length mt:tRNA probe (Supplementary Table S2) did not recognize any other tRNAs. Alternatively, this could be explained by differences in probe binding, however, the unprocessed mt:mRNAs were of similar intensity for all the blots.

In addition, *mldr*^{C} mutant larvae had the largest accumulation of unprocessed mt:tRNAs. This is consistent with it being the more severe *mldr* allele, as well as with our observations that Drosophila are most sensitive to perturbation in Mldr levels. For mt:tRNA^{Ile} processing, *mldr* mutants showed several band sizes of unprocessed mt:tRNAs, which may reflect the potential influence of *mldr* mutations on the specificity of the 5′ end cleavage (Figure 5B). In contrast, the *scu* mutations affected mt:tRNA^{Ile} 5′-end processing of the same cleavage sites equally. *rswl RNAi* also showed a variety of band sizes for mt:tRNA^{Ile} cleavage. By size, these bands cannot be clearly associated with putative RNA transcripts including tRNA^{Ile}. It is possible that these detected bands are products of miscleavage by Rswl deficient mt:RNase P,

suggesting a potential role of Rswl in restricting substrate recognition.

mt:RNase P and disease

Many mitochondrial diseases are associated with point mutations in mtDNA (60). While mt:tRNAs encode for a relatively small proportion of mtDNA, over 50% of the disease-causing mutations found in mtDNA are found in the mt:tRNAs (61). However, most of these mt:tRNA mutations do not occur in the anticodon or discriminator bases that are necessary for codon recognition and aminoacylation. Therefore, these disease-causing mt:tRNA mutations likely impact such processes as post-transcriptional modifications, interaction with the translation machinery or mt:tRNA processing. There is evidence that normal mt:tRNA processing is critical as mutations in precursor mt:tRNAs that impair mt:tRNA 5′-end maturation, as well as in human PRORP, can give rise to disease (19–20,23,62). Studying how loss of Mldr, Scu or Rswl function affects cellular function is therefore important for promoting the understanding of the mechanisms of these mitochondrial diseases.

SUPPLEMENTARY DATA

Supplementary Data are available at NAR Online.

ACKNOWLEDGEMENTS

We would like to thank Drs Frank Shewmaker and Xin Xiang for critically reading the manuscript. We would also like to thank the USU Biomedical Instrumentation Core. The Drosophila Genomics Resource Center, supported by NIH grant 2P40OD010949-10A1, provided reagents. Stocks obtained from the Bloomington Drosophila Stock Center (NIH P40OD018537) and Vienna Drosophila Resource Center were used in this study.

FUNDING

National Institutes of Health [1R01GM117141 to M.K.]; Uniformed Services University [USUHS BIO-71-3019 to R.T.C.]; National Institutes of Health/Department of Defense [CHIRP HU0001-14-2-0041 to R.T.C.]. Funding for open access charge: NIH R01 GM117141.
Conflict of interest statement. None declared.

REFERENCES

1. Gissi,C., Iannelli,F. and Pesole,G. (2008) Evolution of the mitochondrial genome of Metazoa as exemplified by comparison of congeneric species. *Heredity (Edinb.)*, **101**, 301–320.
2. Jackman,J.E. and Alfonzo,J.D. (2013) Transfer RNA modifications: nature's combinatorial chemistry playground. *Wiley Interdiscip. Rev. RNA*, **4**, 35–48.
3. Paris,Z., Fleming,I.M. and Alfonzo,J.D. (2012) Determinants of tRNA editing and modification: avoiding conundrums, affecting function. *Semin. Cell Dev. Biol.*, **23**, 269–274.
4. Phizicky,E.M. and Hopper,A.K. (2010) tRNA biology charges to the front. *Genes Dev.*, **24**, 1832–1860.
5. Berthier,F., Renaud,M., Alziari,S. and Durand,R. (1986) RNA mapping on Drosophila mitochondrial DNA: precursors and template strands. *Nucleic Acids Res.*, **14**, 4519–4533.
6. Torres,T.T., Dolezal,M., Schlotterer,C. and Ottenwalder,B. (2009) Expression profiling of Drosophila mitochondrial genes via deep mRNA sequencing. *Nucleic Acids Res.*, **37**, 7509–7518.
7. Mercer,T.R., Neph,S., Dinger,M.E., Crawford,J., Smith,M.A., Shearwood,A.M., Haugen,E., Bracken,C.P., Rackham,O., Stamatoyannopoulos,J.A. *et al.* (2011) The human mitochondrial transcriptome. *Cell*, **146**, 645–658.
8. Ojala,D., Montoya,J. and Attardi,G. (1981) tRNA punctuation model of RNA processing in human mitochondria. *Nature*, **290**, 470–474.
9. Hartmann,R.K., Gossringer,M., Spath,B., Fischer,S. and Marchfelder,A. (2009) The making of tRNAs and more - RNase P and tRNase Z. *Progress Mol. Biol. Translat. Sci.*, **85**, 319–368.
10. Rossmanith,W. (2012) Of P and Z: mitochondrial tRNA processing enzymes. *Biochim. et Biophys. Acta*, **1819**, 1017–1026.
11. Guerrier-Takada,C., Gardiner,K., Marsh,T., Pace,N. and Altman,S. (1983) The RNA moiety of ribonuclease P is the catalytic subunit of the enzyme. *Cell*, **35**, 849–857.
12. Holzmann,J., Frank,P., Löffler,E., Bennett,K.L., Gerner,C. and Rossmanith,W. (2008) RNase P without RNA: identification and functional reconstitution of the human mitochondrial tRNA processing enzyme. *Cell*, **135**, 462–536.
13. Gobert,A., Gutmann,B., Taschner,A., Gossringer,M., Holzmann,J., Hartmann,R.K., Rossmanith,W. and Giege,P. (2010) A single Arabidopsis organellar protein has RNase P activity. *Nat. Struct. Mol. Biol.*, **17**, 740–744.
14. Taschner,A., Weber,C., Buzet,A., Hartmann,R.K., Hartig,A. and Rossmanith,W. (2012) Nuclear RNase P of Trypanosoma brucei: a single protein in place of the multicomponent RNA-protein complex. *Cell Reports*, **2**, 19–25.
15. Vilardo,E., Nachbagauer,C., Buzet,A., Taschner,A., Holzmann,J. and Rossmanith,W. (2012) A subcomplex of human mitochondrial RNase P is a bifunctional methyltransferase–extensive moonlighting in mitochondrial tRNA biogenesis. *Nucleic Acids Res.*, **40**, 11583–11593.
16. Brzezniak,L.K., Bijata,M., Szczesny,R.J. and Stepien,P.P. (2011) Involvement of human ELAC2 gene product in 3′ end processing of mitochondrial tRNAs. *RNA Biol.*, **8**, 616–626.
17. Suzuki,T., Nagao,A. and Suzuki,T. (2011) Human mitochondrial tRNAs: biogenesis, function, structural aspects, and diseases. *Annu. Rev. Genet.*, **45**, 299–329.
18. Bindoff,L.A., Howell,N., Poulton,J., McCullough,D.A., Morten,K.J., Lightowlers,R.N., Turnbull,D.M. and Weber,K. (1993) Abnormal RNA processing associated with a novel tRNA mutation in mitochondrial DNA. A potential disease mechanism. *J. Biological Chem.*, **268**, 19559–19564.
19. Chatfield,K.C., Coughlin,C.R. 2nd, Friederich,M.W., Gallagher,R.C., Hesselberth,J.R., Lovell,M.A., Ofman,R., Swanson,M.A., Thomas,J.A., Wanders,R.J. *et al.* (2015) Mitochondrial energy failure in HSD10 disease is due to defective mtDNA transcript processing. *Mitochondrion*, **21**, 1–10.
20. Deutschmann,A.J., Amberger,A., Zavadil,C., Steinbeisser,H., Mayr,J.A., Feichtinger,R.G., Oerum,S., Yue,W.W. and Zschocke,J. (2014) Mutation or knock-down of 17beta-hydroxysteroid dehydrogenase type 10 cause loss of MRPP1 and impaired processing of mitochondrial heavy strand transcripts. *Hum. Mol. Genet.*, **23**, 3618–3628.
21. Li,R. and Guan,M.X. (2010) Human mitochondrial leucyl-tRNA synthetase corrects mitochondrial dysfunctions due to the tRNALeu(UUR) A3243G mutation, associated with mitochondrial encephalomyopathy, lactic acidosis, and stroke-like symptoms and diabetes. *Mol. Cell. Biol.*, **30**, 2147–2154.
22. Rossmanith,W. and Karwan,R.M. (1998) Characterization of human mitochondrial RNase P: novel aspects in tRNA processing. *Biochem. Biophys. Res. Commun.*, **247**, 234–241.
23. Wang,S., Li,R., Fettermann,A., Li,Z., Qian,Y., Liu,Y., Wang,X., Zhou,A., Mo,J.Q., Yang,L. *et al.* (2011) Maternally inherited essential hypertension is associated with the novel 4263A>G mutation in the mitochondrial tRNAIle gene in a large Han Chinese family. *Circ. Res.*, **108**, 862–870.
24. Haack,T.B., Kopajtich,R., Freisinger,P., Wieland,T., Rorbach,J., Nicholls,T.J., Baruffini,E., Walther,A., Danhauser,K., Zimmermann,F.A. *et al.* (2013) ELAC2 mutations cause a

mitochondrial RNA processing defect associated with hypertrophic cardiomyopathy. *Am. J. Hum. Genet.*, **93**, 211–223.
25. Vilardo,E. and Rossmanith,W. (2015) Molecular insights into HSD10 disease: impact of SDR5C1 mutations on the human mitochondrial RNase P complex. *Nucleic Acids Res.*, **43**, 5112–5119.
26. Yarham,J.W., Elson,J.L., Blakely,E.L., McFarland,R. and Taylor,R.W. (2010) Mitochondrial tRNA mutations and disease. *Wiley Interdiscip. Rev. RNA*, **1**, 304–324.
27. Lewis,D.L., Farr,C.L. and Kaguni,L.S. (1995) Drosophila melanogaster mitochondrial DNA: completion of the nucleotide sequence and evolutionary comparisons. *Insect. Mol. Biol.*, **4**, 263–278.
28. Dietzl,G., Chen,D., Schnorrer,F., Su,K.C., Barinova,Y., Fellner,M., Gasser,B., Kinsey,K., Oppel,S., Scheiblauer,S. *et al.* (2007) A genome-wide transgenic RNAi library for conditional gene inactivation in Drosophila. *Nature*, **448**, 151–156.
29. Sen,A., Damm,V.T. and Cox,R.T. (2013) Drosophila clueless is highly expressed in larval neuroblasts, affects mitochondrial localization and suppresses mitochondrial oxidative damage. *PLoS One*, **8**, e54283.
30. Sen,A., Kalvakuri,S., Bodmer,R. and Cox,R.T. (2015) Clueless, a protein required for mitochondrial function, interacts with the PINK1-Parkin complex in Drosophila. *Dis. Model Mech.*, **8**, 577–589.
31. Schneider,C.A., Rasband,W.S. and Eliceiri,K.W. (2012) NIH Image to ImageJ: 25 years of image analysis. *Nat. Methods*, **9**, 671–675.
32. Torroja,L., Ortuno-Sahagun,D., Ferrus,A., Hammerle,B. and Barbas,J.A. (1998) scully, an essential gene of Drosophila, is homologous to mammalian mitochondrial type II L-3-hydroxyacyl-CoA dehydrogenase/amyloid-beta peptide-binding protein. *J. Cell Biol.*, **141**, 1009–1017.
33. Brand,A.H. and Perrimon,N. (1993) Targeted gene expression as a means of altering cell fates and generating dominant phenotypes. *Development*, **118**, 401–415.
34. Kelley,L.A., Mezulis,S., Yates,C.M., Wass,M.N. and Sternberg,M.J. (2015) The Phyre2 web portal for protein modeling, prediction and analysis. *Nat. Protoc.*, **10**, 845–858.
35. Li,F., Liu,X., Zhou,W., Yang,X. and Shen,Y. (2015) Auto-inhibitory mechanism of the human mitochondrial RNase P protein complex. *Sci. Rep.*, **5**, 9878.
36. Reinhard,L., Sridhara,S. and Hallberg,B.M. (2015) Structure of the nuclease subunit of human mitochondrial RNase P. *Nucleic Acids Res.*, **43**, 5664–5672.
37. Lustbader,J.W., Cirilli,M., Lin,C., Xu,H.W., Takuma,K., Wang,N., Caspersen,C., Chen,X., Pollak,S., Chaney,M. *et al.* (2004) ABAD directly links Abeta to mitochondrial toxicity in Alzheimer's disease. *Science*, **304**, 448–452.
38. Yang,J., Yan,R., Roy,A., Xu,D., Poisson,J. and Zhang,Y. (2015) The I-TASSER Suite: protein structure and function prediction. *Nature Methods*, **12**, 7–8.
39. Haelterman,N.A., Jiang,L., Li,Y., Bayat,V., Sandoval,H., Ugur,B., Tan,K.L., Zhang,K., Bei,D., Xiong,B. *et al.* (2014) Large-scale identification of chemically induced mutations in Drosophila melanogaster. *Genome Res.*, **24**, 1707–1718.
40. Kirby,K., Hu,J., Hilliker,A.J. and Phillips,J.P. (2002) RNA interference-mediated silencing of Sod2 in Drosophila leads to early adult-onset mortality and elevated endogenous oxidative stress. *Proc. Natl. Acad. Sci. U S A*, **99**, 16162–16167.
41. Macchi,M., El Fissi,N., Tufi,R., Bentobji,M., Lievens,J.C., Martins,L.M., Royet,J. and Rival,T. (2013) The Drosophila inner-membrane protein PMI controls crista biogenesis and mitochondrial diameter. *J. Cell. Sci.*, **126**, 814–824.
42. Sandoval,H., Yao,C.K., Chen,K., Jaiswal,M., Donti,T., Lin,Y.Q., Bayat,V., Xiong,B., Zhang,K., David,G. *et al.* (2014) Mitochondrial fusion but not fission regulates larval growth and synaptic development through steroid hormone production. *Elife*, **3**, e03558.
43. Xie,X. and Dubrovsky,E.B. (2015) Knockout of Drosophila RNase ZL impairs mitochondrial transcript processing, respiration and cell cycle progression. *Nucleic Acids Res.*, **43**, 10364–10375.
44. Flint,D.H., Tuminello,J.F. and Emptage,M.H. (1993) The inactivation of Fe-S cluster containing hydro-lyases by superoxide. *J. Biol. Chem.*, **268**, 22369–22376.
45. Gardner,P.R. and Fridovich,I. (1991) Superoxide sensitivity of the *Escherichia coli* aconitase. *J. Biol. Chem.*, **266**, 19328–19333.
46. Howard,M.J., Karasik,A., Klemm,B.P., Mei,C., Shanmuganathan,A., Fierke,C.A. and Koutmos,M. (2016) Differential substrate recognition by isozymes of plant protein-only Ribonuclease P. *RNA*, **22**, 782–792.
47. Sanchez,M.I., Mercer,T.R., Davies,S.M., Shearwood,A.M., Nygard,K.K., Richman,T.R., Mattick,J.S., Rackham,O. and Filipovska,A. (2011) RNA processing in human mitochondria. *Cell Cycle*, **10**, 2904–2916.
48. Kissinger,C.R., Rejto,P.A., Pelletier,L.A., Thomson,J.A., Showalter,R.E., Abreo,M.A., Agree,C.S., Margosiak,S., Meng,J.J., Aust,R.M. *et al.* (2004) Crystal structure of human ABAD/HSD10 with a bound inhibitor: implications for design of Alzheimer's disease therapeutics. *J. Mol. Biol.*, **342**, 943–952.
49. Powell,A.J., Read,J.A., Banfield,M.J., Gunn-Moore,F., Yan,S.D., Lustbader,J., Stern,A.R., Stern,D.M. and Brady,R.L. (2000) Recognition of structurally diverse substrates by type II 3-hydroxyacyl-CoA dehydrogenase (HADH II)/amyloid-beta binding alcohol dehydrogenase (ABAD). *J. Mol. Biol.*, **303**, 311–327.
50. Rauschenberger,K., Scholer,K., Sass,J.O., Sauer,S., Djuric,Z., Rumig,C., Wolf,N.I., Okun,J.G., Kolker,S., Schwarz,H. *et al.* (2010) A non-enzymatic function of 17beta-hydroxysteroid dehydrogenase type 10 is required for mitochondrial integrity and cell survival. *EMBO Mol. Med.*, **2**, 51–62.
51. Gardner,P.R., Nguyen,D.D. and White,C.W. (1994) Aconitase is a sensitive and critical target of oxygen poisoning in cultured mammalian cells and in rat lungs. *Proc. Natl Acad. Sci. U.S.A.*, **91**, 12248–12252.
52. Tennessen,J.M., Baker,K.D., Lam,G., Evans,J. and Thummel,C.S. (2011) The Drosophila estrogen-related receptor directs a metabolic switch that supports developmental growth. *Cell Metabol.*, **13**, 139–148.
53. Celotto,A.M., Frank,A.C., McGrath,S.W., Fergestad,T., Van Voorhies,W.A., Buttle,K.F., Mannella,C.A. and Palladino,M.J. (2006) Mitochondrial encephalomyopathy in Drosophila. *J. Neurosci.*, **26**, 810–820.
54. Fergestad,T., Bostwick,B. and Ganetzky,B. (2006) Metabolic disruption in Drosophila bang-sensitive seizure mutants. *Genetics*, **173**, 1357–1364.
55. Zhang,Y.Q., Roote,J., Brogna,S., Davis,A.W., Barbash,D.A., Nash,D. and Ashburner,M. (1999) stress sensitive B encodes an adenine nucleotide translocase in Drosophila melanogaster. *Genetics*, **153**, 891–903.
56. Liu,F. and Altman,S. (1994) Differential evolution of substrates for an RNA enzyme in the presence and absence of its protein cofactor. *Cell*, **77**, 1093–1100.
57. Sugita,C., Komura,Y., Tanaka,K., Kometani,K., Satoh,H. and Sugita,M. (2014) Molecular characterization of three PRORP proteins in the moss Physcomitrella patens: nuclear PRORP protein is not essential for moss viability. *PLoS One*, **9**, e108962.
58. Koutmou,K.S., Zahler,N.H., Kurz,J.C., Campbell,F.E., Harris,M.E. and Fierke,C.A. (2010) Protein-precursor tRNA contact leads to sequence-specific recognition of 5′ leaders by bacterial ribonuclease P. *J. Mol. Biol.*, **396**, 195–208.
59. Terzioglu,M., Ruzzenente,B., Harmel,J., Mourier,A., Jemt,E., Lopez,M.D., Kukat,C., Stewart,J.B., Wibom,R., Meharg,C. *et al.* (2013) MTERF1 binds mtDNA to prevent transcriptional interference at the light-strand promoter but is dispensable for rRNA gene transcription regulation. *Cell Metabol.*, **17**, 618–626.
60. Wallace,D.C. (1992) Diseases of the mitochondrial DNA. *Annual Rev. Biochem.*, **61**, 1175–1212.
61. Ruiz-Pesini,E., Lott,M.T., Procaccio,V., Poole,J.C., Brandon,M.C., Mishmar,D., Yi,C., Kreuziger,J., Baldi,P. and Wallace,D.C. (2007) An enhanced MITOMAP with a global mtDNA mutational phylogeny. *Nucleic Acids Res.*, **35**, D823–D828.
62. Rossmanith,W. and Karwan,R.M. (1998) Impairment of tRNA processing by point mutations in mitochondrial tRNA(Leu)(UUR) associated with mitochondrial diseases. *FEBS Lett.*, **433**, 269–274.

Supplemental Figure Legends

Figure S1. All three mt:RNase P proteins localize to mitochondria. (A-F) Germ cells expressing Rswl-myc (A, C) and Scu-FLAG (D, F) using the germline driver *nosGAL4*. Both Rswl (A) and Scu (D) colocalize with mitochondria (B, E). The merged images are shown in C and F, respectively. (G-O) S2R+ cells transfected with constructs encoding myc-tagged Rswl (G), Scu (J), and Mldr (M). All three colocalize with mitochondria (H, K, N and merge, I, L, O). White = anti-myc (A, G, J, M), anti-ATP synthase (B, E, H, K, N). Green = anti-myc (C, I, L, O), anti-FLAG (F). Magenta = anti-ATP synthase (C, F, I, L, O). Scale bar = 5 μm in F for A-F and in O for G-O.

Figure S2. Representative field of S2R+ cells transfected with myc-tagged Scully. S2R+ cells transfected with Scu-myc express lower levels of myc (A, arrowheads) that co-localizes with mitochondria (B, arrowheads) but also express very high levels of Scu-myc containing frequent large aggregates (A, arrows). White = anti-myc (A), anti-ATP synthase (B). Green = anti-myc (C). Magenta = anti-ATP synthase (C). Scale bar = 10 μm in C for A-C.

Figure S3. Mutations in *mldr* and *scu* cause pupation defects. Graph indicating the range of various pupal defects. Micrographs show the representative classes of defects scored. Wild type (WT) pupation usually results in full eversion of the anterior spiracles (WT, arrow). Occasionally, eversion is not completed (nubs, arrow). Pupae mutant for *mldr* and *scu* frequently display defects in spiracle eversion (nubs, club, arrows). A substantial portion of scu^{4058} and $mldr^{C}$ do not even form compact pupal cases, but rather larval-like pupal cases (larval). Consistent with pupation rates, $mldr^{C}$ also contains many dead third instar wandering larvae (wandering). Controls are an average of all the sibling controls for each genotype. Error bars = s.d..

Figure S4. Overexpressing Roswell does not cause any obvious mitochondrial morphology defects. (A) Using tubGAL4 to overexpress UAS-rswl-myc results in larvae that are close to normal third instar size. (B-D) Germ cells overexpressing *UAS-rswl-myc*. (B) Two germ cells, the one on the left has high levels of *UAS-rswl-myc* expression. (C) The corresponding image labelled with ATP synthase shows that the mitochondria in both the *rswl-myc* expressing (left) and non-expressing cell (right) have the same normal morphology. (D) The merge of A and B. The black hole in the center of each cell is the nucleus. White = anti-myc (B) and anti-ATP synthase (C). Green = anti-myc (D). Magenta = anti-ATP synthase (D). Scale bar = 10 μm in C for A-C.

Table S1. *RNAi* knockdown of *rswl*, *scu* and *mldr*. The percent pupation and eclosion is shown for each *RNAi* line crossed to both *tubGAL4* and *ActGAL4*, with pairwise sibling controls for comparison. This table contains information also found in Table 1.

Table S2. Northern blot mt:tRNA probes. Each northern blot probe for Figure 5 used the full-length mt:tRNA sequence.

Figure S1

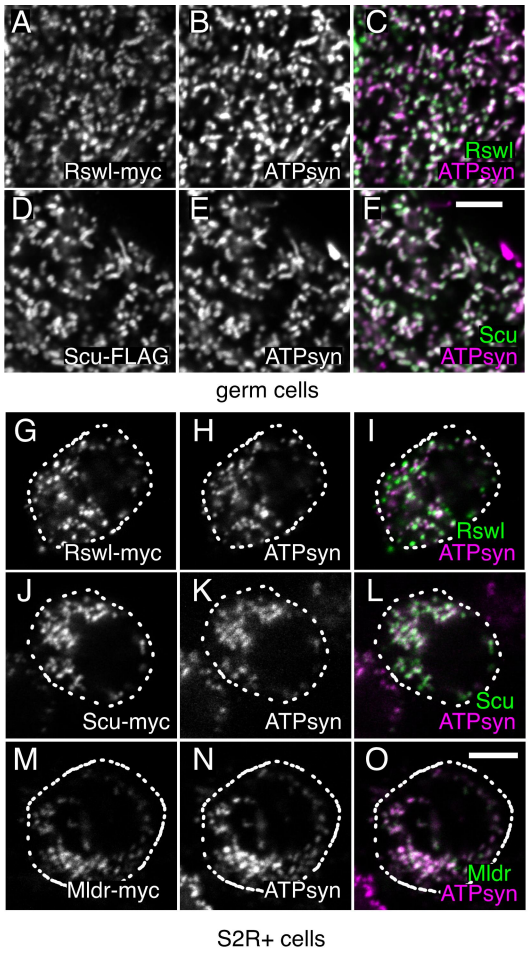

A
Rswl-myc
B
ATPsyn
C
Rswl
ATPsyn
D
Scu-FLAG
E
ATPsyn
F
Scu
ATPsyn
germ cells
G
Rswl-myc
H
ATPsyn
I
Rswl
ATPsyn
J
Scu-myc
K
ATPsyn
L
Scu
ATPsyn
M
Mldr-myc
N
ATPsyn
O
Mldr
ATPsyn
S2R+ cells

Figure S2

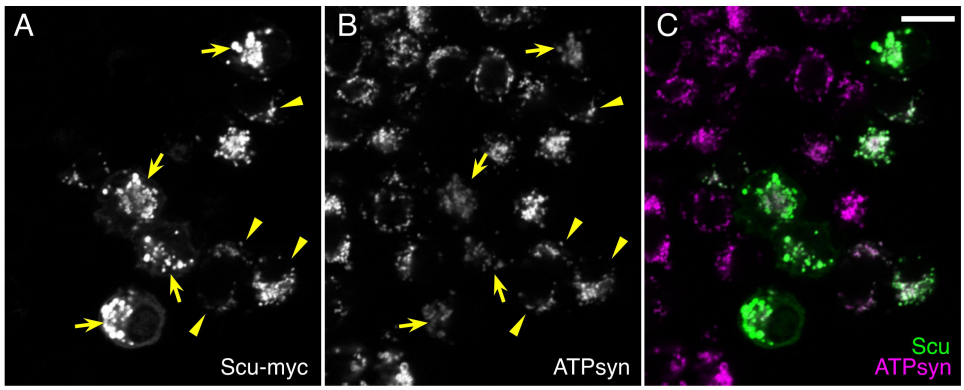


Figure S3

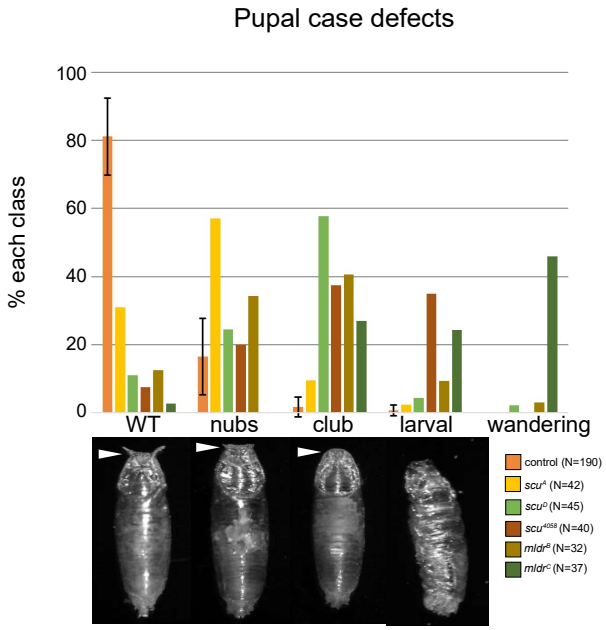

Pupal case defects
% each class
100
80
60
40
20
0
WT
nubs
club
larval
wandering
control (N=190)
scu4 (N=42)
scuO (N=45)
scu4058 (N=40)
mldr6 (N=32)
mldrC (N=37)

Figure S4

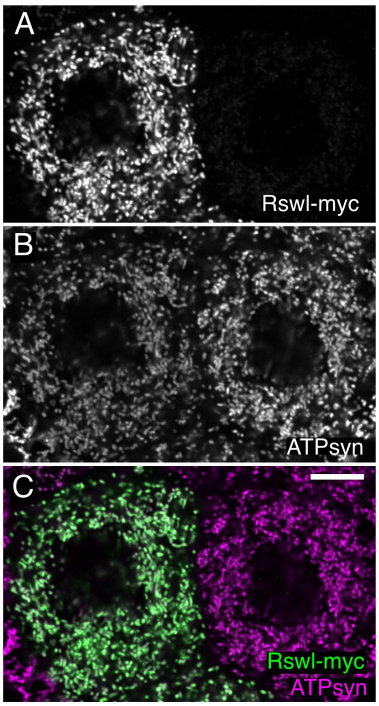


Table S1 mt:RNase P *RNAi* knockdown pupation and eclosion rates.

	RNAi		Sibling control[b]	
	% pupation[a]	% eclosion	% pupation	% eclosion
tubGAL4/ UAS-rswl ^{GD12447}	0	0	85 ± 5	98 ± 1.8
ActGAL4/ UAS-rswl ^{GD12447}	92 ± 3.3	0	98 ± 1.7	98 ± 1.7
UAS-scu $^{TRiP.HMS02305}$*/+; tubGAL4/+*	86 ± 7.2	0	98 ± 2.5	98
UAS-scu $^{TRiP.HMS02305}$*/+; ActGAL4/+*	85 ± 5	0	83 ± 3.3	100
UAS-scu $^{TRiP.GL01078}$*/ tubGAL4*	92 ± 1.7	0	95 ± 2.9	97 ± 3.3
UAS-scu $^{TRiP.GL01079}$*/ ActGAL4*	88 ± 3.3	49 ± 2	85 ± 2.9	96 ± 2.0
tubGAL4/ UAS-mldr ^{KK108043}	83 ± 1.7	8 ± 5.1	92 ± 1.7	97 ± 3.3
actGAL4/ UAS-mldr ^{KK108043}	92 ± 4.4	18 ± 0.6	73 ± 3.3	100

[a] ± s.e.m. [b] GFP$^+$ sibling larvae.

Table S2. Northern blot mt:tRNA probes.

probes	5’ to 3’ sequence
$tRNA^{Ile}$	GGGCAAUGAAUGCAGAAAACUGCAUGAUUUACCCUAUCAAGGTAAUCCUUUU UAUCAGGCAAUUCAUU
$tRNA^{Val}$	GGGCAAUUUAUAUUGAUUUGCACAAAAAUCUUUUCAAUGUAAAUGAAAUACU UUACUUAAUAAGCUUUAAAUUG
$tRNA^{Leu\ (CUN)}$	GGGUACUAUUUGUAAUAAAAAUCACAUAUAUAAAUUCUAAAUUUAUUGCACU AAUCUGCCAAAAUAGU
$tRNA^{Gly}$	GGGUAUCUAUACUAUUAAUUAAUAGACCUUAUGAUUGGAAGUCAAAUAUACU UUUAUACUAUAUAGAU